High bandwidth microrheology of complex fluids and biopolymer networks

Atakhorrami, M.

2006

document version
Publisher's PDF, also known as Version of record

High-bandwidth microrheology of complex fluids and biopolymer networks

Maryam Atakhorrami

This thesis was reviewed by:

prof.dr. A.M. Dogterom
prof.dr. P. Janmey
prof.dr. P.D. Olmsted
dr. Rinke J. Wijngaarden
prof.dr. B.M. Mulder

High-bandwidth microrheology of complex fluids and biopolymer networks
Maryam Atakhorrami

Cover: Simon Tindemans

ISBN 90-6464-5-21-3

VRIJE UNIVERSITEIT

High-bandwidth microrheology of complex fluids and biopolymer networks

ACADEMISCH PROEFSCHRIFT

ter verkrijging van de graad Doctor aan
de Vrije Universiteit Amsterdam,
op gezag van de rector magnificus
prof. dr. T. Sminia,
in het openbaar te verdedigen
ten overstaan van de promotiecommissie
van de faculteit der Exacte Wetenschappen
op donderdag 16 februari 2006 om 13.45 uur
in de aula van de universiteit,
De Boelelaan 1105

door

Maryam Atakhorrami

geboren te Roodbar, Iran

promotor: prof.dr. C.F. Schmidt
copromotor prof.dr. F.C. MacKintosh

Dit werk maakt deel uit van het onderzoekprogramma van de Stichting voor Fundamenteel Onderzoek der Materie (FOM), die financieel wordt gesteund door de Nederlandse Organisatie voor Wetenschappelijk Onderzoek (NWO).

To my mother Nabat,
and to the memory of my father, Ali

Contents

High-bandwidth microrheology of complex fluids and biopolymer networks

Maryam Atakhorrami

This thesis was reviewed by:

prof.dr. A.M. Dogterom
prof.dr. P. Janmey
prof.dr. P.D. Olmsted
dr. Rinke J. Wijngaarden
prof.dr. B.M. Mulder

High-bandwidth microrheology of complex fluids and biopolymer networks
Maryam Atakhorrami

Cover: Simon Tindemans

ISBN 90-6464-5-21-3

VRIJE UNIVERSITEIT

High-bandwidth microrheology of complex fluids and biopolymer networks

ACADEMISCH PROEFSCHRIFT

ter verkrijging van de graad Doctor aan
de Vrije Universiteit Amsterdam,
op gezag van de rector magnificus
prof. dr. T. Sminia,
in het openbaar te verdedigen
ten overstaan van de promotiecommissie
van de faculteit der Exacte Wetenschappen
op donderdag 16 februari 2006 om 13.45 uur
in de aula van de universiteit,
De Boelelaan 1105

door

Maryam Atakhorrami

geboren te Roodbar, Iran

promotor: prof.dr. C.F. Schmidt
copromotor prof.dr. F.C. MacKintosh

Dit werk maakt deel uit van het onderzoekprogramma van de Stichting voor Fundamenteel Onderzoek der Materie (FOM), die financieel wordt gesteund door de Nederlandse Organisatie voor Wetenschappelijk Onderzoek (NWO).

To my mother Nabat,
and to the memory of my father, Ali

Chapter 1

General introduction

The goal of this thesis is to develop and apply a method that can quantitatively probe the viscoelastic properties of biomaterials, and to acquire a better understanding of the microscopic origins of the complex dynamical properties underlying the rheology of cytoskeletal biopolymer networks on micrometer length scales. To do so, we develop a microrheology technique based on particle tracking with the use of optical tweezers and interferometry. We test these methods and apply them to Cytoskeletal actin solutions as a model system. This chapter aims to give a brief general introduction to this field. The outline of this chapter is following: first we give an introduction to rheology, and the essential definitions of linear viscoelastisity, following with the second section describing the microrheology experiments. In the third section we describe the experimental approach and we discuss the two model systems, namely worm-like micelle solutions and actin networks. Finally, we describe the outline of the thesis is described.

1. Rheology

Rheology is the science of the deformation and flow of all types of matter from gases to solids. The equations of rheology describe the interrelation between force fields, deformation fields and time. The word comes from the Greek "ρειν" meaning "to flow", and was first used by E. C. Bingham in 1929. The history of rheology, however, goes back to the Sumerian, Chinese, Egyptian and Greek peoples. The earliest known application of viscosity effects was in ancient Egypt at around 1500BC. Prince Amenemhet made for the king a "clepsydra", or a water clock. He noticed that water would flow more slowly or quickly through a small opening as a

result of the temperature changes. He made a 7 degree correction to the drainage angle of the water clock, to account for the viscosity change of water by temperature, which is significant between day and night in tropical climate [1]. At a later time, rheology appeared in the notebooks of Leonardo da Vinci and Galileo. In the seventeenth century Robert Hooke did a great deal of work on the elasticity of solids, and Isaac Newton, in his famous *Principia,* discusses the response of fluids to a steady shearing motion [2].

All materials have rheological properties, which means that they respond to mechanical force by deformation of various kinds. Purely viscous fluids dissipate all the dynamical energy through viscous flow (liquid-like), purely elastic materials store all the applied energy in fully reversible deformations (solid-like), and there is a large range of soft materials between the two extremes, which exhibit viscous as well as elastic properties and are therefore called viscoelastic. The viscoelastic properties are dependent on the time scale on which the response of the sample is probed, as well as on the magnitude of the applied stress [3,4]. Viscoelastic properties of materials originate from the microscopic response of their molecular components to the applied stress, implying that rheology can be used as a tool to acquire knowledge about the microscopic dynamics of soft materials.

Biological materials with all of their complexity and their active functions are a unique type of soft condensed matter. The mechanical properties of cells as the fundamental building blocks of living organisms are essential for many cell functions, such as cell crawling, division, and mechanosensing. Physicists have realized that cells have material properties that are distinct from materials made of common, flexible polymers. For instance, when cells are crawling, they change their rigidity by orders of magnitude. They can also become stiffer under applied stress to minimize deformation, in order to maintain their shape and functions. The mechanical response of cells is controlled by the cytoskeleton. The cytoskeleton is an elastic composite network of highly dynamic, structured and interconnected protein filaments and membranes. Cytoskeletal filaments are semiflexible, in other words, they have a persistence length that is much larger than their monomer size which sets them apart from common technical polymers. The wide range of length scales in

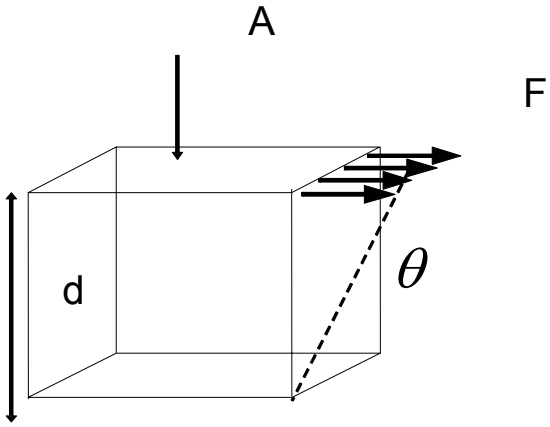

Figure 1: A cube of fluid, with a top area A and a height d has been subjected to a simple shear by applying force F resulting in a deformation of angle θ.

the cytoskeleton has as a consequence different regimes of mechanical response to applied stress. One of the other important features of the cytoskeleton is its non-equilibrium character which is due to the continuous polymerization of the filaments as well as the activity of motor proteins. Therefore the cytoskeleton serves as an active complex fluid that can respond to biochemical signals. To quantitatively describe these complexities has been challenging for physicists.

In any study of the viscoelastic behavior of materials, one wants to determine the relation between stress and strain under particular boundary conditions. For a linearly elasti system, this reduces to determining the time (or frequency) dependence of the elastic moduli or compliances corresponding to the type of chosen deformation. When the stress is sufficiently small, linear behavior is guaranteed. In the following I give a brief introduction to rheological measurements under simple shear.

Consider a cube of side d and area A, under a simple shear by a force F, as shown in Fig 1. A shear stress $\sigma = F / A$ is applied; the shear strain γ is then the tangent of the angle of deformation θ, which, for a small deformation, is the same as the angle. The complex shear modulus then is $G = \sigma / \gamma$, with a real part G', and an

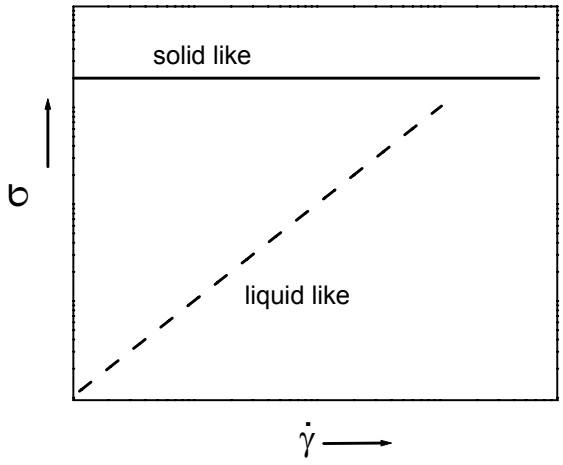

Figure 2: Illustration of stress dependence on shear rate, for solid-like and liquid-like materials.

imaginary part G''. This deformation represents a change in shape but not in the volume. The shear rate $\dot{\gamma}$ is defined as the relative speed of deformation of the top layer relative to the bottom layer $\dot{\gamma} = (v_{top} - v_{bottom})/d$, where v is velocity. In the extreme case of a purely elastic medium, the shear stress is independent of the shear rate, as illustrated in Fig 2. Indeed, in this case the medium responds to the applied force similar to a Hookean spring $F = -kx$ and G' plays the role of a spring constant. On the other hand, for a simple liquid the shear rate is related linearly to the applied stress by the fluid viscosity η, in the form of $\dot{\gamma} = \eta\sigma$. The behavior of most materials is dependent on the time scale on which the stress is applied. On very short time scales, the behavior is often viscoelastic, on intermediate time scales it can be predominantly elastic (solid-like), and as time increases one often sees, especially in amorphous materials, viscous (liquid-like) behavior.

Simple shear experiments are the most important type of deformation in the study of viscoelasticity, because they can be performed on solids and liquids alike. A classical way of measuring rheological properties is to measure the in-phase and out-of-phase material response to a small-amplitude oscillatory shear strain $\gamma = \gamma_0 \sin(\omega t)$. Here γ_0 is the amplitude of strain and $\omega = 2\pi f$ is the frequency of

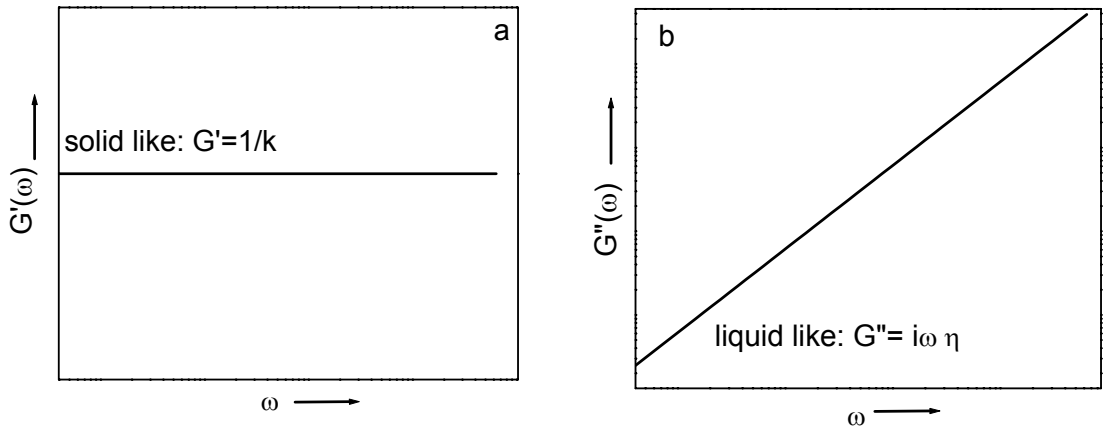

Figure 3: Illustration of shear modulus versus frequency ω, (a) for solid like and (b) liquid-like (here is water) materials. η is the viscosity (for water 0.969 mPas) and k is the Hookian spring constant.

oscillation. The periodic deformation provides information corresponding to a time scale $t = (2\pi/\omega)$. When the applied strain is small enough to not deform the sample beyond the range of the linear elastic response, in a homogeneous material, the affine deformation controls the time dependent stress response, $\sigma(t) = \gamma_0[G'(\omega)\sin(\omega t) + G''(\omega)\cos(\omega t)]$. $G'(\omega)$ is in phase with the strain and called elastic or storage modulus, and $G''(\omega)$ is out-of-phase with the strain and is called viscous or loss modulus. The complex shear modulus of viscoelastic materials is $G(\omega) = G'(\omega) + iG''(\omega)$. When the ratio of $G''/G' >> 1$, materials are liquid-like, and when $G''/G' << 1$ materials are solid-like. For a simple liquid, the loss modulus $G''(\omega)$ increases linearly with frequency with the slope of the viscosity η while the loss modulus is zero, and for a solid-like medium, the elastic modulus $G'(\omega)$ is frequency independent as is shown in Fig 3. In viscoelastic fluids the form of the frequency dependence of the shear modulus is related to stress relaxation mechanisms of the medium. In general, the compressional modulus is not relevant for soft networks embedded in nearly incompressible fluids at high frequencies.

Various geometries like concentric cylinders, cone-and-plate and parallel plates are used in commercial instruments to probe rheological properties of complex fluids such as suspensions, polymer solutions, gels, emulsions, and

surfactant mixtures [3,4]. Commercial rheometers typically require milliliter volume samples and can probe frequencies up to tens of Hertz. The high end of the frequency range is set by inertial effects [3,4]. For this reason the conventional rheometers can probe dynamics associated with large length scales and typically collective relaxations of the systems. Moreover, the conventional measurements are averaged measures over bulk sample volumes, and do not give any information about the heterogeneities of the samples.

2. Microrheology

Many complex soft materials including biological samples, are difficult to obtain in large volumes, and exhibit complex length-scale dependent dynamics. This requires new methods to probe small volumes and extend the probe frequency range. These methods, which locally deform a sample on the length scales of microns and measure the time-dependent response of the fluid to these deformations, are collectively called microrheology. With these methods we can probe the phenomena involved in the storage and dissipation of mechanical energy in microliter volumes and on micrometer or sub-micrometer length scales [5,6,7,8]. Different methods have been developed and can be divided into the broad classes of particle tracking, diffusing wave spectroscopy (DWS) and Atomic/Scanning force microscopy (A/SFM) [7,8]. Each of these methods covers a part of the desired frequency window between 10^{-2} and 10^{6} Hz, and shear moduli window between 10^{-5} to 10^{6} Pa. Typically measurements are done using micron-sized probes. The probes can be actively manipulated, using an external force (optical, magnetic, etc.)[9,10-12], or monitoring their passive Brownian motion in thermal equilibrium [13-23]. Passive methods are based on tracking the probes' motion using video microscopy [17,24,22] or laser tracking [5,14,15,23,25-28]. These techniques are uniquely useful for measuring soft materials.

2.1 Physical background of passive microrheology

In passive microrheology, the Brownian motion of colloidal particles is used to obtain the viscoelastic response of the medium to their motion. The Brownian

motion is the result of random kicks of the solvent molecules against the particles in the fluid in thermal equilibrium. In a purely viscous fluid the mean square displacement of a particle is directly proportional to time in the *x* direction, with a proportionality constant *D*, which is known as the diffusion constant for translational motion. In general, the relation $<\Delta x^2>=2Dt^{\beta}$ holds, where $0<\beta<1$, $\beta = 1$ represents a purely viscous fluid, and $\beta = 0$ for an elastic medium. This exponent is of key relevance in microrheological measurements which determines the relative viscous and elastic contribution to the shear modulus.

The diffusion coefficient *D* is related to the frictional coefficient of the particle. This friction coefficient for a spherical particle with radius *R* in a viscous fluid with viscosity η is the well known Stokes friction $6\pi R\eta$, and the relation to the diffusion coefficient, the Stokes-Einstein relationship $D=(k_BT/6\pi R\eta)$ is one manifestation of the fluctuation-dissipation theorem of statistical physics.

2.2 Shear modulus from complex response function

In passive microrheology no active stress is applied, so, irrespective of the amplitude of the thermal motions, by definition, linear response parameters are measured. Equations can nevertheless be written as if there was a small external force. The response of a probe particle to a small oscillatory force $f(\omega)$ is: $x(\omega)=\alpha(\omega)\times f(\omega)$ with the complex response function: $\alpha(\omega)=\alpha'(\omega)+i\alpha''(\omega)$. The real part $\alpha'(\omega)$ is the in-phase response and $\alpha''(\omega)$ is the out-of-phase response. The fluctuation-dissipation theorem relates the imaginary part of the response function to the power spectral density of the position fluctuations via $<|\Delta x(\omega)|^2>=(2k_BT/\omega)\alpha''(\omega)$ [29]. The real component $\alpha'(\omega)$, which is not directly measured can then be computed from $\alpha''(\omega)$ (if that is known for a large enough range of frequencies) through a Kramers-Kronig integral [30]:

$$\alpha'(\omega)=\frac{2}{\pi}P\int_0^{\infty}\frac{\varsigma\alpha''(\omega)}{\varsigma^2-\omega^2}=\frac{2}{\pi}\int_0^{\infty}\cos(t\omega)\int_0^{\infty}d\varsigma\alpha''(\varsigma)\sin(t\varsigma) \qquad (1)$$

where P is a principal-value integral [25,5]. The complex response function $\alpha(\omega)$ is related to the complex shear modulus via the generalized Stokes Einstein relation $G(\omega)=1/6\pi R\alpha(\omega)$ [5], and thus one can obtain the complex shear modulus $G(\omega)=G'(\omega)+iG''(\omega)$.

2.3 One- and two-particle microrheology

Microrheology is still a developing technique, which requires further investigation into its capabilities and limitations. One of the obvious questions is: how does microrheology compare with conventional macroscopic bulk rheology? An attempt to answer this question necessitates to consider the importance of the length scales probed with microrheology as compared with other macroscopic rheology techniques.

The formalism discussed above is based on tracing the motion of individual particles in the sample, so it is called one-particle microrheology (1PMR). Based on measurements with actin polymers, Crocker *et al* [17] suggested that 1PMR does not measure bulk rheology. They proposed that the inter-particle response functions, which are computed from the cross-correlated motions of two particles, can be used instead. This method is now known as two-particle microrheology (2PMR). Later Levine and Lubensky [32] showed that cross-correlated motion of particles can probe longer length scales and that the result is independent of the particle size, shape and local interactions. Therefore 2PMR should measure the macroscopic shear modulus [17,20,22].

The principle of two-particle microrheology is similar to that of one-particle microrheology, the only difference being that one calculates the inter-particle response function from the cross-correlated motions of a pair of particles, parallel to their center-line $< \Delta x^1(\omega)\Delta x^2(\omega) >= (2k_BT/\omega)\alpha''_{\parallel}(\omega)$, and perpendicular to their center line $< \Delta y^1(\omega)\Delta y^2(\omega) >= (2k_BT/\omega)\alpha''_{\perp}(\omega)$, where the numbers 1 and 2 denotes the particle number. The real part of the inter-particle response function, $\alpha'_{\parallel,\perp}$, can be found from the respective Kramers-Kronig integral as described above. Here we assumed that particles are displaced along the *x* direction. The shear modulus then is calculated from the Oseen relation [33 32, ,34, 35] $G(\omega) = 1/4\pi r\alpha_{\parallel}(\omega) = 1/8\pi r\alpha_{\perp}(\omega)$, where *r* is the separation distance between two-particles and the medium is assumed to be incompressible. The assumption of incompressibility results in the real part of the ratio of the parallel to the perpendicular inter-particle (complex) response functions $\alpha_{\perp}/\alpha_{\parallel} = (3-4\sigma)/4(1-\sigma)$ to be equal to 0.5, where σ is the Poisson ratio which is 0.5 for a practically (for our purposes) incompressible material such as water. The ratio can, in turn, be used to measure compressibility of the medium that

the particles are imbedded in [32,34] for frequencies at which the fluid inertia can be neglected. The Poisson ratio σ in the above equation is bounded by $-1 \le \sigma \le 0.5$.

In the above formalism we have used the generalized Stokes Einstein relationship in obtaining the macroscopic viscoelastic modulus. For this to be valid, it is necessary that the medium around the particles can be treated as a continuum viscoelastic medium. This requires that the size of the probe particles (in 1PMR) or the distance between two particles (in 2PMR) is larger than of the medium's internal length scales. For example in a polymer network, the particles should certainly be larger than the characteristic mesh size.

Recent theoretical studies [25,5,32,36] have shown that the generalized Stokes Einstein relationship describes the thermal response of a particle within a certain frequency range of $\omega_B \le \omega \le \omega^*$. The lower limit corresponds to frequencies where the longitudinal (or compressional) modes become significant compared to the shear modes that are excited in the system. A thermally driven particle is coupled to all the thermally excited modes of the system, including the longitudinal modes of the elastic network. At frequencies below ω_B the network compresses and the solvent drains from denser parts of the network. Above ω_B the elastic network is strongly coupled with the incompressible fluid, and longitudinal modes of the network are suppressed. In this regime the probe motion is entirely due to excited shear modes [5]. The crossover frequency can be determined from balancing local viscous and elastic forces, and the viscous coupling will be dominant at $\omega_B \ge G'\xi^2/\eta R^2$, where ξ is the characteristic length scale of the elastic network with elastic modulus of G', η the viscosity of the medium and R the radius of the particle. This crossover frequency for soft materials with mesh size of one tenth of the particle size embedded in the medium with η = 1mPas and G' of 1Pa is expected to be about 10Hz.

The upper frequency limit of ω^* is due to the onset of fluid inertial effects. In the Stokes limit the response of the liquid to the motion of a particle is instantaneous everywhere and decays as 1/*r*. This picture neglects the time dependence introduced by fluid inertia which is relevant for length scales bigger than $\delta = \sqrt{\eta/\rho\omega^2}$. Here δ is the viscous penetration depth and ρ is the fluid density. Fluid inertia for a particle

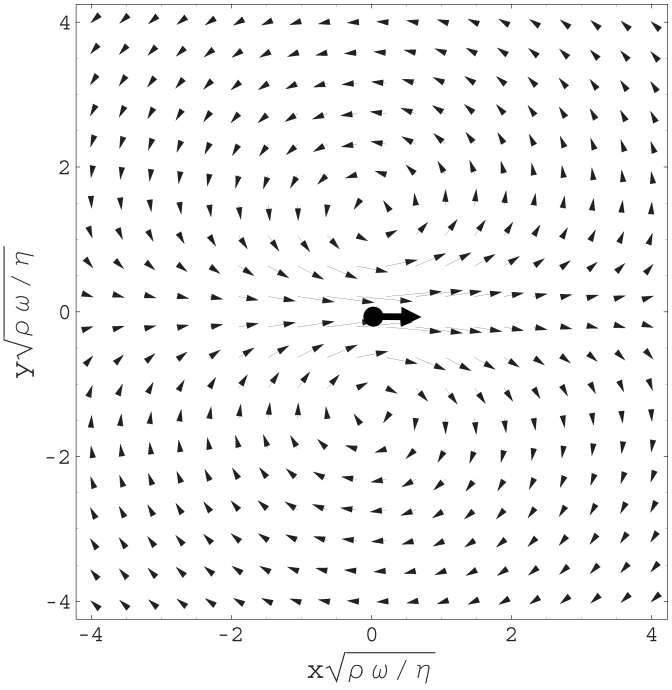

Figure 4: The displacement field around a point force applied to the origin (as shown by the filled circle and arrow) in simple liquid displays a clear vortex-like structure. Here the projection of vortex is shown in (x-y) plane. Distances are shown in units of the penetration depth.

with 1μm dimension does not strongly affect the single particle displacement response function up to ~100 kHz, (as is shown in part IV of this thesis). However this point should be reexamined for the inter-particle response functions used to obtain 2PMR. The reason is that the important length scale in that method is the particle separation distance *r*. The physical concept underlying the inertial effect is the following. Any instantaneous disturbance of the fluid must be confined to a small region after a short interval of time because of fluid inertia. In an incompressible liquid, this enforces a back flow at short times (high frequency), which creates a vortex ring in three dimensions. The diffusive spreading of this vortex carries the momentum/stress into the fluid. In Fig. 4 the vortex-like structure of the displacement field caused by a point force applied to the origin in a simple liquid is shown. The figure shows a two-dimensional (*x-y* plane) projection of the vortex ring which propagates in three dimensions. For particle separations $r < \delta$, the

inter-particle response is not affected by fluid inertia, while for the larger distances $r > \delta$ the fluid inertia will modify the inter-particle response function. This concept, based on the solution of the Navier-Stokes equation, considering the time-dependent inertial response of simple liquids, has been derived by Oseen and is known since 1927 [35]. It has been indirectly observed as the "long-time tail" in scattering experiments [37- 40] but it has not been directly observed up to now. In part IV of this thesis we describe how we directly mapped this inertial-induced vortex pattern in simple and viscoelastic fluids by probing the distance-dependent fluctuation correlation of two particles in parallel to their centerline (x in Fig. 4) and perpendicular to that (y in Fig. 4).

In order to minimize the inertial effect in the shear moduli measured by 2PMR, we chose the particle separations to be less than 20μm and we used the parallel inter-particle response functions, which are less affected, to calculate the shear moduli. Nevertheless, for soft media, such as worm-like micelles, the effect could be seen (chapter 6). The inertia of the probe particles can be neglected up to MHz frequencies [36, 5].

3. Experimental approach

Biopolymer networks such as the actin networks in *vitro* were the main focus of this study. They exhibit a wide range of dynamics on various time and length scales. Therefore it is necessary to measure with large bandwidth to probe the different dynamics associated with the existing different length scales. This was our main motivation for developing a broadband one- and two-particle microrheology method. Other existing microrheology methods, based on video tracking of multiple particles are limited to a frequency range of ~0.01 to ~30 Hz [17, 20, 22]. At such low frequencies, the rheological properties of biopolymers are very sensitive to the sample preparations and experimental details. For instance, the low-frequency dependent rheological properties of actin networks which have been fairly intensively studied, are very sensitive to the length distribution of actin filaments and the remaining cross-linking proteins, all of which are typically different for different purification methods [16,41]. This has caused discrepancies between the

results from different groups and confusions in the interpretation of the experiments. Moreover, there is still a lack of a good theoretical model for low-frequency dynamics. Current models of semiflexible polymer networks are well established just at high frequencies, where the network response reflects single-filament response [25,42-44].

We have succeeded in building a high-bandwidth microrheometer with which we can measure up to 100kHz, using a pair of optical tweezers that trace the motion of a pair of Brownian colloidal particles using laser interferometry. We trap two spherical Brownian particles simultaneously and sample their displacements at a rate of 195kHz. Then the frequency dependent single- and inter-particle response functions are calculated and linear shear moduli are obtained. When constructing such a setup, some experimental considerations should be taken into account with regard to optical traps. The most important points are (i) when two traps are made from two perpendicular polarization of one wavelength laser, there is leakage of the signal due to cross-talk between the two orthogonal polarizations of the laser, (ii) the laser trapping potential has an effect on the measured single- and inter-particle response functions and the shear modulus, (iii) the quadrant photo diode needs to have high bandwidth sensitivity, (iv) sample heating can become a problem when highly focused lasers are used. In the part I of this thesis we study the first two points. The other two points, (iii) and (iv) have been studied in [45,46]. All the results presented in this thesis, were obtained with the methods explained in part I, and the reproducibility of the data was typically examined for different samples (minimum 3 samples) and probe particles (minimum 40 different particles in each sample) at various places in the samples.

Furthermore, for the first time, we have directly compared the shear moduli measured with microrheology with those measured with macrorheology (using a special piezo-rheometer) in a wide overlapping frequency range up to 10 kHz. This is a general test for the applicability of the technique. This macro-rheometer used here (Fig 5) was made of two glass plates mounted horizontally between two piezoelectric ceramics separated by 100μm. The bottom plate is sinusoidally oscillated with a vertical amplitude of about 1 nm. This movement squeezes the sample and causes mainly shear strain with some extensional flow in the very center

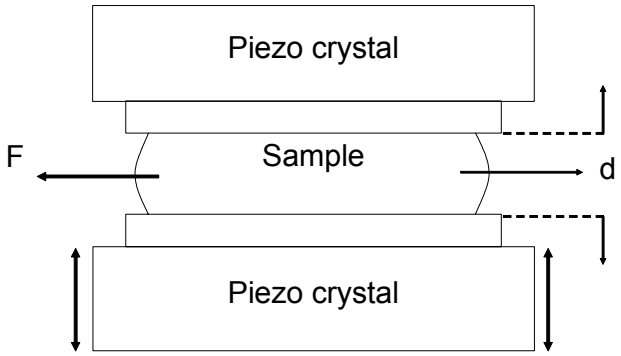

Figure 5: Sketch of the piezorheometer used to measure the macroscopic shear modulus.The sample is placed between two glass surfaces separated by a distance d (~50μm to 100μm). The lower plate moves sinusoidally with $\omega = 2\pi f$, and squeezes the sample between the two plates. The top plate with use of lock-in amplifier measures the induced pressure.

of the sample. The vertical stress transmitted to the upper plate is measured by the other piezoelectric element. A very small strain amplitude in the range of (10^{-6} to10^{-4}) is imposed to the sample so that the sample structure is not altered by the flow. In this setup the temperature can be controlled and to avoid evaporation, it is hermetically sealed. More detail of this setup can be found from [47, 48].

In the context of this thesis, we have studied two complex fluids. First, wormlike-micelle solutions and second entangled and crosslinked actin networks. In the following sections we give a general introduction to these two systems.

3.1 Wormlike Micelles

Micelles are self-assembled aggregates of surfactant molecules in a solvent. Surfactants are amphiphilic molecules with a hydrophilic head with (ionic or polar) groups and a hydrophobic tail (usually hydrocarbon chain(s)); therefore they are semi-soluble in both polar and non-polar solvents, but in both cases they self assemble in such a geometry that the solvent compatible parts are in contact with the

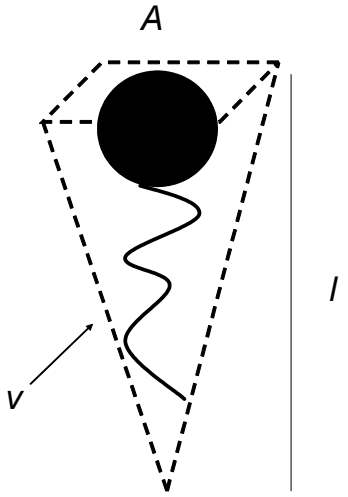

Figure 6: Diagram illustrated the packing parameter $P = v/lA$. A is the area occupied by the surfactant head group, l is the extended surfactant tail length, and v is the volume occupied by the tail.

solvent and the other parts are not. These assemblies are called micelles. Micelles are formed when the concentration of surfactant molecules is greater than the Critical Micelle Concentration (CMC) and the temperature is higher than a critical temperature (Krafft temperature) [3].

Micelles can exist in different shapes, including spherical and cylindrical. The shape is largely controlled largely by the molecular geometry of the surfactant, but also strongly influenced by the solution conditions (temperature, salt type and concentration, etc). The geometry of micelles is characterized by the packing parameter $P = v/Al$, where v is the volume and l is the extended length of the hydrophobic part of the surfactant. The parameter A is the surfactant area occupied by the head group as illustrated in Fig6. When P increases towards 1/2, the micelles form elongated tubes [49]. When the overall length (or contour length) of such tubes is larger than the persistence length (the length over which it is rigid) they become wormlike [49, 3]. At high enough concentration these wormlike micelles become entangle with each other, similar to long synthetic polymers [3]. There are two important differences between worm-like micelles and polymers, which are mainly the consequence of the self assembly process of micelle formation in contrast to

polymers that are typically made of chemically identical monomeric groups in linear chains. The differences are i) the length of flexible chains is broadly distributed and determined by thermodynamical equilibrium of the surfactant solution and ii) there is an additional crucial process for stress relaxation in addition to reptation of polymers along a confinement "tube", namely breaking and recombination of micelles [50-53].

The growth of wormlike micelles is a statistical process, so that they exist in a polydisperse distribution of lengths with nanometers in diameter, tens of nanometers persistence length and up to micrometers in length [51]. These length scales make worm-like micelles an excellent model system to examine the validity of our experimental one-and two-particle microrheology methods using micron-sized particles. Because the probe size is much bigger than the intrinsic length scales in solution, we do not expect any discrepancy between one- and two- particle microrheology. This is studied in chapters 4 and 6 .

3.2 Linear rheology of entangled wormlike micelle solutions

The dynamical behavior of womlike micelles is modeled based on the theory of polymer dynamics [54,51]. In this model the stress relaxation in an entangled classical polymer solution is described via a reptation mechanism in which the polymer chain diffuses along its contour path and by which the imposed stress is gradually completely relaxed [54]. On top of that, in worm like micelles or so-called living polymers the imposed stress can also relax by their ability to break and recombine. The kinetics of breakage and reconnection is dependent on the surfactant type and the salinity. In the dilute limit when the micelles are not interconnected, they break along their contour by forming end- caps. They also can reconnect end-to-end by elimination of end-caps. In addition, in a network, the network junctions can break and reconnect. Also, at low salt concentrations micelles can make branches. There is a characteristic time for breakage, τ_b, and for reconnection, τ_r. When τ_b or τ_r are much longer than the reptation time τ_{rep}, then the stress relaxation is dominated by the reptation process and the system behaves like a "dead" polymer solution. However, when the breakage/recombination time is much

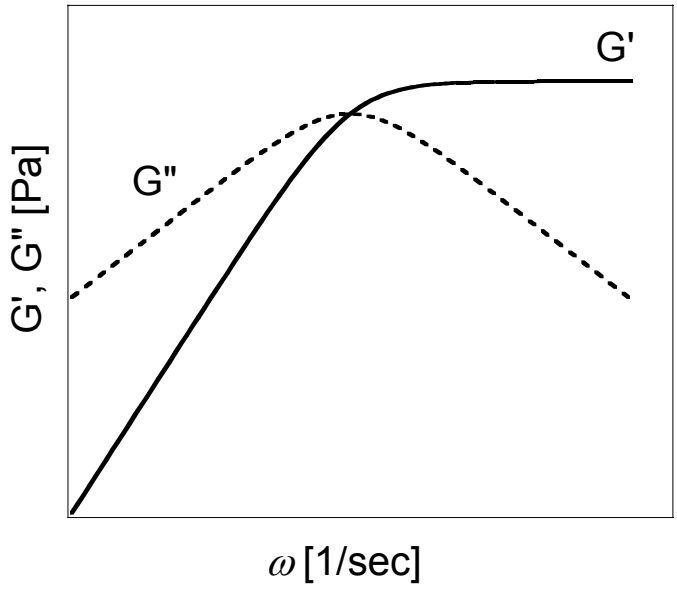

Figure 7: Illustration of the storage modulus *G′* and loss modulus *G″* for a Maxwell fluid plotted as a function of ω.

shorter than the reptation time, the stress relaxation process leads to a monoexponential or Maxwellian stress relaxation.

The Maxwell model for viscoelastic medium is described by a spring (elastic element) and dashpot (viscous element) connected in series [4]. The spring creates the elastic plateau in the shear modulus G_0 and the dashpot the viscosity η. In a Maxwell fluid, the imposed stress relaxes as $G = G_0 \exp(-t/\tau)$ with $\tau = \eta/\dot{\gamma}$, where $\dot{\gamma}$ is the shear rate. The Maxwell behavior under harmonic oscillation (in frequency representation) is obtained as:

$$G'(\omega) = \frac{G_0 \omega^2 \tau^2}{(1+\omega^2\tau^2)} \text{ and } G''(\omega) = \frac{G_0 \omega \tau}{(1+\omega^2\tau^2)} \quad (2)$$

In these equations it is evident that when $\omega\tau >> 1$, G' approaches a constant plateau, under this condition the medium behaves as an elastic body. At low frequencies when $\omega\tau << 1$, $G' \sim \omega^2$ and $G'' \sim \omega$, and the medium behaves as a simple liquid. The crossover time corresponding between these regions, is in the case of worm-like micelles, related to the breakage and recombination times $\tau = (\tau_b \tau_r)^{1/2}$ and known as

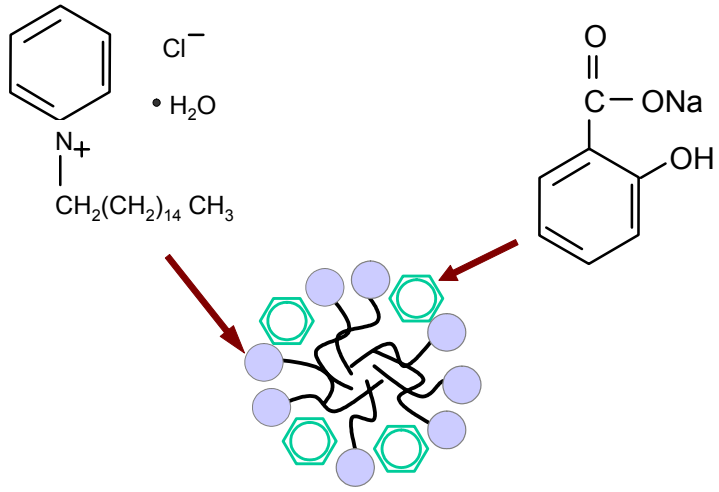

Figure 8: Sketch of the molecular structure of the micelles that we used: cetylpyridinium chloride (CPyCl) as surfactant (circles) was diluted in brine (0.5M NaCl) and Sodium salicylate (NaSal) was used as binding counterions.

the terminal relaxation time [50, 51,55]. Long worm-like micelles break and reconnect rapidly, therefore in equilibrium typically $\tau_b \sim \tau_r$. Fig 7 illustrates the expected viscoelastic behavior of a Maxwell fluid.

In our experiments we used cetylpyridinium chloride (CPyCl) as surfactant diluted in brine (0.5M NaCl). Sodium salicylate (NaSal) was used as a strongly binding counterion. The molar ratio was kept at Sal/Cpy = 0.5. A schematic representation is given in Fig.8. The Kraft temperature for this system is ~19°C, which is below 21°C, the stabilized room temperature in our laboratory. This system has been studied well and is known to have Maxwellian behavior [55], and in the concentration range of this study (0.5wt% to 8wt%) it forms entangled worm-like micelles.

The main purpose of our experiments with micelles was to validate the experimental method, and to establish the validity of one- and two-particle microrheology in a system with internal length scales much smaller than the probe

size. Further, for the first time, the shear moduli measured with microrheology are directly compared with those measured by macrorheology (using a special piezo-rheometer) in a wide overlapping frequency range up to 10 kHz. Part II of this thesis focuses on worm-like micelles and high-frequency rheology of different micelle concentrations.

In a more complex system, such as entangled actin networks, in which the length scales such as the persistence length and the filament length, are larger than micron, we expect to see a difference in the results between one-and two-particle microrheology. In these systems we used the differences between both methods to learn about the local dynamics as well as the macroscopic shear modulus. In the next section we give general introduction to actin.

3.3 Cytoskeletal actin filaments

The cytoskeleton of most eukaryotic cells consists of a network of protein filaments. There are three principal types of filaments: (i) microtubules: are stiff tube-like structures with an outer diameter of ~25nm and inner diameter of ~18nm. They determine the position of the membrane and direct the intracellular transport. (ii) Intermediate filaments: are rope-like structures composed of several inter-wined proteins with a final diameter of ~10nm, which provide mechanical strength and resistance to shear stress. (iii) Actin filaments: are cable-like structures that are the thinnest of all, with a diameter of ~7nm. Actin filaments are mainly located in the cell cortex [56, 57], determine the shape of the cell surface and are essential for whole cell locomotion. Regulation of the structure and interaction of these three basic filaments, in cooperation with a large number of accessory proteins provides the cell with a wide range of activities and structures which are essential for living organisms. One of the large challenges in biophysics is to understand the dynamic properties of the cell cytoskeleton. We are approaching the problem using a bottom-up approach, in which we first look at the network of purified proteins *in vitro* as a well-controlled model system. In this thesis we study the mechanical properties of actin networks in the form of entangled and cross linked network in *vitro*.

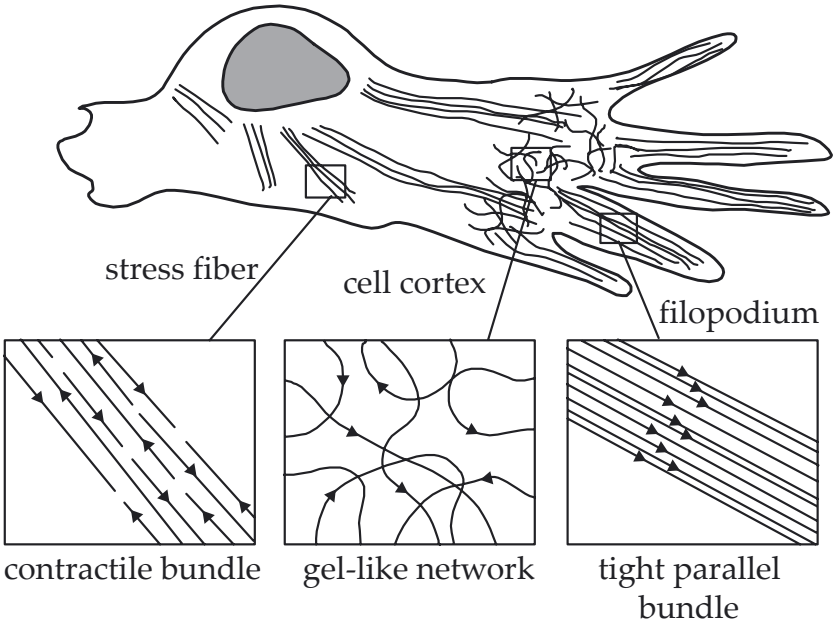

Figure 9: A crawling cell, indicating three areas with different arrangements of actin filaments with arrows pointing towards the actin plus ends. Stress fibers are contractile and exert tension. Filopodia are spike-like projections of the plasma membrane that allow the cell to explore its environment, and the cortex is underlying the plasma membrane. Varying the rheology of cytoskletal actin in different regions is crucial for cell locomotation. (figure is adapted from *Molecular Biology of the Cell* [56])

In cells, actin filaments form many types of cell-surface protrusions [56]. Some of these are dynamic structures, such as lamellipodia and filopodia that cells use to explore territory and pull themselves around. Others are stable structures such as the regular bundles of stereocilia on the surface of hair cells in the inner ear, which tilt as rigid rods in response to sound. In animal cells actin filaments are organized into two types of arrays: bundles and web-like (gel-like) structures. These form with the help of actin binding proteins. In Fig. 9 a schematic of a crawling cells with different arrangements of actin filaments is shown.

Filamentous actin (F-actin) is assembled as a right handed helix of uniformly oriented actin monomers (G-actin) with a period of 37nm (Fig 10). The process of

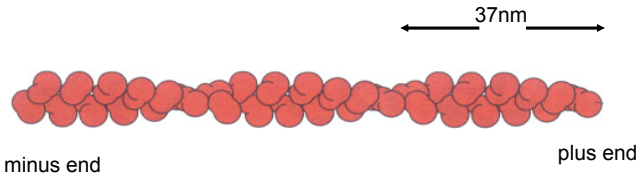

Figure 10: The structure of an actin filament. Actin filament is made of actin monomer. Actin monomer (G actin) having a abinding site for ATP or ADP in the middle. One filamnet consists of two protofilaments, held together by lateral contacts, winding around each other as two parallel strands of a helix repeating in each 37nm [56].

actin polymerization starts with the assembly of three G-actin monomers into a trimer in the presence of K^+ and Mg^{2+}. This trimer provides the nucleus for polymerization, from which the protein assembles into a helical polymer by addition of monomers to the exposed end of the growing filament. There are two ends for growing filament: a plus end which is the fast-growing end and a minus-end, which is the slow growing end. For this process ATP hydrolysis by actin itself is essential.

Actin was purified (by Karen Vermeulen) from rabbit skeletal muscle, following standard protocols [58] and diluted in G-buffer. For each experiment, frozen G-actin was thawed and mixed with 1/10 volume of 10 times concentrated F-buffer and left to polymerize for a minimum of 1 hour. As an example see in Fig. 11, showing fluorescently labeled F-actin filaments after 1.5 hour polymerization at room temperature. As can be seen from this typical example, actin filaments are strongly polydisperse.

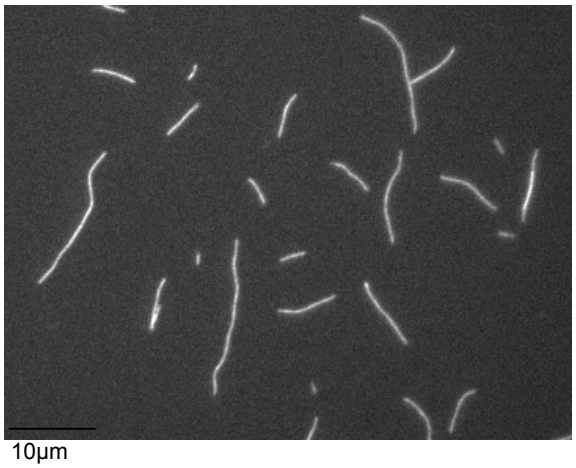

Figure 11: Fluorescently labeled F-actin after polymerization for 1.5 hour at room temperature.

3.4 Dynamic shear modulus of actin solutions

From a materials point of view F-actin is a model system for semiflexible polymer dynamics [59]. Most biopolymers are semiflexible, i.e. a polymer for which the aspect ratio of l_p/a is large, where l_p is the persistence length and a is the filament diameter. *In vitro* F-actin solutions exhibit a polydisperse distribution of lengths with a (difficult to determine) average length of L ~17 µm, l_p ~ 15-17 µm and a = 7 nm, yielding to an aspect ratio of ~2000. One of the distinct properties of semiflexible polymers is that they can make viscoelastic gels at very low concentrations, in the case of actin at a volume fraction of about $5x10^{-5}$, or about 50 µg/ml [60]. Also strikingly different from flexible polymers is that changing the cross-linker density at a constant concentration of polymers can change the low-frequency shear modulus by several orders of magnitude. At high frequencies, a characteristic frequency dependence of the complex shear modulus in the form of $G \sim \omega^{3/4}$ is observed for semiflexible polymers [5,25,42,44] which is in contrast to flexible polymers, with flexible polymers exhibiting $\omega^{1/2}$ to $\omega^{2/3}$ [61] high frequency scaling laws.

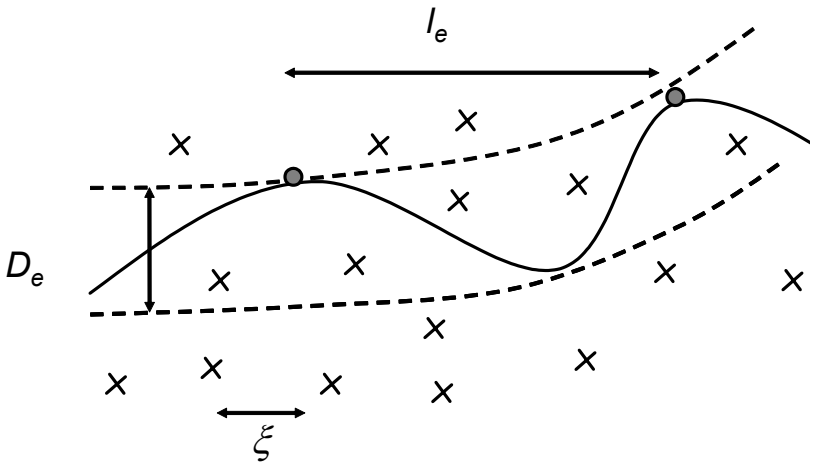

Figure 12: Illustration of the plane of a single filament (line) showing the intersection of out-of plane filaments (crosses). The mesh size ξ is the average distance between filaments. The polymer is constrained to a "tube" (broken lines) with diameter D_e.

Several theoretical models have been developed to explain the unique behavior of semiflexible polymer systems at high frequencies [42,44] and at low frequencies [43, 62, 63]. In the following a brief description of the physical picture is presented that we have used to model the high frequency rheology measurements.

In an entangled solution of F-actin the average distance between filaments, or mesh size (in micron), is related to the actin concentration as $\xi = 0.3/\sqrt{c_A}$ where cA is measured in mg/ml [64]. At low frequencies, the steric constraints of surrounding filaments, do not allow large-amplitude bending fluctuations, and the filament is effectively constrained to an effective tube with diameter of $D_e \sim l_e^{3/2} l_p^{-1/2}$ as shown in Fig. 12, where $l_e \sim \xi^{4/5} l_p^{1/5}$ is the distance between filaments entanglements [65]. The macroscopic shear modulus of a solution of actin filaments is determined by the mechanism used by the polymers to relax the imposed shear. Which mechanism is available depends on the probed frequency range. Filaments can relax the imposed deformation either by transversal diffusion in the tube or by reptation. In entangled

actin solutions with uncontrolled lengths the reptation time is of the order of $\tau_{rep} \sim L^3$ ~250s or more due to the large length of actin [43,65] which corresponds to very low frequencies. This frequency regime is followed by a plateau (in G') reflecting collective filament dynamics which are not very well understood, but which include the orientation and curvature dynamics of the confinement tubes [43,65].

For frequencies higher than the plateau in entangled (or crosslinked) solutions, that are accessible with our experimental technique (f >0.1Hz), we can understand the macroscopic shear modulus from single filament relaxation between two effective entanglement points, following the theoretical predictions of Gittes and Mackintosh [42] and Morse [44]. They assumed that a semiflexible polymer network is an isotropic, random array of long extended chains that are subject to constraints on the scale of an effective entanglement length le (or similarly the distance between cross-linking points in the cross-linked network), which is typically smaller than the persistence length *lp*. The applied distortions of the network at high frequencies are affine and shear strain implies extension or compression in the fluctuating segments dependent on their orientation with respect to the shear direction. The longitudinal relaxation of the chain conformation through the viscous solvent, which is a balance between stress in solution and tension in the filaments, will result in a specific frequency (time) dependence of the shear modulus of the form $G(\omega) \sim 1/15(\rho\kappa l_p(-2i\zeta/\kappa)^{3/4}\omega^{3/4}) - i\omega\eta$, where $\kappa = l_p k_B T$ is the bending energy in the absence of tension, ρ is the spatial filament density, ζ ~0.0023Ns/m2 [42] is the lateral drag coefficient and $i\omega\eta$ is the solvent contribution. This relation shows that at high frequencies the shear modulus does not depend on the contour length or entanglement length and that each filament contributes independently to the total shear modulus trough its thermal bending fluctuations. This relation provides a quantitative prediction for the high frequency shear modulus of an actin solution $G(\omega) \sim 1.6Pa(c/mgml^{-1})(\omega/2\pi)^{3/4} i^{3/4}$. Using our high-frequency two-particle microrheology method we could show for the first time direct experimental proof for this prediction (chapter 7). This single filament model can explain the frequency dependence of the modulus of the crosslinked actin solutions and the high-frequency properties of entangled actin solutions.

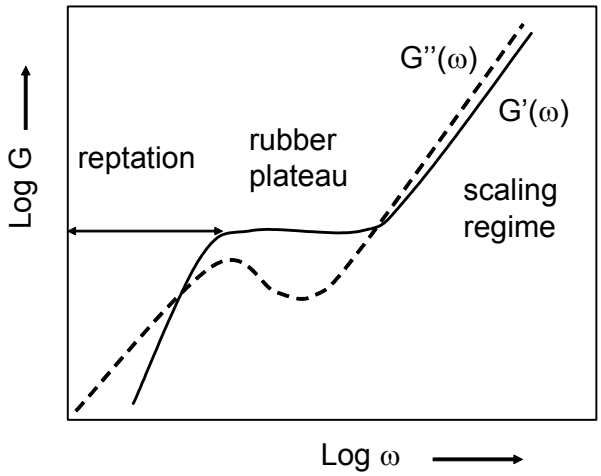

Figure 13: Simplified illustration of the complex shear modulus G′ (line) and G″ (broken line) versus frequency $\omega = 2 \pi f$, predicted for semiflexible polymer solutions [42,43].

However the model does not predict the behavior of the shear modulus at frequencies intermediate between the plateau regime and the high-frequency regime in entangled actin solutions which we explore in chapter 7. A schematic representation of the expected frequency dependence of the shear modulus, (*G′* and *G″*) for a semiflexible polymer network is shown in Fig. 13.

The microrheology methods discussed in this thesis have also been used to study a number of other systems: (i) solutions of mono disperse fd virus, as a model system for short monodisperse semi-flexible polymers, and (ii) solutions of hyaluronic acid, a highly charged polymer occurring in many biological tissues such as joint fluid or cartilage. Although the microrheology experiments were initially motivated by the need to study biomaterials in small volumes, they can also open a new window for the understanding of the microscopic dynamics of complex fluids such as colloidal systems. We have used active and passive microrheology in aging colloidal systems, in order to answer the question wether the fluctuation-dissipation

theorem can be used in an aging (non equilibrium) system and what the high frequency dynamics are that are involved in the rheology changes in aging colloidal systems. These studies are not included in this thesis because my involvement was not central, but can be found in the following references [66-69].

1.4 Outline of this thesis

This thesis is consist of a bundle collection of published or (to be) submitted papers and is organized in four parts:

Part I consists of two chapters which explain the experimental methods as well as the data evaluation methods used throughout the thesis to measure one- and two- particle microrheology using optical tweezers. Chapter 2 describes the experimental setup. We use two lasers of different wavelengths for optically trapping probe particles and for measuring their motions. In chapter 3 we present an extensive study of the thermal motions of one and two particles in the presence of optical traps. We present a method to account for the trapping potentials in order to obtain the medium rheological properties in simple Newtonian fluids, water, and in viscoelastic solutions of filamentous fd virus.

Part II comprises three chapters, in which high-bandwidth microrheology and macrorheology of wormlike micelle solutions are compared. In chapter 4 we show a comparison of one- and two-particle microrheology with macrorheology results over a large range of frequencies for four samples, followed by chapter 5 in which we examine a larger concentration of wormlike micelles with one-particle microrheology and macrorheology. Here the focus is more on the high frequency rheological properties of wormlike micelle solutions. In chapter 6 we compare one- and two-particle microrheology with a greater focus on two-particle microrheology measurements.

Part III comprises two chapters, in which semiflexible actin networks are studied. In chapter 7 we present the results of two-particle microrheology of entangled and cross-linked actin solutions as a model system for semiflexible polymer solutions. In this chapter a quantitative study of the rheology of actin solutions at high frequencies is presented. Also the dynamics of semiflexible

polymer solutions at intermediate frequencies is discussed. In chapter 8 we probe the local dynamics with one-particle microrheology using different particle sizes. We first compare two-particle microrheology with bulk rheology, and then the one-particle microrheology with bulk rheology to reveal the interactions of particles with their local environments. The discrepancies are mainly due to non-continuum elastic deformation of the network around the small probe particles.

Part IV contains two chapters, in which the high-frequency inertial response of fluids, in viscous and viscoelastic media is measured up to 100kHz. For the viscous solutions we used water and water/glycerol, and for the viscoelastic solutions we used actin and wormlike micelle solutions. In chapter 9, we use the cross-correlated response function of two Brownian particles to map out the flow pattern in the medium. Inertially induced vortex propagation is observed in the medium. In chapter 10, we use actively driven particles to measure the inertial effect in the complex response function in water and in actin solutions. We also investigate the effect of different particle sizes.

1.5 References

[1] G. W. Scott Blair, *A Survey of General and Applid Rheology* (Sir Isaas Pitman&Sons, London, 1949).

[2] D. Doraiswamy, DuPont iTechnologies.

[3] R. G. Larson, *The structure and rheology of complex fluids* (Oxford University Press, Oxford, 1998).

[4] J. D. Ferry, *Viscoelastic properties of polymers* (Wiley, New York, 1980).

[5] B. Schnurr, F. Gittes, F. C. MacKintosh, et al., Macromolecules **30**, 7781 (1997).

[6] F. C. MacKintosh and C. F. Schmidt, Curr. Opin. Colloid Interf. Sci. **4**, 300 (1999).

[7] T. A. Waigh, Rep. Prog. Phys. **68**, 685 (2005).

[8] M. L. Gardel, M. T. Valentine, and D. A. Weitz, in *Microscale diagnostic techniques*, edited by K. Breuer (Springer Verlag, 2005).

[9] F. Amblard, B. Yurke, A. Pargellis, et al., Review of Scientific Instruments **67**, 818 (1996).

[10] B. Fabry, G. N. Maksym, J. P. Butler, et al., Phys. Rev. Lett. **87**, 148102 (2001).

[11] M. Keller, J. Schilling, and E. Sackmann, Rev. Sci. Instrum. **72**, 3626 (2001).

[12] X. Trepat, M. Grabulosa, L. Buscemi, et al., Rev. Sci. Instrum. **74**, 4012 (2003).

[13] T. G. Mason and D. A. Weitz, Phys. Rev. Lett. **75**, 2770 (1995).

[14] T. G. Mason, K. Ganesan, J. H. v. Zanten, et al., Phys. Rev. Lett. **79**, 3282 (1997).

[15] D. J. Pine, D. A. Weitz, P. M. Chaikin, et al., Phys. Rev. Lett. **60**, 1134 (1988).

[16] Jingyuan Xu, William H. Schwarz, Josef A. Käs, et al., Biophys J, **74,**, 2731 (1998).

[17] J. C. Crocker, M. T. Valentine, E. R. Weeks, et al., Phys. Rev. Lett. **85**, 888 (2000).

[18] T. G. Mason, Rheologica Acta **39**, 371 (2000).

[19] A. W. C. Lau, B. D. Hoffman, A. Davies, et al., Phys. Rev. Lett., 198101 (2003).

[20] D. T. Chen, E. R. Weeks, J. C. Crocker, et al., Phys. Rev. Lett. **90,**108301 (2003).

[21] L. Starrs and P. Bartlett, Faraday Discussions **123**, 323 (2003).

[22] M. L. Gardel, M. T. Valentine, J. C. Crocker, et al., Phys. Rev. Lett. **91**, 158302 (2003).

[23] K. M. Addas, C. F. Schmidt, and J. X. Tang, Phys. Rev. E **70**, 021503 (2004).

[24] A. W. C. Lau, B. D. Hoffman, A. Davies, et al., Phys. Rev. Lett. **91** (2003).

[25] F. Gittes, B. Schnurr, P. D. Olmsted, et al., Phys. Rev. Lett. **79**, 3286 (1997).

[26] J. Xu, A. Palmer, and D. Wirtz, Macromolecules **31**, 6486 (1998).

[27] J. Xu, V. Viasnoff, and D. Wirtz, Rheol. Acta **37**, 387 (1998).

[28] L. Starrs and P. Bartlett, Journal of Physics-Condensed Matter **15**, S251 (2003).

[29] L. D. Landau, E. M. Lifshitz, and L. P. Pitaevskii, *Statistical Physics* (Pergamon Press, Oxford, New York, 1980).

[30] P. M. Chaikin and T. C. Lubensky, *Principles of Condensed Matter Physics* (Cambridge University Press, Cambridge, New York, 1995).

[31] F. Gittes, B. Schnurr, W. Moehler, et al., Biophysical Journal **74**, A361 (1998).

[32] A. J. Levine and T. C. Lubensky, Phys. Rev. Lett. **85**, 1774 (2000).

[33] LD Landau and EM Lifshitz *Fluid Mechanics*. (Oxford, Butterworth-Heinemann, 2000).
[34] A. J. Levine and T. C. Lubensky, Phys. Review E **65** (2002).
[35] C.W.Oseen, *Neuere Methoden und ergebnisse in der hydrodynamik*, Leipzig, (1927).
[36] A. J. Levine and T. C. Lubensky, Phys. Rev. E **6304** (2001).
[37] B. J. Alder and T. E. Wainwright, Phys. Rev. A **1**, 18 (1970).
[38] B.J. Alder and T.E. Wainwright, Phys. Rev. Lett. **18**, 988 (1967).
[39] G.L. Paul and P. N.Pusey, Journal of Physics A **14**, 3301 (1981).
[40] D. A. Weitz, D. J. Pine, P. N. Pusey, et al., Phys. Rev. Lett. **63**, 1747 (1989).
[41] Jingyuan Xu, James F, Casella, et al., Cell Motility and the Cytoskeleton **42**, 73–81 (1999).
[42] F. Gittes and F. C. MacKintosh, Phys. Rev. E **58**, R1241 (1998).
[43] D. C. Morse, Macromolecules **31**, 7044 (1998).
[44] D. C. Morse, Phys. Rev. E **58**, R1237 (1998).
[45] E. J. G. Peterman, F. Gittes, and C. F. Schmidt, Biophysical Journal **84**, 1308 (2003).
[46] E. J. G. Peterman, M. A. van Dijk, L. C. Kapitein, et al., Review of Scientific Instruments **74**, 3246 (2003).
[47] P. Hebraud, F. Lequeux, and and J.F. Palierne, Langmuir **16**, 8296 (2000).
[48] D. Constantin, J. F. Palierne, E. Freyssingeas, et al., Europhys. Lett. **58**, 236 (2002).
[49] L. M. Walker, Current Opin. Colloid Interf. Sci. **6**, 451 (2001).
[50] M. Cates, macromoleculs **20**, 2289 (1987).
[51] M. E. Cates and S. J. Candau, Journal of Physics-Condensed Matter **2**, 6869 (1990).
[52] R. Granek and M. E. Cates, Journal of Chemical Physics **96**, 4758 (1992).
[53] J. F. Berret, J. Appell, and G. Porte, Langmuir **9**, 2851 (1993).
[54] M. Doi and S. F. Edwards, *The Theory of Polymer Dynamics* (Clarendon Press, Oxford, 1988).
[55] H. Rehage and H. Hoffmann, Journal of Physical Chemistry **92**, 4712 (1988).
[56] B. Alberts, A. Johnson, J. Lewis, et al., *Molecular Biology of the Cell* (Garland Publishing, Inc., New York&London, 2002).
[57] J. Howard, *Mechanics of motor proteins and the cytoskeleton* (Sinauer Associates, Sunderland, 2001).
[58] J. D. Pardee and J. A. Spudich, in *Structural and Contractile Proteins (PartB: The Contractile Apparatus and the Cytoskeleton)*, edited by D. W. Frederiksen and L. W. Cunningham (Academic Press, Inc., San Diego, 1982), Vol. 85, p. 164.
[59] F. C. MacKintosh and P. A. Janmey, Curr. Opinion in Solid State and Mater. Sci. **2**, 350 (1997).
[60] F. C. MacKintosh, J. Käs, and P. A. Janmey, Phys. Rev. Lett. **75**, 4425 (1995).
[61] M. Doi and S. Edwards, *The Theory of Polymer Dynamics* (Oxford Science Publications, Oxford, 1986).
[62] A. C. Maggs, Phys. Rev. E **57**, 2091 (1998).

[63] H. Isambert and A. C. Maggs, Macromolecules **29**, 1036 (1996).
[64] C. F. Schmidt, M. Baermann, G. Isenberg, et al., Macromolecules **22**, 3638 (1989).
[65] D. C. Morse, Macromolecules **31**, 7030 (1998).
[66] Fatima Bouchama, Maryam Atakhorrami, Christoph F. Schmidt, et al., (in Preparation).
[67] S. Jabbari-Farouji, D. Mizuno, M. Athakhorrami, et al., (submitted to Phys.Rev.lett).
[68] S. Jabbari-Farouji, M. Athakhorrami, D. Mizuno, et al., (in Preparation).
[69] S. Jabbari-Farouji, D. Mizuno, M. Athakhorrami, et al., (in Preparation).

One- and Two-Particle Microrheology with Optical Tweezers

This part is based on the following papers:

M. Atakhorrami, K.M. Addas and C.F. Schmidt," Twin optical traps for two-particle cross-correlation measurements: eliminating cross-talk" (manuscript in preparation), (Chapter 2)

M. Atakhorrami, J. Kwiecinska, K.M. Addas, G.H. Koenderink, J.X. Tang, A.J. Levine, F.C. MacKintosh and C.F. Schmidt, "Correlated fluctuations of microparticles in viscoelastic solutions: quantitative measurement of material properties by microrheology in the presence of optical traps" (submitted Physical Review E), (Chapter 3)

Chapter 2

Twin optical traps for two-particle cross-correlation measurements: eliminating cross-talk

Abstract

Correlated motions of two micron-sized particles can be conveniently detected using two optical traps with interferometric displacement detection. When the correlations become small, the elimination of crosstalk between the two beams becomes important. We have used dual optical traps created by either two orthogonally polarized laser beams derived from one laser source, or by two independent lasers of different wavelengths. High NA lenses (objective and condenser) in the optical path introduce depolarization, and thereby lead to optical cross-talk. We have characterized the cross-talk in this case and demonstrate that the use of two independent laser eliminates cross-talk entirely.

2.1 Introduction

A tightly focused laser beam can trap a dielectric object in a three dimensional "potential well", if the size of the object is on the order of the laser wavelength. Laser-based optical trapping was first introduced by Art Ashkin [1] and is now used in a large range of applications from atomic physics to medicine. Optical traps (or optical tweezers) are usually built into a light microscope with a high-numerical-aperture (NA) objective. Trapping forces range from 200 pN to sub-pN on a micron sized objects, and the displacement of the trapped particle can be measured with sub-nanometer precisions by laser interferometry [2,3,4].

High-precision position detection by lasers with and without optical trapping is, among many other applications, used to study the mechanical properties of motor proteins [5,6,7], of single biopolymers [8, 9] or to measure the viscoelastic properties of complex fluids in microliter volumes and with high bandwidth in so-called microrheology techniques [10,11]. Passive microrheology, is one of the commonly used methods, based on particle tracking. The motions are tracked by laser interferometry and auto- or cross-correlations of position fluctuations of one (one-particle microrheology) or two (two-particle microrheology) colloidal particle(s) are calculated. Viscoelastic properties, i.e. shear elastic moduli, are then derived from the single- particle or inter-particle response functions, which are related to the position fluctuations via the fluctuation-dissipation theorem [12-16].

A number of experiments such as measuring hydrodynamic correlations in fluids or gels [17,15,18], or different assays in molecular motor experiments [5,6,7] and also two-particle microrheology experiments [17,19-22], are performed using a pair of optical traps, which hold a pair of colloidal particles at a well-defined distance. The position fluctuations of both particles are detected simultaneously using quadrant photo diodes (QPD) [4,23,24]. Two optical traps are commonly created using one linearly polarized laser beam, which is split into two orthogonally polarized and independently steered beams using a polarizing beam splitter [13,23,25,26]. Typically the laser creating the traps is also used in combination with QPDs for position detection.

Using polarization to split a single beam into two, creates a cross-talk problem when very weak cross correlations need to be detected (as is typically the case in 2-particle microrheology). Polarized light is partially depolarized when passing trough a highly curved surface as a collimated beam or through a flat surface as a divergent of convergent beam [27, 28]. When optical traps are generated by high-NA lenses, a portion of light will thus be depolarized both at the internal lens surfaces and at the cover slip surfaces. The measured depolarization of the electric field in a high aperture objective lens (NA= 1.4, oil immersion) can be substantial, up to 10 percent of the integrated focal intensity [29,30]. The depolarization introduces cross talk in the position (force) detection when the same laser light is used for trapping and detection. Cross-correlated position functions are a measure of the "real" correlation between a pair of trapped objects; if there is any cross-talk, an extra correlation introduces to the results, which is an artifact.

We have used a dual trap optical tweezers made with a 1064nm wavelength laser (4W, cw) to perform one- and two-particle microrheology with 195kHz sampling frequency [16,17,21,22]. Cross-talk in our setup initially contaminated the cross-correlation measurements. This is more pronounced for the motion in perpendicular direction to the center-line of the particles and for large separations between the two particles, because the position cross-correlation function decays inversely with particle separation, while cross-talk is independent of the particles separation. Therefore the cross- talk will dominate a weak position signal for larger separations and can dominate the weak position cross-correlation signal.

In this paper we show and explain the technical construction of the setup used for one- and two- particle microrheology measurements. We quantify the cross talk and present a method to reduce the cross talk. Finally an alternative method to eliminate cross-talk altogether, using a second laser, is explained.

2.2 Experimental setup

2.2.1 Twin optical traps with one laser

A custom built inverted microscope [31,13] was equipped with two optical traps. Figure 1 shows a sketch of the setup.

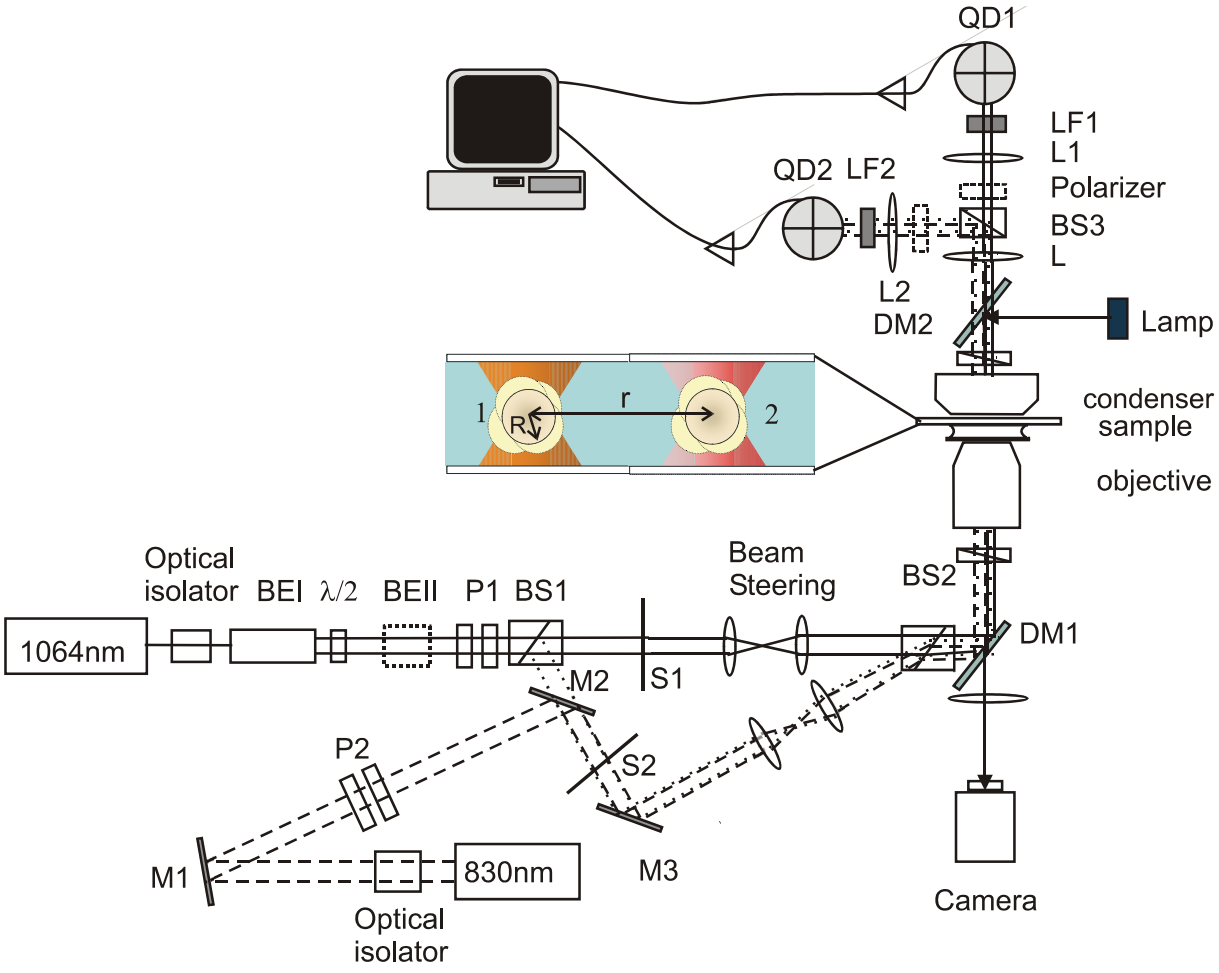

Figure 1: Sketch of the experimental setup, in two possible configurations, as described in the text. (*i*) One laser (1064nm) is used and split into two beams with orthogonal polarizations: 1 (solid line, laser trap 1) and 2 (dotted line, laser trap 2). (*ii*) Two independent lasers are used by flipping up M2: 1064nm (solid line, laser trap 1) and 830nm (broken line, laser trap 2).

We used a linearly polarized near infrared laser (ND:YV0$_4$, cw, λ = 1064nm, maximum power = 4W, Compass, Coherent), protected against back reflections to enhance stability with an optical isolator (37 dB isolation, Optics for Research, Caldwell, NJ). A 3x beam expander (BEI) (CVI Laser Corp., Albuquerque, NM) was

used to increase the beam width to ≈ 3.9 mm and to extend the Rayleigh range. The laser was usually operated at a constant power of about 2 W for maximum stability, and a combination of $\lambda/2$ plate and polarizer (P1 in Fig.1) was used to adjust the power. The laser beam then was split into two orthogonally polarized beams by a Glan-Thompson polarizing beam splitter (BS1). The ratio of the powers in the two beams depends on the orientation of the polarizer in P1 relative to the beam splitter and can thus be altered if necessary. Here the polarizer in P1 was mostly set at an angle of 45 degree with respect to the vertical and therefore both traps had close to equal strength. Two shutters S1 and S2 were placed in the laser paths on the optical table, which allowed us to switch on and off each of the traps independently. In this one-laser configuration mirror M2 was flipped down, so that the deflected laser beam reached mirror M3 and was directed towards the second Glan-Thompson beam splitter BS2 that recombined the two beams. The lateral and axial position of both laser foci in the specimen plane were independently adjustable using two pairs of telescope lenses (f = 80 mm). The second telescope lens images the point about which the beam is bent by moving the first lens into the back-focal plane of the objective. This guarantees that the intensity distribution in the back focal plane of the objective and all conjugated planes including the detector plane remains unchanged when the traps are moved in the specimen plane.

A dichroic mirror (DM1) (590DCLPxt, Chroma Corp.) was placed below an oil-immersion infinity-corrected objective (100x, 1.3NA; Neofluar, Zeiss) and coupled the beams into the microscope imaging beam path which was perpendicular to the optical table. After passing through the sample, the laser light was collected by an oil immersion condenser (1.4NA, Zeiss) and passed through a second dichroic mirror (DM2) (740DCSPxr, Chroma Corp.) towards the detectors. The light from the two perpendicularly polarized traps was separated by BS3, providing independent and simultaneous position detection for both traps. A further lens L (f = 50mm) was placed below the polarizing beam splitter BS3 to collimate the divergent beams and to, in combination with lenses L1 and L2, to image the condenser back focal plane onto the quadrant photo diodes (QD1 and QD2). QD1 was a specialized silicon PN quadrant photodiode operated under a reverse bias voltage of 100V (10mm diameter, YAGG444-4A, Perkin Elmer, Vaudreuil, Canada) to guarantee fast detection at

1064nm [32] and QD2 was a standard silicon PN photo diode, operated under a reverse bias voltage of 15V (10mm diameter, Spot9-DMI, UDT, Hawthorne, CA). Laser line filters LF1 and LF2 (D1064/10, Chroma Corp.) were placed in front of both detectors to block room light. Lenses L1 and L2 were also used to center the beams on the detectors.

For imaging the samples we used the microscope in differential interference contrast (DIC) mode, with Köhler illumination [33]using a fiber coupled 100W mercury arc lamp (546-nm line). The illumination light was coupled into the condenser via DM2 (740DCSPxr, Chroma Corp.), which transmits the laser light, but reflects the illumination light. Images were recorded by an Ultricon tube camera (model VT1000, Dage-MTI). Focusing in the sample was controlled by a DC motor which moves both objective and condenser with respect to the fixed sample. The sample is mounted on a 3-axis piezo stage (Nano-LP-100, MAD CITY LABS, INC. 2524 Todd Drive, Madison, WI 53713), with 0.7nm precision.

The signals from the quadrant photo diodes were converted to voltages and amplified by low-noise pre-amplifiers, [31,13] and combined by analog electronics to get voltages proportional to the x and y positions of the trapped particles with respect to the centers of the traps in the plane normal to the optical axes. The four displacement signals were finally sampled via an (A/D) converter (200kHz, ChicoPlus board with AD16 A/D module, Innovative Integration, Simi Valley, CA). The digitized data was processed by a custom-written LABVIEW (National Instruments, Austin, TX, USA) data acquisition program. Every data file was recorded at the chosen sampling frequency to the length of about 8.5 milion data point (2^{23}) and the recorded position fluctuation data are processed off-line. Both traps are calibrated using the power spectral method [34], using bead diameter and solvent viscosity as input parameters to calculate a conversion factor to actual displacement from the high-frequency Brownian bead fluctuations in water.

2.2.2 Twin optical traps with two independent lasers

In the configuration of optical traps with independent lasers two different laser wavelengths are used to create the two optical traps. The first laser was the near-

infrared 1064nm laser described above. The second laser (broken line in Fig.1) had a wavelength λ = 830nm (diode laser, cw, maximum power 140mW, IQ1C140, Laser 2000). It was guided into the path of the deflected 1064nm beam by mirror M2 (dotted line in Fig.1). The choice of wavelength of the laser (λ = 830nm) avoids the need for a specialized infrared detector. The rest of both optical paths was identical to those in the first method. The 830nm laser was polarized vertically to the table, as was the deflected 1064nm beam. As for the 1064nm laser, an optical isolator (IO-3-820-LP narrow adjustable Isolator, 760-860nm) was used in front of the 830nm Laser Power wass adjusted with a $\lambda/2$ plate and polarizer (P2). LF2 is replaced with a 830nm laser line filter (D830/10, Chroma Corp).

In this configuration the laser intensities and the trap strengths of the optical traps were independent. QD1 measured the 1064nm signal from trap 1, and QD2 measured the 830nm signal from trap 2. Signals were processed and data files were recorded as described above. Both traps are calibrated separately for each of the wavelengths as described before.

2.2.3 Sample Preparation

We used pure water as a simple liquid medium with η=0.969mPa, at 21.4°C temperature controlled lab. The spherical silica particles (R = 0.58μm, Van't Hoff Laboratory, Utrecht University, Utrecht, Netherlands) were added to the 20 μl of water at the final dilution of 10^{-5} volume%. Sample chambers were made of a coverslip glued onto a microscope slide with two narrow strips of double-stick tape giving an inner chamber height of ~ 70μm. In order to avoid an increase of viscosity due to the vicinity of the glass surfaces, particles were trapped near the surface and then moved to a distance of ~20 to 40 μm from the bottom surface (cover slip). The lab temperature was stabilized to 21.4 ± 1°C.

2.3 Results

Cross-talk measurements were first performed with the twin traps made from orthogonally polarized beams from the 1064nm laser. For detection, the two beams were separated by the polarizing beam splitter BS3. Leakage through the beam

splitters and depolarization in the microscope path as well as misalignment of the polarizers can in principle generate crosstalk, i.e. can lead to light from one trap ending up on the detector belonging to the other trap. Depolarization of light by the trapped particle itself can cause further cross-talk. We designate the leakage of light from trap 1 (broken line in Fig.1) into detector 2 (line in Fig.1) as the cross-talk from 1 to 2 and vice versa. Crosstalk can be characterized in different ways. We first measured the relative integrated power of the signals in the respective "wrong" channels without any trapped particles. This can be done with a calibrated power meter in the place of the detectors or from the average current measured by the QDs themselves, which is linearly proportional to the laser intensity. Here we have used the latter method. We used two different type of QD, as mentioned before, and we checked that the sensitivity of both detectors was tested to be the same.

cross-talk	underfilled objective [V]	one laser, overfilled objective	one laser, with additional polarizers	two lasers [V]	detector dark noise [V]
1 to 2	1.9%±0.2%	1.6%	1.5%	0.009	0.009
2 to 1	7.6%±0.2%	10.6%	1.1%	0.017	0.017

Table 1: Comparison of measured cross talk from 1 to 2 and from 2 to 1, when twin traps are either made with one laser (1064nm) and orthogonal polarizations, with a laser beam underfilling the objective back-focal plane or with an expanded beam overfilling the objective, using additional polarizers after BS3, or when twin traps are generated with two separate lasers of wavelengths 1064nm and 830nm.

Cross-talk from 2 to 1 was measured when the light with a polarization vertical to the optical table (trap 2) was switched on (shutter S2 open) and the other laser beam with a polarization horizontal to the optical table (trap 1) was switched off (shutter S1 closed). The average voltage read by QD2 is proportional to the trapping light

intensity, and the voltage read by QD1 is proportional to the leakage due to incomplete polarization or due to depolarization of beam 2. The fraction of light thus measured on QD1 can come both from trap 1 and from trap 2. Only the part passing through trap 2 will be contributing to actual cross-talk between displacement signals of trapped particles. Similarly, the cross-talk from 1 to 2 was measured when S1 was open and S2 was closed. The measured amounts of cross-talk are listed in Table 1 as ratios of the averaged voltage signals read in the respective detectors. Changing the incoming laser intensity did not affect the percentage of measured cross-talk. An average result for 7 different laser intensities is presented in column 2 of Table 1. Cross-talk from 1 to 2 was 1.9% and from 2 to 1 was 7.6%. The asymmetry of the measured cross-talk points to leakage in BS3, which is likely due to the fact that the laser light can not be perfectly collimated going through BS3. In these measurements the laser beam diameter at full width of half maximum (fwhm) intensity was measured with a beam profiler (WinCam-PCIProduct) to be 3.9mm right before the objective. This is smaller than the back aperture of objective of 4.2mm. Therefore the back aperture was not overfilled. When the back aperture was overfilled by using an additional 3X beam expander BEII, placed after the $\lambda/2$ plate and polarizer in the 1064nm laser path (in Fig1), the cross talk from 2 to 1 increase as it is shown in column 3 of Table 1.

A simple way to clean up leakage in BS3 is to use two additional prism polarizers right after BS3, before the lenses L1 and L2 which will focus the beam again. This reduced the cross-talk and also made it symmetric. The results of the integrated intensity measurements as described above are listed in column 4 of Table 1. The remaining ~1% cross-talk can still introduce artifacts in cross-correlation measurements, in particular when weak correlations are studied between relatively far-separated particles.

To eliminate also this remaining cross-talk in the instrument, we used two independent lasers of different colors as explained above to construct the twin traps. The control measurements of cross-talk signals, again measured as integrated intensities, in this configuration are presented in column 5 of Table 1. In this case the absolute voltage reading is given, measured with maximal laser power in the respective other beams (10V for highest power) it should be compared to the dark

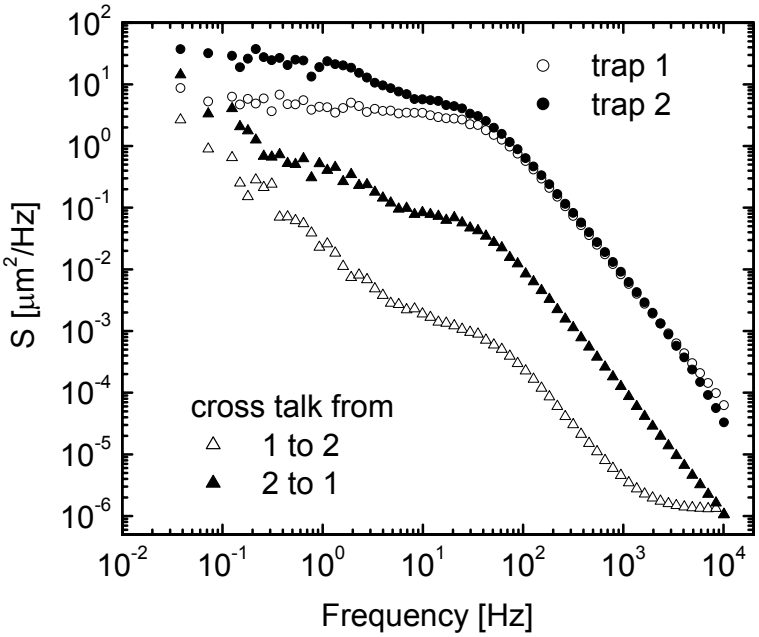

Figure 2: Power spectral densities of displacement fluctuations of particles (0.58μm radius silica beads) trapped in traps 1 and 2 (circles) when twin optical traps were made from orthogonally polarized light derived from a single laser. Cross-talk signals from the detector belonging to the respective other (empty) trap are plotted as triangles. The laser power was ~2mW corresponding to trap stiffness of 0.9pN/m were equal in trap 1 and trap 2. Sampling frequency was 20kHz. Without additional polarizers after BS3, cross-talk was not symmetric as also observed in the integrated intensities (Table 1).

noise signal from the detector and amplifier produced without any light on the detector. As can be seen, there was no detectable cross-talk. The dark noise level (column 6) was subtracted from all voltages before calculating ratios in columns 2-4.

Depolarization is expected either when a collimated beam hits a strongly curved interface or equivalently when a strongly convergent or divergent beam hits a flat interface between media with different indices of refraction.

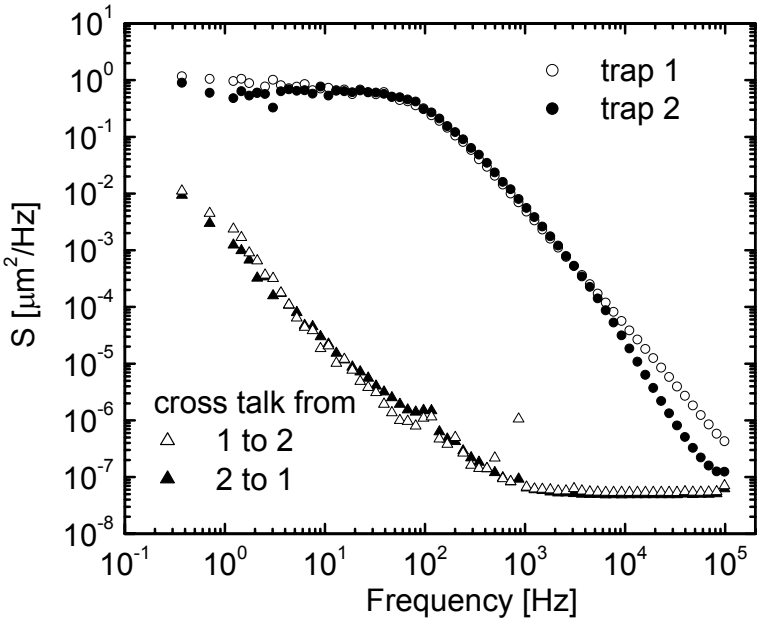

Figure 3: Power spectral densities of displacement fluctuations of particles (0.58μm radius silica beads) trapped in traps 1 and 2 (circles) when twin optical traps were made from orthogonally polarized light derived from a single laser, but with additional polarizers inserted after BS3. Cross-talk signals from the detector belonging to the respective other (empty) trap are plotted as triangles. The laser power was ~2.6mW, corresponding to a trap stiffness of 1.7pN/m in both trap 1 and trap 2. The sampling frequency was 195kHz. The high frequency additional decay in the PSD in trap 2 is due to the slow response of the standard QPD used for that trap at 1064nm [32].

To examine what portion of the cross-talk is due to the depolarization from the glass-water-glass interfaces in the sample chamber, we replaced the water in the sample chamber by index matching oil of objective. The amount of cross talk measured with this sample chamber was slightly lower than with a water-filled chamber: cross talk from 1 to 2 was 1.5%±0.1% and cross talk from 2 to 1 was 6%±0.2%. That do not have a major contribution thus suggests that the main depolarization is not due to the interfaces.

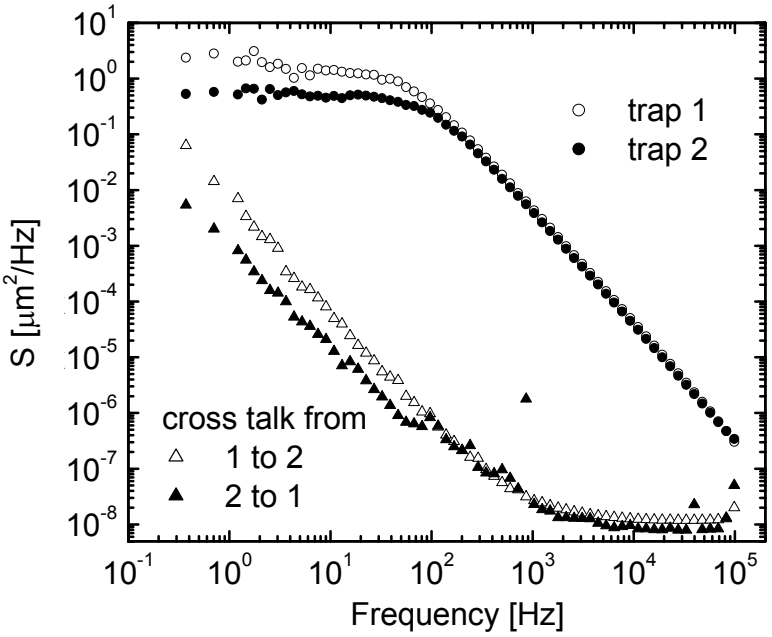

Figure 4: Power spectral densities of displacement fluctuations of particles (0.58μm radius silica beads) trapped in traps 1 and 2 (circles) when twin optical traps were made from two independent lasers (830nm and 1064nm). Cross-talk signals from the detector belonging to the respective other (empty) trap are plotted as triangles. Laser powers were (~1.8mW), corresponding to a trap stiffness of 1.1pN/m, in trap 1 and (~3mW), corresponding to trap stiffness of 1.8pN/m, in trap 2. The sampling frequency was 195kHz.

Furthermore we tested both for depolarization by the trapped particles and how much of the cross-talk actually comes from the opposite trap. With both laser beams on and a bead caught only in one trap, the cross-talk was measured by calculating displacement power spectral densities (PSD) from the signals of both detectors. The displacement power spectral densities is the Fourier transform of the auto-correlations of the measured position fluctuations $u(t)$: $S(\omega) = \int \langle u(t)u(0)\rangle e^{i\omega t} dt$, where $\omega = 2\pi f$ is the radial frequency.

PSDs are plotted in Fig. 2. Here one particle was trapped in one of the laser foci (e.g trap1), while the other trap (e.g trap2) was empty, and vice versa. No additional polarizers were used after BS3. The PSDs of a trapped particle in water is, apart from noise contributions, expected to be a Lorentzian [34]. Noise at low frequencies is predominantly 1/*f* noise from laser beam pointing fluctuations. At high frequencies shot noise creates a flat spectrum. As can be seen in Fig. 2, cross-talk from the loaded trap (*e.g.* trap 2) adds an extra component to the PSD of empty trap (*e.g.* trap1), consisting of an attenuated version of the Lorentzian characterizing the fluctuations of the bead trapped in trap 2. Use of additional polarizers after BS3 reduced the cross-talk in this case so that there was not any effect observed in the spectra of the empty trap as shown in Fig. 3. Using two different lasers of different colors likewise eliminated the cross-talk as presented in Fig. 4.

In summary, we have shown that cross-talk on the order of a few percent can easily occur in twin optical trap/twin detector experiments. If this level of cross-talk is detrimental, for example for the measurement of weak hydrodynamic couplings between trapped colloids, one needs to be careful in aligning the optics and eliminating the cross-talk by using additional polarizers. Alternatively and much more simply, one can use two independent lasers with different wavelengths to build a twin optical trap. This entirely eliminates cross-talk when the appropriate laser line filters are used.

2.4 Acknowledgments

We thank Jens-Christian Meiners, Daisuke Mizuno, Erwin Peterman, for helpful discussion. Joost van Mameren, Frederick Gittes and Mark Buchanan for help with data-evaluation software. This work was supported by the Foundation for Fundamental Research on Matter (FOM).

2.5 References

[1] A. Ashkin, Phys. Rev. Lett. **24**, 156 (1970).

[2] M. J. Lang and S. M. Block, Am. J. Phys. **71**, 201 (2003).

[3] Keir C. Neuman and S. M. Block, Rev. Sci. Instrum. **75**, 2787 (2004).

[4] F. Gittes and C. F. Schmidt, Optics Lett. **23**, 7 (1998).

[5] M. W. Allersma, M. J. deCastro, R. Fondecave, et al., Biophys. J. **74**, A50 (1998).

[6] C. Veigel, M. L. Bartoo, D. C. S. White, et al., Biophys. J. **75**, 1424 (1998).

[7] C. Veigel, F. Wang, M. L. Bartoo, et al., Nature Cell Biology **4**, 59 (2002).

[8] Amit D. Mehta, Matthias Rief, James A. Spudich, et al., SCIENCE **283**, 1689 (1999).

[9] C. Bustamante, Z. Bryant, and S. B. Smith, Nature **421**, 423 (2003).

[10] F. C. MacKintosh and C. F. Schmidt, Curr. Opin. Colloid Interf. Sci. **4**, 300 (1999).

[11] T. A. Waigh, Rep. Prog. Phys. **68**, 685 (2005).

[12] L. D. Landau, E. M. Lifshitz, and L. P. Pitaevskii, *Statistical Physics* (Pergamon Press, Oxford, New York, 1980).

[13] B. Schnurr, F. Gittes, F. C. MacKintosh, et al., Macromolecules **30**, 7781 (1997).

[14] F. Gittes, B. Schnurr, P. D. Olmsted, et al., Phys. Rev. Lett. **79**, 3286 (1997).

[15] L. A. Hough and H. D. Ou-Yang, Physical Review E **65**, 021906 (2002).

[16] K. M. Addas, C. F. Schmidt, and J. X. Tang, Phys. Rev. E **70**, 021503 (2004).

[17] M. Atakhorrami, G.H. Koenderink, C.F. Schmidt, et al., Phys.Rev.Lett. **95,** 208302 (2005).**(Chapter9)**

[18] J. C. Meiners and S. R. Quake, Phys. Rev. Lett. **82**, 2211 (1999).

[19] L. Starrs and P. Bartlett, Journal of Physics-Condensed Matter **15**, S251 (2003).

[20] S. Henderson, S. Mitchell, and P. Bartlett, Phys. Rev. E **6406**, art. no. (2001).

[21] M. Atakhorrami and C. F. Schmidt, Rheologica Acta.(in print) **(Chapter 6)**

[22] M.Buchanan, M.Atakhorrami, J. F. P. and, et al., Macromolecules. **38** (21): 8840 (2005).**(Chapter 4)**

[23] M. W. Allersma, F. Gittes, and C. F. Schmidt, in *Mat. Res. Soc. Symp. Proc.*, edited by B. Mulder, V. Vogel and C. F. Schmidt, 1998), Vol. 489, p. in press.

[24] S. B. Smith, Y. J. Cui, and C. Bustamante, Science **271**, 795 (1996).

[25] K. Visscher, S. P. Gross, and and S. M. Block, IEEE J. Sel. Top. Quantum Electron. **2**, 1066–1076 (1996).

[26] E. Fallman and a. O. Axner, Appl. Opt. **36**, 2107–2113 (1997).

[27] S. Inoué, Exp.Cell Research **3**, 199 (1951).

[28] S. Inoué and A. W. L. HYDE, J. BioPHYsic,AND BIOCHEM. CYTOL **3**, 831 (1957).

[29] K. BAHLMANN and a. S. W. HELL, Journal of Microscopy, **200**, 59 (2000).

[30] K. Bahlmann and a. S. W. Hell, Applied Physics Letters **77**, 612 (2000).

[31] M. W. Allersma, F. Gittes, M. J. deCastro, et al., Biophys. J. **74**, 1074 (1998).

[32] E. J. G. Peterman, M. A. van Dijk, L. C. Kapitein, et al., Rev. Scien. Inst. **74**, 3246 (2003).

[33] M. W. Davidson and M. and Abramowitz, Optical Microscopy. Online PDF-recourse (1999).

[34] F. Gittes and C. F. Schmidt, in *Methods in Cell Biology* (Academic Press, 1998), Vol. 55, p. 129.

Chapter 3

Correlated fluctuations of microparticles in viscoelastic solutions: quantitative measurement of material properties by microrheology in the presence of optical traps

Abstract

The Brownian motions of microscopic particles in viscous or viscoelastic fluids can be used to measure rheological properties. This is the basis of recently developed one- and two-particle microrheology. For increased temporal and spatial resolution, some microrheology techniques employ optical traps, which introduce additional forces on the particles. We have systematically studied the effect that confinement of particles by optical traps has on their auto- and cross-correlated fluctuations. We show that trapping causes anti-correlations in the motion of two particles at low frequencies. We demonstrate how these anti-correlations depend on trap strength and the shear modulus of viscoelastic media. We present a method to account for the effects of optical traps, which permits the quantitative measurement of viscoelastic properties in one- and two-particle microrheology over an extended frequency range in a variety of viscous and viscoelastic media.

3.1 Introduction

Complex fluids are commonly characterized by their viscoelastic properties. Considerable interest has in recent years also been devoted to biomaterials. These materials typically show a very complex time-dependent behavior related to their intrinsic length scales ranging from nm to μm. To probe this mechanical behavior over the required wide frequency range, new rheological techniques are needed since most conventional rheometers are restricted to frequencies less than about 50Hz due to the inertia of the macroscopic probe [1].

In part in an effort to increase the bandwidth (up to MHz), various active and passive (fluctuation-based) microrheology (MR) techniques have been developed in recent years [2-11] that explore the viscoelastic properties of soft complex fluids by measuring the response of the medium to the motion of embedded micron-sized particles. In passive MR the samples are in thermal equilibrium and the probe particles execute Brownian motion. The complex response function of the particle is obtained via the fluctuation-dissipation theorem and a Kramers-Kronig integral, which relates the real and imaginary parts of the response function. A Generalized Stokes-Einstein (GSE) relation relates the complex shear modulus of the medium to the complex response function of the particle [2,4,5,12].

Microrheology in its simplest form can be done with a single probe particle (1PMR) where the rheological properties of the material are extracted from the displacement autocorrelation function of individual fluctuating particles. Such measurements probe the dynamics on length scales that of particle to system size. Two-particle microrheology (2PMR), on the other hand, uses the correlated fluctuations of two particles at a separation distance r, which can be much larger than the probe particle size and thus probe the mechanics of the medium on a length scale comparable to the inter-particle separation [11, 13, 14, 15].

Tracking of particles in transparent media can be done by video microscopy [16] which has the advantage of allowing one to image ~ 100 particles simultaneously and to rapidly obtain good statistics. Standard video microscopy, however, is limited in frequency to 50/60Hz with a spatial resolution of 10 to 50nm. An alternative method giving higher spatial and temporal resolution is based on

laser trapping of individual particles combined with interferometric displacement detection. To apply this method to 2PMR one uses a pair of focused laser beams to produce two optical traps in the sample holding a pair of (spherical) particles at a separation distance *r*. Position fluctuations of each of the trapped particles are detected with quadrant photodiodes, with a bandwidth from ~ 0.1Hz to 100kHz with a spatial resolution of better than 1nm [17, 5, 18]. The detection range of the laser focus is on the order of only 1μm. Therefore the particle has to be kept in focus if one wants to record motions over longer times. In a predominantly viscous solution the particle can be confined and moved about by the laser traps themselves. In a viscoelastic medium such as a polymer solution or network, the probe particles are confined, and the laser has to be targeted on the particle. Even in that case, elevated laser power is necessary to avoid shot noise when detecting particle motion at high frequencies.

Optical trapping introduces an additional force on the particles that is determined by the laser power rather than by the inherent mechanical properties of the medium. This will influence the thermal motions so we must re-examine the relationship between the observed fluctuations of the particles and the rheological properties of the medium in which they are embedded. If not corrected for, the trapping potential introduces a systematic artifact in the magnitude of the storage modulus derived from the particle fluctuations, especially at low frequencies. In this paper we quantify both theoretically and experimentally the effects of the traps on the measured particle response functions in viscous and viscoelastic fluids using water and an aqueous solution of fd-virus. We demonstrate that the response functions measured with 1PMR and 2PMR at low frequencies reflect a combination of the viscoelastic confinement by the medium and the trapping forces on the particles and we present a procedure to correct microrheology data for the trap effect.

3.2 Materials

As an example of a purely viscous fluid we have used pure water. As an example of a viscoelastic medium, we have used a 10mg/ml solutions of monodisperse filamentous virus particles, fd-virus. The fd-bacteriophages were prepared by a standard method [19] and details are described elsewhere [20]. The concentrated stock solution of virus rods was diluted to 10mg/ml at pH 7 by adding a buffer solution with an ionic strength I = 50mM (5mM imidazole, 1mM NaN_3, and 46.5mM KCl).

As probe particles we used silica beads of radius R = 0.58μm ±5% (Van't Hoff Laboratory, Utrecht University, Utrecht, Netherlands), diluted to a final volume fraction of ~ 10^{-5}. After mixing the particles with the solutions, we pipetted the solutions into sample chambers with a ~ 20μl volume, made of a coverslip and microscope slide attached with two narrow strips of double-stick tape (thickness 70μm). After filling, the sample chambers were sealed at both ends with Apiezon H vacuum grease (M&I Materials LTD, Manchester, UK).

3.3 Experimental method

Two independent polarized laser beams with wavelengths λ=1064nm (ND:YV04, Compass, Coherent) and λ = 830nm (diode laser, CW, IQ1C140, Laser 2000) provided a pair of optical traps in a custom-built light microscope [14, 21]. A schematic sketch of the experiment is shown in Fig. 1, where two particles, labeled 1 and 2, at a separation distance r are trapped in the two laser foci. To avoid surface effects, particles were trapped at a minimum distance of 20μm away from all chamber surfaces. The laser intensity was varied for each wavelength individually using λ/2 plates and polarizers placed in the laser paths. The position fluctuations of each of the particles relative to the center of the trap were detected in the x and y directions (normal to the optical axis) simultaneously using a back focal plane interferometric method with quadrant photodiode (QPD) detection [22]. The λ = 1064nm laser was detected with a PIN photodiode with reverse bias voltage of 100V (YAGG444-4A, Perkin Elmer, Vaudreuil, Canada) [18], while the λ = 830nm light was detected with a standard silicon-type PIN photo diode, operated with a reverse bias voltage of 15V

(10mm diameter, Spot9-DMI, UDT, Hawthorne, CA). The particle position signals were digitized using an A/D board (200kHz, ChicoPlus, Innovative Integration, Simi Valley, CA) at 195kHz and anti-alias filtered above 100kHz and recorded with a Labview program (National Instruments, Austin, TX, USA) for 80 seconds per run.

Position measurements were calibrated using the power spectrum method [23]. For fd solutions we used calibration data taken for the same batch of particles, but trapped in buffer. For water, we calibrated with the very same particles that were used for the measurements. The trap stiffness was obtained in water as a function of the laser power [23]. The lab temperature was stabilized to 21.4 ± 1°C.

3.4 Data analysis method

Thermal (Brownian) particle motions are exactly described by linear response theory [24]. We therefore relate the Fourier transform of the displacement $u_\alpha^{(j)}(\omega)$ of particle j (1 or 2) in direction α (x or y) to the Fourier transform of the applied force $F_\beta^{(k)}(\omega)$ applied to particle k in direction β via the response function $\chi_{\alpha\beta}^{(j,k)}(\omega)$ as: $u_\alpha^{(j)}(\omega) = \chi_{\alpha\beta}^{(j,k)}(\omega) F_\beta^{(k)}$. Here, $\omega = 2\pi f$ is the radial frequency and we have used the Einstein summation convention in which both coordinate directions (Greek indices) β and particle numbers (Latin indices) k are summed over. The single-particle response functions $\chi_{\alpha\beta}^{(1,1)}(\omega)$ and $\chi_{\alpha\beta}^{(2,2)}(\omega)$ refer to the displacement responses of particles 1 and 2 to forces applied to the same particle. The $\chi_{\alpha\beta}^{(j,k)}(\omega)$ for $j \neq k$ refer to the inter-particle response functions, *e.g.*, describing how particle 1 responds to forces on particle 2. Each of these, in general complex, response functions can be separated into real (in-phase) and imaginary (out-of-phase) parts in the usual way: $\chi_{\alpha\beta}^{(j,k)}(\omega) = \chi'^{(j,k)}_{\alpha\beta}(\omega) + i\chi''^{(j,k)}_{\alpha\beta}(\omega)$.

In thermal equilibrium, and in the absence of external forces, the fluctuation-dissipation theorem [24] relates the imaginary part of the (single- or inter-particle) response functions to the equilibrium fluctuation spectrum of $u_\alpha^{(j)}(\omega)$:

$$\chi''^{(j,k)}_{\alpha\beta}(\omega) = \frac{\omega}{2k_B T} S_{\alpha\beta}^{(j,k)}(\omega) , \qquad (1)$$

where $k_B T$ is the thermal energy and the $S_{\alpha\beta}^{(j,k)}(\omega)$ are given by

$$S_{\alpha\beta}^{(j,k)}(\omega) = \int \left\langle u_\alpha^{(j)}(t) u_\beta^{(k)}(0) \right\rangle e^{i\omega t} dt . \qquad (2)$$

In our experiments we chose a coordinate system with x and y spanning the plane perpendicular to the optical axis (laser propagation direction), and in which the x-axis lies along the line connecting the centers of the two particles. In this coordinate system all $S_{\alpha\beta}^{(j,k)}$ are identically zero for $\alpha \neq \beta$ (here and throughout this paper we shall assume that the viscoelastic medium is homogeneous and isotropic in the absence of probe particles). For the remaining and only non-zero components of $S_{\alpha\beta}^{(j,k)}$ we introduce the short-hand notation: $S_{\parallel}^{(j,k)} \equiv S_{xx}^{(j,k)}$, $S_{\perp}^{(j,k)} \equiv S_{yy}^{(j,k)}$. We do not analyze particle fluctuations along the z-axis, perpendicular to the focal plane. Such fluctuations would also be given by $S_{\perp}^{(j,k)}$ if neither the medium nor the laser trap broke the axial rotational symmetry of the two-particle system. In practice the laser trap does break this symmetry, as the effective trapping potential is broader along the optical axis than in the plane perpendicular to that axis. In the event that these $S_{zz}^{(j,k)}$ correlations were measured, the resulting data could be analyzed using a trivial extension of the theory presented in this work.

At the risk of only apparently ambiguous notation, we shall also use a shorthand for the single-particle correlation functions, in which $S_{\parallel}^{(j)} \equiv S_{\parallel}^{(j,j)}$ and $S_{\perp}^{(j)} \equiv S_{\perp}^{(j,j)}$. Furthermore, in a medium that respects time-reversal invariance (assumed hereafter), all correlation functions must be symmetric under time reversal t so that $S_{\parallel}^{(1,2)}(\omega) = S_{\parallel}^{(2,1)}(\omega) \equiv S_{\parallel}(\omega)$ and correspondingly for $S_{\perp}$. Thus, there are six non-zero correlation functions $S_{\parallel,\perp}^{(j)}$ and $S_{\parallel,\perp}$, which can be used to directly determine the imaginary parts of the six corresponding response functions $\chi_{\parallel,\perp}^{(j)}$ and $\chi_{\parallel,\perp}$ for j = 1,2 using the Fluctuation-Dissipation theorem. Finally, for isolated particles (*i.e.*, in the absence of another particle trapped close by) in isotropic and homogeneous media, or for large separations between particles, the isotropy of the system requires that $S_{\parallel}^{(j)} = S_{\perp}^{(j)}$. In this case, the four $S_{\parallel,\perp}^{(j)}$ (or $\chi_{\parallel,\perp}^{(j)}$) reduce to just two correlation (response) functions $S^{(j)}$ (or $\chi^{(j)}$).

From the various imaginary parts of the response functions $\chi_{\alpha\beta}^{(j,k)}(\omega)$, we obtain the real parts (and hence, the full complex quantities) via a Kramers-Kronig integral [24 ,5]:

$$\chi'^{(j,k)}_{\alpha\beta} = \frac{2}{\pi}\int_0^\infty \frac{\zeta}{\omega^2+\zeta^2}\,\chi''^{(j,k)}_{\alpha\beta}(\omega)\,d\zeta\,. \qquad (3)$$

For isolated particles in the absence of optical traps, the complex response functions $\chi^{(j)}$ are related to the complex shear modulus *G* of the medium by a GSE relation [25, 4, 5,6]:

$$\chi^{(j)}(\omega) \to \alpha^{(j)}(\omega) = \frac{1}{6\pi RG(\omega)} \tag{4a}$$

where we have assumed the same particle radius *R* for both particles *j* = 1, 2, which is the case for our experiments. Here, we have introduced a new symbol α for the response functions, since it will be important to distinguish the *measured* response functions in the presence of traps (for which we shall consistently use χ), from those response functions that would be observed in the absence of traps (α). The latter characterize the part of the response due entirely to the medium, and they are thus the quantities of interest for rheology. Thus, we shall refer to these α as either *corrected* or *medium* response functions. The arrow in the above equation signifies that the measured response function χ directly reflects the *actual* rheology of the medium only in the absence of the trapping potentials.

Likewise, in the absence of traps, the inter-particle response functions $\chi_{\parallel,\perp}$ are given by generalizations of the Oseen tensor [26]:

$$\chi_{\parallel}(\omega) \to \alpha_{\parallel}(\omega) = \frac{1}{4\pi rG(\omega)} \quad \text{and} \quad \chi_{\perp}(\omega) \to \alpha_{\perp}(\omega) = \frac{1}{8\pi rG(\omega)}, \tag{4b}$$

where *r* is the separation between the particles. These expressions neglect inertia, which is a good approximation in the low frequency range studied here. While both of these expressions can be used to determine the modulus *G*, we find experimentally that the perpendicular channel is noisier than the parallel one.

In the presence of optical traps, additional forces are applied to the particles from the laser potentials. Thus, the displacements of each of the particle $u_{\alpha}^{(j)}(\omega)$ are modified by both trap potentials on the pair of particles. We model an optical trap as a Hookean spring characterized by a single isotropic trap stiffness or spring constant. In frequency representation, the additional trapping force in the α^{th} direction on particle *j* is $-k^{(j)}u_{\alpha}^{(j)}(\omega)$, where $k^{(j)}$ is the trap stiffness holding particle *j* in the laser focus (here, no summation on *j* is implied). Thus, given an external force applied to that particle, $F_{\alpha}^{(j)}(\omega)$, the total force acting on it is $F_{\alpha}^{(j)}(\omega) - k^{(j)}u_{\alpha}^{(j)}(\omega)$. In terms of the (medium) response functions α, we can now write the displacements

$$u_x^{(1)}(\omega) = \alpha^{(1)}(\omega) \times \left(F_x^{(1)}(\omega) - k^{(1)} u_x^{(1)}(\omega)\right) + \alpha_{\parallel}(\omega) \times \left(F_x^{(2)}(\omega) - k^{(2)} u_x^{(2)}(\omega)\right) \quad (5a)$$

and

$$u_x^{(2)}(\omega) = \alpha_{\parallel}(\omega) \times \left(F_x^{(1)}(\omega) - k^{(1)} u_x^{(1)}(\omega)\right) + \alpha^{(2)}(\omega) \times \left(F_x^{(2)}(\omega) - k^{(2)} u_x^{(2)}(\omega)\right) \quad (5b)$$

There is a similar pair of equations with x replaced by y and parallel by perpendicular. Of course, the measured response functions χ are those that relate the $u_\alpha^{(j)}$ to $F_\alpha^{(j)}$ alone. These can be found by solving the above equations for $u_\alpha^{(j)}$. This results in expressions for the χ that are nonlinear in the α. For example, the linear response coefficient relating $u_x^{(1)}$ to $F_x^{(1)}$ is

$$\chi_{xx}^{(1,1)} = \chi_{\parallel}^{(1)} = \frac{\alpha^{(1)} + k^{(2)}\alpha^{(1)}\alpha^{(2)} - k^{(2)}(\alpha_{\parallel})^2}{1 + k^{(1)}\alpha^{(1)} + k^{(2)}\alpha^{(2)} + k^{(1)}k^{(2)}\alpha^{(1)}\alpha^{(2)} - k^{(1)}k^{(2)}(\alpha_{\parallel})^2}. \quad (6a)$$

This nonlinear relationship should be distinguished from the fundamental *linear response* assumption that we make. Although the relationships among the various χ and α are nonlinear, we are still describing the *linear* response of the medium. Thus, for instance, we assume that forces and corresponding displacements are sufficiently small for the linear relationships in Eqs. 5a and b to be valid. In contrast, the higher-order terms beyond the leading term $\alpha^{(1)}$ do not depend on the amplitude of the displacement or force. These higher-order terms give relative contributions of order k/GR, kR/Gr^2, $k^2/(Gr)^2$, and $k^2/(GR)^2$, which depend on the trapping potentials k and the geometry of our experiments. Since these corrections do not depend on the amplitude of motion, they cannot be assumed to be small. Note also that the presence of the pair of traps breaks the rotational symmetry of the single-particle response, since

$$\chi_{yy}^{(1,1)} = \chi_{\perp}^{(1)} = \frac{\alpha^{(1)} + k^{(2)}\alpha^{(1)}\alpha^{(2)} - k^{(2)}(\alpha_{\perp})^2}{1 + k^{(1)}\alpha^{(1)} + k^{(2)}\alpha^{(2)} + k^{(1)}k^{(2)}\alpha^{(1)}\alpha^{(2)} - k^{(1)}k^{(2)}(\alpha_{\perp})^2} \quad (6b)$$

differs from the expression in Eq. (6a) by terms second order in both trap stiffness and inter-particle response. For the other particle, the corresponding expressions can be obtained by interchanging indices 1 and 2. The inter-particle response functions are given by

$$\chi_{xx}^{(1,2)} = \chi_{\parallel} = \frac{\alpha_{\parallel}}{1 + k^{(1)}\alpha^{(1)} + k^{(2)}\alpha^{(2)} + k^{(1)}k^{(2)}\alpha^{(1)}\alpha^{(2)} - k^{(1)}k^{(2)}(\alpha_{\parallel})^2} \tag{6c}$$

and

$$\chi_{yy}^{(1,2)} = \chi_{\perp} = \frac{\alpha_{\perp}}{1 + k^{(1)}\alpha^{(1)} + k^{(2)}\alpha^{(2)} + k^{(1)}k^{(2)}\alpha^{(1)}\alpha^{(2)} - k^{(1)}k^{(2)}(\alpha_{\perp})^2}. \tag{6d}$$

From an examination of the above equations, it is clear that in the limit of vanishing trapping potentials, the experimentally measured response functions χ reduce to the appropriate medium response functions α. These latter response functions that are thus (in the presence of optical traps) not directly accessible via experiment are necessary in order to determine the rheological properties of the medium. The experimentally accessible (measured) response functions χ, however, can be used to calculate the rheologically useful response functions α by inversion of the above equations. This inversion is facilitated by the observation that, within linear response, the parallel and perpendicular motions/response functions completely decouple. This, together with the symmetry properties mentioned above leads to two separate sets, each of three nonlinear equations that must be inverted. The resulting expressions for the parallel case are:

$$\alpha^{(1)} = \frac{\chi_{\parallel}^{(1)} + k^{(2)}(\chi_{\parallel})^2 - k^{(2)}\chi_{\parallel}^{(1)}\chi_{\parallel}^{(2)}}{1 - k^{(1)}\chi_{\parallel}^{(1)} - k^{(2)}\chi_{\parallel}^{(2)} - k^{(1)}k^{(2)}(\chi_{\parallel})^2 + k^{(1)}k^{(2)}\chi_{\parallel}^{(1)}\chi_{\parallel}^{(2)}}, \tag{7a}$$

$$\alpha^{(2)} = \frac{\chi_{\parallel}^{(2)} + k^{(1)}(\chi_{\parallel})^2 - k^{(1)}\chi_{\parallel}^{(1)}\chi_{\parallel}^{(2)}}{1 - k^{(1)}\chi_{\parallel}^{(1)} - k^{(2)}\chi_{\parallel}^{(2)} - k^{(1)}k^{(2)}(\chi_{\parallel})^2 + k^{(1)}k^{(2)}\chi_{\parallel}^{(1)}\chi_{\parallel}^{(2)}}, \tag{7b}$$

$$\alpha_{\parallel} = \frac{\chi_{\parallel}}{1 - k^{(1)}\chi_{\parallel}^{(1)} - k^{(2)}\chi_{\parallel}^{(2)} - k^{(1)}k^{(2)}(\chi_{\parallel})^2 + k^{(1)}k^{(2)}\chi_{\parallel}^{(1)}\chi_{\parallel}^{(2)}}. \tag{7c}$$

Similarly, for the perpendicular motion:

$$\alpha_{\perp} = \frac{\chi_{\perp}}{1 - k^{(1)}\chi_{\perp}^{(1)} - k^{(2)}\chi_{\perp}^{(2)} - k^{(1)}k^{(2)}(\chi_{\perp})^2 + k^{(1)}k^{(2)}\chi_{\perp}^{(1)}\chi_{\perp}^{(2)}}. \tag{7d}$$

Here, the additional pair of equations obtained for perpendicular motion can be obtained from Eqs. (7a,b) by replacement of parallel with perpendicular throughout, which must give the same values for $\alpha^{(1)}$ and $\alpha^{(2)}$ in isotropic and homogenous media. We also note that among the various second-order correction terms, the ones involving the inter-particle response are smaller than those involving the single-particle response by a factor of order $(R/r)^2$. Thus, for instance, the broken rotational symmetry of the single-particle response functions is expected to be small, even if second-order corrections due to the traps are otherwise relevant.

Here $k^{(1)}$ and $k^{(2)}$ are linearly dependent on the laser power and are known for each experiment. Specifically in our experiments $k^{(1)}$ is the trap stiffness of laser focus with λ = 1064nm and $k^{(2)}$ is the trap stiffness of laser focus with λ = 830nm.

Using Eqs. 4a and b we can extract the rheological properties of the medium as measured with one- and two-particle microrheology from the response functions α after correcting the measured response functions χ using Eqs. 7a–d. Through this manipulation of the raw data we can thus prevent systematic errors that would otherwise be introduced by the trapping potentials.

3.5 Results and discussion

In this section we verify experimentally how the optical trapping potential modifies the complex particle response functions. We demonstrate how this effect can be corrected for to measure shear moduli of viscous and viscoelastic fluids with 1PMR and 2PMR. We first present results for 1PMR, then for 2PMR, in both cases for water and fd solutions. The *measured* response functions χ are compared with the predictions of Eqs. 6a–d. Then, we obtain the corrected (medium) response functions α from the *measured* response functions using Eqs 7a–d. The shear moduli of the medium were calculated from the complex response functions after the correction for the traps. In order to demonstrate the necessity of correcting for trapping effects, we also calculated the (apparent) complex shear moduli without correcting for the trapping potential, *i.e.* directly from the correlation data using Eqs 4a, and b.

We measured the auto- and cross-correlated displacement fluctuations of the two particles simultaneously in each sample and for every power setting, so that the trap stiffness of each individual optical trap was the same for the measured single-

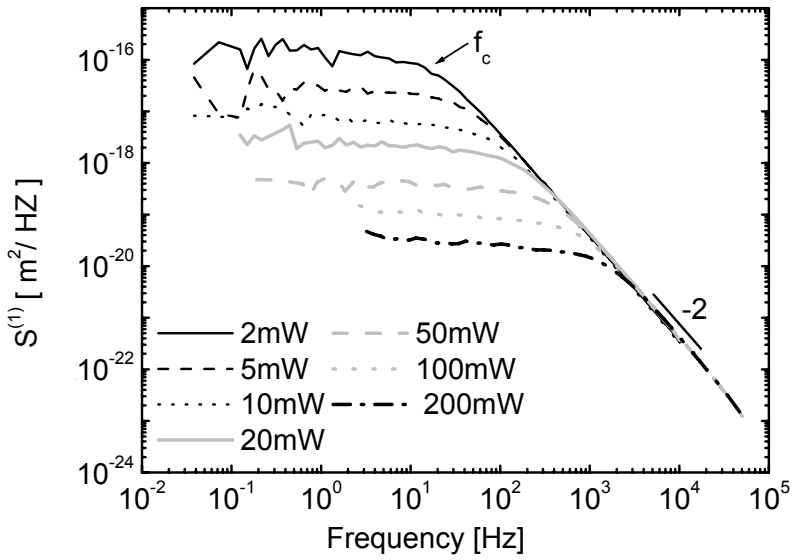

Figure 2: Displacement auto-correlations of a particle trapped in water as a function of frequency. The laser intensity (wavelength λ = 1064nm) was varied between 2 and 200mW. The corner frequency fc changes with laser intensity; the high frequency power-law slope is –2. Laser noise (increasingly prominent for stronger confinement at higher powers) was cut off at the low-frequency end of the curves.

and inter-particles response functions. The silica particle pairs (radius R = 0.58μm) were trapped at a separation distance of r = 2.7μm. The strength of the laser traps was varied by changing the laser intensity from 2 to 200mW (measured with a power meter before the incident beam enters the microscope path). Here we present the single-particle response functions measured with the laser trap of wavelength λ = 1064nm. Results for the second trap with λ = 830nm (not shown) were equivalent. The inter-particle response functions are similar in parallel and perpendicular to center-line of particles, we present thus just the results for parallel channel. Data are presented as a function of frequency, f ($f = \omega/2\pi$).

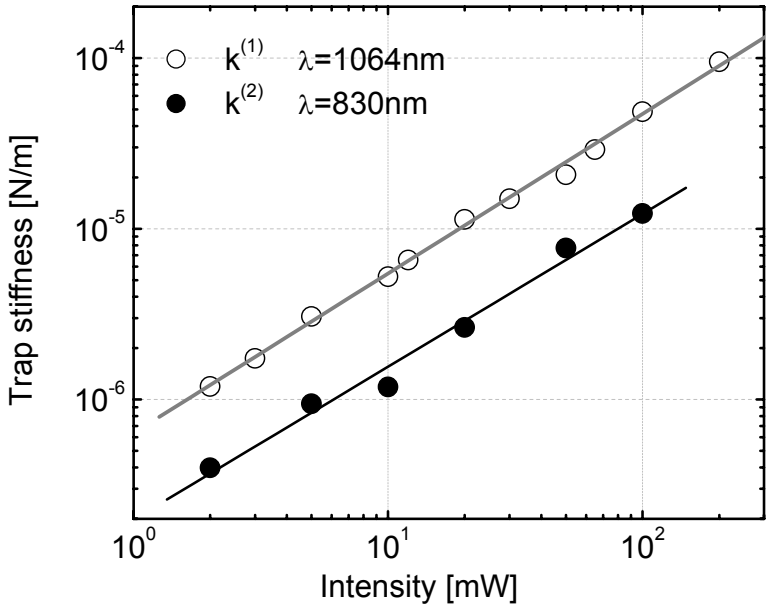

Figure 3: Trap stiffnesses of two laser traps generated by independent lasers (λ = 1064 and 830nm) measured from the fluctuations of two silica particles (R = 0.58μm) in water. The trap stiffnesses increased linearly with the laser intensities (measured before the beams entered the objective) for both traps.

3.5.1 One-particle microrheology (1PMR)

In 1PMR we measure the displacement auto-correlations of a single particle in a laser trap. The Fourier transform of this correlation function as defined in Eq. 1 for a thermally excited particle in a purely viscous fluid and laser trap takes the form of a Lorentzian [23, 27]:

$$S\ (f) = \frac{k_B T}{\gamma \pi^2 \left(f_c^2 + f^2\right)}, \tag{8}$$

where f_c is the characteristic (corner) frequency which divides the curve $S\ (f)$ into two regimes. For frequencies $f < f_c$, the laser trap provides the dominant force on the particle and the $S\ (f)$ is essentially constant, $S\ (f) \sim S_0 (f) = 4\gamma k_B T / k^2$. At higher frequencies $f >> f_c$, hydrodynamic drag forces acting on the particle dominate the

trapping forces and $S(f)$ decays as $1/f^2$, which is equivalent to free Brownian motion in a purely viscous solution. The trap stiffness can be calculated most conveniently from the corner frequency as $k=2\pi f_c \gamma$, where $\gamma=6\pi\eta R$ is the Stokes drag on a spherical particle with radius *R*.

Figure 2 shows a log-log plot of the position auto-correlation $S^{(1)}(f)$ of a silica particle (R = 0.58μm) trapped in water at different laser powers. The laser intensity was varied from 2 to 200mW, corresponding to corner frequencies between 11Hz and 1.3kHz. As expected, the corner frequency shifts to higher frequencies as the trap stiffness increases. Also, the area under $S^{(1)}(f)$ decreases as the particle is more tightly trapped (larger k) indicating that the rms amplitude of the position fluctuations decreases in accordance with the equipartition theorem. At high frequencies, where the particle is freely diffusing, all the measurements for different laser powers fall onto one line with a power-law slope of -2. The sampling frequency for low laser powers of 2, 5 and 10mW was 20kHz, while for higher laser intensities of 20, 50, 100 and 200mW a sampling rate of 195kHz was used.

Figure 3 shows that the trap stiffness depends linearly on laser intensity. The quoted laser powers were measured before the laser beams entered the microscope objective and are about a factor of 2 higher than power in the sample, with the absorption of light being different for the two different wavelengths [28] and the power passed through the objective also dependent on how much of the laser beam overfills the objective back aperture. Due to slightly varying alignments, the quoted laser powers are only a rough indication of trapping strengths and for calculations of the trap effect on the complex response functions, we used the measured trap stiffnesses, obtained from the corner frequencies of the auto-correlation spectra measured for the same silica particles in water.

In viscoelastic solutions the auto correlation spectra are not Lorentzian and we can not fit for a corner frequency to obtain the trap stiffness k for the same particle as used for the experiments. There are two alternative methods to find k, (i) one can trap a particle from the same batch at the same laser power in water, introducing an error due to polydispersity and (ii) one can use the low frequency data points for $G'(\omega)$ to extract k provided that the low frequency apparent $G'(\omega)$ is

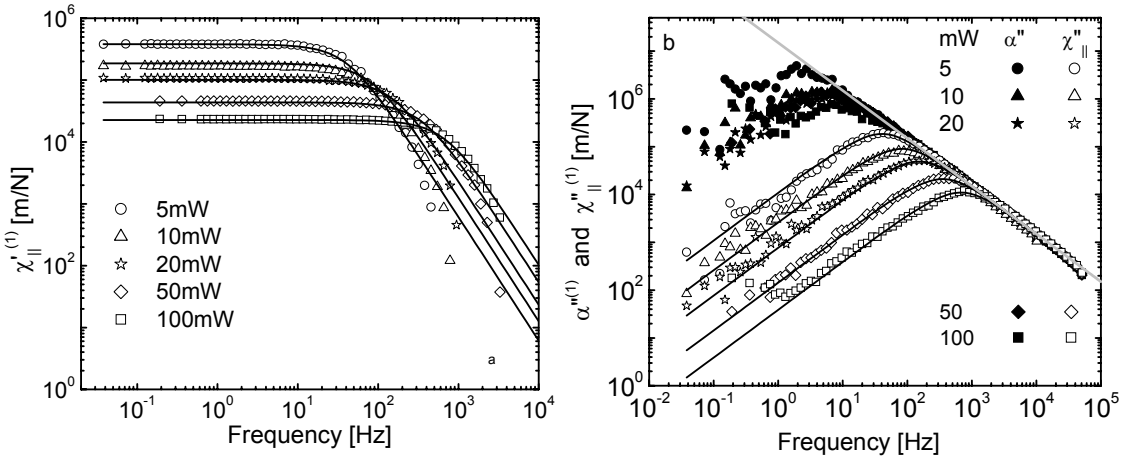

Figure 4: Frequency dependence of **(a)** the real part $\chi'^{(1)}_{\parallel}(f)$ and **(b)** the imaginary part $\chi''^{(1)}_{\parallel}(f)$, of the *measured* single-particle response functions in water, for x displacements (empty symbols). The data agree well with theoretical prediction (solid dark lines) calculated from Eq. 6a without any adjustable parameters. In **(b)** the solid symbols are *medium* response functions $\alpha''^{(1)}(f)$, calculated from $\chi'^{(1)}_{\parallel}(f)$ and $\chi''^{(1)}_{\parallel}(f)$ by eliminating the trap effect according to Eq. 6a. The solid gray line is the expected Stokes result for a sphere in a viscous fluid.

dominated by the trap. The error of this method increases with the elastic modulus of the solution.

A prediction for the *measured* response function of one particle trapped in a laser focus in water can be calculated from Eqs. 6a and b, using the known trap stiffness $k^{(1)}$ and $k^{(2)}$ in each measurement. From the stationary Stokes results [29], the response function of one particle in a simple viscous fluid of viscosity η and subject to no trapping potential is $\alpha^{(1)} = \alpha^{(2)} = 1/(6\pi R\eta(i\omega))$, while the inter-particle response function of two such particles along their centers is given by $\alpha_{\perp} = 2\alpha_{\parallel} = 1/(8\pi r\eta(i\omega))$ [30]. We insert these quantities in Eqs. 6a, and b and obtain a theoretical prediction of the *measured* response function in water.

Figures 4a and b show log-log plots of the real and imaginary parts of the *measured* single-particle response function in water, compared to the predicted ones. The $\chi'^{(1)}_{\parallel}(f)$ and $\chi''^{(1)}_{\parallel}(f)$ are plotted for different laser intensities between 5 and 100mW (same data as in Fig. 2). Figures 4a-b, show very good agreement of the

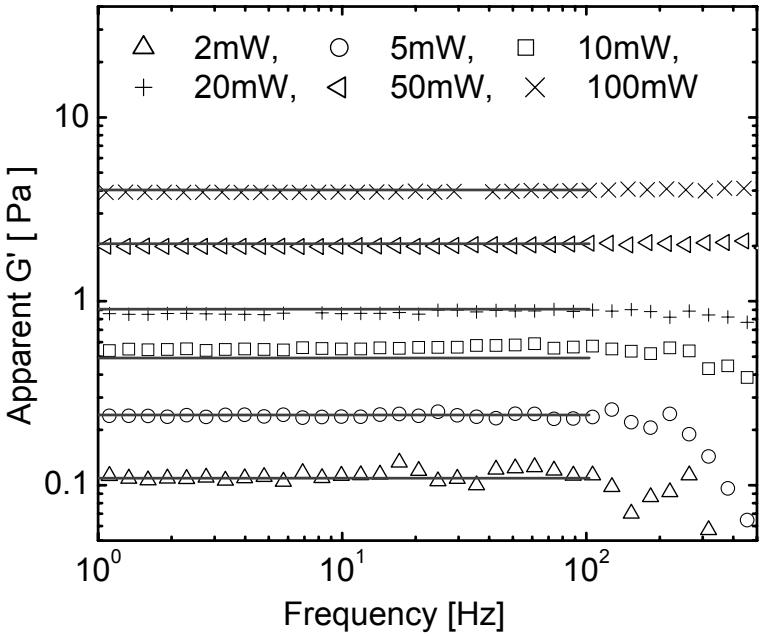

Figure 5: Apparent storage moduli (caused by the trap) as a function of frequency, measured in water with 1PMR for different laser powers (measured before the objective, see legend). The solid lines are the theoretical predictions based on the measured trap stiffnesses.

experimental data with the theoretical predictions with no adjustable parameters. In this calculation we used the trap stiffnesses $k^{(1)}$ and $k^{(2)}$ shown in Fig. 3. The filled symbols in Fig. 4b represent the imaginary part of the *medium* single-particle response function, $\alpha''^{(1)}(f)$, calculated from the *measured* one using Eq. 7a. The $\alpha''^{(1)}(f)$ thus obtained should be equal to the simple Stokes result for a viscous fluid of $1/(6\pi R\eta(i2\pi f))$ (gray line in Fig. 4b). This is evidently the case at high frequencies for all different laser powers, where all of the $\chi''^{(1)}_{\parallel}(f) = \alpha''^{(1)}(f)$ collapse onto the gray line. At lower frequencies, however, the $\chi''^{(1)}_{\parallel}(f)$ diverge from the gray line in a power dependent way. The corrected response functions $\alpha''^{(1)}(f)$ collapse onto the Stokes result except for deviation for even lower frequencies. These are due to the laser beam pointing fluctuations.

If one calculates an (apparent) shear modulus from the uncorrected response function $\chi''_{\parallel}(f)$, one finds a non zero storage modulus in the purely viscous medium, which is due to the laser traps. Figure 5 shows this apparent storage modulus as a function of frequency for different laser powers from 2 to 200mW. Since water does not have a storage modulus, the measured (frequency independent) values of 0.1 to 4.4Pa are completely due to the laser trap and are therefore proportional to the laser intensity. The solid lines are calculated from the independently measured trap stiffnesses $k^{(1)}/(6\pi R)$.

Unlike water, solutions of semiflexible fd particles have an storage (*real*) component to the shear modulus. Thus measured response functions using 1PMR contain a contribution of the *actual* elasticity of the medium as well as of the laser trap.

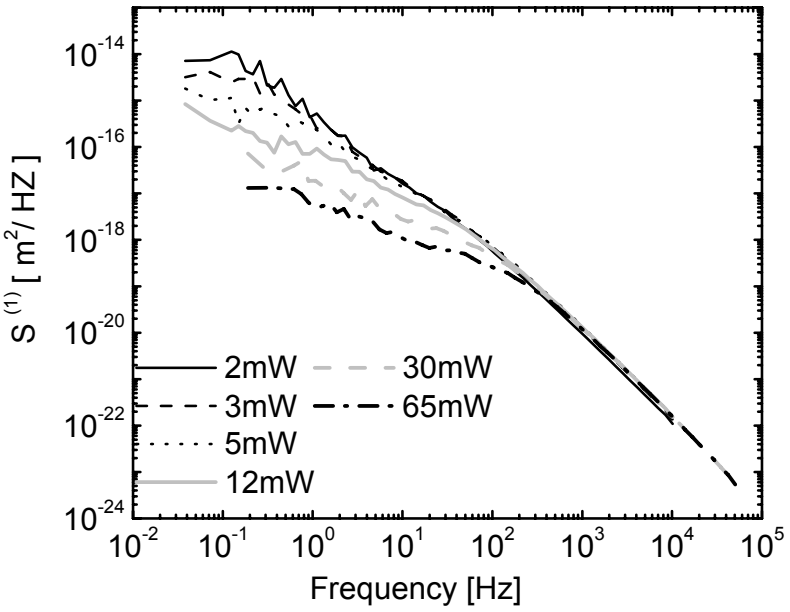

Figure 6: Displacement auto-correlations as a function of frequency of a particle of radius R = 0.58μm in a 10 mg/ml fd virus solution for different laser intensities (measured before the objective, see legend). The sampling rate was 20kHz for low powers 2, 3, and 5mW and 100kHz for high powers 12, 30 and 65mW.

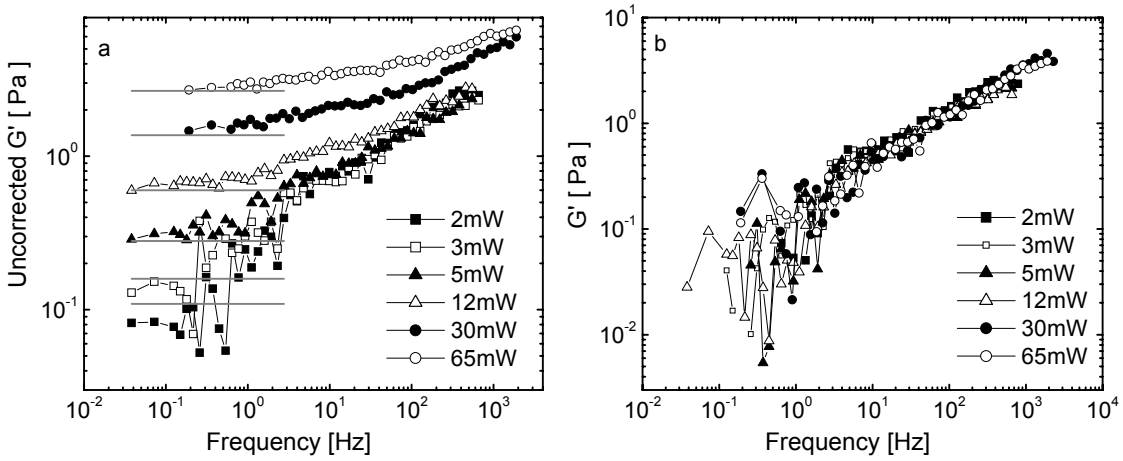

Figure7: (a) *Uncorrected* storage moduli $G'(f)$ for an fd solution measured with 1PMR using different laser powers (measured before the objective, see legend). The gray lines are the expected moduli corresponding to the $G'(f)$ measured in water for the same power settings. (b) *actual* storage moduli $G'(f)$ calculated using the response functions corrected for the traps using Eq. 7a.

The autocorrelation function $S^{(1)}(f)$ of one particle in fd solution is plotted in Fig. 6 as a function of frequency for different laser powers. As the laser power is increased, the rms amplitude (area under the curve) of the position fluctuations becomes smaller, similar to the behavior observed for a particle in water. Due to the viscoelastic nature of the fd solution the autocorrelation function of one particle are not Lorentzian [20], but, as in water, the spectra $S^{(1)}(f)$ for all the different laser powers coincide at frequencies larger than a characteristic frequency that is linearly dependent on the trap strength.

To highlight the systematic effect of the laser trap on the data, we calculated the storage modulus $G'(f)$ as measured by the 1PMR method without first removing the effect of the trap (Fig. 7a and b). These data were obtained with the same particle size and laser power settings as the water data in Fig. 6. The trap stiffnesses were calculated from the first data points of the *uncorrected* $G'(f)$ as described above to correct the measured response function. The *uncorrected* $G'(f)$ increase proportionally to the laser intensity at low frequencies. The *uncorrected* moduli

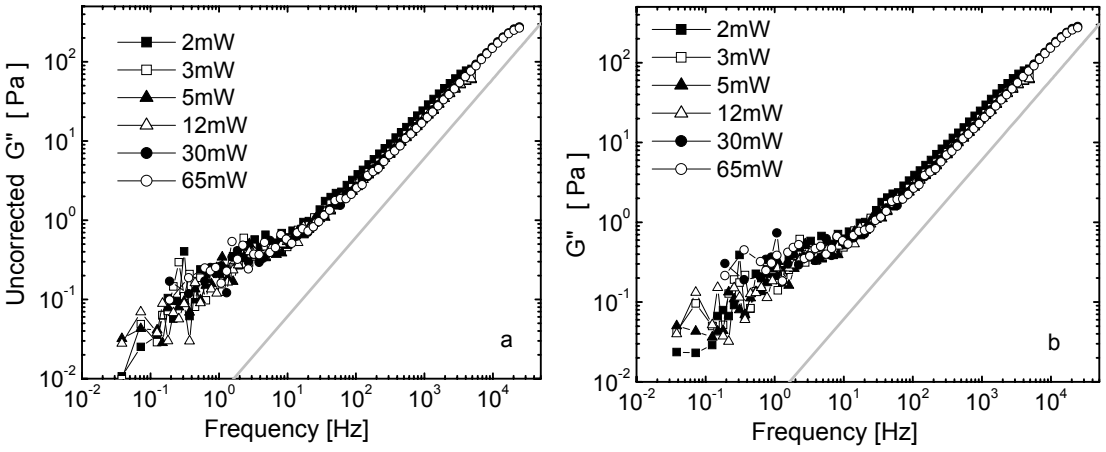

Figure 8: (a) Uncorrected loss moduli $G''(f)$ and (b) actual loss moduli $G''(f)$ (obtained with Eq. 7a), measured in x direction with 1PMR for a 10mg/ml fd solution for different laser powers (measured before the objective, see legend). The gray line shows the loss modulus of the buffer. The trapping laser does not have a significant effect on G".

determined using low power settings (2, 3, 5 and 12mW) converge to the *actual* storage modulus (Fig. 7b) of the medium at high frequencies. At larger laser powers (30 and 65mW), the *uncorrected* storage moduli are affected by the trap up to the largest probed frequency of 2kHz. At low frequencies the trap dominates the moduli which can be seen from the comparison to gray lines in Fig. 7 reflecting the pure trap effect.

We used Eq. 7a to correct the *measured* single-particle response functions $\chi^{(1)}$ for the trap effect, and obtain the single-particle response functions $\alpha^{(1)}$. We then applied Eq. (4) to calculate the complex shear moduli $G(f)$. The results for the storage modulus $G'(f)$ are plotted in Fig. 7b. As expected, the moduli $G'(f)$ fall onto one curve for all laser powers, which represents the storage modulus of the fd solution [20].

The *uncorrected* loss moduli $G''(f)$ from 1PMR at various laser powers are plotted in Fig. 8a. There is no significant effect from the trapping laser on the

uncorrected $G''(f)$, and all the measurements fall onto one curve even before correction, which does not change much with correction (Fig. 8b).

We note that in order to record the single- and inter-particle simultaneously, in all of these measurements two particles are trapped, so both $k^{(1)}$ and $k^{(2)}$ have nonzero values. In measurements with just one trapping laser ($k^{(1)} \neq 0$ and $k^{(2)} = 0$), Eq. 7a simplifies to:

$$\frac{1}{\alpha^{(1)}} = \frac{1}{\chi^{(1)}} - k^{(1)}. \tag{9}$$

We conclude that to correct for the trap effect in 1PMR and to get the *actual* storage modulus of a viscoelastic solution, it is sufficient to subtract a constant of $k/(6\pi R)$ from the *uncorrected* storage modulus.

3.5.2 Two-particle microrheology

To obtain the shear modulus of a medium from 2PMR we calculate the cross-correlation displacement of two hydrodynamically coupled particles trapped in two separate laser foci. In this case the correction for trap effects becomes slightly less straightforward.

Again, we first show data for particles trapped in water, as a purely viscous fluid. The Fourier transforms of the cross-correlation functions, $S_{\parallel,\perp}(f)$, of two thermally fluctuating particles in a viscous solution have a power-law slope of –2 at high frequencies just as was the case for single particles [21]. Figure 9 shows inter-particle correlation function ($S_{\parallel}(f)$) obtained using Eq. 2 at different laser powers for both traps with the trap stiffness of both traps as shown in Fig. 2. At low frequencies, where the confinement by the traps is dominant, the motion of the particles becomes anti-correlated, i.e., $S_{\parallel}(f)$ becomes negative (not visible in the log-log plot). At high frequencies, the viscous drag is dominant so that the $S_{\parallel}(f)$ are independent of trap power and overlap with a (power-law) slope of -2.

Figures 10a and b show linear-log plots of the *measured* real and imaginary parts of the inter-particle response functions $\chi'_{\parallel}(f)$ and $\chi''_{\parallel}(f)$ for different powers. Using an approach similar to that of the previous section, we calculated $\chi_{\parallel}(f)$ in water from Eq. 6c. The predictions from the measured trap stiffnesses (lines) are in

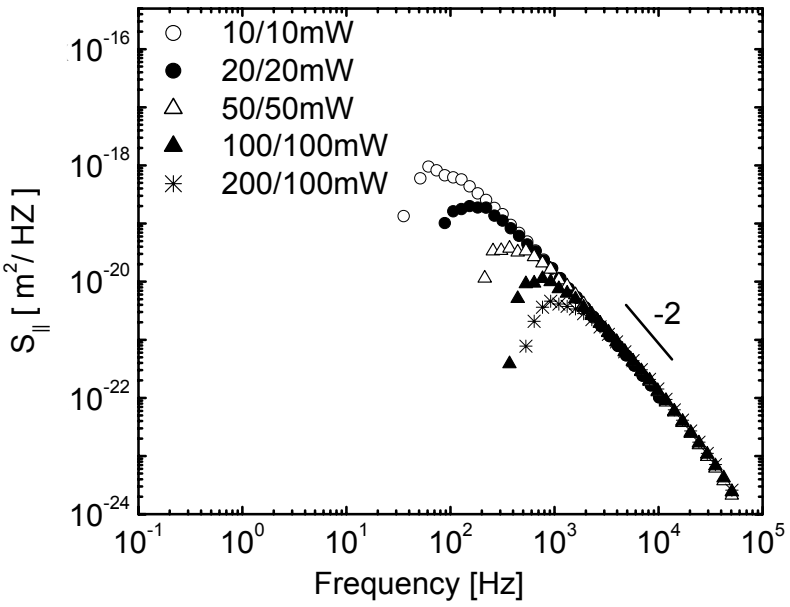

Figure 9: Inter-particle displacement correlation functions as a function of frequency of a pair of particles (radius R = 0.58μm) separated by a distance r = 2.7μm, trapped with different laser powers in water. Laser intensities were varied in parallel in the two traps (measured before the objective, legend: 1064/830 nm powers). Low-frequency anti-correlations are not plotted in this log-log plot. At high frequencies, all curves superimpose onto one curve with slope –2.

good agreement with the measured $\chi'_{\parallel}(f)$ and $\chi''_{\parallel}(f)$. It is evident that the maxima in $\chi'_{\parallel}(f)$ shift up in frequency and down in amplitude with increasing the laser power. This can be calculated formally from Eq. 6c with the Stokes assumption for the frequency of the maximum of $\chi'_{\parallel}(f)$ which corresponds to the frequency of the zero-crossing of the $\chi''_{\parallel}(f)$:

$f_{Max} = \frac{\sqrt{k^{(1)}k^{(2)}(4-9(R/r)^2)}}{24\pi^2\eta R}$ and for the amplitude of the maximum:

$\chi^1_{Max} = \frac{3k^{(2)}}{2Rk^{(1)}(k^{(1)}+k^{(2)})}$.

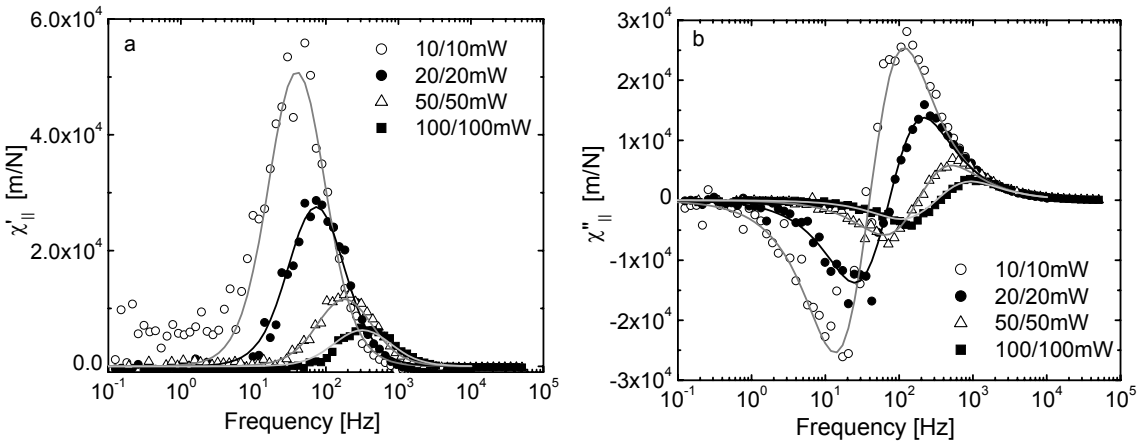

Figure 10: (a) Real part and (b) imaginary part of the inter-particles response functions of two particles in water as a function of frequency in the parallel direction, trapped with different laser powers varied in parallel in the two traps (measured before the objective, legend: 1064/830 nm powers). The theoretical predictions of Eq. 6c, calculated with the trap stiffness determined from corner frequency are plotted for comparison (lines).

The apparent storage and loss moduli calculated from the response functions $\chi'_{\parallel}(f)$ and $\chi''_{\parallel}(f)$ at various trapping powers without correcting for the laser trapping potentials are plotted in Fig. 11a and b. As expected in water this results in constant apparent $G'(f)$ which is entirely due to the laser traps (Fig. 11a). Noise at frequencies below 10Hz is due to the lower number of data points at low frequencies for each data set.

The (apparent) loss moduli $G''(f)$ for different laser powers calculated from uncorrected response functions are shown in Fig. 11b The frequency-dependent anti-correlation of $\chi''_{\parallel}(f)$ caused by the trap (shown in Fig. 10) is observed here as missing data points at low frequencies in a log-log plot of $G''(f)$. The solid gray lines in both figures show the theoretical predictions of the *apparent* modulus determined from the uncorrected response functions $\chi'_{\parallel}(f)$ and $\chi''_{\parallel}(f)$ using measured trap stiffnesses and Stokes assumptions in water.

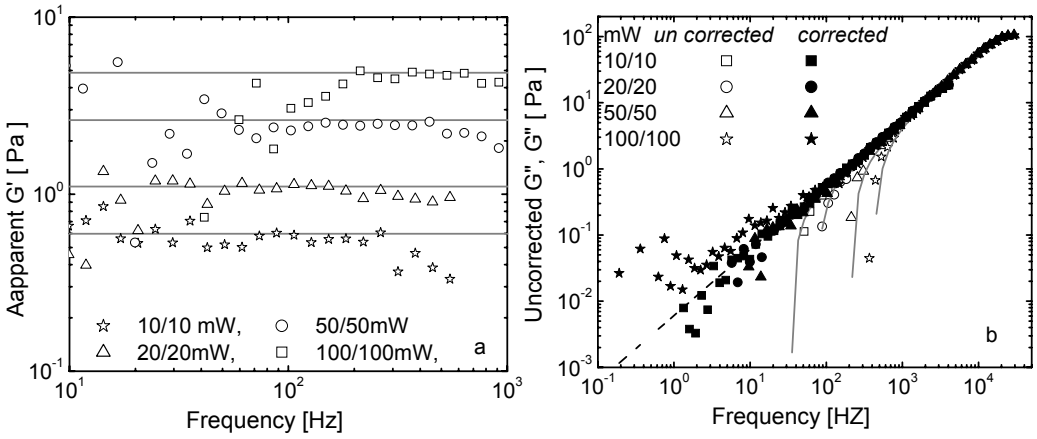

Figure 11: (a) Apparent storage modulus $G'(f)$ and (b) apparent loss modulus $G''(f)$ (empty symbols) measured in parallel direction with 2PMR in water as a function of frequency with different laser powers varied in parallel in the two traps (measured before the objective, legend: 1064/830 nm powers). The gray lines are the calculated apparent moduli $G'(f)$ and $G''(f)$ from the predicted response $\chi_{\parallel}(f)$ as in Eq. 6c. Filled symbols in (b) show the corrected loss modulus of water calculated using $\alpha_{\parallel}(f)$ and the expected loss modulus for water, $G''(f) = 2\pi f \eta$ plotted as a broken line.

In Figure 11 a and b, we obtain the *actual* moduli $G'(f)$ and $G''(f)$ from $\alpha'_{\parallel}(f)$ and $\alpha''_{\parallel}(f)$, the corrected response functions according to Eq. 7c. The storage modulus $G'(f)$ is largely scattered around an average value of close to 0, as expected for water (data not shown); $G''(f)$ now extends to lower frequencies. The data are consistent with the expected value of $G''(f) = 2\pi f \eta$ for water, plotted as the broken line.

Finally, we examined the effect of the traps on the inter-particle response functions in viscoelastic solutions of fd virus. Fig. 12 shows $S_{\parallel}(f)$ for different laser powers. At high frequencies all curves fall on top of each other, as expected. At low frequencies anti-correlated motion is observed again (negative values of $S_{\parallel}(f)$ not plotted), from a frequency on that depends on the trap strength.

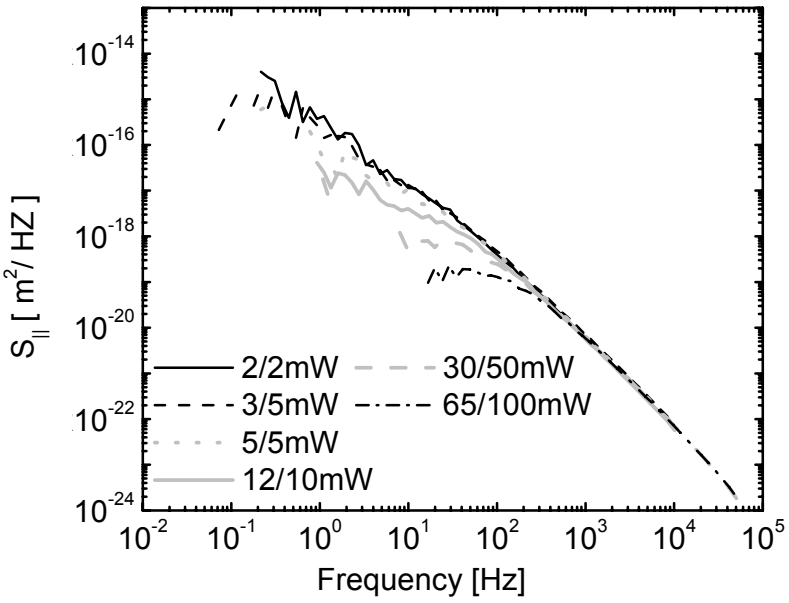

Figure 12: Inter-particle correlation functions in parallel direction of two particles separated by a distance r = 2.7μm in a 10mg/ml fd solution, as a function of frequency. The trap powers were varied in parallel (measured before the objective, legend: 1064/830 nm powers). A power-dependent anti-correlation is observed at low frequencies.

The anti-correlation occurs at frequencies that are one decade smaller than for the same measurement in water due to the higher viscosity and elasticity of the fd solution.

Fig. 13a and b compares the storage moduli of the fd solutions measured with 2PMR derived from uncorrected and from corrected response functions. Fig. 13a shows the *uncorrected* results, while Fig. 13b shows the corrected or *actual* $G'(f)$. The trap potentials make the *apparent* storage moduli $G'(f)$ approach a constant at low frequencies for high laser powers and change the slope of the curves even at higher frequencies (Fig. 13a). The curves for the corrected $G'(f)$ (corrected for both laser traps) collapse onto one curve for all laser powers (Fig. 13b), independent of trapping force.

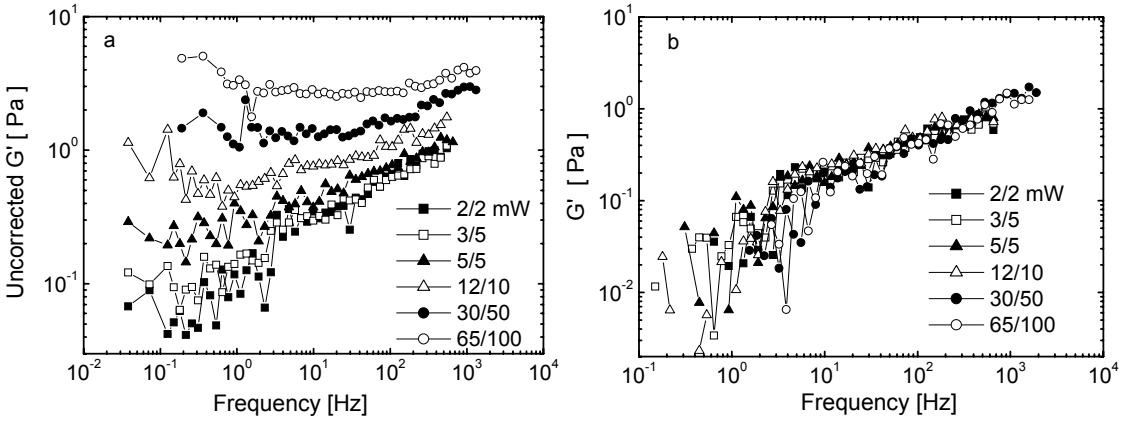

Figure 13: Storage shear modulus of a 10mg/ml fd solution as a function of frequency $G'(f)$, measured with 2PMR in parallel direction. The trap powers were varied in parallel (measured before the objective, legend: 1064/830 nm powers), with the (a) *uncorrected* modulus $G'(f)$ and (b) the *actual* modulus $G'(f)$ calculated using the corrected response functions in Eq. 7c.

Fig. 14 a and b demonstrate that the loss moduli of the fd solution measured with 2PMR are much less affected by the traps than the storage moduli. Fig. 14b shows the *uncorrected* $G''(f)$ derived from the uncorrected response functions, while Fig. 14b shows the *corrected* $G''(f)$. The missing low-frequency range in the *uncorrected* case *of* $G''(f)$ is due to the trap-induced anti-correlation, observed for powers above 30 mW; The trap correction to the response functions removes the anti-correlation effect and therefore extends the frequency range to lower frequencies (Fig. 14b).

3.6 Discussion

Correlations in the motion of trapped particles in time domain have been studied in purely viscous solutions before [31, 32]. Hough and Ou-Yang [33] derived formally different but in essence equivalent results for the response functions.

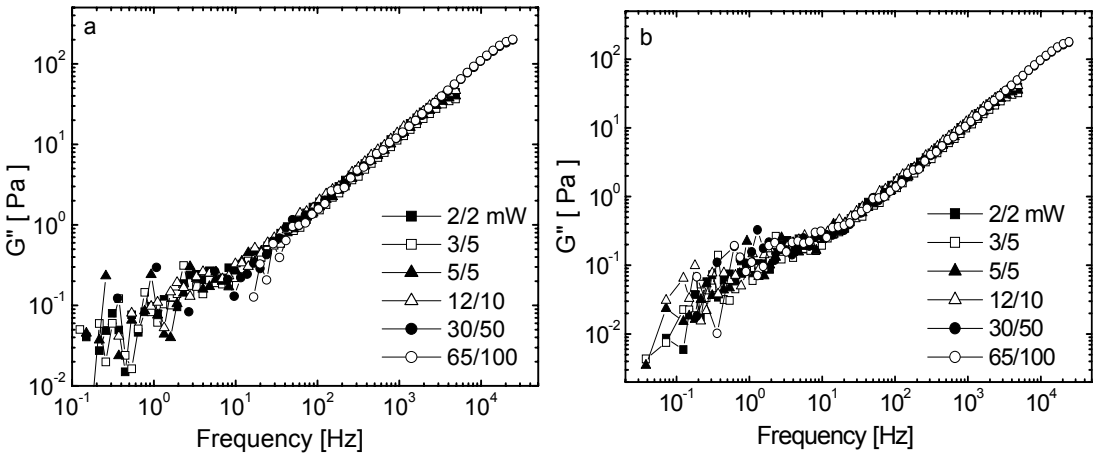

Figure 14: Loss moduli of a 10mg/ml fd solution as a function of frequency $G''(f)$, measured with 2PMR in parallel direction. The trap powers were varied in parallel (measured before the objective, legend: 1064/830nm powers). The *uncorrected* $G''(f)$ in (a) and *actual* modulus in (b) $G'(f)$ calculated using the corrected response functions (Eq. 7c) do not show a significant difference for the lower powers. For higher laser powers 12, 30 and 65mW correction eliminates the negative values at low frequencies (not plotted in (a)).

Because we use correlated Brownian fluctuations in optical traps to measure viscoelastic properties of soft materials we need to correct for such additional correlations. We have here used our formal representation of single and inter-particle response functions to develop a correction procedure for one and two particle microrheology. We have shown that it is straightforward to correct 1PMR results by subtracting a constant from $G'(\omega)$. If there is a second particle trapped in the vicinity, in principle, there will be an effect of both traps on the observed particle. The effect of the second trap predicts an asymmetry in the measured response function, which was found to be negligible under the conditions (R/r = 0.21) we used. In 2PMR, however, the effect of both traps on both particles has to be taken into account in a symmetric way. In 2PMR it is simpler to correct the particle response functions before calculating medium shear moduli. The correction is more involved,

including higher order terms in the storage constants, even if linear elasticity is assumed. It is particularly notable and at first glance counter-intuitive, that trapping two particles leads to anticorrelated fluctuations at low frequencies, an effect that is more pronounced in purely viscous media than in viscoelastic media. This is different from the anticorrelated fluctuations occurring at very high frequencies due to solvent inertia [34, 35]. The Fourier transform of the cross-correlation function of particle displacement thus becomes negative at low frequencies (and cannot be log-log plotted as usual).

Intuitively, the anti-correlations seen at low frequency can be understood in the following way. Along any particular axis, the relative motion of two particles in traps can be decomposed into in-phase (together) and out-of-phase (opposite) motion. In a simple liquid, the latter experiences a greater drag or dissipation. Thus, since the motion is strongly over-damped, the latter mode will always dominate at long times [31]. In the time domain, in fact, the resulting motion is always anti-correlated. This is because the effective spring constant, and therefore the overall amplitude is the same for both modes.

By contrast, when plotting corrrelation functions in the frequency domain, as we do in our experiments, the result is anti-correlations at low frequencies and positive correlations at high frequencies. This is because, although the slower decay of the out-of-phase motion results in low-frequency anti-correlations, the more rapid initial decay of the in-phase mode gives rise to dominant positive correlations at high frequencies. Equivalently, this can be seen from a simple force balance argument. At high frequencies, the forces due to the viscoelastic medium dominate the trapping forces, and the instantaneous propagation of stress means that one particle tends to move with the other. At frequencies below the characteristic relaxation time of a single trapped particle, however, the trapping forces tend to dominate, meaning that when one particle is displaced to one side of its trap, the (opposing) restoring force tends to make the second particle displace to the opposite side of its trap. Again, this latter regime corresponds to frequency/time scales such that the second particle is effectively undamped in its motion in response to the first particle. The frequency scale for the crossover from anti-correlated to positively correlated motion/fluctuations is determined by the relaxation frequency of a single

particle in its trap. This frequency will tend to increase with increasing laser power (observed above), and is also expected to decrease for more viscoelastic media (also observed above). Furthermore, since the anti-correlations are the direct result of the traps, they also tend to disappear (or shift to lower frequencies) with increasing storage modulus of the medium.

With the rigorous and complete correction procedure we have developed here it is simple to extract the true medium response parameters from either particle fluctuation recordings or responses to actively driven particles when optical trapping is used. We expect this method to be useful in applications of laser-interferometry based active and passive microrheology in many different soft media.

3.7 Acknowledgments

We thank Jens-Christian Meiners for helpful discussion. Joost van Mameren, Frederick Gittes and Mark Buchanan for help with data-evaluation software. This work was supported by the Foundation for Fundamental Research on Matter (FOM), AJL was supported in part by NSF-DMR0354113 and JXT was supported in part by NSF DMR 0405156 and J. I. Sulkowska was supported by the European Community-Access to Research Infrastructures action of the Improving Human Potential Program, Contract no. RII-CT-2003-506350.

3.8 References

[1] R. G. Larson, *The structure and rheology of complex fluids* (Oxford University Press, Oxford, 1998).

[2] T. G. Mason and D. A. Weitz, Phys. Rev. Lett. 75, 2770 (1995).

[3] T. G. Mason, K. Ganesan, J. H. v. Zanten, et al., Phys. Rev. Lett. 79, 3282 (1997).

[4] F. Gittes, B. Schnurr, P. D. Olmsted, et al., Phys. Rev. Lett. 79, 3286 (1997).

[5] B. Schnurr, F. Gittes, F. C. MacKintosh, et al., Macromolecules 30, 7781 (1997).

[6] A. J. Levine and T. C. Lubensky, Phys. Rev. Lett. 85, 1774 (2000).

[7] F. C. MacKintosh and C. F. Schmidt, Curr. Opin. Colloid Interf. Sci. 4, 300 (1999).

[8] A. W. C. Lau, B. D. Hoffman, A. Davies, et al., Phys. Rev. Lett. 91, 198101 (2003).

[9] F. G. Schmidt, B. Hinner, E. Sackmann, et al., Phys. Rev. E 62, 5509 (2000).

[10] L. Starrs and P. Bartlett, Faraday Discussions 123, 323 (2003).

[11] J. C. Crocker, M. T. Valentine, E. R. Weeks, et al., Phys. Rev. Lett. 85, 888 (2000).

[12] A. J. Levine and T. C. Lubensky, Phys. Rev. E 4, 6304 (2001).

[13] D. T. Chen, E. R. Weeks, J. C. Crocker, et al., Phys. Rev. Lett. 90, 10831 (2003).

[14] M. W. Allersma, F. Gittes, M. J. deCastro, et al., Biophys. J. 74, 1074 (1998).

[15] M.Buchanan, M.Atakhorrami, J.F.Palierne, et al., Phys. Rev. E 72, 011504 (2005).**(Chapter 5)**

[16] J. C. Crocker and D. G. Grier, J. Colloid Interface Sci. 179, 298 (1996).

[17] F. Gittes and C. F. Schmidt, Biophys. J 74, A183 (1998).

[18] E. J. G. Peterman, M. A. van Dijk, L. C. Kapitein, et al., Rev. Sci. Instrum. 74, 3246 (2003).

[19] J. Sambrook, E. F. Fritsch, and T. Maniatis, *Molecular Cloning: A Laboratory Manual* (Cold Spring Harbor Laboratory Press, Cold Spring Harbor, 1989).

[20] K. M. Addas, C. F. Schmidt, and J. X. Tang, Phys. Rev. E 70, 021503 (2004).

[21] M.Atakhorrami et al, not published.**(Chapter 2)**

[22] F. Gittes and C. F. Schmidt, Optics Lett. 23, 7 (1998).

[23] F. Gittes and C. F. Schmidt, in *Methods in Cell Biology* (Academic Press, 1998), Vol. 55, p. 129.

[24] L. D. Landau and E. M. Lifshitz, Statistical physics.(Pergamon Press, Oxford, NewYork, 1980).

[25] T. G. Mason and D. A. Weitz, Phys. Rev. Lett,74, 1250 (1995).

[26] A. J. Levine and T. C. Lubensky, Phys. Rev. E 63, 1510 (2001).

[27] K. Berg-Sørensen and H. Flyvbjerg, Rev. Sci. Instrum. 75 (2004).

[28] Keir C. Neuman and S. M. Block, Rev. Sci. Instrum. 75, 2787 (2004).

[29] LD Landau and EM Lifshitz, *Fluid Mechanics* (Butterworth-Heinemann, Oxford, 2000).

[30] C.W.Oseen, *Neuere Methoden und ergebnisse in der hydrodynamik*, Leipzig, 1927.

[31] J. C. Meiners and S. R. Quake, Phys. Rev. Lett. 82, 2211 (1999).
[32] S. Henderson, S. Mitchell, and P. Bartlett, Phys. Rev. E 64, 061403 (2001).
[33] L. A. Hough and H. D. Ou-Yang, Phys.Rev. E 65, 021906 (2002).
[34] M. Atakhorrami, G.H. Koenderink, C.F. Schmidt, et al., Phys.Rev. Lett. 95, 208302 (2005).**(Chapter 9)**
[35] T. B. Liverpool and a. F. C. MacKintosh, submitted to Phys.Rev.Lett. 95, 208303 (2005).

Wormlike Micelle Solutions

II

This part is based on the following papers:

1. **M. Atakhorrami**, M. Buchanan, J.F. Palierne, and C.F. Schmidt, "Comparing macrorheology and one- and two-point microrheology in wormlike micelle solutions " Macromolecules 2005, 38(21)8840. (Chapter 4)
2. M. Buchanan, **M. Atakhorrami**, J.F. Palierne, F.C. MacKintosh, and C. F. Schmidt, "High-frequency microrheology of wormlike micelle" Phys. Rev. E (2005) 72: 011504. (Chapter 5)
3. **M. Atakhorrami** and C.F. Schmidt, "High-bandwidth one- and two-particle micrhorheology in solutions of wormlike micelles" (in print Rheologica Acta), (Chapter 6)

Chapter 4

Comparing macrorheology and one- and two-point microrheology in wormlike micelle solutions

Abstract

We present here a comparison between three rheological techniques to verify a recently developed optical microrheology technique. As a model viscoelastic fluid we have used worm-like micelle solutions which are well characterized Maxwell fluids. Using the same samples, we have measured the viscoelastic response function using macroscopic rheology, as well as one-particle and two-particle microrheology. With all three techniques we have obtained frequency dependent complex shear moduli over large and overlapping frequency ranges. Excellent agreement of the results from all three techniqes was observed. This was expected given that characteristic length scales of the solution, such as persistence length and mesh size, were significantly smaller than the probe particle size. Our results provide a much needed quantitative verification of microrheology on a simple model system.

4.1 Introduction

The shear elastic properties of viscoelastic materials, such as polymer or colloidal solutions, are commonly measured by mechanical rheometers. Storage and loss moduli of a material can be measured by application of strain while measuring stress or vice versa, and probe geometries of order centimeters are typically used. Recently developed optical microrheology techniques, in contrast, use micron-sized particles that are embedded in the material, to obtain the viscoelastic response parameters [1]. In contrast to macroscopic mechanical rheology techniques, there is no strain applied to the material during the measurement. This is particularly useful in complex fluids where even small imposed strains can cause a structural reorganization of the material, and change its viscoelastic properties.

Response parameters can be measured either by actively manipulating the probe particles with magnetic fields or with light (optical traps)[2], or in a passive mode by merely recording the thermal fluctuations of the particles. Various methods have been utilized to measure the displacement fluctuations of the embedded particles. Video tracking or "rheological microscopy" has been applied to a variety of polymer systems such as λ-DNA solutions [3] as well as to biological cells [4]. The highest frequency that can be measured using this technique is half the video frequency (Nyquist frequency), typically 25 or 30Hz. Higher bandwidths can be reached using diffusing wave spectroscopy (DWS) [5,6] or optical trapping techniques combined with laser interferometry with fast photodiodes to track individual particles [7,8].

The complex shear modulus of the embedding medium can be calculated from the Brownian motion of the particle using results from linear response theory [9]. In the linear response regime, the fluctuation-dissipation theorem relates position fluctuations to the imaginary part of the response function. A Kramers-Kronig integral then makes it possible to calculate the real part of the response function. Generalized Stokes-Einstein relationships, which differ for the one-particle and the two-particle method, can then be used to extract the complex shear modulus [8, 10]. Data analysis has also been performed in a different way, using a Laplace transform of the mean-square displacement and then employing a fitting procedure

assuming the analytic form of the storage and loss elastic modulus [5, 11, 12]. Here we use the first method to obtain the viscoelastic modulus directly from the data, avoiding any fitting procedures.

In general, microrheology is a useful tool to probe spatially resolved viscoelastic properties of inhomogeneous materials and it can be applied to study small samples, such as biological cells. Furthermore, the technique has a bandwidth of up to MHz, much larger than conventional macrorheology, and it is sensitive enough to measure low elastic moduli (<1 Pa) that are not accessible to macrorheometers. Passive microrheology is ideally suited to investigate materials that respond non-linearly to low strains, such as many biopolymer systems.

Since microrheology techniques are relatively new and have been applied initially to samples such as actin solutions or cells which are problematic in macrorheology, there is still a need to rigorously determine under what conditions one can expect to measure the same bulk shear moduli as measured by conventional rheometers. A number of possible effects can lead to differing results, which at the same time opens up new and interesting possibilities to characterize materials on a microscopic scale. One possibility is that the probe particle locally perturbs its environment on the same scale that it probes, e.g. by causing local depletion or enrichment of the medium, [13]. This is expected to occur if there are characteristic length scales in the sample that are on the order of or larger than the probe size. Non-stick boundary conditions on the surface of the probes would also affect the results [14]. Furthermore, if the sample is a polymer solution, compressional or free draining modes should in principle be measurable since there is no constant-volume constraint. The fluctuation-dissipation theorem which is used in the passive modes might not be applicable in non-equilibrium or glassy systems. Local perturbation effects can be circumvented and at the same time quantified by measuring the correlated fluctuations of pairs of probe particles, a method termed two-particle microrheology [13,15,16]. Evidence for depletion effects has been reported in λ-DNA solutions where a difference between one and two particle results was observed [3].

To-date there has been no clear quantitative comparison of microrheology with macrorheology on a well-characterized system. This has been due to the limited overlap over the frequency range between the two techniques. Typical commercial

rheometers measure up to a maximum frequency of about 10Hz. At such low frequencies microrheology tends to give quite noisy results. Furthermore, there is also a limit in the range of elastic moduli one can measure with both techniques: Microrheology performs well in soft systems, but gets less accurate from ~100Pa upwards, while macrorheology is often not very accurate below 10Pa. Microrheology to date has been extensively used on biopolymer solutions, such as actin networks or cells, for which macrorheology has been notoriously inaccurate [17] or impossible.

We report here on rheology experiments with a simple and well-studied model system, namely a surfactant forming wormlike micelles in solution. The objective of this paper is to quantitatively compare the results of both one-and two-particle microrheology and macrorheology with the same samples. Technical details of the two-particle microrheology technique will be published elsewhere [18]. The wormlike micelle solutions, made from cetylpyridinium chloride and sodium salicylate in 0.5M sodium chloride brine, exhibit dynamics similar to polymer solutions, however the breakage dynamics ensure a single relaxation time in the slow dynamics [19,20]. This results in very simple and well-understood rheological properties, namely Maxwell behavior at low frequencies [21]. Furthermore, for this sample one-particle microrheology should not be sensitive to depletion or other probe particle effects, since the relevant length scales such as mesh size and persistence length are smaller than the particle size. We expect therefore agreement between all three techniques.

4.2 Experimental Methods

4.2.1 Materials

Wormlike micelles were prepared from surfactant, cetylpyridinium chloride (CPyCl) dissolved in brine (0.5M NaCl) with sodium salicylate (NaSal) as strongly binding counterions. All samples had a molar ratio Sal/Cpy = 0.5. Samples were made in batches of 50 ml and equilibrated and stored at ambient (controlled) lab temperature of 21.5-22.0°C. The microrheology experiments were performed in the same lab at the same temperature. The wormlike micelles have a typical diameter of 2-3nm,

lengths between 100 nm and 1μm and a persistence length of order 10 nm [20]. Experiments were performed with micelle concentrations between 0.5 and 4 wt% i.e. in the semidilute regime (c > c*, c* ~ 0.3 wt%) where micelles are entangled. The average mesh size varies between 30 and 10nm for c between 1 and 5 wt% [20].

4.2.2 Macrorheology

A custom designed piezo-rheometer [22] was used to measure directly the loss and storage shear elastic moduli of the samples. The sample was contained between two glass plates mounted on piezoelectric ceramics. One of the plates was made to oscillate vertically with an amplitude of about 1 nm by applying a sine wave to the ceramic. This movement induces a squeezing flow in the sample and stress transmitted to the second plate is measured by the other piezoelectric element. The strain is extremely small ($\gamma < 10{-}4$) so the sample structure was likely not altered by the flow. The set-up allows us to measure the storage ($G'(\omega)$) and loss ($G''(\omega)$) shear modulus for frequencies ranging from 0.1Hz to 10kHz. All experiments were done at 21.8oC except for *c*p = 4 which was done at 22.4oC. The set-up was hermetically sealed to avoid evaporation.

4.2.3 One-particle microrheology (1PMR)

All experiments were performed using a custom built optical microscope equipped with an optical trap and a laser-interferometric position detection system as described previously [8]. Briefly, an infrared laser (λ =1064 nm, ND:YVO4, Compass, Coherent, Santa Clara, CA, USA) was focused into the sample via a microscope objective lens (Zeiss Neofluar, 100x, oil immersion, NA: 1.3) to optically trap a particle in the sample. The back-focal plane of the condenser collecting the laser light downstream of the trap was imaged onto a special-design PN photodiode operated at a reverse bias voltage of 100 V (YAG444-4A, Perkin Elmer, Vaudreuil, Canada) to avoid high-frequency attenuation [23]. Displacement fluctuations of the trapped particle in the plane normal to the optical axis were recorded on a PC using Labview (National Instruments, Austin, TX, USA) after analog signal conditioning and A/D

conversion with sample frequencies up to 195kHz [8]. The lab temperature was stabilized to 21.4 ± 1°C.

The particles used in the experiments were silica beads of diameter 0.98μm (Bangs Laboratories, Fisher, IN, USA) and 1.16μm (Van't Hoff Laboratory, Utrecht University, Utrecht, Netherlands) for single- and two-point microrheology experiments respectively. A small quantity (below 10^{-3} vol%) was added to each sample before measurements and the sample was then introduced into the sample chamber. The sample chamber consisted of a glass slide and cover slip connected by two strips of double-stick tape (about 75μm thick) and was sealed after loading the sample with grease (Apiezon L) at the open ends. After a bead was trapped, all measurements were performed at a distance of about 20μm from the bottom surface of the sample chamber. The instrument was aligned before each set of experiments and, among other criteria, it was tested that x and y auto-correlation spectra of beads trapped in pure solvent were overlapping. The shear that the solution is exposed to when filling the chamber transiently changes the structure of the sample. To ensure that the samples were completely relaxed and isotropic after the filling procedure and after the probe particle was positioned with the help of the optical trap, particle fluctuations in the directions parallel (x) with and perpendicular (y) to the long axis of the chamber were compared. Averaged auto-correlation spectra of 60 second segments of data typically differed right after filling the chambers, with the x-spectra (in the flow direction) typically showing a higher rms amplitude of motion than the y- spectra, but slowly converged over 5 -15 minutes. After complete relaxation, between 8-16 data sets were recorded for each sample, using different beads (minimum of 3) in different locations of the sample. Data were taken at two different sampling rates, 20 kHz and 195 kHz. At 20 kHz sample rate, the laser power was set low (3 -5mW) to avoid a large effect of the optical trap on the particle fluctuations, at 195 kHz laser power had to be set somewhat higher (15 ~ 30mW) to avoid shot noise at the high-frequency end of the spectrum.

Calibration factors are needed to convert the amplified quadrant diode signals to actual displacements in nanometers. These factors were determined from displacement autocorrelation spectra in water of particles from the same batch as used in the micelle experiments. Auto correlation spectra of particles trapped in a

purely viscous fluid have a Lorentzian shape and from the amplitude of the Lorentzian at high frequencies, calibration factors can be determined if particle size, solvent viscosity and temperature are used as (given) parameters [24]. Three or more particles in water were trapped again 20μm from the glass surface at both the low and high laser power used in the micelle experiments, and their displacement fluctuations were recorded at sampling rates of 20kHz and 195kHz. The variance of the results was around 5%, which is mainly due to particle polydispersity.

4.2.4 Two-particle microrheology (2PMR)

A pair of focused laser beams with wavelengths λ=830 nm (diode laser, CW, IQ1C140, Laser 2000) and λ=1064 nm ($NdVO_4$, see above) (power less than 10mW, measured before coupling into the microscope) was used to weakly trap a pair of silica particles far away from other particles, at several separation distances r between 3 and 20 μm. The x and y position fluctuations of each trapped particles were detected with a pair of quadrant photo diodes, the λ=1064 nm laser was detected as described above, and for the λ = 830 nm we used a standard silicon-type PN photodiode with a reverse bias voltage of 15V (10mm diameter, Spot9-DMI, UDT, Hawthorne, CA).

4.2.5 Data Evaluation

We processed the recorded position fluctuation data off-line to obtain the viscoelastic moduli in a similar manner for both the 1PMR and the 2PMR method. Within linear response a (complex) single- or inter-particle response function $\alpha_{k,l}^{(i,j)}(\omega)$ relates the displacement of each particle in x or y direction $u_k^{(i)}(\omega)$ to the force $F_k^{(i)}(\omega)$ applied to the same particle or to the other one; $u_k^{(i)}(\omega) = \alpha_{k,l}^{(i,j)}(\omega) \times F_{k,l}^{j}(\omega)$, written in Fourier space, where i, j = 1,2 are particles labels, k, l = x, y are coordinate directions and $\omega = 2\pi f$ is the radial frequency. For example, $\alpha_{x,x}^{(1,1)}(\omega)$ is the single-particle response function relating the x-displacement of particle 1 to the force acting on particle 1 in x direction, or $\alpha_{x,x}^{(1,2)}(\omega)$ is the inter-particle response function relating the x-displacement of particle 1 to the force applied to particle 2 in x direction.

For 1PMR we calculate the Fourier transform of the displacement autocorrelation $S_k^{(i)}$ of each particle from the recorded position fluctuations $u_k^i(t)$:

$$S_k^{(i)} = \int \left\langle u_k^i(t) u_k^i(0) \right\rangle e^{i\omega t} dt \quad (1)$$

in all experiments reported here the medium was homogeneous. Thus we calculate an averaged $S_{Auto} = 1/4\left\langle S_x^1 + S_y^1 + S_x^2 + S_y^2 \right\rangle$. We chose the coordinate system such that the *x*-axis is parallel to the line connecting the centers of the two particles and the *y*-axis perpendicular to that.

For 2PMR we calculate the Fourier transforms of the two displacement cross-correlations that are non-zero to first order:

$$S_{\parallel}(\omega) = \int \left\langle u_x^{(1)}(t) u_x^{(2)}(0) \right\rangle e^{i\omega t} dt \quad \text{(parallel to center line)} \quad (2a)$$

$$S_{\perp}(\omega) = \int \left\langle u_y^{(1)}(t) u_y^{(2)}(0) \right\rangle e^{i\omega t} dt \quad \text{(perpendicular to center line)} \quad (2b)$$

From these correlation functions we first obtain the imaginary parts of the complex response functions $\alpha_{Auto}(\omega) = \alpha'_{Auto}(\omega) + \alpha''_{Auto}(\omega)$ and $\alpha_{\parallel,\perp}(\omega) = \alpha'_{\parallel,\perp}(\omega) + \alpha''_{\parallel,\perp}(\omega)$, which, in thermal equilibrium and in the absence of external forces, are related to the correlation functions by the fluctuation-dissipation theorem [9]:

$$\alpha''_{Auto}(\omega) = \frac{\omega}{2k_B T} S_{Auto}(\omega) \quad \text{and} \quad \alpha''_{\parallel,\perp}(\omega) = \frac{\omega}{2k_B T} S_{\parallel,\perp}(\omega) \ , \quad (3)$$

where $k_B T$ is the thermal energy.

The real parts of the response functions are then computed by a Kramers-Kronig integral over the imaginary parts:

$$\alpha_{auto}' = \frac{2}{\pi} \int_0^\infty \frac{\zeta \alpha_{auto}''(\omega)}{\omega^2 + \zeta^2} d\zeta \quad \text{and} \quad \alpha_{\parallel,\perp}' = \frac{2}{\pi} \int_0^\infty \frac{\zeta \alpha_{\parallel,\perp}''(\omega)}{\omega^2 + \zeta^2} d\zeta \ . \quad (4)$$

In principle, there is a systematic error expected for α' due to the finite integration limits in the KK-integral [8]. This error is here generally negligible when we sample at 195kHz. Since the error is in α' it will be more apparent in samples with large G'. In the data presented here, the maximum G_0 = 10 Pa where we can still neglect the effect. However, for stiffer samples a small error will arise in α'.

So far we have calculated response properties of the particles. These are determined by the viscoelastic properties of the embedding medium via generalized Stokes-Einstein relationships [8, 15]:

$$\alpha_{auto}(\omega) = \frac{1}{6\pi R G(\omega)} \ , \quad \alpha_{\parallel}(\omega) = \frac{1}{4\pi r G(\omega)} \quad \text{and} \quad \alpha_{\perp}(\omega) = \frac{1}{8\pi r G(\omega)} \quad (5)$$

where $G(\omega)$ is the complex shear modulus, R is the particle radius, and r is the separation distance between the two particles. While both the parallel and the perpendicular inter-particle response can be used to determine $G(\omega)$ in 2PMR, we find experimentally that the perpendicular channel is noisier than the parallel one. Furthermore, at higher frequencies solvent inertia becomes visible and the effect is larger on the perpendicular channel [25]. We thus present in the following the data measured by the parallel inter-particle response function as the 2PMR results.

The optical traps limit the Brownian motion of the particles and have an effect on the storage modulus calculated from the fluctuation data if not corrected for [26]. The response functions $\alpha'(\omega)$ and $\alpha''(\omega)$, were corrected for the trap effect before calculating $G(\omega)$ as described elsewhere [26]. For the lower sampling rate (20 kHz, laser power ≤ 5mW) the trap effect was negligible for all micelle concentrations except for 0.5 wt%, where the correction amounted to decrease of $G'(\omega)$ of 50% at 5 Hz up to less than 1% at 1kHz. Heating of the samples in the trap focus is negligible because of the low laser power [27].

4.3 Results and Discussion

Figure 1 shows a comparison of complex shear moduli measured with mechanical macrorheology and with microrheology. $G'(\omega)$ and $G''(\omega)$ curves are shifted vertically for clarity. Surfactant concentrations were c_p = 0.5, 1, 2 and 4 wt. %. 2PMR and 1PMR data were taken simultaneously as described above, averaging over x and y fluctuations of both particles (four independent data sets) over a total recording time of 200 to 300 seconds gives relatively smooth curves for 1PMR.

In 2PMR curves are clearly more noisy because there is just one independent data set for each recording (parallel direction) and the amplitude of the cross-correlation is smaller than the amplitude of the auto-correlation and decays as $1/r$. With increasing micelle concentration storage and loss moduli show a trend expected for an increasingly elastic polymer network [28]. There is disagreement between macro and microrheology data at frequencies <1Hz (panels B and D). This is most likely due to small errors in the trap correction, which becomes dominant at the lowest frequencies in $G'(\omega)$.

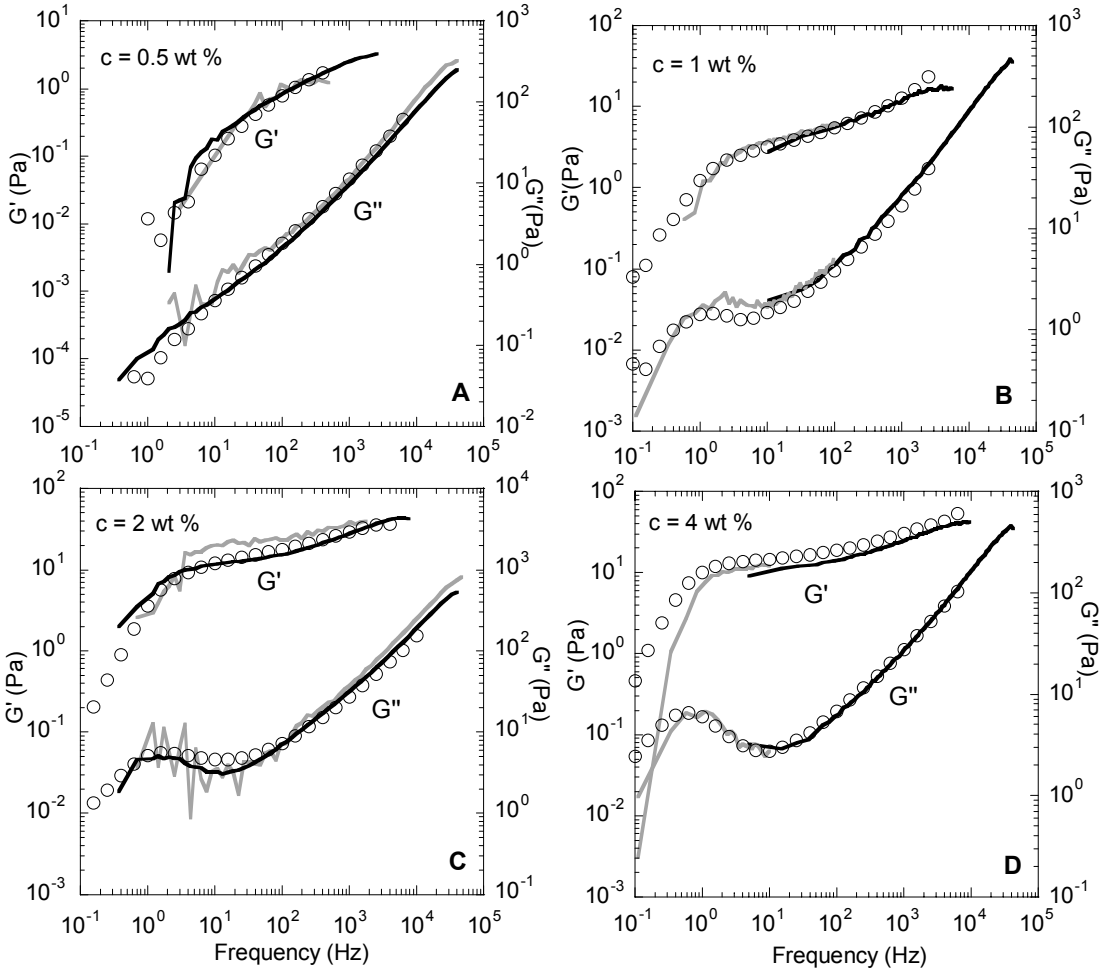

Figure 1: The loss modulus (right axes) and elastic modulus (left axes) for four surfactant concentrations 0.5 (A), 1(B), 2(C) and 4(D) wt% are plotted as a function of frequency. Curves are in (A) and (C): macrorheology (circles), 1PMR (black lines) and 2PMR (gray lines) in 0.5 and 2wt%; in (B) and (D): 1PMR with 20 kHz sampling rate (gray line) and 1PMR with 195 kHz sampling rate (black lines). All microrheology data were logarithmically binned with the factor of 1.2 relating the widths of successive bins.

Agreement between all three techniques quantitatively validates the new microrheology methods. It is theoretically expected when certain criteria are met. First, the micelle solution must be homogeneous on the scale of the particle size. Second, the particle should not perturb the local environment in which it moves on a scale comparable to its own size. When the particle size is much larger than any network length scale such as the mesh size or the polymer persistence length, as is the case here, this criterion will be met. In semiflexible polymer systems this is not the case and discrepancies have been found between 1PMR and 2PMR [29,30]. Third, there should be a non-slip boundary condition between the micelles and the particle surface. Particularly at elevated frequencies viscous coupling is expected to ensure non-slip boundary conditions. Our results demonstrate that for the wormlike micelle solutions studied all criteria were satisfied. In particular, the good agreement between one- and two-particle microrheology demonstrates that local perturbations around the probes such as depletion, enrichment or slip boundary conditions did not occur to a measurable degree. Our results here are in contrast to what has been claimed for polystyrene solutions [31].

In 2PMR one expects a minimal distance between two particles where approximation of a homogeneous medium and a Stokes flow field would cease to be valid. The distance which this corresponds to is the larger of either particle size or internal length scales of the system. Here we did not observe any deviations from $1/r$ scaling in 2PMR results down to a distance of 4 μm, for the D = 1.16 μm particles [32].

Previous work using diffusing wave spectroscopy (DWS) had found agreement between that implementation of microrheology and conventional macrorheology in polymer and emulsion systems at low frequencies [5, 6]. However, the range of comparison was severely restricted (< 20Hz) due to the limitations of the mechanical rheology.

4.4 Conclusions

We have verified that there is excellent agreement between mechanical rheology probing a sample at macroscopic scales and one- and two particle microrheology

experiments up to high frequencies. With a piezo-actuated mechanical rheometer we could extend the range for comparison to 10 kHz, much above what has been achievable with commercial rheometers. The system chosen for the comparison, worm-like micelles in high salt concentrations, has strongly screened electrostatic interactions and structural length scales much smaller than the particle size. We have shown here that in such a system microrheology and in particular the relatively simple one-particle technique is sufficient to probe the bulk rheological properties of the medium. These results should now make it possible to use the advantages of microrheology, such as small sample size, high bandwidth and high sensitivity, to quantitatively study a variety of systems.

4.5 Acknowledgements

We thank J.F. Berret, M.E. Cates, P. Bartlett, L. Starrs. F.C. Mackintosh and A. Levine for helpful discussions and E. Peterman, J. van Mameren, and G. Koenderink for technical help. This work was supported by the Foundation for Fundamental Research on Matter (FOM).

4.6 REFERENCES

[1] MacKintosh, F. C.; Schmidt, C. F. Curr. Opin. Colloid Interf. Sci. 1999, 4, 300-307.

[2] Ashkin, A. Proc. Natl. Acad. Sci. U. S. A. 1997, 94, 4853-4860.

[3] Chen, D. T.; Weeks, E. R.; Crocker, J. C.; Islam, M. F.; Verma, R.; Gruber, J.; Levine, A. J.; Lubensky, T. C.; Yodh, A. G. Physical Review Letters 2003, 90.

[4] Rehage, H.; Hoffmann, H. J. Phys. Chem. 1988, 92, 4712-4719.

[5] Mason, T. G.; Weitz, D. A. Phys. Rev. Lett. 1995, 75, 2770-2773.

[6] Cardinaux, F.; Cipelletti, L.; Scheffold, F.; Schurtenberger, P. Europhysics Letters 2002, 57, 738-744.

[7] Mason, T. G.; Ganesan, K.; Zanten, J. H. v.; Wirtz, D.; Kuo, S. C. Phys. Rev. Lett. 1997, 79, 3282-3285.

[8] Schnurr, B.; Gittes, F.; MacKintosh, F. C.; Schmidt, C. F. Macromolecules 1997, 30, 7781-7792.

[9] Landau, L. D.; Lifshitz, E. M.; Kosevich, A. M.; Pitaevskii, L. P. Theory of Elasticity, 3rd. english ed.; Pergamon Press: Oxford, 1986.

[10] Chaikin, P. M.; Lubensky, T. Principles of Condensed Matter; Cambridge University Press: Cambridge, 1994.

[11] Mason, T. G. Rheologica Acta 2000, 39, 371-378.

[12] Bird, R. B.; Armstrong, R. C.; Hassager, O. Dynamics of Polymeric Liquids; John Wiley and Sons: New York, 1977.

[13] Crocker, J. C.; Valentine, M. T.; Weeks, E. R.; Gisler, T.; Kaplan, P. D.; Yodh, A. G.; Weitz, D. A. Phys. Rev. Lett. 2000, 85, 888-891.

[14] Starrs, L.; Bartlett, P. Faraday Discussions 2003, 123, 323-334.

[15] Levine, A. J.; Lubensky, T. C. Phys. Rev. Lett. 2000, 85, 1774-1777.

[16] Levine, A. J.; Lubensky, T. C. Physical Review E 2002, 65.

[17] Xu, J.; Palmer, A.; Wirtz, D. Macromolecules 1998, 31, 6486-6492.

[18] M. Atakhorrami et al. not published. **(Chapter 2)**

[19] Walker, L. M. Current Opin. Colloid Interf. Sci. 2001, 6, 451-456.

[20] Berret, J. F.; Appell, J.; Porte, G. Langmuir 1993, 9, 2851-2854.

[21] Ferry, J. D. Viscoelastic properties of polymers, 3d ed ed.; Wiley: New York, 1980.

[22] P. Hebraud; F. Lequeux; Palierne, a. J. F. Langmuir 2000, 16, 8296.

[23] Peterman, E. J. G.; van Dijk, M. A.; Kapitein, L. C.; Schmidt, C. F. Review of Scientific Instruments 2003, 74, 3246-3249.

[24] Gittes, F.; Schmidt, C. F. In Methods in Cell Biology; Academic Press, 1998; Vol. 55, pp 129-156.

[25] M. Atakhorrami, G.H. Koenderink, C.F. Schmidt, F. C. MacKintosh. Phys.Rev.Lett. 2005, 95, 208302. **(Chapter 9)**

[26] M. Atakhorrami; J. Kwiecinska; Karim M. Addas; G.H. Koenderink; Alex Levine; F.C. MacKintosh; Schmidt, a. C. F. submitted to Phys.Rev.E.**(Chapter 3)**

[27] Peterman, E. J. G.; Gittes, F.; Schmidt, C. F. Biophysical Journal 2003, 84, 1308-1316.

[28] M.Buchanan; M.Atakhorrami; J.F.Palierne; and, F. C. M.; C.F.Schmidt. Phys. Rev. E 2005, 72, 011504.**(Chapter 5)**

[29] Gardel, M. L.; Valentine, M. T.; Crocker, J. C.; Bausch, A. R.; Weitz, D. A. Phys. Rev. Lett. 2003, 91, 158302.

[30] Koenderink, G. H.; Atakhorrami, M.; MacKintosh, F. C.; Schmidt, C. F. submitted to Phys.Rev.Letters 2005. **(Chapter 7)**

[31] Starrs, L.; Bartlett, P. Journal of Physics-Condensed Matter 2003, 15, S251-S256.

[32] Atakhorrami, M.; Schmidt, C. F. (in print) Rheologica Acta. **(Chapter 6)**

Chapter 5

High-frequency microrheology of wormlike micelles

Abstract

We have measured the frequency-dependent shear modulus of entangled solutions of wormlike micelles by high-frequency microrheology and have compared the results with those from macrorheology experiments done on the same samples. Using optical microrheology based on laser interferometry we have measured loss and storage moduli over six decades in frequency up to about 100kHz. We present data over a decade in concentration in the entangled regime and find good agreement between micro- and macrorheology, thus validating recently developed microrheology techniques. By collapsing data for different concentrations, we furthermore determine both the concentration scaling of the plateau modulus and a power-law exponent of the complex shear modulus at high frequencies.

5.1 Introduction

Microrheology is a powerful new technique for studying the viscoelastic properties of complex fluids and soft materials with high bandwidth and spatial resolution [1-8].To determine the viscoelastic behavior of a particular system using this technique one must employ a number of assumptions and subtle physical approximations in evaluating the data. Until now a rigorous comparison between established conventional rheology and microrheology on a stable, well known system has been lacking. Here we set out to provide such a comparison using entangled solutions of wormlike micelles.

Microrheology techniques are based on tracking the motions of micron-sized probe particles embedded in the system to be studied. Variations of the technique include active and passive methods, as well as single- and multiple-particle methods [8]. In the passive methods, such as the one applied here, the fluctuation-dissipation theorem of linear response theory [9] is used to extract viscoelastic parameters [5,6,8,10] of the material from the thermal equilibrium fluctuations of the embedded particles. In contrast to typical macroscopic mechanical rheology, no strain is applied to the material during the measurement, and linear response parameters can be measured directly without extrapolation. This is particularly useful in soft materials and complex fluids where even a small imposed strain can cause reorganization of structure within the material and thus change its viscoelastic properties (*e.g.* strain hardening or shear thinning). Furthermore, when using micron-sized probes, probe and solvent inertial effects are largely negligible up to frequencies of ~100kHz. Microrheology thus achieves a bandwidth far beyond that of conventional macroscopic rheometers, with the exception of specialized designs, such as ones using resonant probes [11,12] or the instrument we use here for comparison, which is based on piezoelectric actuators and reaches 10kHz [13].

In contrast to common instruments such as plate-and-cone rheometers, there is no constant-volume constraint on the medium around the probe in microrheology. Therefore the probe motions can couple to pure shear modes as well as to compressional modes. This opens a new window to study the latter in complex fluids, but it also complicates the comparison with macrorheology, especially at low

frequencies. If the material studied is a polymer solution, the viscoelastic response measured by microrheology will asymptotically approach pure shear response due to the viscous coupling of polymer to solvent at higher frequencies [6,14 -16].

The thermal motion of a single particle reflects the viscoelastic properties of its environment on roughly the scale of the probe particle radius since this is the length scale on which the strain-field around the particle decays [6,17]. This sets the spatial resolution of the method and therefore results in micrometer resolution for micrometer particles. Ideally one wants to measure material properties that are not perturbed by the presence of the probe particle itself. From the preceding argument it is evident that this will not be the case if the particle perturbs the medium on a length scale comparable to its radius. The probe can influence the material near its surface in several ways, *e.g.* by physical *entropic* depletion or by chemical or electrostatic interaction with the material. How deep into the material such a perturbation propagates depends on the characteristic length scales of the material in relation to the probe size. If the probe particle is smaller than material scales (such as polymer persistence length, contour length, Debye length etc.), perturbations will decay over a distance of order the probe size and true bulk properties are not measured. If all material scales are smaller than the particle, surface effects should be negligible. Biopolymer solutions and gels made of, for example, filamentous actin [6,7], DNA [18], or polysaccharides [7] typically have intrinsic length scales as large as a micrometer. In this case it may be insufficient to analyze the fluctuations of an isolated probe particle. A way to avoid probe effects and determine the bulk viscoelastic behavior in these cases is to measure the correlated fluctuations of pairs of particles separated by more than the relevant material length scales (two-particle microrheology) [7,19]. In this study we have selected a system with small characteristic length scales, so that single-particle microrheology should not be influenced by local surface effects.

The polymer system studied here was an entangled solution of wormlike micelles. Wormlike micelles are cylindrical assemblies of amphiphilic molecules that form spontaneously in aqueous solutions at particular concentrations and temperature conditions. Their properties have been well studied, both experimentally and theoretically [20-22]. We have used cetylpyridinium chloride

(CPyCl) as the surfactant and sodium salicylate (NaSal) as a strongly-binding counter ion. The wormlike micelles formed in this system have a diameter of 2-3nm, contour lengths of 100nm-1μm and a persistence length of order 10nm [20]. At the concentrations we used (1-8wt%), the mesh size varies from about 30 to 10nm [22]. Despite their rather exotic structure and dynamics, wormlike micelles exhibit well defined rheological properties, similar to those of covalently linked linear polymers. When entangled wormlike micelles are sheared, relaxation of stress occurs via reptation and scission [23]. Both processes, occurring simultaneously, lead to a single dominating relaxation time being observed. Systems with one relaxation time are known as Maxwell fluids and have been studied extensively [22,24]. In general, studies performed on wormlike micelles have focused on low-frequency properties where the simple mechanical analogue, the Maxwell model, consisting of a dashpot and a spring in series, can be used to model the viscoelastic response. Higher frequency rheology has been performed on micelle systems confirming the Maxwell regime at somewhat elevated frequencies [25,26].

We have chosen wormlike micelle solutions as a model system to quantitatively test the underlying principles of microrheology and to provide a benchmark performance test. Specifically, we have performed detailed comparisons between single particle microrheology and a macroscopic technique using a piezorheometer [13] over a frequency range from 0.1Hz to about 10kHz. We have performed experiments with both techniques for micelle solutions covering a range of shear moduli ranging from 1Pa to 200Pa at low-frequency. Our results demonstrate excellent agreement between the two techniques and make a strong case for the validity of single-particle microrheology for soft materials with intrinsic length scales below the probe size. At high frequencies the (single relaxation time) Maxwell model does not apply anymore and internal micelle dynamics become important, presenting a continuous spectrum of relaxation times. We introduce simple scaling arguments to interpret the high-frequency dynamic properties of micelle solutions in a regime where collective network dynamics cross over to single filament dynamics.

This paper is organized as follows. In section 2, we present the theoretical background and cover some fundamental aspects of microrheology and data

evaluation. In section 3 we outline the experimental procedure, sample preparation, and how data is collected and analyzed. In section 4 we present our results, comparing microrheology and macrorheology and investigating the scaling behavior of the shear moduli at high and low frequencies. In section 5 we discuss the results.

5.2 Theoretical background

In optical microrheology, the complex viscoelastic modulus, $G = G' + iG''$ can be obtained from direct measurement of the displacement fluctuations of micrometer size dielectric particles [2,5,6]. By relying on fundamental principles such as the fluctuation-dissipation theorem [9,27], one can in many cases obtain the frequency-dependent shear modulus G of materials in this way. In a general viscoelastic material, the position x of an embedded particle is related, within the linear regime, to the applied force f by a response function α via $x_\omega = \alpha(\omega) f_\omega$. Here, the various quantities represent complex Fourier transforms, and thus depend on frequency ω. In particular, the response function itself is complex, exhibiting both storage (elastic-like) and loss (dissipative or viscous-like) character for viscoelastic materials.

In the absence of any externally applied forces, random thermal or Brownian forces will give rise to fluctuations of the particle position. These fluctuations are fundamentally related to the temperature of the system and the response function or compliance α via the fluctuation-dissipation theorem [9,27]. One common expression of the (classical) fluctuation-dissipation theorem relates the power-spectral-density (PSD) $\left\langle |x_\omega|^2 \right\rangle$ of particle fluctuations to the imaginary part of the response function $\alpha'' = \mathrm{Im}(\alpha)$:

$$\left\langle |x_\omega|^2 \right\rangle = \frac{2kT}{\omega} \alpha''(\omega) . \qquad (1)$$

In our experiments, we measure the power spectral density (PSD) of the displacement fluctuations, which is then directly used to determine the imaginary response function, as shown above. In addition to the fluctuation-dissipation theorem, linear response theory also shows that the real and imaginary parts of the response function α can be obtained from each other. Specifically, provided that the PSD, and thus $\alpha''(\omega)$, can be determined over a wide frequency range, it is possible to determine the real part $\alpha'(\omega)$ using a Kramer-Kronig relation

$$\alpha'(\omega) = \frac{2}{\pi}\int_0^\infty \frac{\xi\,\alpha''(\xi)}{\omega^2 + \xi^2} d\xi \,. \tag{2}$$

We use numerical integration to obtain the real part of the compliance, and thus the full, complex α. In an incompressible, linear viscoelastic medium, the geometry-dependent compliance is related to the complex shear modulus $G(\omega) = G'(\omega) + iG''(\omega)$ of the embedding medium via [5,6]

$$G(\omega) = \frac{1}{6\pi R\alpha(\omega)} \tag{3}$$

In principle, the integral in the Kramers-Kronig relation above must be performed out to infinite frequency. In practice, however, one has only a finite data set for the PSD, and thus $\alpha''(\omega)$. Due to the finite range of the KK integral $\alpha'(\omega)$ will be slightly underestimated. By evaluating the integral above assuming $\alpha''(\omega)$ continues to infinity with a slope of -1 (*i.e.*, as for a simple viscous liquid), we can obtain an analytic correction. Although not necessarily physically correct, it allows us to estimate how much of an effect the finite data set has. Specifically, we assume that $\alpha''(\omega)$ continues from the Nyquist frequency ω_N with a slope of -1. Thus, $\alpha''(\omega) = \alpha''_N\,\omega_N / \omega$ where numerator is determined from the data. By integrating this part from ω_N to infinity one obtains a frequency-dependent correction of $\alpha'(\omega)$.

$$\alpha'_c(\omega) = -\frac{\alpha''_N\,\omega_N}{\omega}\ln\left|\frac{\omega_N - \omega}{\omega_N + \omega}\right| \tag{4}$$

This correction may lead to underestimate of both $G'(\omega)$ and $G''(\omega)$ for the higher concentration data where the correction is large (see Figure 4). If high accuracy is desired in this range, data should be taken at high sampling rates at the cost of large memory usage. In an incompressible medium, the response function is related to the (complex) shear modulus G by the Generalized Stokes-Einstein relation in Eq. (3).

Using this we can extract the storage and loss moduli $G'(\omega)$ and $G''(\omega)$ from the response functions $\alpha'(\omega)$ and $\alpha''(\omega)$, via

$$G'(\omega) = \frac{1}{6\pi R}\left(\frac{\alpha'(\omega)}{\alpha'(\omega)^2 + \alpha''(\omega)^2}\right) \tag{5}$$

and

$$G''(\omega) = \frac{1}{6\pi R}\left(\frac{-\alpha''(\omega)}{\alpha'(\omega)^2 + \alpha''(\omega)^2}\right) \tag{6}$$

5.3 Experimental Methods

5.3.1 Materials

Wormlike micelles were prepared from the surfactant cetylpyridinium chloride (CPyCl) dissolved in brine (0.5M NaCl) with strongly binding counterions, sodium salicylate (NaSal). Chemicals were obtained from Sigma Chemical Co.(Sigma-Aldrich Chemie B.V. Zwijndrecht, The Netherlands). In this study all samples have a molar ratio Sal/CPy = 0.5. A tiny quantity, below 10^{-3} *vol* %, of silica particles with a diameter of 0.98 μm (Bangs Laboratories, Fishers, IN, USA) was added to each sample before measurement. The micellar solutions were stored at (controlled) ambient temperature (between 21.5 and 22.0°C) which was above the Krafft point of this system.

5.3.2 Macrorheology

A custom-built piezorheometer [13] was used to measure the viscous and elastic shear moduli of wormlike micelle samples prepared in parallel with the ones used for microrheology. Details of this technique can be found in the literature [28]. Briefly, samples are contained between two glass plates mounted horizontally between two piezoelectric ceramics. One of the plates is sinusoidally oscillated with a vertical amplitude of about 1 nm. This movement squeezes the sample and causes mainly shear strain with some extensional flow in the very center of the sample. The vertical stress transmitted to the second plate is measured by the other piezoelectric element. The imposed strain is extremely small so that the sample structure is not altered by the flow. This instrument allowed us to measure the storage (G') and loss (G'') shear modulus for frequencies ranging from 0.1Hz to 10kHz. The temperatures at which we measured were 21.8°C for c_p = 1 and 2%, 22.4°C for c_p = 4%, 22.6°C for c_p = 5 and 8%, and 22.0°C for c_p = 6%. The set-up was hermetically sealed to avoid evaporation.

5.3.3 Microrheology

All microrheology experiments were performed on a custom-built optical microscope equipped with differential interference contrast optics and with optical traps essentially as described earlier [6,29]. Briefly, an infrared laser (λ = 1064nm, $NdVO_4$, COMPASS, Coherent, Santa Clara, CA, USA) was coupled into the sample via the microscope objective lens (Zeiss, Neofluar, 100X, NA = 1.3) with immersion oil (n_{oil} =1.5, Cargille LTD, Cedar Grove, NJ, USA) and used to trap particles. A quadrant photodiode (YAG444-4A, Perkin Elmer, Vaudreuil, Canada) was used to measure the lateral (x and y) displacements of the trapped particle relative to the laser focus by back-focal-plane interferometry [30]. In this detection scheme the backfocal plane of the condenser (Zeiss, NA = 1.4, oil) collecting the laser light after the interaction with the probe particle is imaged onto the quadrant photodiode. The diode current signals are amplified by a low-noise analog differential amplifier (custom built), then digitized with a 200 kHz A/D board (AD16 board on a ChicoPlus PC-card, Innovative Integration, Simi Valley, CA, USA) and processed and stored on hard disk using Labview (National Instruments, Austin, Texas, USA). Time-series data was stored and later (off-line) calibrated to displacement in nm as described below, using independently measured calibration factors from particles trapped in water samples. We can track particle motions with a bandwidth of about 100 kHz in our set-up [31].

The laboratory temperature was stabilized to between 21.5 and 22.0°C. Micelle samples were doped with silica particles as described above and then introduced into a sample chamber. Sample chambers were assembled of a microscope slide and a coverslip separated by spacers of double-stick tape and sealed with grease (Apiezon L, M&I Materials Ltd, Manchester, UK.). The inner height of the sample chambers was about 70μm. Probe particles were trapped and were moved to about 20μm above the glass surface. In order to ensure that the samples were completely relaxed and isotropic after the filling procedure and the probe positioning, x- (aligned with the long axis of the chamber) and y-fluctuations were measured, and averaged power spectral densities (PSD) of 60 second segments of data were obtained. The instrument was aligned before each set of experiments and, among other criteria, it was tested that x and y PSDs of beads trapped in pure

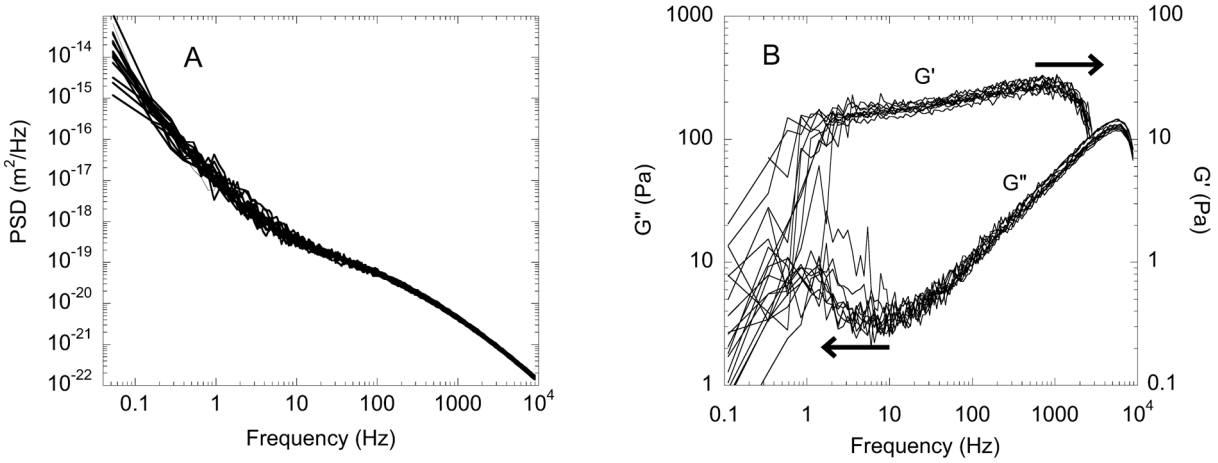

Figure 1: Power spectral densities (PSD) of thermal bead motion in a wormlike micelle solution (A), and storage (*G′*) and loss (*G′′*) modulus of the solution derived from the PSDs (B). The scatter in amplitude and shape of the curves illustrates reproducibility for 16 different runs using 3 different beads (d = 0.98 μm) in the same sample (c_p = 4). The vertical axes for *G′* and *G′′* in (B) are shifted apart for visibility.

solvent were overlapping. Immediately after manipulating the wormlike micelles samples, x and y PSDs were not overlapping, with the x-spectra (in the flow direction) typically showing a higher rms amplitude of motion than the y-spectra, due to shear-induced structural changes in the solutions. After typically about 15 minutes, PSDs overlapped and we used this as a criterion that the samples had come to equilibrium.

For each sample, once they had fully relaxed, we obtained between 8-16 data sets. Each data file was about 5MB. In most samples 8 data sets were sufficient, however in the high concentration samples up to 16 runs were required to obtain better averaging and to reduce noise in the data. For each sample we measured at two different sample frequencies. Careful attention was paid to checking for anisotropic behavior (difference in x and y PSDs) that occasionally occurred due to the movement of small air bubbles or a leak in the chamber. Data sets that showed anisotropic behavior were eliminated. Figure 1 shows a typical set of data to illustrate reproducibility from run to run with different beads. PSDs were then

averaged for all beads in the sample and for x- and y-directions, before shear elastic parameters were calculated.

Data were taken at two sample rates in order to cover maximum bandwidth. To capture the low-frequency end of the spectrum, we sampled at 20kHz and recorded for 60s (0.1 to 10kHz bandwidth). In order to minimize the elastic contribution from the trap we used a low laser power of ~3mW which gave a trap stiffness of 1.6pN/nm (measured in buffer), resulting in an apparent added constant of G' ~ 0.1Pa in the final result for the shear moduli. The trap effect was corrected for by subtracting this constant [32] . At the high sampling rate of 195kHz a higher power of ~30mW was required to avoid shot noise, which resulted in a correction of G' ~ 1Pa. Shot noise is visible as a *turning-up* of the PSD at high frequencies. At both high and low laser powers heating of the sample due to the laser was estimated to be less than 1°C and therefore considered negligible [33]. Time series data was further processed off-line on a PC, using LabView software to obtain real and imaginary part of the complex shear modulus of the wormlike micelle solutions according to equations 5 and 6. Final results wear smoothed by logarithmic binning with a factor of 1.05 relating the widths of successive bins. Data was thus averaged into N bins where N is determined by the algorithm $N= \log_{1.05}(n/100)$ where n is the total number of data points before binning.

Calibration factors to convert stored voltage time-series data to actual displacement time series were determined from measurements of the PSDs of the same beads as used in the wormlike micelle experiments in water. PSDs of beads trapped in a purely viscous fluid have a Lorentzian shape and from the amplitude of the Lorentzian at high frequencies, calibration factors can be determined if bead size, solvent viscosity and temperature are used as (given) parameters [34]. Silica beads in water were trapped 20μm from the glass surface at both the low and high laser power used in the micelle experiments, and their displacement fluctuations were measured at sampling rates of 20kHz and 195kHz respectively. Typically the x- and y- position components of three or more particles were measured and an average PSD was obtained [34]. The variance on these runs is approximately 5% which is likely mainly due to bead polydispersity (compare with Figure 1).

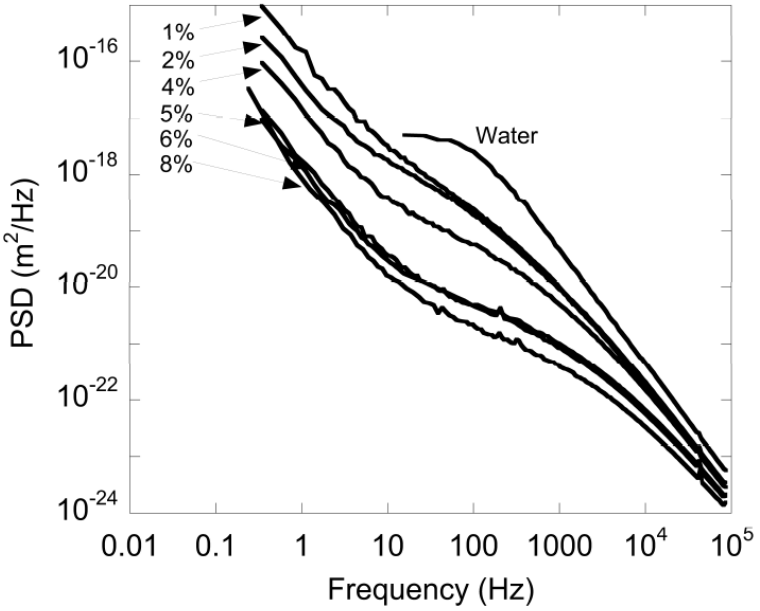

Figure 2: Power spectral densities of displacement fluctuations for 0.98μm diameter beads in water and in wormlike micelle solutions of concentrations, c_p = 2, 4, 6 and 8wt%. PSDs are each an average of 8 spectra recorded from 3 different beads in the respective sample, smoothed by logarithmic binning. Data were taken for each concentration at 20kHz and at 195kHz sampling rates and were merged for each concentration.

5.4 Results

Microrheology experiments on flexible wormlike micelles were performed in the semidilute regime ($c > c^* \sim 0.3$ wt%) where the micelles are entangled. The entanglement length has been reported to vary between 30 and 10nm for c_P = 1 to 8wt% respectively [22].

5.4.1 Comparing Microrheology and Macrorheology

Figure 2 shows the PSDs for water and wormlike micelle solutions at c_P = 1, 2, 4, 5, 6 and 8wt%. Following the procedure outlined above real and imaginary parts of the complex compliance were determined by use of a Kramers-Kronig integral [9]. Frequency-dependent viscoelastic moduli were then calculated from the compliance and corrected for the trapping effect as described. Figure 3 shows the effect of correcting the compliance for the finite high-frequency cut-off of the Kramers-Kronig integral on the final results for the shear elastic moduli, G' and G'', as described above. Gray lines are uncorrected and black lines are corrected storage and loss moduli for concentrations c_P = 2, 5 and 8wt%. At high concentrations and low sampling rates the correction is significant, while at high sampling rates it is minor. In the following, only corrected curves are presented. Shear moduli obtained from the fluctuation analysis of 0.98μm diameter beads, averaged over about 3 beads in each case, and macrorheology data obtained with the piezorheometer are presented in Figure 4 for micelle concentrations c_P = 1, 2, 4, 5, 6, 8wt%. Each panel shows a comparison between shear elastic moduli, derived from macrorheology (symbols) and microrheology (lines) for three concentrations. Storage moduli, G', are plotted on the left, and loss moduli, G'', on the right. Microrheology data were taken at two different sampling rates: 195kHz (solid lines) and 20kHz (dashed line).

Over a large range of concentrations excellent agreement between microrheology and macrorheology is observed. For the microrheology data the low frequency data is taken at a lower sampling frequency and lower power allowing us access to the lower frequency range. Due to the extended time required for these runs and the increase in noise in the data it is important to verify an overlap of data with the high sampling rate data. In our data excellent agreement over a decade in

the mid-range frequency region between high and low sampling rate runs is observed.

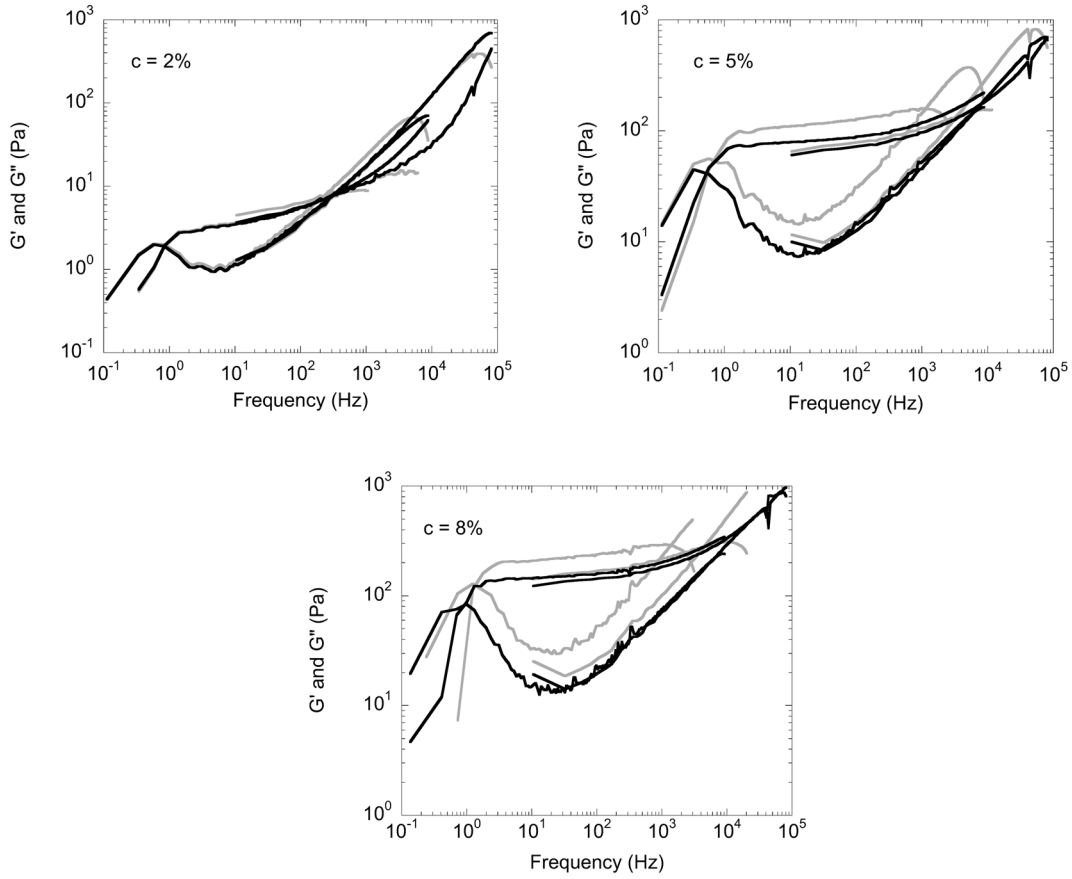

Figure 3: Comparison of complex shear moduli of wormlike micelle solutions of concentrations c_P = 2, 5 and 8wt%, uncorrected (gray lines) and corrected (black lines) for the finite high-frequency cut-off of the Kramers-Kronig integral. Moduli were measured by microrheology with probe particles of 0.98μm diameter at 20kHz and at 195kHz sampling rates. The correction effect is more pronounced for low sampling rates and high concentrations. Data curves are averages of 8 spectra recorded from 3 different beads in each case, smoothed by logarithmic binning.

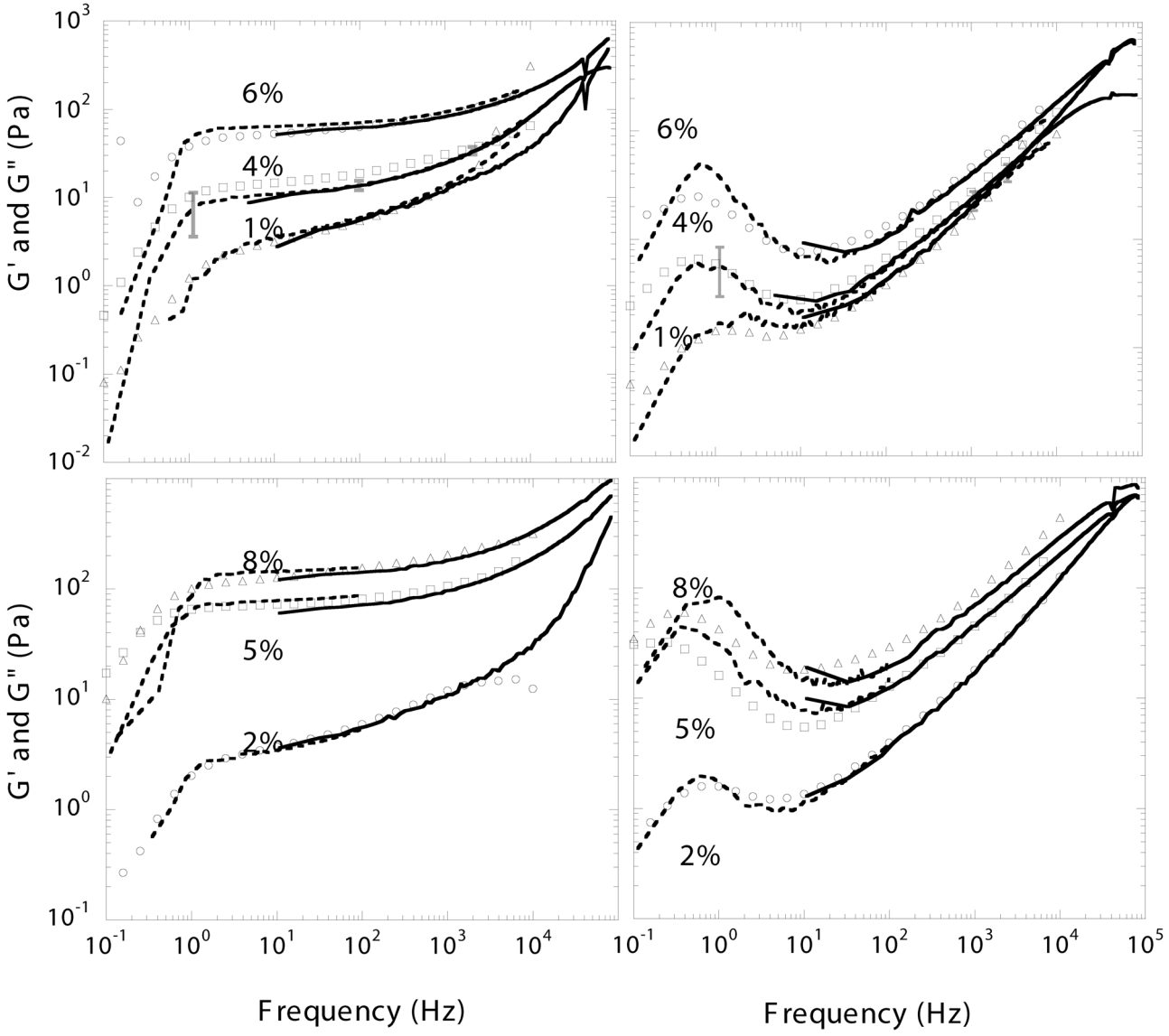

Figure 4: Complex shear moduli (G' on the left, G'' on the right) for wormlike micelle solutions of concentrations c_P= 1, 2, 4, 5, 6 and 8wt% as labeled in the plots. Lines are microrheology results with probe particles of 0.98μm diameter (solid line 195kHz sampling rate, dashed line 20kHz sampling rate). Data was averaged from 8 recorded spectra from 3 different beads, smoothed by logarithmic binning. Symbols are macrorheology results obtained with the piezorheometer.

5.4.2 Scaling behavior and high-frequency viscoelasticity

Maxwell behavior in the low-frequency regime for viscoelastic fluids is usually demonstrated in a Cole-Cole plot of normalized loss modulus plotted against normalized storage modulus (Figure 5). With a single relaxation time τ, the moduli become: $G(\omega) = i\omega\nu_0 / (1 + i\omega\tau)$ where the zero time shear modulus is $G_\infty = \nu_0 / \tau$, which will result in a half-circle with radius 0.5 in the Cole-Cole plot. Our data demonstrate this behavior (see Figure 5) at the low-frequency end of the moduli. The relaxation times can be determined from the crossovers of *G′* and *G′′* in Figure 6.

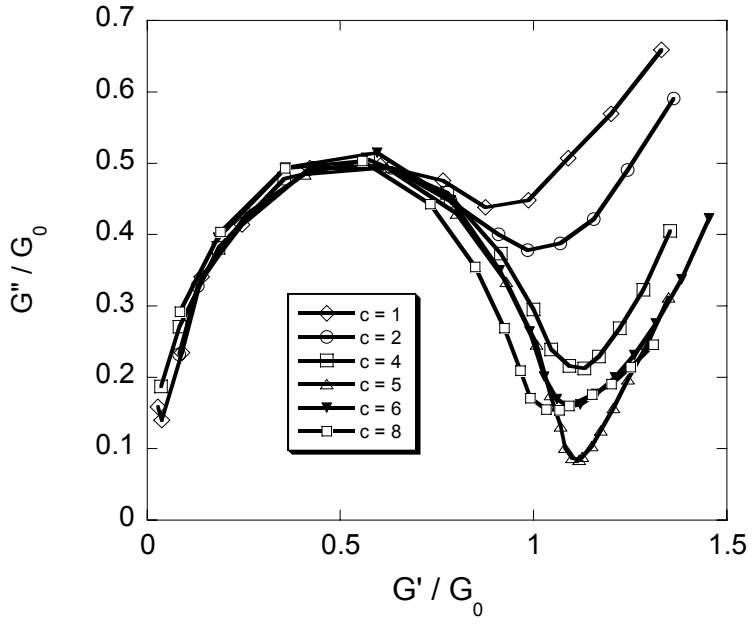

Figure 5: Cole-Cole plot of normalized viscous modulus against normalized elastic modulus for wormlike micelle solutions of concentrations cp = 1, 2, 4, 5, 6 and 8 wt%, measured with the piezorheometer on macroscopic samples. Data curves follow Maxwell behavior at low frequencies.

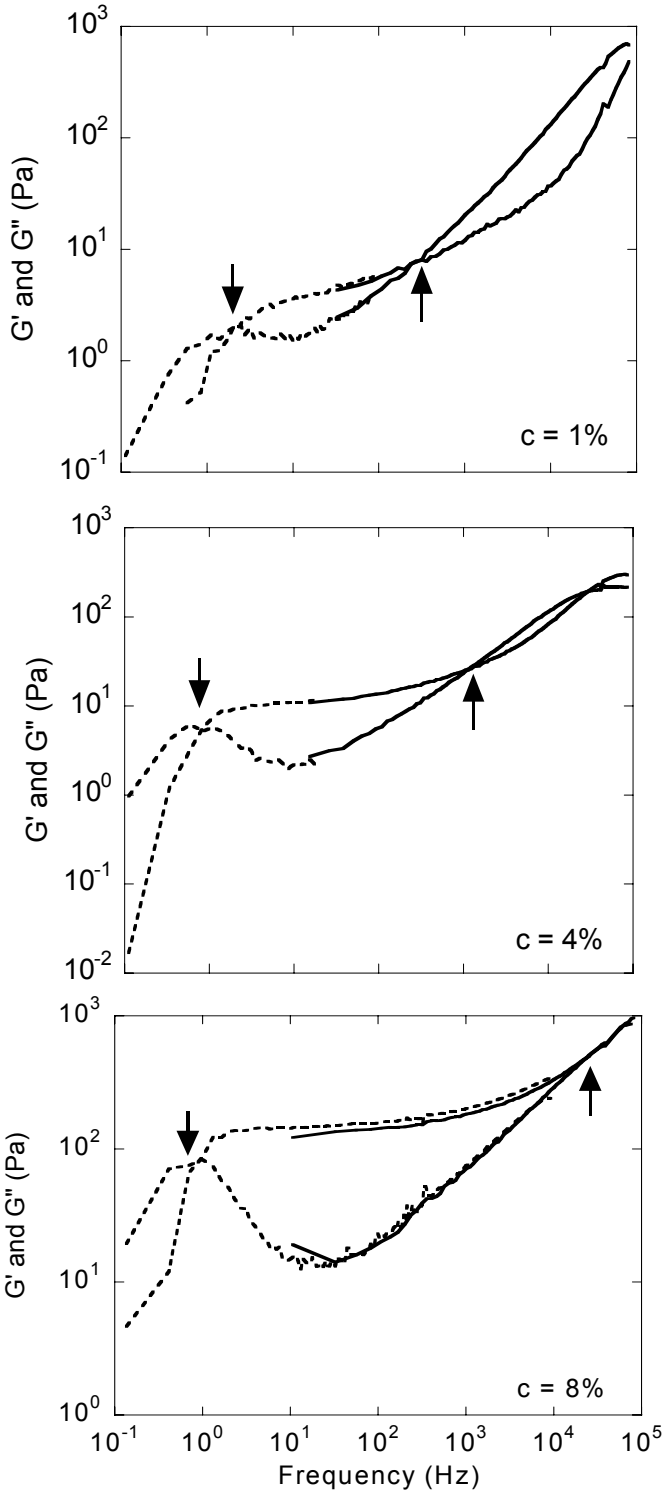

Figure 6: Cross-over frequencies: Storage and loss shear moduli were measured for wormlike micelle solutions of concentrations cp = 1, 4 and 8wt%, by microrheology with probe particles of 0.98μm diameter (solid line 195kHz sampling rate, dashed line 20kHz sampling rate). Moduli are plotted (without shifting curves apart) to identify the crossover points of the two moduli.

As concentration increases the high-frequency crossover moves to higher frequency indicated by upwards pointing arrows, while the low-frequency cross-over moves to lower frequencies. Curves are at each concentration averages of 8 spectra recorded from 3 different beads, smoothed by logarithmic binning. Frequencies for the high-frequency cross-overs are: 316Hz, 1144Hz and 60000Hz.

Deviations from the circle reflect additional internal dynamics of the micelles [35]. At the high-frequency end these will be dominated by the bending fluctuations of individual micelles which leads to a continuum of relaxation times, commonly resulting in a power-law form of the moduli [36,37].

The elastic plateau in $G'(\omega)$ reflects the collective dynamics of the entangled micelles and is maintained for frequencies above $1/\tau$ until the largest characteristic microscopic time scale of the system is reached, which is typically the relaxation time of a single mesh in a flexible polymer network. In simple physical terms, this crossover separates the plateau regime caused by collective network dynamics from the single-filament regime (e.g. Rouse behavior of flexible polymers) at higher frequencies [36]. The increase of the complex shear modulus at high frequencies can be understood as a progressive reduction of the compliance of individual filaments under periodic stress with increasing frequency. The compliance mainly arises from the relaxation of lateral undulation modes. Such modes typically exhibit a power law dispersion, with relaxation time decreasing with wavelength, leading to power-law behavior of the shear modulus. In rheology, crossovers such as this one can be extremely broad, covering many decades in frequency. It is evident from our data (Figure 4), that, particularly for the more concentrated solutions, the high frequency scaling regime is not reached within the bandwidth of our experiments.

The mesh size of the entangled solution decreases with increasing polymer concentration and the crossover frequency marking the end of the plateau is expected to rise accordingly. The plateau value of G' itself also increases with polymer concentration. Both effects can be seen in Figure 6. In fact, these two effects are not independent, as is demonstrated empirically in Figure 7.

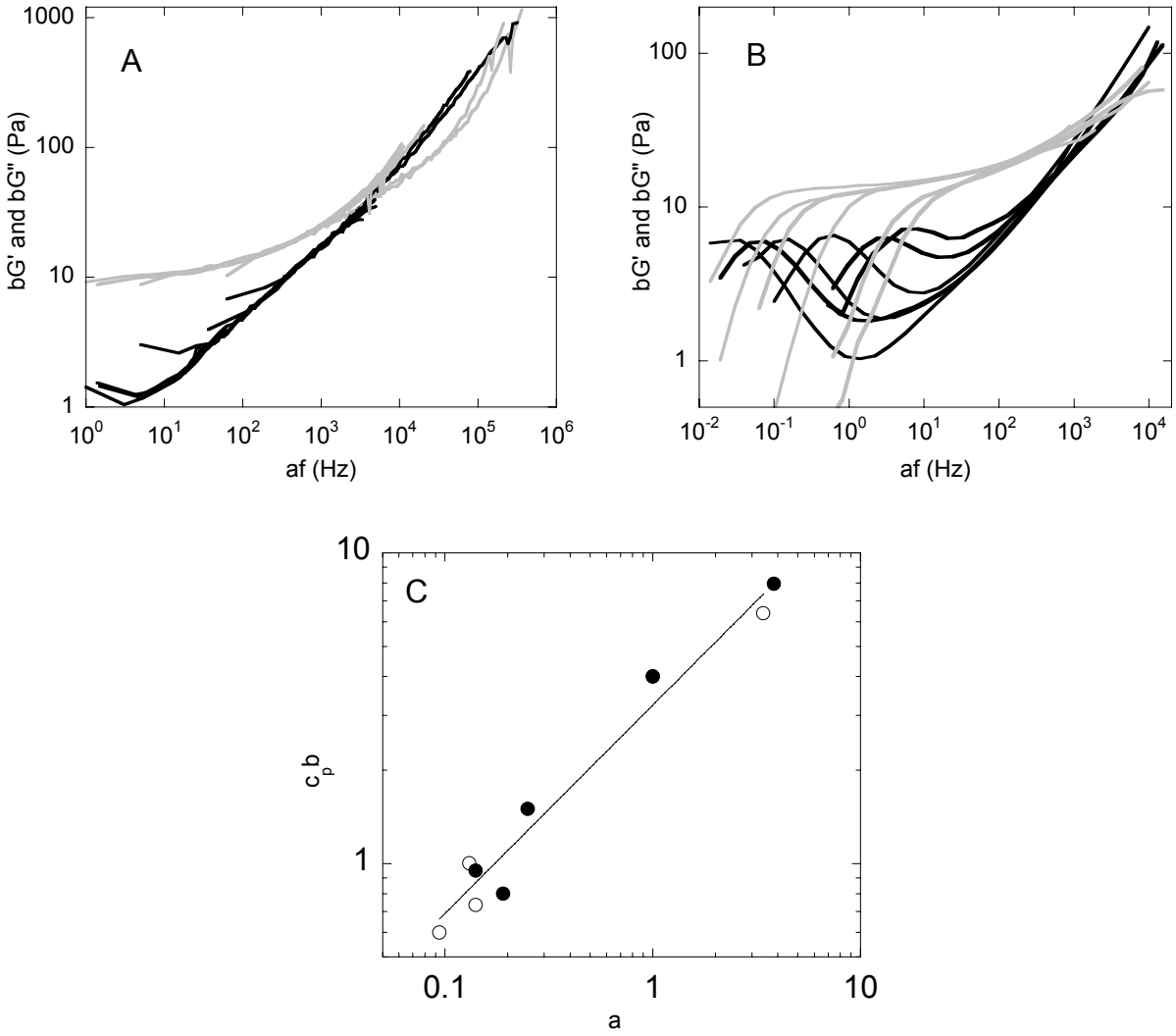

Figure 7: Scaling analysis of storage and loss moduli: Scaling factors *a* and *b* were determined for every set of *G′* and *G′′* curves such that *bG′* and *bG′′* versus *af* collapse onto the respective 4% reference curves. (A)Moduli from microrheology with probeparticles of 0.98μm diameter for wormlike micelle solutions of concentrations c_P = 1, 2, 4, 5, 6 and 8 wt%. (B) Macrorheology results (piezorheometer) for samples from the same stocks. (C) Plot of *bc* versus *a* to extract the high-frequency scaling exponent *z* of both moduli and the concentration scaling exponent of *G′* in the plateau regime. Filler data points are macrorheology and unfilled are microrheology.

We can make these ideas more precise, and actually infer the characteristics of the high-frequency scaling regime from carefully analyzing the transition regime as follows. The approach is to collapse both the *G′* and *G′′* curves simultaneously by rescaling the frequency and moduli axes. This is similar to what was done in Ref. [38] for colloidal gels, but we must account for the single-filament bending dynamics of the micelles [39].

We consider a simple model describing both the plateau and the high-frequency regimes. The storage modulus is assumed to behave at low frequencies as

$$G'(\omega) \sim c_p^y , \tag{7}$$

while both real and imaginary parts of the high-frequency modulus are assumed to increase with frequency ω according to

$$G'(\omega) \sim G''(\omega) \sim c_p \omega^z \tag{8}$$

In simple terms, we assume that the complex viscoelastic response of semidilute micelle solutions has two distinct contributions: (1) a frequency-independent component dominated by $G'(\omega)$ at low frequencies, and (2) a high-frequency component due to the relaxation of polymer between entanglements. The former represents the plateau, which is expected to depend on network architecture, *e.g.*, the mesh size. It is expected to increase with concentration as a power-law with the exponent *y* that is left as a fit parameter. The latter, being a single-filament effect, is expected to depend linearly on concentration c_p. For flexible polymers, the exponent *z* is expected to be in the range 0.5-0.7, depending on hydrodynamic interactions [36]. Following Ref. [38], we collapse the family of frequency-dependent shear moduli by introducing scaling factors *a(c)* and *b(c)* for each pair of *G′* and *G′′* curves at a given concentration, chosen for the best empirical collapse of the data. The *G′* and *G′′* graphs were scaled after water $G''(\omega) = \omega \eta_{water}$ was subtracted from the *G′′*. The data collapse was done independently for both microrheology and macrorheology data (Figure 7 a, b).

Specifically, we chose the intermediate data set for 4% as a reference, and rescaled the modulus as *bG* and frequency as *af* for each of the other data sets for concentrations 1%, 2%, 5%, 6% and 8% to match the 4% data. This method is sufficient since we are only interested in the scaling of the scaling factors. Assuming the model with exponents *y* and *z* expressed above, this means that $b \sim c_p^{-y}$ and that

$a \sim c_p^{(1-y)/z}$, which means that $bc_p \sim a^z$. Thus, by plotting $c_p b(c)$ versus $a(c)$, we expect a power-law relationship between the scaling factors, with the high-frequency scaling exponent z. The exponent z was found to be 0.67 from the combined plot of factors derived from macro- and microrheology (Figure7c). The exponent y was calculated to be 1.89. At the low-frequency end the scaling is observed to break down as one approach the Maxwell regime. This is expected because the terminal relaxation is not included in the model assumption of Eqs.(7) and (8).

5.5 Discussion

For wormlike micelles the characteristic length scales of both individual micelles (diameter ~3nm, persistence length ~10nm) and of the polymer solution (mesh size ~30nm) are much smaller than the probe particle size. Furthermore, at the ionic strength of the brine we used, charge interactions are effectively screened with a Debye screening length of about 0.4nm (0.5M NaCl). Therefore single-particle microrheology should report correct bulk shear moduli. Consistent with this expectation, our experimental results (Figures 3 and 4) show excellent agreement between single particle and mechanical rheology. This result verifies both the microrheology technique with the calibration and data evaluation procedures we used here as well as the assumptions involved. In particular, the assumption of strong coupling between polymer and solvent, limiting the dynamics to incompressible shear, appears to be justified down to the lowest frequencies we measured of 10^{-2}Hz. A deviation from strong coupling should have shown up as a growing decrease of the microrheology-moduli below the macrorheology values towards low frequencies. No such systematic difference was observed. On the other hand, a change of the Poisson ratio from 1/2 even all the way to 0 would only cause a slight decrease (~5%) of the shear modulus. Such an effect is difficult to resolve due to noise at low frequencies.

In some systems with relatively large internal characteristic length scales, the presence of the particle will locally affect the embedding medium so strongly that shear elastic moduli derived from single-particle microrheology will differ from average bulk values [26,40]. In particular, we have also performed similar

experiments with the filamentous fd virus [44], and with the cytoskeletal protein actin [44], in the first case although the persistence length of fd is about 1 micrometer and comparable to bead sizes used, there was no measurable difference between one- and two-particle microrheology. In the second case (actin), there were strong probe particle effects at low and high frequencies [43]. In such cases, if spatial resolution and high bandwidth are desired, two-particle microrheolgy should be used. The price to pay is increased noise and that of a more complex experimental set-up. Even in a system with small characteristic scales, slip boundary conditions have been suggested as a possible explanation for the discrepancies observed between one- and two-particle microrheology [40].

It is important that we have here found good agreement between single-particle microrheology and macrorheology in a simple system. This unambiguously proves the foundations of the technology and makes it now possible to quantitatively exploit the unique strengths of microrheology to study less simple systems. Apart from seeing effects created by the presence of the probe particle itself (which in themselves can be interesting), microrheology can be used e.g. to map microscopic inhomogeneities, to study local non-affine (bending) deformations of semiflexible or bundled polymers or to measure low-frequency compressional elasticity of a polymer solution. In other words, what from one point of view might have been seen as a disadvantage of this new technique, namely that results don't always agree with conventional rheology, is clearly emerging as an advantage providing more experimental access to phenomena that could not be studied with conventional rheology. One can, however, confidently exploit the capabilities of microrheology that go beyond those of conventional rheology only after it has been shown that agreement can be reached in simple systems, which we have done here.

The second new result presented here is the high-frequency rheology data extending beyond the Maxwell regime. Earlier macrorheological work [24] had been technically limited to about 5Hz. At high frequencies we expect an asymptotic cross-over from elastic response determined by collective network dynamics to response dominated by short-range single-filament relaxation. The crossover frequency is expected to be concentration dependent, determined by the longest relaxation time of a segment of wormlike micelle between two entanglement points which should

roughly be equivalent to the mesh size in the entangled solution. In our experiments (Figure 6) the bandwidth is not sufficient to go far beyond this crossover frequency into the asymptotic scaling regime, and the log-log slopes of G' and G'' are not constant for large enough intervals to make a precise statement about scaling exponents. Nevertheless, the superposition method we have presented above can still be used to infer the asymptotic scaling behavior, even if only the transition between regimes is captured in the data. This only works, however, if the transition takes place directly between two scaling regimes without other intervening complex dependencies.

For entangled micelles one would expect the high-frequency single-filament behavior to be somewhere between that of flexible polymers and that of semi-flexible polymers. For our system, the entanglement length was approximately 30nm for c_P=1 while the persistence length was of order 10nm. Semi-flexible polymers show high-frequency scaling in the shear elastic modulus with an exponent of about 3/4~[5,6,41,42]. Our results point to a slightly lower exponent of about 0.67. There is no model to calculate the exact scaling behavior of a given polymer between the limits of semiflexible and flexible behavior, but an exponent of slightly less than 3/4 is reasonable. For Zimm dynamics, for a flexible chain including hydrodynamic effects, an exponent of about 5/9 is expected [36]. In the case of a chain with a persistence length somewhat larger than the monomer size assuming a more extended conformation, one might expect less of an effect from hydrodynamic interactions and therefore Rouse- rather than Rouse-Zimm dynamics. For that case an exponent of 1/2 is expected.

There may of course also be an influence of the particular dynamics of wormlike micelles that have so far not been considered. The breaking and reannealing dynamics might, for example, also influence the scaling exponent. The extraction of the scaling exponent from the transition regime data rests, as described, on the assumption that the transitions leads directly to the asymptotic high frequency scaling. A distinct possibility is that other dynamic regimes might follow the plateau regime before asymptotic scaling is reached [41].

Further experiments either with systems with intrinsically slower dynamics or of a similar system in a more viscous environment will be necessary to further explore high frequency rheology of wormlike micelle solutions.

5.6 Acknowledgments

We would like to thank J. Berret, J. Candau, M. Cates, P. Bartlett and L. Starrs for useful discussions and E. Petermann, A. Levine and J. van Mameren for discussions and technical help. This research has been supported by a Marie Curie Fellowship of the European Community (contract number HPMF-CT-20001-01278) for MB, and by the Foundation for Fundamental Research on Matter (FOM).

5.7 References

[1] F. Ziemann, J. Radler, and E. Sackmann, Biophys. J. 66, 2210 (1994).

[2] T.G. Mason and D.A. Weitz, Phys. Rev. Lett. 74, 1250 (1995).

[3] F. Amblard, A.C. Maggs, B. Yurke, A.N. Pargellis, and S. Leibler, Phys. Rev. Lett. 77, 4470(1996).

[4] T.G. Mason, K. Ganesan, J.H. vanZanten, D. Wirtz, and S.C. Kuo, Phys. Rev. Lett. 79, 3282(1997).

[5] F. Gittes, B. Schnurr, P.D. Olmsted, F.C. MacKintosh, and C.F. Schmidt, Phys. Rev. Lett.79, 3286 (1997).

[6] B. Schnurr, F. Gittes, F.C. MacKintosh, and C.F. Schmidt, Macromolecules 30, 7781 (1997).

[7] J.C. Crocker, M.T. Valentine, E.R. Weeks, T. Gisler, P.D. Kaplan, A.G. Yodh, and D.A.Weitz, Phys. Rev. Lett. 85, 888 (2000).

[8] F.C. MacKintosh and C. F. Schmidt, Curr. Opin. Colloid Interf. Sci 4, 300 (1999).

[9] L.D. Landau and E.M. Lifshitz, Statistical Physics (Butterworth and Heinemann, 1980), 3rded.

[10] A. Ashkin, Proc. Nat. Acad. Sci. USA. 94, 4853 (1997).

[11] T.M. Stokich, D.R. Radtke, C.C. White, and J.L. Schrag, J. Rheol. 38, 1195 (1994).

[12] J.L. Schrag and R.M. Johnson, Rev. Sci. Instr 42, 224 (1971).

[13] P. Hebraud, F. Lequeux, and J.F. Palierne, Langmuir 16, 8296 (2000).

[14] A.J. Levine and T.C. Lubensky, Phys. Rev. E. 63, 041510 (2001).

[15] F. Brochard and P.G. Degennes, Macromolecules 10, 1157 (1977).

[16] S.T. Milner, Phys. Rev. E. 48, 3674 (1993).

[17] L.D. Landau and E.M. Lifshitz, Theory of Elasticity (Butterworth and Heinemann, 1986), 3rded.

[18] D.T. Chen, E.R. Weeks, J.C. Crocker, M.F. Islam, R. Verma, J. Gruber, A.J. Levine, T.C. Lubensky, and A. G. Yodh, Phys. Rev. Lett. 90, 108301 (2003).

[19] A.J. Levine and T.C. Lubensky, Phys. Rev. E. 65, 011501 (2002).

[20] L.M. Walker, Curr. Opin. Colloid Interf. Sci. 6, 451 (2001).

[21] R. Granek and M.E. Cates, J. Chem. Phys. 96, 4758 (1992).

[22] J.F. Berret, J. Appell, and G. Porte, Langmuir 9, 2851 (1993).

[23] M.E. Cates and S.J. Candau, J. Phys.-Cond. Mat 2, 6869 (1990).

[24] H. Rehage and H. Hoffmann, J. Phys. Chem. 92, 4712 (1988).

[25] D. Constantin, J.F. Palierne, E. Freyssingeas, and P. Oswald, Europhys. Lett. 58, 236 (2002).

[26] F. Cardinaux, L. Cipelletti, F. Scheffold, and P. Schurtenberger, Europhys. Lett. 57, 738(2002).

[27] L.D. Landau and E.M. Lifshitz, Fluid Mechanics (Butterworth and Heinemann, 1987), 3rd ed.
[28] M. Cagnon and G. Durand, Phys. Rev. Lett. 45, 14181421 (1980).
[29] M.W. Allersma, F. Gittes, M.J. deCastro, R.J. Stewart, and C. F. Schmidt, Biophys. J. 74,1074 (1998).
[30] F. Gittes and C.F. Schmidt, Biophys. J. 74, A183 (1998).
[31] E.J.G. Peterman, M.A. van Dijk, L.C. Kapitein, and C. F. Schmidt, Rev. Sci.Instr. 74, 3246(2003).
[32] M. Atakhorrami, J. Kwiecinska, K.M. Addas, G.H. Koenderink, A. Levine, F. MacKintosh, and C. Schmidt, submitted toPhys.Rev.E.**(Chapter 3)**
[33] E.J.G. Peterman, F. Gittes, and C.F. Schmidt, Biophys. J. 84, 1308 (2003).
[34] F. Gittes and C.F. Schmidt, Meth. Cell Biol, Vol 55 55, 129 (1998).
[35] M.S. Turner and M.E. Cates, Langmuir 7, 1590 (1991).
[36] M. Doi and S. Edwards, The Theory of Polymer Dynamics, vol. 73 of International series of monographs on physics (Oxford Science Publications, Oxford, 1986).
[37] J.D. Ferry, Viscoelastic Properties of Polymers (Wiley, New York, 1980).
[38] V. Trappe and D.A. Weitz, Phys. Rev. Lett. 85, 449 (2000).
[39] M. Gardel, J. Shin, F. MacKintosh, L. Mahadevan, P. Matsudaira, and D. Weitz, Phys. Rev.Lett.93, 188102 (2004).
[40] L. Starrs and P. Bartlett, J. Phys.-Cond. Mat. 15, S251 (2003), sp. Iss. SI.
[41] D.C. Morse, Phys. Rev. E. 58, R1237 (1998), part A.
[42] F. Gittes and F.C. MacKintosh, Phys. Rev. E. 58, R1241 (1998).
[43] M. Atakhorrami, G.H. Koenderink, J.F. Palierne F.C. MacKintosh, and C.F. Schmidt, manuscript in preparation. (**Chapter 7)**
[44] K.M. Addas, M. Atakhorrami, J.X Tang, A. Levine, F.C. MacKintosh, and C.F. Schmidt, manuscript in preparation.

Chapter 6

High-bandwidth one- and two-particle micrhorheology in solutions of wormlike micelles

Abstract

We have developed a large bandwidth two-particle microrheology technique to measure loss and storage moduli of viscoelastic materials from 0.1 Hz to about 100 kHz using laser trapping and interferometry. We found quantitative agreement between one- and two-particle microrheology results in entangled solutions of wormlike micelles chosen as a simple model viscoelastic system. These results validate both experimental method and data interpretation. The consistent results also prove that in a simple system, where the solutions length scales are much smaller than the micron probe size, one-particle microrheology can accurately measure bulk viscoelastic parameters.

6.1 Introduction

Microrheology collectively refers to a family of recently developed techniques to measure the viscoelastic properties of complex fluids and soft materials with high bandwidth and high spatial resolution [1-10].

These techniques are based on tracking the motions of micron-sized probe particles embedded in the system to be studied. Variations of the technique include active ones in which the probe particles are manipulated with magnetic fields or with laser light (optical tweezers) and passive ones in which the thermal fluctuations of particles are recorded. In the passive methods, the fluctuation-dissipation theorem in linear response theory [11] is used to extract viscoelastic parameters [6-8] of the material from the thermal equilibrium fluctuations of the embedded particles. We focus here on passive microrheology where, in contrast also to typical macroscopic mechanical rheology, no strain is applied to the material during the measurement, and linear response parameters can be measured directly without extrapolation. This is particularly useful in soft materials and complex fluids where even a small imposed strain can cause reorganization of structure within the material and thus change its viscoelastic properties (e.g. strain hardening or shear thinning).

Several methods have been utilized to measure the displacement fluctuations of embedded particles in passive microrheology. Video tracking has been applied to a variety of polymer systems such as λ-DNA solutions [12] as well as to biological cells [13]. The highest frequency that can be measured by video tracking is half the video frequency. This is a disadvantage when probing the rheological properties of complex fluids exhibiting a wide range of characteristic length and time scales. Much higher andwidths of 100kHz to 1 MHz can be reached using diffusing wave spectroscopy (DWS) with dense solutions of probe particles [3] , [14] or laser trapping techniques combined with interferometry using fast photodiodes to track individual particles [7, 10].

A potential problem for microrheology are local perturbations that can be introduced by the presence of the probe particles. The thermal motion of a particle reflects the viscoelastic properties of its environment on roughly the scale of the probe particle radius since this is the length scale on which the strain field around

the particle decays [7, 8]. Ideally one wants to measure material properties that are not perturbed by the presence of the probe particle itself. Measuring the thermal fluctuations of individual particles (one-particle microrheology, 1PMR) can thus only achieve that, if the particle does not perturb the medium on a length scale comparable to its radius. The probe can influence the material near its surface in several ways, e.g. by physical entropic depletion or by chemical or electrostatic interaction with the material. How deep into the material such a perturbation propagates, depends on the characteristic length scales of the material. In the limit where the probe particle is smaller than material scales such as polymer persistence length, contour length, Debye length etc., what are measured are not the bulk properties. Micorheology provides in this limit access to local dynamics that are not measurable with conventional rheology. In the limit where all material scales are smaller than the particle, surface effects should become negligible.

Many biopolymer solutions or networks such as the cytoskeleton of cells and its components (actin, microtubules and intermediate filaments [15], typically have intrinsic length scales as large as micrometers. A way to nevertheless circumvent local probe effects and determine the bulk viscoelastic behavior in these materials by microrheology is to measure the cross-correlated fluctuations of pairs of particles separated by more han the relevant material length scales, a method dubbed two-particle microrheology (2PMR) [8, 10, 16]. 2PMR has been tested and compared with 1PMR experimentally in several systems with varying properties. Results from 1PMR and 2PMR differed in systems with length scales bigger or in order of the probe particles size, λ-DNA solutions [12 , 16, 17] and entangled actin solutions. Another system studied is non-adsorbing polystyrene in decalin [10], where, surprisingly, 1PMR and 2PMR gave different results, which the authors explained by slip boundary conditions.

The experimental situation is thus somewhat unclear. A careful analysis is needed, best done with a simple model system, to resolve ambiguities and to make it possible to take advantage of the capabilities of microrheology to complement conventional rheology. It is advantageous to measure with high bandwidth, particularly in systems, such as actin solutions, [18] where interesting dynamic transitions occur over a wide range of frequencies and good data at high frequencies

will be essential for modeling [19]. We have here implemented 1PMR and 2PMR in the same experiment, using laser trapping and interferometry to track particle position fluctuations up to 100 kHz. We have selected solutions of worm-like micelles as a model system with small characteristic length scales, where we expect agreement between 1PMR and 2PMR. Worm-like micelles (WLM) are cylindrical tubes of amphiphilic molecules that self-assemble in aqueous solution under particular ionic and temperature conditions. Properties of WLM have been well studied, both theoretically [20, 21] and experimentally by scattering and conventional rheology techniques [22-24]. We have published earlier results with 1PMR elsewhere [25]. In [26] we have compared results with those from macroscopic rheology.

WLM were assembled with cetylpyridinium chloride (CPyCl) as the surfactant and sodium salicylate (NaSal) as strongly-binding counter ion. WLM formed in this system have a diameter of 2-3nm, contour lengths of 100nm-1μm and a persistence length of order 10nm [22], Despite their somewhat complex structure and dynamics, wormlike micelles exhibit well defined rheological properties, similar to those of covalently linked linear polymers. When entangled wormlike micelles are sheared, relaxation of stress occurs via reptation and scission [21]. Both processes, occurring simultaneously, lead to a single dominating relaxation time (in our case about 1s) being observed at long times. Systems with one relaxation time are known as Maxwell fluids and have been studied extensively [27, 23]. In general, studies performed on wormlike micelles have focused on low-frequency properties where the simple mechanical analogue, the Maxwell model, consisting of a dashpot and a spring in series, can be used to model the viscoelastic response. Higher frequency rheology has been performed on micelle systems confirming the Maxwell regime at somewhat elevated frequencies [28, 24].

Our results demonstrate good agreement between one- and two-particle microrheology over a wide frequency range between 0.1Hz and about 100kHz. The results make a strong case for the validity of 1PMR for soft materials with intrinsic length scales much smaller than the probe size, and they provide a critical performance test for our implementation of high-bandwidth 2PMR.

6.2 Experimental section

6.2.1 Materials

Worm-like micelles were prepared from the surfactant cetylpyridinium chloride (CPyCl) dissolved in brine (0.5M NaCl) with as strongly binding counterion sodium salicylate (NaSal) (chemicals fromSigma-Aldrich Chemie B.V. Zwijndrecht, The Netherlands). In this study all samples have a molar ratio Sal/CPy = 0.5. The micellar solutions were stored at (controlled) ambient temperature (between 21.5 and 22.0°C) which was above the Krafft point of this system. Samples were prepared in three different concentrations: c = 0.5wt%, 1wt% and 2wt%.

As probe particles we used for all measurements silica beads (R = 0.580 μm ± 5% and R = 1.05 ± 5% (a kind gift of the Van't Hoff Laboratory, Utrecht University, Utrecht, Netherlands). Beads were diluted to a final volume fraction of ~10-5. After mixing the particles with the solutions, we pipetted the solutions into sample chambers with about 20 μl volume, made of a coverslip and a microscope slide joined with two strips of double-stick tape (thickness ~70μm). The sample chambers were sealed at both ends with Apiezon H vacuum grease to prevent evaporation and slow flow.

6.2.2 Experimental method

Two separate polarized laser beams with wavelengths λ = 1064nm (Nd:YVO4, Compass, Coherent, Santa Clara, CA, USA) and λ = 830nm (diode laser, CW, IQ1C140, Laser 2000) were focused to diffraction limited beam waists through a microscope objective (Neofluar, 100x, NA 1.3 oil, Zeiss) providing a pair of optical traps in a custom-built light microscope [29]. Two different color lasers were used to avoid crosstalk between the two traps, which does occur when one laser beam is split by polarizing beam splitters due to partial depolarization of both beams in the objective [30]. A schematic sketch of the experiments is shown in Fig. 1, where two particles, labeled 1 and 2, separated by a distance r along the x-axis are trapped in the two laser foci. To avoid the influence of the chamber surface, particles were trapped at a minimum distance of 20 μm from all chamber surfaces.

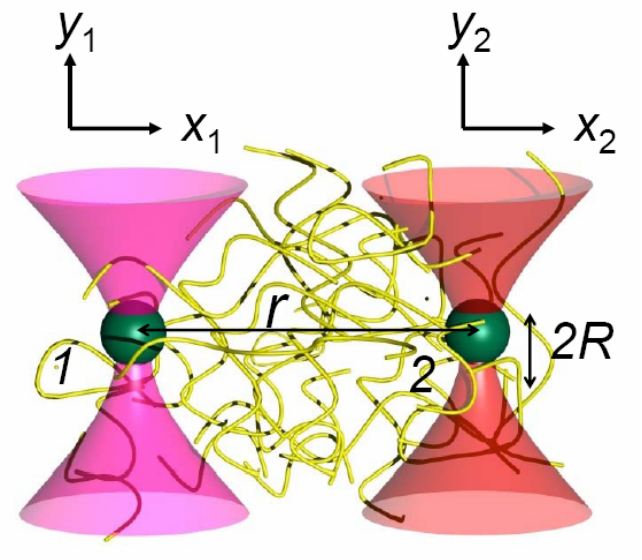

Figure 1: Schematic of the one/two-particle microrheology experiment. A pair of silica particles (radius R) is trapped by a pair of laser traps at a separation distance r. The position fluctuations of each particle in the x and y directions are simultaneously detected with quadrant photodiodes. The two particles are normally arranged such that the cross-correlated position fluctuations are measured in one detector axis parallel and in the other perpendicular to the centerline.

The laser intensity was varied for each wavelength individually using $\lambda/2$ plates and prism polarizers placed in the laser paths. The position fluctuations of each of the particles with respect to the center of its trap were detected in the x and y directions simultaneously with quadrant photo diodes (QPD) using back-focal-plane interferometric detection [29,31]. A laser line filter for the respective wavelength was placed in front of each of the QPDs to suppress any residual crosstalk from imperfect beam splitting. To avoid the slow response at 1064nm of standard silicon QPDs [32]; [33], a special QPD (10mm diameter, YAGG444-4A, Perkin Elmer, Vaudreuil, Canada), operated with a reverse bias of 100V, was used for the detection of the 1064nm beam, while the 830 nm light was detected with a standard silicon-type QPD (10mm diameter, Spot9-DMI, UDT, Hawthorne, CA) operated with a reverse bias voltage of 15 V. The particle position time series were acquired and stored with a Labview program (National Instruments, Austin, TX, USA), and digitized using an

A/D board (195 kHz, ChicoPlus, Innovative Integration, Simi Valley, CA) at 195 kHz Positions measured in voltages were calibrated to displacements using the high-frequency amplitude of the Brownian motion power spectral densities of beads from the same batch of particles in water, recorded right after the measurements were done. Trap stiffnesses were obtained in the same measurements [34]. In all experiments presented here, laser power (~10mW) and thereby the trap stiffness (~5pN/nm) were kept at a minimum to minimize the artifacts introduced by the laser traps. The lab temperature was stabilized to 21.4 ± 1°C.

After filling the chambers with worm-like micelle solutions, we trapped two particles and moved them to a desired separation distance *r*, 20μm above the surface. Then we waited for about 10 minutes to let the system relax. As a criterion for the relaxation of possible structural perturbations from the process of filling the sample into the chamber, we checked sample isotropy for each particle looking for overlap of the averaged displacement correlation functions of *x* and *y* for both particles. Then we recorded between 5-10 data sets of each 80 seconds duration for every pair of particles in each *r*.

6.3 Data analysis

In the linear response regime the Fourier transform of the displacement $u_\alpha^{(j)}(\omega)$ of particle *j* (1 or 2) in direction α (*x* or *y*) is related to the Fourier transform of the applied force $F_\beta^{(k)}(\omega)$ applied to particle *k* in direction β via $u_\alpha^{(j)}(\omega) = \chi_{\alpha\beta}^{(j,k)}(\omega) F_\beta^{(k)}$.

Here, $\omega = 2\pi f$ is the radial frequency, and $\chi_{\alpha\beta}^{(j,k)}(\omega)$ is the response function. Here both coordinate directions β and particle number *k* are summed over. The $\chi_{\alpha\beta}^{(j,k)}(\omega)$ for $j = k$ refer to the single- particle response functions and for $j \neq k$ to the inter-particle response functions. The single-particle response function describes the response of particles 1 or 2 to forces applied to the same particle. The inter-particle response function describes how particle 1 responds to forces on particle 2 etc. Each of these, in general complex response functions can be separated into real (in-phase) and imaginary (out-of-phase) part in the usual way: $\chi_{\alpha\beta}^{(j,k)}(\omega) = \chi'^{(j,k)}_{\alpha\beta}(\omega) + i\chi''^{(j,k)}_{\alpha\beta}(\omega)$.

In thermal equilibrium and in the absence of external forces, the fluctuation-dissipation theorem [35] relates the imaginary part of (single- or inter-particle) response functions to the thermal position fluctuations $u_\alpha^{(j)}(\omega)$:

$$\chi''^{(j,k)}_{\alpha\beta}(\omega) = \frac{\omega}{2k_BT}\omega S^{(j,k)}_{\alpha\beta}(\omega) \quad (1)$$

where k_BT is the thermal energy and the position correlation functions $S^{(j,k)}_{\alpha\beta}(\omega)$ are given by

$$S^{(j,k)}_{\alpha\beta}(\omega) = \int \left\langle u_\alpha^{(j)}(t)\, u_\beta^{(k)}(0)\right\rangle e^{i\omega t}\, dt\,. \quad (2)$$

In our experiments we have chosen the *x*-axis along the line connecting the centers of the two particles and *y* perpendicular to that (and the laser beam axis). With this coordinate system, all $S^{(j,k)}_{\alpha\beta}$ are negligible (to first order) for $\alpha \neq \beta$, [36], and the relevant nonzero components of this tensor are $S^{(j,k)}_{xx} = S^{(j,k)}_{\parallel}$ and $S^{(j,k)}_{yy} = S^{(j,k)}_{\perp}$ (for $j \neq k$). We shall use a shorthand notation for the single-particle correlation functions: $S^{(j)}_{\parallel} \equiv S^{(j,j)}_{\parallel}$ and $S^{(j)}_{\perp} \equiv S^{(j,j)}_{\perp}$. In a time-reversal invariant medium, the various correlation functions must be symmetric in time *t* and $S_{\parallel}(\omega) \equiv S^{(1,2)}_{\parallel}(\omega) = S^{(2,1)}_{\parallel}(\omega)$ similarly for the perpendicular components. Thus, there are six non-zero correlation functions for *j* = 1,2, $S^{(j)}_{\parallel,\perp}$ (single-particle) and $S_{\parallel,\perp}$ (two-particle), along with six corresponding response functions $\chi^{(j)}_{\parallel,\perp}$ and $\chi_{\parallel,\perp}$. Finally, for isolated particles in isotropic and homogeneous media, or for large separations between particles, we can expect rotational symmetry, for which, $S^{(j)}_{\parallel} = S^{(j)}_{\perp}$. In this case, the four $S^{(j)}_{\parallel,\perp}$ (or $\chi^{(j)}_{\parallel,\perp}$) reduce to two non-zero single-particle correlation functions $S^{(j)}$ and related response functions $\chi^{(j)}$.

Using the fluctuation-dissipation theorem (Eq. 1), we obtain the imaginary parts of the response functions $\chi^{(j,k)}_{\alpha\beta}(\omega)$. From these we then obtain the real parts (and hence, the full complex quantities) via a Kramers-Kronig integral [35]; [7]:

$$\chi'^{(j,k)}_{\alpha\beta} = \frac{2}{\pi} P\int_0^\infty \frac{\zeta}{\omega^2+\zeta^2}\chi''^{(j,k)}_{\alpha\beta}(\omega)d\zeta \quad (3)$$

The measured response functions (χ^j and $\chi_{\parallel,\perp}$) include the effect of the (weak) laser trapping force which limits the fluctuations of the particles. Sufficient laser power is required to, first, hold the particles in the foci against sedimentation and diffusion, and, second, to limit shot noise in photon detection at high frequencies.

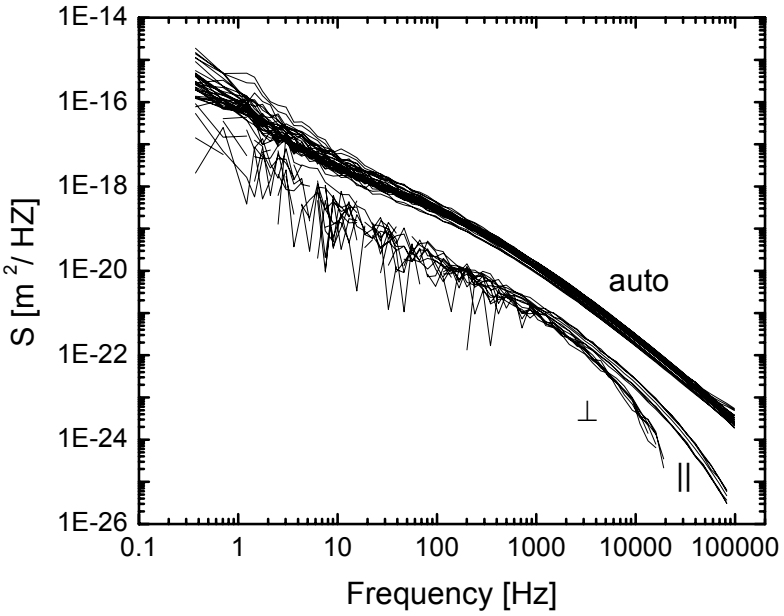

Figure 2: Spread of the raw data. Top curves: single-particle correlation functions S^j in x and y for both particles recorded for 80 s each sequentially for the same particle pair at same location and distance. Bottom curves: inter-particle correlation functions in x direction, $S_{\parallel}$ and y direction, $S_{\perp}$ versus frequency for c = 1wt% (R = 1.05μm, r = 5μm). In this plot the data are not scaled with particle radius R or distance r.

To obtain the single- and inter-particle response functions generated by the medium alone, α^j and $\alpha_{\parallel,\perp}$ respectively, and eventually the shear modulus of the medium, we must subtract the contribution from the laser traps from the measured response functions Details are described in [37].

The complex shear modulus $G(\omega)$ of the medium is related to the $\alpha^{(j)}$ by a general Stokes-Einstein relationship (GSER) [3, 6]:

$$\alpha^{(j)}(\omega) = \frac{1}{6\pi R^j G(\omega)} \tag{4a}$$

where R^j is the particles radius. In all experiments presented here we use the same particles size for both particles.

Similar relationships which are generalizations of the Oseen tensor [38] hold for the inter-particle response functions $\alpha_{\parallel,\perp}$

$$\alpha_{\parallel}(\omega)=\frac{1}{4\pi rG(\omega)} \quad \text{and} \quad \alpha_{\perp}(\omega)=\frac{1}{8\pi rG(\omega)}, \tag{4b}$$

where r is the separation between the particles. These expressions completely characterize the linear response at any point in the medium to a force at another point. Here we assume that particle and fluid inertia are negligible and that the medium is incompressible. As Levine and Lubensky had suggested, incompressibility of the medium results in ratio $\alpha_{\perp}/\alpha_{\parallel}=0.5$,[36] this can be used as a check on the medium incompressibility.

6.4 Results and discussion

First we examined the homogeneity of the sample by choosing different particles at different locations. A typical example of data spread for different data sets recorded sequentially for one particular pair of particles at a given location and distance (c = 1 wt%, R = 1.05 μm, r = 5 μm) is shown in Fig. 2. Here each of the calculated S^j and $S_{\parallel,\perp}$ (according to Eq. (2)) are smoothed by logarithmic binning.

To confirm that correlation functions from data taken at different bead separations obey the 1/r scaling implicit in Eq. (4), we have plotted in Figs. 3a and b the scaled inter-particle correlation functions $4\pi rS_{\parallel}$ and $8\pi rS_{\perp}$ versus frequency (0.1 to 100 kHz) for c = 1 wt%, R = 1.05 μm, and r between 4 and 16 μm. The scaled single-particle result, $6\pi RS^j$ is also plotted (black lines). Data superimpose well up to about 2 kHz, but we see a systematic frequency dependent decrease of both parallel (Fig. 3a) and perpendicular (Fig. 3b) inter-particle correlations which is due to fluid inertia [39]; [40]. The larger r is, the earlier occurs this steep decrease and for the same distance the inertial effect is larger in the perpendicular direction. Figs. 3a and b show that the single particle correlation function is not affected by solvent inertia up to 100kHz.

Figure 4 shows a comparison of the storage and loss moduli obtained from 1PMR and 2PMR for the same sample (c = 1 wt%). The 1PMR results are averaged from different particles for R = 1.05 μm (gray line). The 2PMR results are averaged

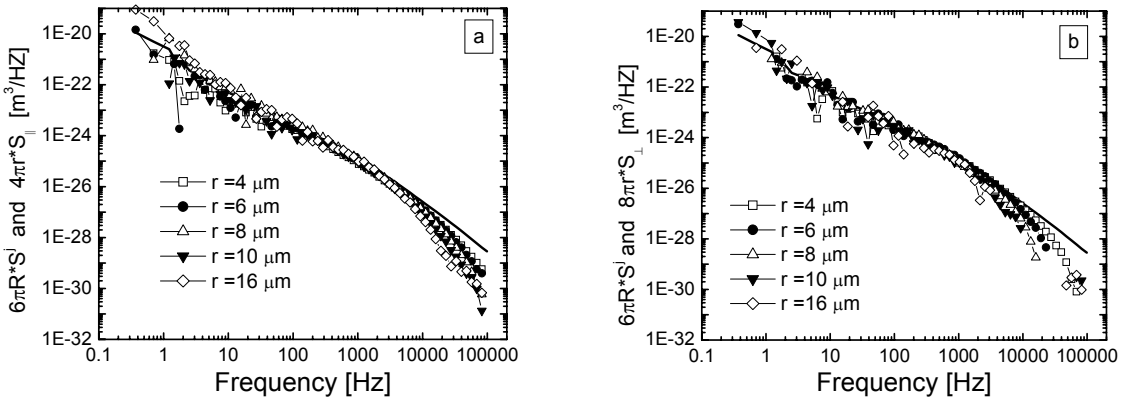

Figure 3: Inter-particle correlation functions scaled by the Oseen expectation: $4\pi r S_{\parallel}$ (a) and $8\pi r S_{\perp}$ (b) plotted versus frequency for c = 1wt% (R = 1.05 μm, r = 4 to 16 μm). In both (a) and (b) the single-particle correlation function, normalized by Stokes expectation ($6\pi R S^{j}$), is plotted for comparison. Plotted curves are the result of averaging 5 different data sets from the same particle pairs and repeated for three different particle pairs with the same given separation distance at different locations in the sample.

over all distances (r = 4 to 16 μm) and are plotted separately for the parallel (x-x) (filled symbols) and perpendicular (y-y) (empty symbols) geometry. At frequencies smaller than ~ 5 kHz all results are superimpose. At higher frequencies two effects are observed: i) The loss moduli G'' measured from the perpendicular channel of the inter-particle response function only extend to ~ 20 kHz. At this frequency displacements become anticorrelated due to solvent inertia. ii) G'' calculated from the parallel channel of inter-particle response function first show a gradual increase over the 1PMR results with frequency. The discrepancy is eventually a factor of ~ 1.3. This is again due to solvent inertia as shown in Figs.3 a and b. The solvent inertia leads to a break down of 1/r scaling, correlations decay more rapidly with increasing distance. Since the shear modulus is inversely proportional to the response function; a more rapidly decaying response function causes an increase in G''. Because of the larger effect of inertia in the perpendicular direction we will here

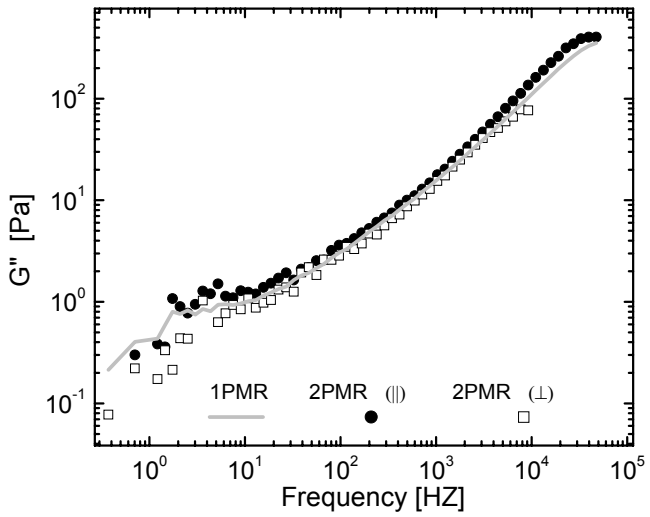

Figure 4: Comparison of loss modulus G″ measured by 1PMR (gray line) and 2PMR (symbols). 2PMR results obtained from the inter-particle correlation in the direction parallel to the center line (filled symbols) and perpendicular to it (empty symbols) are plotted separately. Plotted curves are obtained from averaging 5 data sets for particles with R = 1.05 μm and distances r = 4 to 16 μm in c =1wt%.

present only the shear moduli measured from the inter-particle response function in parallel directions.

In Figure 5 shear moduli measured with 1PMR and 2PMR are plotted versus frequency for three different concentrations of c = 0.5 wt% , 1wt% and 2wt%. Results from both methods agree within the error margins of the data. 2PMR curves are always noisier than those from 1PMR when calculated from the same data set. The reasons are i) There are 4 independent data sets, (each x- and y-direction of each particles) to average over for 1PMR, as opposed to just one data set obtained for the inter-particle response function (parallel direction) for the same particle pair. ii) The amplitude of the cross-correlation signal decays as $1/r$, so that distance-independent noise sources rapidly become relevant.

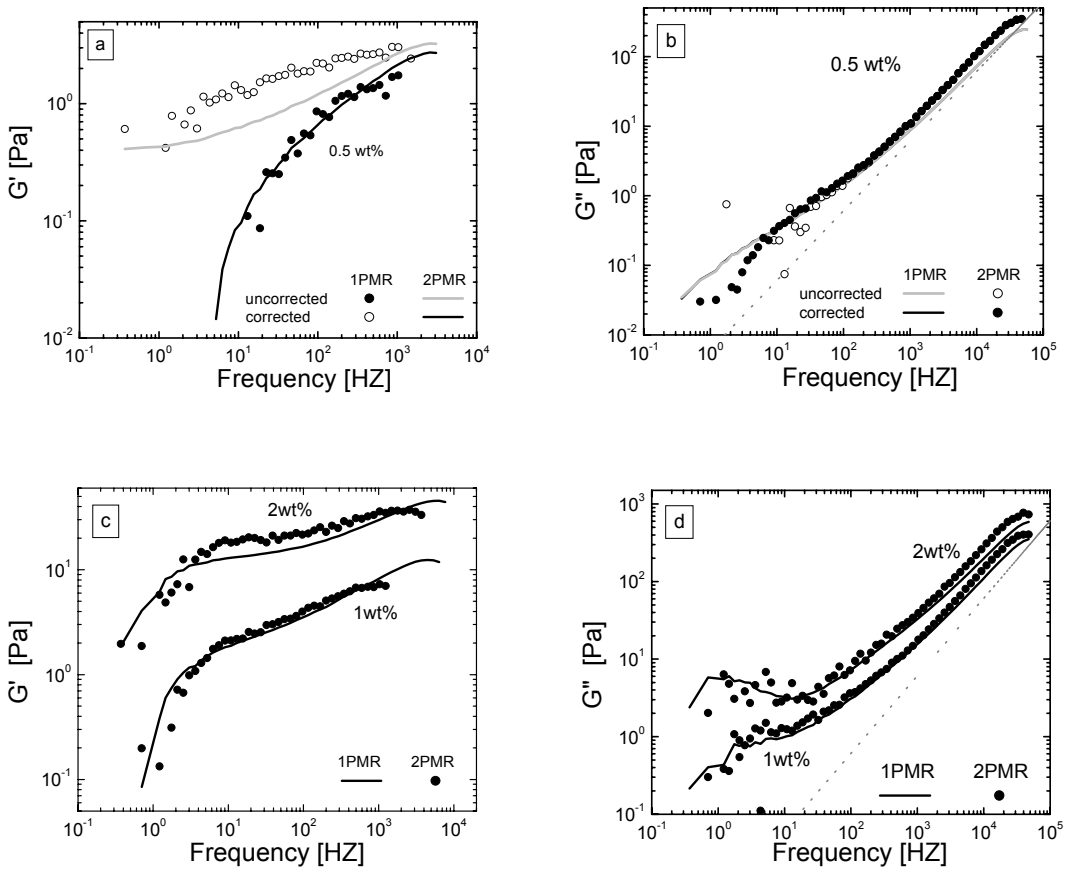

Figure 5: Comparison of storage (a and c) and loss (b and d) moduli obtained from 1PMR (dark lines) and 2PMR (filled symbols) in wormlike micelle solutions with concentrations c = 0.5 wt% with (R = 0.58 μm, r = 2 μm to 16 μm), 1wt % with (R = 1.05 μm and r = 5 μm to 16 μm) and 2 wt % with (R = 0.58 μm and r = 4 μm to 10 μm). In (a) and (b) storage moduli obtained from 1PMR (lines) and 2PMR (symbols) are plotted both before (gray line, empty symbols) and after (black line, filled symbols) correcting for the laser trap effect.. Thin dashed lines in (b) and (d) correspond to the solvent viscous modulus $G"= 2\pi f \eta$.

Figs 5 a, and b demonstrate the trap-correction effect on the resulting shear moduli of the c = 0.5wt% sample. The shear moduli calculated by applying Eq.(4a and b) to the measured response functions (χ^j and $\chi_{\|,\perp}$) are plotted as gray lines (1PMR) and empty symbols (2PMR), the shear moduli calculated from the corrected response

functions (α^j and $\alpha_{\parallel,\perp}$) for the same data set are plotted as black lines and filled symbols respectively. The uncorrected storage moduli shows different frequency dependencies and are larger than the corrected values of G' in the whole probed frequency range. Both curves superimpose, however, when the corrected response functions (α^j and $\alpha_{\parallel,\perp}$) are used to calculate G'. The trapping force had a relatively large effect in the c = 0.5wt% sample, where the trap stiffnesses for both laser traps with wavelengths (λ = 830 nm and λ =1064 nm) were 6.4 pN/m, 4.3 pN/m respectively. This added up to an "apparent elastic modulus" of 0.34 Pa, 0.59 Pa respectively which is large compared to the very small elastic modulus of the solution, G' ~ 0.096 Pa at 10Hz. The loss moduli were not effected substantially by the traps (Fig. 5b), and the loss moduli measured with both techniques overlap in the whole frequency range. This is expected since the laser traps essentially behave as harmonic springs contributing to the real parts of the response functions only. The real part of response function in turn has only a small effect on the loss moduli. The trapping effects were practically negligible in c = 1wt% and 2wt%, since the elastic moduli of these samples are much larger than the effect of the laser traps.

In Figs 5c and d the response function was corrected for the trapping effect and the shear moduli were calculated from the corrected response functions, although the trapping laser has a negligible contribution to the storage moduli in these samples, because of the large storage moduli of the solutions.

An advantage of 2PMR is that the shear modulus is calculated from two independent measurements. Comparing the parallel and perpendicular results provides a further consistency check of the method. At high frequencies the ratio of responses $\alpha_\perp / \alpha_\parallel$ has to be equal to 0.5 since the polymer network will be tightly coupled to the fluid, enforcing incompressibility [41]. The ratio $\alpha_\perp / \alpha_\parallel$ is plotted in fig. 6 versus frequency from (10 Hz to 10 kHz) for c = 1wt%. For most of the frequency range it is close to 0.5, as expected for an ideal incompressible material with a Poisson ratio υ = 0.5. At lower frequencies one can expect to eventually observe compressibility. In the extreme case of a totally compressible fluid (υ = 0) we can calculate the ratio of $\alpha_\perp / \alpha_\parallel$ = 0.75. The ratio appears to show a trend to increase at low frequencies, consistent with compressibility. At frequencies below 100Hz,

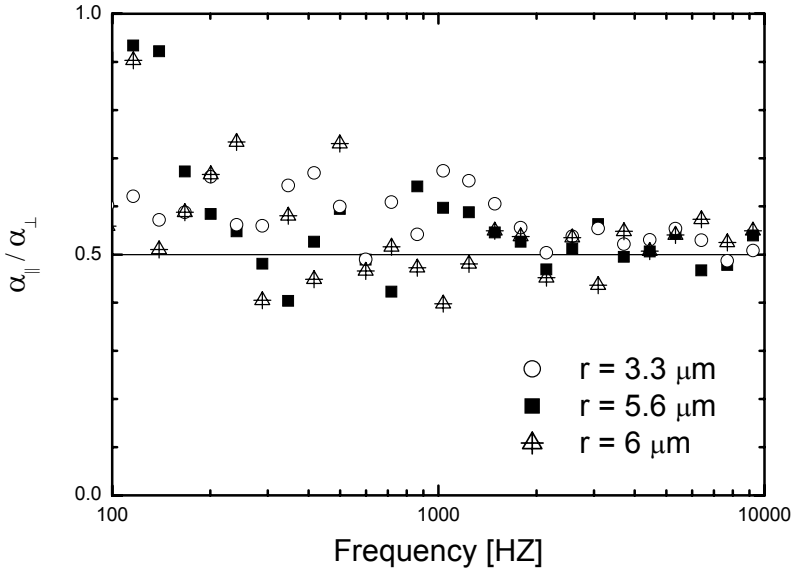

Figure 6: Ratio of parallel to perpendicular inter-particle response functions as a function of frequency in c = 1 wt% for different particle distances r = 3.3 μm, r = 5.6 μm and r = 6 μm

however, the noise in the data increases so much, that it is, with the current data, not possible to prove or exclude compressibility.

6.5 Conclusions

In a solution of entangled wormlike micelles, a relatively simple viscoelastic material, microrheology using micron-sized probe particles, can provide an accurate measurement of shear elastic moduli over a large bandwidth. A stringent test of this relatively new method had been outstanding up to now. By comparing two-particle microrheology results with one-particle microrheology results and finding good agreement, we could establish the validity of the technique.

We could only achieve these results after a careful elimination of spurious correlations in the signals from optics and electronics. Using two different lasers

with different wave lengths was crucial. Discrepancies between the two methods were theoretically not expected in worm-like micelle solutions where the length scales, such as persistence length (nm) and mesh size (nm), are significantly smaller than the probe particle size (μm). The experimental agreement therefore also confirms the modeling and data evaluation approaches.

For the worm-like micelle system (and presumably just the same for other comparable materials) our results demonstrate that one-particle microrheology is sufficient for measuring bulk viscoelastic parameters. One-particle microrheology has the advantages of less experimental complexity and less noise in the data. We are convinced that the method of microrheology with all its variations can in the future be applied to a large variety of soft-matter and biological systems.

6.6 Acknowledgments

We thank Frederick MacKintosh, Mark Buchanan, Alex Levine, Gijsje Koenderink and Karim.M Addas for helpful discussions, Joost van Mameren, Frederick Gittes and Joanna Kwiecinska for help with data-evaluation software. This work was supported by the Foundation for Fundamental Research on Matter (FOM).

6.7 References

[1] Waigh, T.A., Rep. Prog. Phys., 2005. 68: p. 685-742.

[2] Ziemann, F., J. Radler, and E. Sackmann, Local measurements of viscoelastic moduli of entangled actin networks using an oscillating magnetic bead micro-rheometer. Biophys. J., 1994. 66: p. 2210-2216.

[3] Mason, T.G. and D.A. Weitz, Optical Measurements of Frequency-Dependent Linear Viscoelastic Moduli of Complex Fluids. Physical Review Letters, 1995. 74(7): p. 1250-1253.

[4] Mason, T.G., et al., Particle tracking microrheology of complex fluids. Phys. Rev. Lett., 1997. 79: p. 3282-3285.

[5] Amblard, F., et al., Subdiffusion and anomalous local viscoelasticity in actin networks (vol 77, pg 4470, 1996). Physical Review Letters, 1998. 81(5): p. 1136-1136.

[6] Gittes, F., et al., Microscopic viscoelasticity: shear moduli of soft materials determined from thermal fluctuations. Phys. Rev. Lett., 1997. 79: p. 3286-3289.

[7] Schnurr, B., et al., Determining microscopic viscoelasticity in flexible and semiflexible polymer networks from thermal fluctuations. Macromolecules, 1997. 30: p. 7781-7792.

[8] Crocker, J.C., et al., Two-point microrheology of inhomogeneous soft materials. Phys. Rev. Lett., 2000. 85: p. 888-891.

[9] MacKintosh, F.C. and C.F. Schmidt, Microrheology. Curr. Opin. Colloid Interf. Sci., 1999. 4: p. 300-307.

[10] Starrs, L. and P. Bartlett, One- and two-point micro-rheology of viscoelastic media. Journal of Physics-Condensed Matter, 2003. 15(1): p. S251-S256.

[11] LD Landau and EM Lifshitz, Fluid Mechanics. 2000, Oxford: Butterworth-Heinemann.

[12] Chen, D.T., et al., Rheological microscopy: Local mechanical properties from microrheology. Physical Review Letters, 2003. 90(10).

[13] Lau, A.W.C., et al., Microrheology, stress fluctuations, and active behavior of living cells. Physical Review Letters, 2003. 91(19).

[14] Cardinaux, F., et al., Microrheology of giant micelle solutions. Europhys. Lett., 2001.

[15] Alberts, B., et al., Molecular Biology of the Cell. 4th ed. 2002, New York&London: Garland Publishing, Inc.

[16] Gardel, M.L., et al., Microrheology of entangled F-actin solutions. Phys. Rev. Lett., 2003. 91(15): p. 158302.

[17] M. Atakhorrami, G.H. Koenderink, J.F. Palierne, F.C. MacKintosh and C.F. Schmidt, manuscript in preparation **(Chapter 8)**.

[18] MacKintosh, F.C. and P.A. Janmey, Actin gels. Curr. Opinion in Solid State and Mater. Sci., 1997. 2: p. 350-357.

[19] Koenderink, G.H., et al., Submitted to Phys.Rev.Letter, 2005.

[20] Granek, R. and M.E. Cates, Stress-Relaxation in Living Polymers - Results from a Poisson Renewal Model. Journal of Chemical Physics, 1992. 96(6): p. 4758-4767.
[21] Cates, M.E. and S.J. Candau, Statics and Dynamics of Worm-Like Surfactant Micelles. Journal of Physics-Condensed Matter, 1990. 2(33): p. 6869-6892.
[22] Walker, L.M., Rheology and structure of worm-like micelles. Current Opin. Colloid Interf. Sci., 2001. 6: p. 451-456.
[23] Rehage, H. and H. Hoffmann, Rheological Properties of Viscoelastic Surfactant Systems. Journal of Physical Chemistry, 1988. 92(16): p. 4712-4719.
[24] Cardinaux, F., et al., Microrheology of giant-micelle solutions. Europhysics Letters, 2002. 57(5): p. 738-744.
[25] M.Buchanan, et al., Physical Review E, 2005. 72: p. 011504.
[26] M.Buchanan, et al., Macromolecules, 2005. 38(21): p. 8840.
[27] Berret, J.F., J. Appell, and G. Porte, Linear Rheology of Entangled Wormlike Micelles. Langmuir, 1993. 9(11): p. 2851-2854.
[28] Constantin, D., et al., High-frequency rheological behaviour of a multiconnected lyotropic phase. Europhysics Letters, 2002. 58(2): p. 236-242.
[29] Allersma, M.W., et al., Two-dimensional tracking of ncd motility by back focal plane interferometry. Biophys. J., 1998. 74: p. 1074-1085.
[30] Atakhorrami, M. and C.F. and Schmidth, in preperation. **(Chapter 1)**.
[31] Gittes, F. and C.F. Schmidt, Interference model for back-focal-plane displacement detection in optical tweezers. Optics Lett., 1998. 23: p. 7-9.
[32] Peterman, E.J.G., et al., Extending the bandwidth of optical-tweezers interferometry. Review of Scientific Instruments, 2003. 74(7): p. 3246-3249.
[33] K. Berg-Sørensen, a. and H. Flyvbjerg, Rev. Sci. Instrum., 2004. 75(594).
[34] Gittes, F. and C.F. Schmidt, Signals and noise in micromechanical measurements, in Methods in Cell Biology. 1998, Academic Press. p. 129-156.
[35] Landau, L.D., E.M. Lifshitz, and L.P. Pitaevskii, Statistical Physics. Pergamon international library of science, technology, engineering, and social studies. 1980, Oxford, New York: Pergamon Press.
[36] Levine, A.J. and T.C. Lubensky, One- and two-particle microrheology. Phys. Rev. Lett., 2000. 85: p. 1774-1777.
[37] M. Atakhorrami, et al., trapping effect in microrheology. (submitted to Phys Rev E, **(Chapter 3)**.
[38] Levine, A.J. and T.C. Lubensky, Response function of a sphere in a viscoelastic two-fluid medium. Physical Review E, 2001. 6304(4): p. art. no.-041510.
[39] M. Atakhorrami, et al., Short-time inertial response of viscoelastic fluids: observation of vortex propagation. Phys.Rev.Lett, 2005. 95(208302). **(Chapter 9)**
[40] Liverpool, T.B. and a.F.C. MacKintosh, Inertial effects in the response of viscous and viscoelastic fluids. Phys.Rev.Lett, 2005. 95: p. 208303.

[41] Levine, A.J. and T.C. Lubensky, Two-point microrheology and the electrostatic analogy. Physical Review E, 2002. 65(1).

Actin Networks

III

This part is based on the following papers:

1. G.H. Koenderink, **M. Atakhorrami**, F.C. MacKintosh, and C.F. Schmidt," High-frequency stress relaxation in semi-flexible polymer solutions and networks" (submitted to Physical Review Letters), (Chapter 7)
2. **M. Atakhorrami**, G.H. Koenderink, J.F. Palierne, F.C. MacKintosh and C.F. Schmidt," Cytoskeleton networks at the micron scale: anomalous dynamics due to non-continuum elasticity" (manuscript in preparation), (Chapter 8)

Chapter 7

High-frequency stress relaxation in semi-flexible polymer solutions and networks

Abstract

We measure the linear viscoelasticity of sterically entangled as well as chemically crosslinked networks of actin filaments over more than five decades of frequency. The high-frequency response reveals rich dynamics unique to semiflexible polymers, in particular a previously unobserved relaxation due to rapid axial tension propagation. For high molecular weight, and for crosslinked gels, we obtain quantitative agreement with theoretical predictions of the shear modulus in both amplitude and frequency dependence.

The machinery that drives essential functions of cells such as locomotion and division is based on an elastic network of interconnected semiflexible protein filaments, collectively referred to as the cytoskeleton [1]. A major component of the cytoskeleton is the actin cortex, a dense meshwork of crosslinked actin filaments beneath the plasma membrane. The actin cortex is controlled by a multitude of accessory proteins and is driving many dynamic cell functions. The physical construction of the cytoskeleton with its complex hierarchy of structural length scales makes it possible for the cell to effect large changes in physical properties by small chemical interventions, such as length- or crosslink-control or regulated attachments to other structures in the cell. The unique sensitivity of cytoskeletal networks stems to a large part from the semiflexible character of the constituent filaments, i.e., the fact that their thermal persistence length l_p (17 μm for filamentous (F-)actin [2]) is orders of magnitude larger than molecular scales (7 nm filament diameter of actin [2]).

The mechanical and dynamical (rheological) properties of semiflexible polymers have been the focus of intense research in recent years. Apart from their biological role, these networks have proven to be unique and fascinating polymeric materials in their own right. In contrast to flexible polymer networks, the elastic shear modulus of a semiflexible polymer network can be varied over many orders of magnitude by small changes in crosslinking [3-5], and exhibits strong non-linearities [3, 5-7]. The dynamics and viscoelastic properties of semiflexible solutions and gels have proven to be much richer than those of flexible polymers. Even for single filaments there are multiple distinct modes of relaxation that are qualitatively distinct from those of conventional polymers [6, 8-10]. It has proven challenging, however, to quantitatively probe those dynamic regimes experimentally, because of the extensive bandwidth required.

Here, we have measured the dynamic shear modulus of F-actin solutions and crosslinked gels over a range of frequencies from 1 Hz to nearly 100 kHz. We find quantitative agreement with theory in both amplitude and frequency dependence for the modulus at high frequencies, confirming the principal role of transverse thermal bending fluctuations in determining the solution/network response [11,12]. Furthermore, we demonstrate an intermediate-frequency relaxation mode that is

unique to semiflexible polymers, and is due to rapid stress propagation along the filament backbone leading to a retraction of the chain ends. This effect has been predicted [12-15], but has not been observed previously due to the time resolution required.

We achieve a bandwidth of 100 kHz by using an optical microrheology technique based on laser-interferometric detection of thermal fluctuations of embedded probe particles [10,16]. We have here used two-particle microrheology, measuring the cross-correlated thermal motion of pairs of particles at well-defined separations. Correlations in displacements result from hydrodynamic and elastic interactions transmitted through the intervening material and report bulk viscoelasticity, virtually unaffected by the local particle environment [17,18]. In contrast, the shear moduli derived from one-particle microrheology in actin have been shown to differ from the bulk moduli measured with conventional rheometers [17,19]. Discrepancies are in this case expected because the typically micron-sized probe beads are smaller than characteristic scales of actin filaments such as the persistence length.

Samples were prepared by mixing monomeric actin (G-actin) isolated from rabbit skeletal muscle [20] with silica spheres of 1.16 μm diameter, which were larger than the average mesh size [21] $\xi = 0.3/\sqrt{c_A}$, with c_A the actin concentration (0.5 to 2 mg/ml) [22]. Polymerization was initiated by buffer change [20] and the sample was loaded into a coverslip/microscope slide sample chamber, sealed with vacuum grease, and equilibrated for 1 hour at room temperature. Crosslinking was achieved by mixing G-actin (A) with small amounts of biotinylated actin (B) (ratio $r_{AB} = 50$) and neutravidin (N) ($r_{AN} = 25$). Microrheology was performed using laser interferometry and quadrant-photodiode detection in an inverted microscope, providing subnanometer resolution at 100 kHz bandwidth as described previously [10,16]. Pairs of probe particles located at least 20 μm away from the sample chamber walls were illuminated by two weak (<5 mW) focused laser beams with wavelengths of 1064 and 830 nm, respectively. The photodiode signals corresponding to the displacements of the two particles (labeled 1 and 2) from their respective detector-beam axes in the directions parallel (x) and perpendicular (y) to the line connecting the two particles were digitized at 195 kHz after anti-alias filtering [16]. From the

measured fluctuations $x_{1,2}(t)$ and $y_{1,2}(t)$ we calculated the parallel and perpendicular time-averaged cross-correlation functions, $C_{\parallel} = \int dt e^{i\omega t} < x_1(t)x_2(0) >$ and $C_{\perp} = \int dt e^{i\omega t} < y_1(t)y_2(0) >$. For an isotropic and homogeneous medium, these two components completely characterize the full tensorial correlations. The fluctuation-dissipation theorem relates these correlation functions to the corresponding mutual displacement response functions [23], $\alpha_{\parallel,\perp}(\omega) = \alpha'_{\parallel,\perp}(\omega) + i\alpha''_{\parallel,\perp}(\omega)$:

$$C_{\parallel,\perp}(\omega) = (2k_B T / \omega)\alpha''_{\parallel,\perp}, \quad (1)$$

where $k_B T$ is the thermal energy, and $\alpha''_{\parallel,\perp}$ refer to the imaginary parts of the complex response functions. The respective real parts $\alpha'_{\parallel,\perp}$ are computed from $\alpha''_{\parallel,\perp}$ by Kramers-Kronig integrals [10,23]. The connection between the complex response functions (corrected for the weak harmonic potentials created by the focused lasers [16]) and the complex shear modulus, $G(\omega) = G'(\omega) + iG''(\omega)$, is given by a generalization of the Stokes-Einstein (SE) relation, extended to the two-particle case [10,17,18]:

$$\alpha_{\parallel}(\omega) = 1/((4\pi r)G(\omega)), \quad \alpha_{\perp}(\omega) = 1/((8\pi r)G(\omega)) \quad (2)$$

For a viscous liquid of viscosity η, $G(\omega)) = -i\omega\eta$, and these expressions reduce to the familiar Oseen tensor [24]. Eqs. (2) assume an incompressible viscoelastic medium [10,25], which is a good approximation in our case. This assumption is supported by the fact that we obtain consistent results for $G(\omega)$ from the parallel and perpendicular displacement correlations (data not shown). The shear moduli presented here are based on the less noisy parallel channel. For separation distances r between about 3 and 20 μm there was no distance-dependence of the moduli, consistent with the assumption that the material connecting the particles at these distances behaves as a bulk viscoelastic material [17,18].

Figures 1(a) and (b) show the storage and loss moduli, G′(ω) and G″(ω), of a 1 mg/ml solution of actin filaments without and with crosslinking. The non-crosslinked solution has a low-frequency modulus of around 0.2 Pa, similar to values measured previously with conventional rheology [4] and microrheology [10,19]. The storage modulus shows no discernible elastic plateau over the frequency range studied here. After crosslinking, the storage modulus develops a plateau of around 46 Pa, while the loss modulus is slightly increased at intermediate frequencies and scales with frequency as $G''(\omega) \sim \omega^{3/4}$. Data at high frequencies can be quantitatively

compared with theory. Theoretical models of the viscoelastic response of semiflexible polymer networks [11,12] predict that the shear modulus at high frequencies is entirely controlled by the relaxation of individual polymer chains. When a polymer network is sheared, the thermally undulating filaments are either compressed or stretched, depending on their orientation with respect to the shear direction. Since the filaments are practically inextensible along their contour, the chain conformations re-thermalize by a redistribution of their bending modes, leading to a characteristic scaling of both the storage and loss shear modulus as $G(\omega) \sim \omega^{3/4}$ [11]:

$$G(\omega) \approx \frac{1}{15} \rho \kappa l_p (-2i\zeta / \kappa)^{3/4} \omega^{3/4} - i\omega\eta \qquad (3)$$

Here, the area density of filaments $\rho = c_A \times 3.8 \times 10^{13}$ m^{-2}, the bending stiffness $\kappa = l_p/k_BT$, and the lateral drag coefficient per unit length $\zeta \approx 0.0023$ Ns/m^2, are all known [11]. Thus, the solid lines in Figs. 1(a) and (b) represent the prediction of Eq. (3) with no adjustable parameters. The measured loss modulus $G''(\omega)$ for entangled actin approaches the theoretical prediction only at the highest frequencies probed, while upon crosslinking with practically irreversible biotin-neutravidin bonds, $G''(\omega)$ agrees with Eq. (3) over the whole experimental frequency range. The storage modulus $G'(\omega)$ for entangled actin also remains below the theoretical curve over the whole frequency range probed, while crosslinking leads to better agreement with Eq. (3) above the plateau. (The elastic moduli are cut off at about 10 kHz, due to the high-frequency limit of the Kramers-Kronig integral.) The plateau value of 46 Pa at low frequencies is consistent with theory [3,11] for an average distance between crosslinks of about 1.8 μm.

In a regime where the modulus is dominated by single-filament dynamics, it should be linear in actin concentration c_A. By contrast, collective phenomena (e.g., entanglement) will result in a stronger dependence. The inset of Fig. 1b shows that, within experimental error, the loss modulus (scaled by actin concentration c_A and multiplied by $\omega^{3/4}$) for actin concentrations between 0.5 and 2 mg/ml is close to a linear dependence. There appears to be, however, a slight increase of the scaled modulus with actin concentration. This may reflect a concentration-dependent filament length distribution.

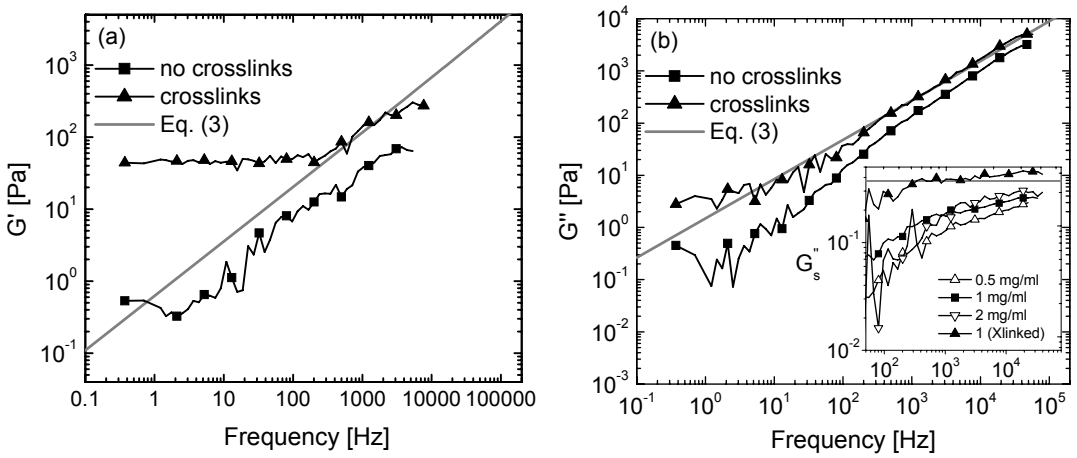

Figure 1: **(a)** Storage modulus $G'(\omega)$ and **(b)** loss modulus $G''(\omega)$ of 1 mg/ml solutions of F-actin filaments without (squares) and with (triangles) crosslinking plotted against frequency $f = \omega/2\pi$. Solid lines: theory, Eq. (3). Inset: scaled loss modulus $G_s(\omega) = (G''(\omega) - i\omega\eta)/(c_A\omega^{3/4})$.

Naïvely one would expect that entangled and crosslinked semiflexible polymer networks are indistinguishable at frequencies above the elastic plateau, where single-filament dynamics are probed. The fact that we find the shear moduli for entangled solutions of actin to be below both the crosslinked and the theoretically predicted modulus implies an additional mechanism for relaxation of stress that disappears with crosslinking. The deviation from Eq. (3) is emphasized in the insert of Fig. 1b, where the loss moduli are multiplied by $\omega^{-3/4}$. This inset also shows that the increased relaxation at intermediate frequencies is present for a range of actin concentrations. It has recently been suggested [12-15] that, in the case of semiflexible polymers of finite length, rapid tension propagation along the filament backbone leads to an additional relaxation of network stress by the retraction or extension of filament ends. Experimental proof of this mechanism has been lacking due to the limited bandwidth of previous experiments. The comparison of crosslinked and entangled networks in Fig. 1 provides one test for this mechanism, since crosslinking prevents filament end retraction. Note that for crosslinked networks we find

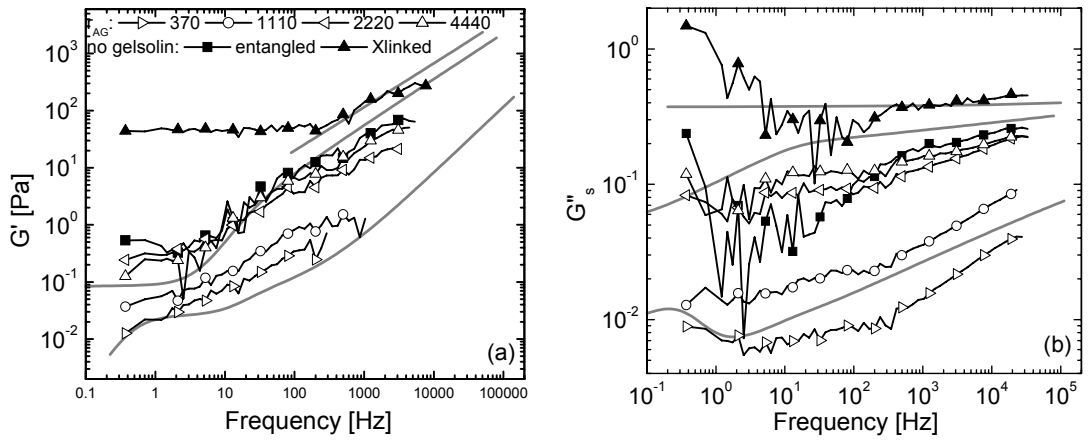

Figure 2: Filament length dependence of the storage modulus G′(ω) (a) and scaled loss modulus G″s (b) of a 1.0 mg/ml solution of F-actin filaments shortened with different amounts of gelsolin as indicated. Solid symbols: unshortened actin (see Fig. 1). Lines: high molecular weight theory, Eq. (3) (top), finite length theory with average lengths 17 μm (middle) and 3 μm (bottom).

quantitative agreement with high molecular weight theory with no adjustable parameters (Eq. (3), solid lines in Fig. 1).

We further test for this relaxation mechanism by examining the polymer length dependence, which should be strong since the time it takes for tension to propagate along a filament of length L increases rapidly with length as $t \sim L^8$ [12-15]. For shorter filaments the transition to the $\omega^{3/4}$ regime should occur at higher frequencies, and the network should be softer at lower frequencies. To control average filament length we added gelsolin, a physiological capping protein that binds to the barbed end of F-actin [26]. G-actin was polymerized at a fixed concentration of 1 mg/ml in the presence of gelsolin at actin/gelsolin molar ratios r_{AG} = 370-6290. Assuming random capping [26], we estimate average lengths between 1 and 17 μm. Figures 2(a) and (b) show that the storage and loss moduli indeed decrease as the filament length is reduced. The slope of $G''(\omega)$ (corrected for the solvent contribution) increasingly approaches 1, which is also consistent with a larger contribution of chain-end retraction to the stress relaxation.

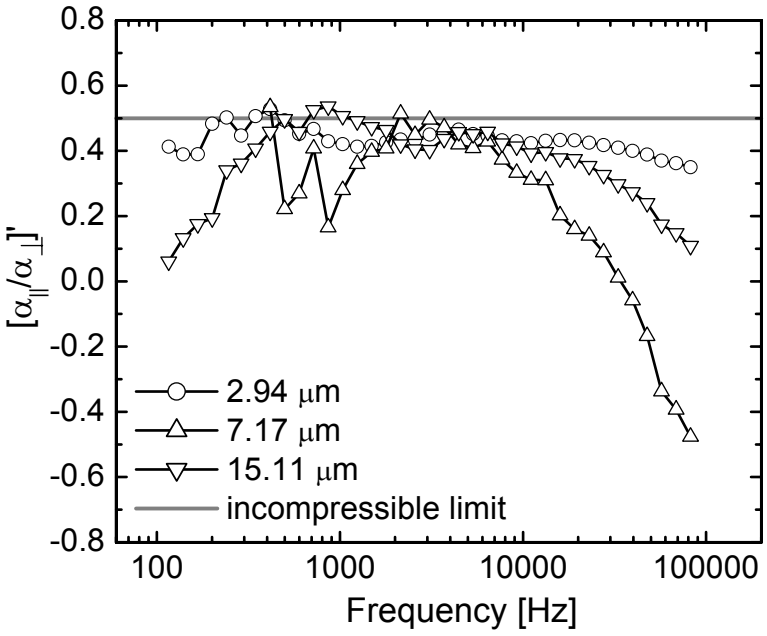

Figure 3: Ratio of the parallel and perpendicular response functions $[\alpha_{\parallel}/\alpha_{\perp}]$ for a pair of 1.16 μm beads in a 1.0 mg/ml actin solution at distances r as indicated. The real part of the ratio is plotted against frequency.

At present, there is no theory that accounts for the longitudinal relaxation while spanning dilute solutions and strongly entangled regimes. The lines in Fig. 2(a-b) are the predictions of Refs. [12,15] for dilute solutions of short chains (3 μm, bottom) and entangled solutions of long chains (17 μm, middle). This theory with chain end corrections, although it does not take into account the exponential length distribution of actin filaments [26], qualitatively captures the trend towards lower shear moduli as the chain length is shortened. The observed change in slope of $G''(\omega)$ to values higher than 3/4 is also consistent with the theoretical predictions.

The shear moduli reported here were all obtained from thermal fluctuations of micron-sized probe particles embedded in the actin solutions/networks, using the generalized SE relation, Eq. (2). This formalism assumes that the probe particles are embedded in an incompressible homogeneous medium [10,25]. Experimentally, the

importance of compressibility can be tested by considering the (real part of the) ratio of the parallel and perpendicular cross-correlated particle displacements [18]:

$$\left[\alpha_{\parallel} / \alpha_{\perp}\right] = \frac{3-4\sigma}{4(1-\sigma)}, \qquad (4)$$

which has physical bounds of 1/2 and 7/8, since the Poisson ratio σ is bounded by 1/2 and -1, where the former corresponds to an incompressible medium [10,25]. Figure 3 shows real part of $[\alpha_{\parallel} / \alpha_{\perp}]$ measured for three different separation distances *r* in an entangled network of actin filaments. The real part of ratio $[\alpha_{\parallel} / \alpha_{\perp}]$ is indeed close to 1/2, consistent with a strong viscous coupling of the actin network to the solvent and in support of the incompressibility assumption. The deviations apparent at high frequencies are quantitatively consistent with fluid inertial effects [16]. At low frequencies we are unable to demonstrate or exclude compressibility because of noise limitations, which are particularly pronounced in the perpendicular channel.

We have measured the complex shear modulus $G(\omega)$ of F-actin solutions and gels over a wide frequency range. We show that at high frequencies the response is dominated by single-filament bending fluctuations and is in quantitative agreement with theory [11,12]. Further, we demonstrate a dynamic mode that is unique to (non-crosslinked) semiflexible polymers, which is due to rapid axial stress relaxation through free filament ends. Both relaxation modes are only apparent at high frequencies which have not previously been accessible. Laser-based particle trapping and tracking methods such as those presented here open an extended view on complex polymer dynamics, which is very relevant for biological systems with their inherently broad distribution of characteristic time scales. Important future challenges include the extension of the high-frequency microrheology technique to include active driving of the particles and the study of the out-of-equilibrium properties of biological systems.

Acknowledgements

We thank A. Levine, D. Head, D.C. Morse, M. Pasquali, and K.M. Addas for helpful discussions, F. Gittes, J. Kwiecinska, and M. Buchanan for help with software development, K.C. Vermeulen for the actin, and P.A. Janmey for the gelsolin. This

work was supported by the Foundation for Fundamental Research on Matter (FOM) and by a European Marie Curie Fellowship (FP6-2002-Mobility-6B, contract 8526).

References

[1] B. Alberts, D. Bray, J. Lewis, M. Raff, K. Roberts, and J.D. Watson, *Molecular Biology of the Cell* (Garland publishing, New York, 1994).

[2] F. Gittes, B. Mickey, J. Nettleton, and J. Howard, J. Cell Biology 120, 923 (1993).

[3] F.C. MacKintosh, J.A. Käs, and P.A. Janmey, Phys. Rev. Lett. 75, 4425 (1995).

[4] J. Xu, W.H. Schwarz, J.A. Käs, T.P. Stossel, P.A. Janmey, and T.D. Pollard, Biophys. J. 74, 2731 (1998).

[5] M.L. Gardel, J.H. Shin, F.C. MacKintosh, L. Mahavedan, P. Matsudaira, and D.A. Weitz, Science 304, 1301 (2004); Phys. Rev. Lett. 93, 188102 (2004).

[6] P.A. Janmey, et al., J. Biol. Chem. 269, 32503 (1994).

[7] C. Storm, J.J. Pastore, F.C. MacKintosh, T.C. Lubensky, and P.A. Janmey, Nature 435, 191 (2005).

[8] F. Amblard, A.C. Maggs, B. Yurke, A.N. Pargellis, and S. Leibler, Phys. Rev. Lett. 77, 4470 (1996).

[9] H. Isambert and A.C. Maggs, Macromolecules 29, 1036 (1996).

[10] F. Gittes, B. Schnurr, P.D. Olmsted, F.C. MacKintosh, and C.F. Schmidt, Phys. Rev. Lett. 79, 3286 (1997); B. Schnurr, F. Gittes, F.C. MacKintosh, and C.F. Schmidt, Macromolecules 30, 7781 (1997).

[11] F. Gittes and F.C. MacKintosh, Phys. Rev. E 58, R1241 (1998).

[12] D.C. Morse, Phys. Rev. E 58, R1237 (1998); Macromolecules 31, 7044 (1998).

[13] R. Everaers, F. Juelicher, A. Ajdari, and A.C. Maggs, Phys. Rev. Lett. 82, 3717 (1999).

[14] M. Pasquali, V. Shankar, and D.C. Morse, Phys. Rev. E 64, 020802 (2001).

[15] V. Shankar, M. Pasquali, and D.C. Morse, J. Rheol. 46, 1111 (2002).

[16] M. Atakhorrami, G.H. Koenderink, J. Kwiecinska, K.M. Addas, A.J. Levine, F.C. MacKintosh, and C.F. Schmidt (unpublished).

[17] J.C. Crocker, M.T. Valentine, E.R. Weeks, T. Gisler, P.D. Kaplan, A.G. Yodh, and D.A. Weitz, Phys. Rev. Lett. 85, 888 (2000).

[18] A.J. Levine and T.C. Lubensky, Phys. Rev. Lett. 85, 1774 (2000); Phys. Rev. E 65, 011501 (2002).

[19] M.L. Gardel, M.T. Valentine, J.C. Crocker, A.R. Bausch, and D.A. Weitz, Phys. Rev. Lett. 91, 158302 (2003).

[20] J.D. Pardee and J.A. Spudich, in *Structural and Contractile Proteins Part B: The Contractile Apparatus and the Cytoskeleton*, edited by D. W. Frederiksen and L. W. Cunningham (Academic Press, San Diego, 1982), p. 164. Actin was purified from rabbit skeletal muscle and stored in G-buffer (2 mM Tris, 0.2 mM $CaCl_2$, 0.2 mM Na_2ATP, 0.5 mM NaN_3, 2 mM DTT, pH 8.0) at -80°C. Thawed actin was polymerized by adding 1/10 of the final sample volume of 10×F-buffer to a final concentration of 2 mM HEPES, 2 mM $MgCl_2$, 50 mM KCl, 1 mM Na_2ATP, 1 mM EGTA, pH 7.5.

[21] C.F. Schmidt, M. Baermann, G. Isenberg, and E. Sackmann, Macromolecules 22, 3638 (1989).

[22] The actin concentration was determined from the absorbance at 280 nm (extinction coefficient 0.65 $cm^{-1}mlmg^{-1}$) and a Bradford assay with a BSA standard.

[23] L.D. Landau and E.M. Lifshitz, *Mechanics: Volume 1, Course of Theoretical Physics* (Elsevier, Oxford, 1960).

[24] C.W. Oseen, *Neuere Methoden und Ergebnisse in der Hydrodynamik* (Akademische Verlagsgesellschaft, Leipzig, 1927).

[25] A.J. Levine and T.C. Lubensky, Phys. Rev. E 63, 041510 (2001).

[26] S. Burlacu, P.A. Janmey, and J. Borejdo, Am. J. Physiol. 262, C569 (1992).

Chapter 8

Cytoskeleton networks at the micron scale: anomalous dynamics due to non-continuum elasticity

Abstract

We probe the local and macroscopic viscoelasticity of entangled F-actin solutions as a model system for the cytoskeleton of the cell. We compare the macroscopic rheology measured with a special custom made piezo- rheometer (up to 10kHz) with high bandwidth one- and two-particle microrheology (up to 100kHz) using optical tweezers. In this way, we confirm that two-particle microrheology measures macroscopic rheology for a wide range of frequency. Simultaneous comparison of one- and two-particle microrheology probed with different particle sizes; demonstrates the local interactions of particles with the surrounding semi-flexible network. One-particle microrheology underestimates the macroscopic modulus, which is due to a depletion of polymers around the particles. Also, non-affine deformations of network around the particles results in an anomalous $\omega^{9/16}$ frequency dependence of the storage modulus at low frequency for small probe sizes.

8.1 Introduction

One of the major challenges for a quantitative understanding of the dynamics of living cells is their extreme structural and dynamic complexity. From a materials perspective, cells are highly structured composites combining soft membranes with more or less rigid polymer networks and organelles against a background of a highly concentrated macromolecular solution. The whole system is out of equilibrium, as active force and motion generation is crucial for many cellular processes. In most cells, the main mechanical component of this composite is the cytoskeleton, of which the principal ingredient is the filamentous protein F-actin [1]. *In vitro* solutions and crosslinked networks of actin alone already have a complex structure with rich dynamics determined by a multitude of characteristic length scales, ranging from monomer size (50Å) through the persistence length (17μm) up to the filament length (up to tens of μm). In networks, additional collective length scales emerge, such as the mesh size (typically of the order of 100 nm in cells), and the entanglement length or crosslink distance. Viscoelastic properties of both *in vitro* actin networks as well as the cytoskeleton *in vivo* are thus expected to be highly dependent on the length and time scales on which they are probed. This has made quantitative mechanical characterization of the cytoskeleton and whole cells challenging.

An ideal set of techniques to explore such rich dynamic behavior in model systems, as well as in cells, is microrheology. These techniques involve the use of micron-sized particles to probe the local mechanics of the medium [2,3]. Conventional rheology, widely used in polymer and materials science, using cm-sized probes can measure macroscopic viscoelastic properties, usually at frequencies below about 20 Hz. With smaller probes one can extend the accessible bandwidth, as well as probe smaller length scales. As long as the probe scale remains above the characteristic length scales of the system, one expects the response/motion of the probe particles to reflect the continuum (visco)elasticity of the medium they are embedded in. This has been confirmed with synthetic polymer solutions of wormlike micelles [4,5] and also with biological material, the filamentous fd virus [6]. When the characteristic length scales of the medium are comparable to the probe size, as is the case with cytoskeletal networks, one can to some extent circumvent the

length scale problem to achieve quantitative results by using two-particle correlation methods [7,8,9].

As we show here, however, one can also exploit the probe size dependence as a new window onto the local structural and dynamic environment of these complex materials. One way to do this is to focus on the deviations from the continuum elastic behavior. Some of the effects one can detect are created by the probe particle itself, while others are intrinsic to the material. An example of the former is the expected entropic depletion near the probe particle [8,10], which is characterized by a concentration decrease of the surrounding polymer matrix near the surface of the particle that becomes measurable when the range of depletion becomes comparable to the probe size. An example of the latter effect is the predicted transition from predominantly locally bending deformations of semiflexible polymers in a network to larger-scale affine deformations involving pure stretching of the (thermally fluctuating) polymers [11-14]. Some evidence for depletion in actin solutions has been reported previously [15,9] but the lack of comparison at high frequencies has prevented a quantitative characterization up to now. Likewise, indications for a deviation from continuum elasticity at small scales and at low frequencies have been suggested [16] and reported in the same studies [15,9].

With much improved technology we have now detected a strong signature in single-particle microrheology results with actin that is consistent with a bead-size dependent depletion effect. We have also found a striking effect of non-continuum elastic response at low frequencies. We present a theoretical model explaining how the transition from non-affine to affine deformations results in a scaling form of the apparent shear modulus with a power-law exponent of 9/16, which is clearly observed in the data.

8.2 Experimental section

8.2.1 Sample preparation

Samples were prepared by polymerizing monomeric actin (G-actin) isolated from rabbit skeletal muscle [17] in the presence of silica probe spheres of different diameters (D = 0.5, 1.16, 2.56, and 5 μm, standard deviation ca. 5% in all cases). The

probe particles were all larger than the average *mesh size* $\xi = 0.3/\sqrt{c_A}$ of the actin networks studied (the actin concentration c_A was varied between 0.5 and 2 mg/ml. Actin polymerization was initiated by adding polymerizing buffer to bring the KCl, $MgCl_2$, and Na_2ATP concentrations to 50 mM, 2 mM, and 1 mM, respectively. The samples were quickly loaded into coverslip/microscope slide sample chambers (volume 20 μl) and sealed with vacuum grease. Samples were equilibrated under constant slow rotation for 1 hour at room temperature.

8.2.2 Macrorheology measurements

High-frequency macrorheology measurements of the linear viscoelastic shear moduli of entangled actin solutions were performed with a custom-built piezorheometer, described in details elsewhere [29,30]. The sample was contained between two glass plates, each mounted on a piezoelectric ceramic. One of the plates oscillates sinusoidally in the vertical direction with an amplitude of about 1 nm. The induced squeezing flow leads mainly to a shear strain, with some extensional flow in the center of the gap. The vertical stress transmitted to the second plate is measured by the other piezoelectric element. The strain is extremely small ($\sim 2 \times 10^{-6}$), ensuring that the sample structure is not altered by the flow. This piezorheometer affords a frequency range of 0.1 Hz to 10 kHz, much wider than the frequency range of conventional rheometers. The set-up was hermetically sealed to avoid evaporation and kept at a constant temperature of 21.4°C. The reproducibility of experiments was tested for three different samples.

8.2.3 Microrheology measurements

Microrheology experiments were performed with a custom-built dual optical tweezer set-up, created by focusing two laser beams with wavelengths λ of 1064 nm (ND:YVO_4, Compass, Coherent, Santa Clara, CA, USA) and 830nm (diode laser, CW, IQ1C140, Laser 2000), respectively, into an inverted microscope [18,19]. Pairs of probe particles were selected that were located at distances equal to at least 10 times the bead diameter away from the walls of the sample chamber and far from other particles (except for D = 5μm, with a minimum distance of 40μm from the surface).

The laser foci were moved into the centers of the selected particles using a pair of telescope lenses in each beam [15,19]. In order to minimize the trapping effect, for the (λ = 1064 and 830nm) laser traps, the trap stiffness of the laser foci was less than 3pN/m, and 2 pN/m, respectively. For the largest particles with diameters of 5 μm, a higher laser power corresponding to 5 pN/m trap stiffness, (measured in water) was required to avoid high-frequency shot noise. The fluctuations of both particles from the centers of their traps were simultaneously monitored in the x and y directions using a back focal plane interferometric method with quadrant photodiode (QPD) detection [20]. We achieved a spatial resolution with instrumental noise generating a noise density of ~ 0.001 nmHz at 195kHz. We typically used a sampling rate of 195kHz. To avoid the wavelength dependent low-pass filtering of the QPD [21], we used a special silicon PN photodiode with a reverse bias voltage of 100 V (YAGG444-4A, Perkin Elmer, Vaudreuil, Canada) for the λ = 1064 nm laser light, while the λ = 830nm light was detected with a standard silicon-type PN QPD operated with a reverse bias voltage of 15 V (10 mm diameter, Spot9-DMI, UDT, Hawthorne, CA). Output voltages were digitized with an A/D interface (195kHz) and recorded in Labview (National Instruments). The output voltages were calibrated by analyzing the thermal motion of probe particles from the same batch for each trap independently in water [22]. In each sample at least 15 pair of particles were probed. The position fluctuation of each pair has been recorded for 80s and repeated for 10 times. The reproducibility of the measurements have been tested for at least 3 different samples with the same procedure.

8.2.4 Analysis of microrheology data

From the measured thermal fluctuations $u_x^1(t)$ and $u_y^1(t)$ of particle 1 and $u_x^2(t)$ and $u_y^2(t)$ of particle 2, we calculated the Fourier transforms of the time averaged auto- and cross-correlation displacement fluctuations by FFT. The auto-correlation functions (e.g. $S_x^1(\omega) = \int \langle u_x^1(t) u_x^1(0) \rangle e^{i\omega t} dt$ for the motion of particle 1 in the x direction) were averaged over x and y directions of both particles ($S_{Auto}(\omega)$). The parallel cross-correlation function was computed from correlated particle motions parallel to the line connecting the centers of the particles: $S_{\parallel}(\omega) = \int \langle u_x^1(t) u_x^2(0) \rangle e^{i\omega t} dt$. The

perpendicular correlation function $S_{\perp}(\omega)=\int\left\langle u_y^1(t)u_y^2(0)\right\rangle e^{i\omega t}dt$ generated the same shear moduli, but was noisier and also more affected by fluid inertia [23,24] at high frequencies, and was therefore not used in averaging. The fluctuation-dissipation theorem relates the fluctuation auto- and cross-correlation functions to the imaginary part of the corresponding single- and inter-particle displacement response functions $\alpha_{Auto,\parallel,\perp}(\omega)=\alpha'_{Auto,\parallel,\perp}(\omega)+i\alpha''_{Auto,\parallel,\perp}(\omega)$ through [25,26]:

$$\alpha''_{Auto,\parallel,\perp}(\omega)=\frac{\omega}{2k_BT}S_{Auto,\parallel,\perp}(\omega)\,, \qquad (1)$$

where k_BT is the thermal energy. The real part of the complex response functions can be computed from its imaginary part by a Kramers-Kronig integral [15, 25, 26]. The connection between the complex response functions and the complex shear modulus, $G(\omega)=G'(\omega)+iG''(\omega)$, is given by a generalization of the Stokes-Einstein relation to the two-particle case [15,7,27]:

$$\alpha_{Auto}(\omega)=\frac{1}{6\pi RG(\omega)}\,,\quad \alpha_{\parallel}(\omega)=\frac{1}{4\pi rG(\omega)} \quad \text{and} \quad \alpha_{\perp}(\omega)=\frac{1}{8\pi rG(\omega)}\,, \qquad (2)$$

where $R=D/2$ is the particle radius, and r is the particle separation. For a viscous liquid of viscosity η, $G(\omega)=i\omega\eta$, and these expressions reduce to the familiar Oseen tensor [28]. These expressions neglect fluid inertia, which is a good approximation for the separation distances used here (10 to 15 μm) for the parallel inter-particle response function. The effect of the optical traps on the shear moduli for the low laser powers used here is likewise negligible. The shear moduli measured by 1PMR are generally less noisy, mostly because the amplitude of the cross-correlation signal decays as 1/*r* and thus the distance-independent noise sources become more relevant for 2PMR. Also, each 1PMR data set is an average over 4 independent channels (the *x*- and *y*-directions of two particles), while the 2PMR result is calculated from only one data set (parallel direction).

8.3 Results and discussions

The high-frequency regime of the linear rheology of entangled and crosslinked actin networks is theoretically well understood, [31,32] in terms of the rapid relaxation of the bending fluctuations of individual deformed filaments.

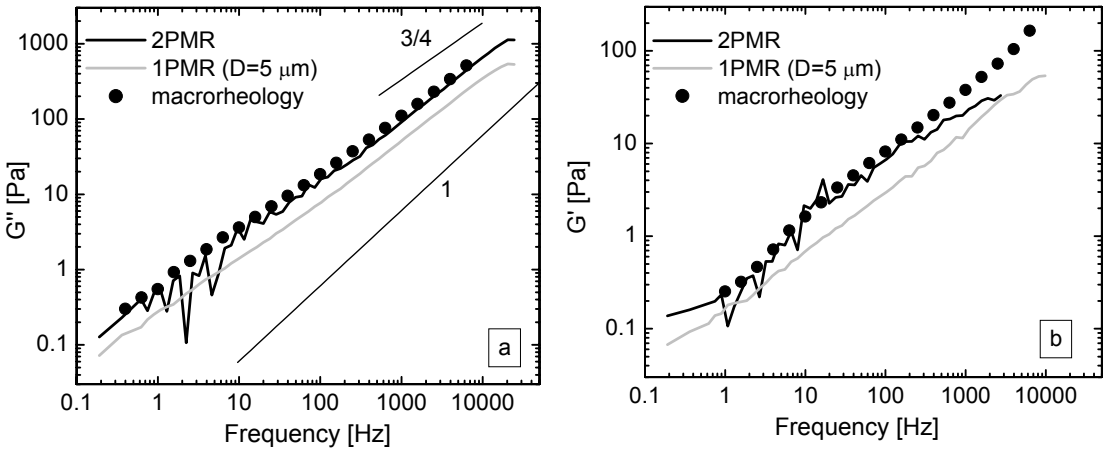

Figure.1: (a) loss moduli $G''(\omega)$ and (b) storage moduli, $G'(\omega)$ measured with 1PMR , 2PMR and macro rheology using the piezo-rheometer for extended frequency range $\omega = 2\pi f$ in an 1mg/ml entangled actin network. Shear moduli obtained from 2PMR with D = 5μm (black line) and D = 1.16μm (black broken line) agree well with the results of macro-rheology measurements (symbols). 1PMR measures smaller moduli than macrorheology with D = 5μm (gray line). Sampling rates used for measurements were 100 kHz (D = 5μm), and 195 kHz (D =1.16μm).

The single-filament model predicts a power-law scaling of the moduli with frequency as $\omega^{3/4}$, and was quantitatively confirmed in recent experiments [33]. The dynamics at intermediate frequencies for non-crosslinked filaments of finite length are expected [34] to involve an additional relaxation mechanism based on the extension/retraction of the filament ends. This mechanism was recently demonstrated using two-particle microrheology [33]. Given the fact that intrinsic length scales in actin networks are of the order of micrometers, one expects that deviations in the local elastic response, reflecting non-affine filament deformations and the break-down of continuum elasticity should be visible on micrometer length scales. Thus 1PMR should be influenced by such local effects while 2PMR with particle separations >10μm might not. Thus we need to confirm that 2PMR measures

macroscopic rheology. Figure 1 (a and b) shows a comparison of macroscopic rheology measurements (symbols) and 2PMR measurements of the storage and loss shear moduli $G'(\omega)$ and $G''(\omega)$ of a 1 mg/ml actin solution over a wide range of frequencies, $\omega = 2\pi f$. The shear moduli measured with 2PMR do not show any significant particle-size dependence (compare the results for 5μm diameter particles (black solid line) and 1.16μm particles (black broken line)) and agree well with the macrorheology data. This provides a strong confirmation that 2PMR measures the macroscopic rheology. At low frequencies, the loss modulus measured with 2PMR remains noisy. Even after extensive averaging of 300 data set of each 80seconds for unknown reasons are much noisier than data for networks of shortened actin filaments. This noise is more pronounced for smaller particles. We speculate that the origin of this noise could be related to the slow relaxation of large scale density fluctuations in these non-ergodic systems. Figure 1 also shows that the shear moduli measured with 1PMR (gray lines) using 5μm particles are below the macroscopic moduli, but have a similar frequency dependence. Apparently, the single-particle response function probes a less rigid local environment.

In order to elucidate the differences between the magnitudes of the shear moduli measured by 1PMR and 2PMR, we used different particle sizes. Figure 2 shows measured loss moduli for probe particles with diameters of 0.52μm (solid line), 1.16μm (broken line), 2.56μm (line with symbol), and 5μm (line with cross), as well as the macroscopic shear values (filled circles). In all cases the $G''(\omega)$ measured with 1PMR data have a smaller magnitude than the macroscopic measured data, while the frequency dependence is similar, particularly at high frequency. The apparent 1PMR loss modulus increases with increasing particle size. The most likely explanation for this behavior is the existence of a steric depletion zone around the particles [7,9,32]. Since individual particle displacements effectively probe a length scale of order the particle diameter, even a small *depletion layer* can significantly affect the measured response, especially for smaller particles.

Such a depletion layer is expected theoretically on very general grounds. For any polymer in the vicinity of an obstacle, or boundary, conformations of the polymer are suppressed because of exclusion by the obstacle. For a dilute solution of flexible polymers, the range of this exclusion is of the order of the radius of gyration,

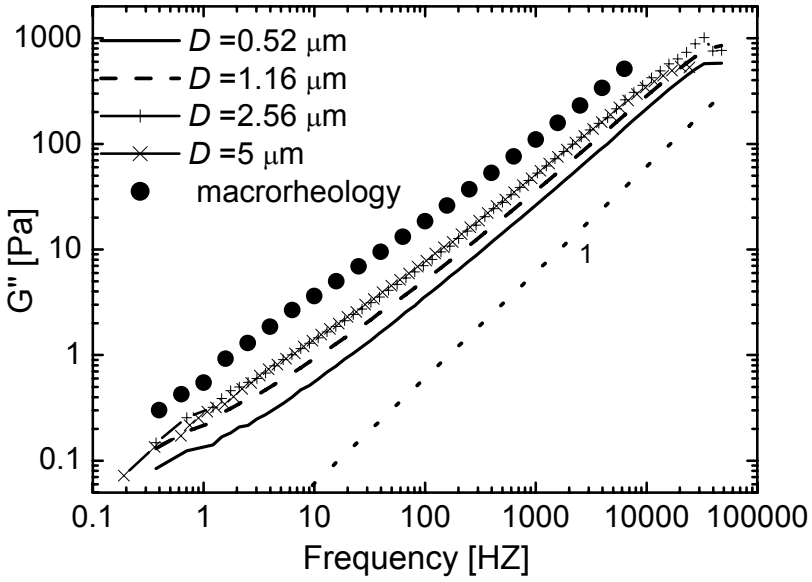

Figure 2: Loss moduli $G''(\omega)$ of 1mg/ml actin, measured with 1PMR compared for different particle diameters of D = 0.52 μm, 1.16 μm (lines), 2.56 and 5μm (line and symbols). The macroscopic shear results are plotted for reference (symbols) and the dotted-line with slope 1 is the loss modulus of the solvent.

or typical overall size of the polymer coil. For entangled solutions of flexible polymers, this length is expected to be of the order of the *mesh size*, or typical distance between neighboring polymers. In the case of semiflexible polymers, the effect is strongly enhanced due to their stiffness: near a hard wall, for instance, semiflexible polymers tend to be excluded from a zone with a thickness of the order of the polymer length or persistence length, whichever is larger. In the vicinity of a spherical probe particle, the situation is more subtle, although a smaller depletion layer can be expected. Nevertheless, estimates based on rigid rods suggest that the depletion layer is still of order the size of the probe particle [10]. In addition to affecting the concentration of polymers, however, the presence of a probe particle is also expected to affect the orientation of polymer: near the surface of the particle,

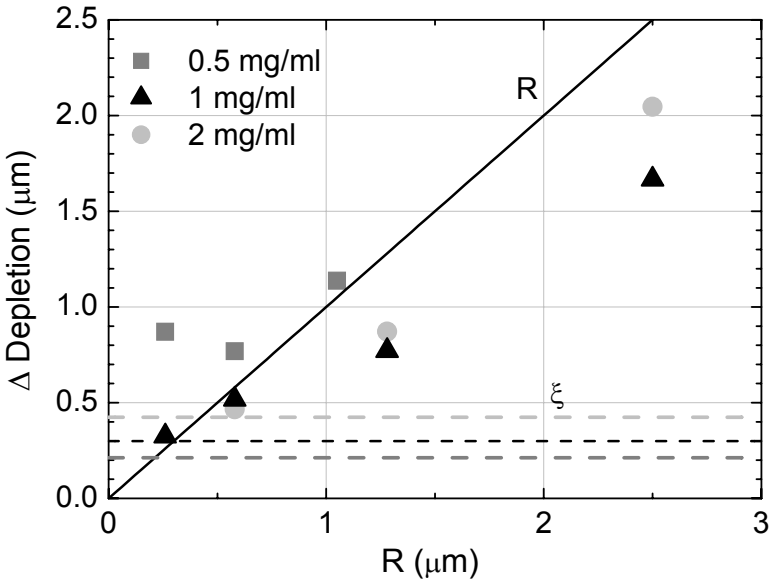

Figure 3: Depletion length computed from the measured data using the shell model (above 10kHz) versus particles radius for different concentrations of actin c = 0.5 (gray square), 1 (black triangle) and 2 mg/ml (light gray circle). The broken lines respected the mesh size for each of the concentrations. The solid line linear dependence to the particle radius (*R*).

polymers will tend to align parallel to the surface, while radial orientations of polymer will be strongly/completely suppressed. For semiflexible polymers, however, this effect is reduced by the lateral fluctuations of the polymer, allowing it to fluctuate out of the way of the probe [35].

Given a depletion layer, a simple model allows us to estimate the effective viscoelastic response function of a particle with a steric depletion layer. This is based on recent work of Levine and Lubensky [27]. In this so-called *shell model*, it is assumed that there is a shell surrounding the particle in which the polymer is depleted, resulting in a region with different viscoelasticity from the macroscopic shear modulus of the medium. This region is assumed to extend over a distance Δ [36] from the surface of the probe.

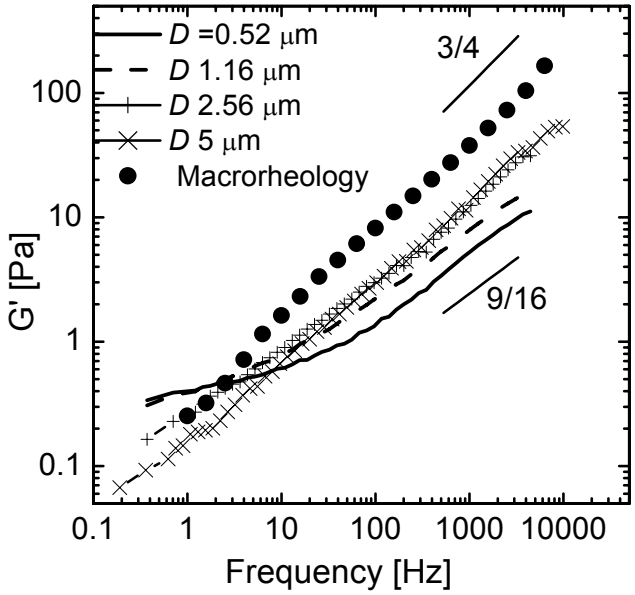

Figure 4: $G'(\omega)$ measured with 1PMR in c = 1mg/ml actin, compared for different particles diameters of D = 0.52, 1.16 (lines), 2.56 and 5μm (line and symbols). The macroscopic shear results are plotted for reference (symbols). The line with slope of 3/4 is the expected high frequency scaling and the line with slope of 9/16 is expected from the non-affine deformation.

As noted above, this length is expected to depend on both the size of the probe particle as well as on the properties (especially the stiffness) of the surrounding polymers.

In the following, we estimate the depletion zone thickness Δ using this model, assuming that the material inside the shell is pure solvent (with known viscosity 0.969 mPa.s) and outside the shell is a continuous viscoelastic network characterized by the shear moduli measured with 2PMR. From the difference between the loss moduli measured with 1PMR and 2PMR at high frequency (above 10 kHz) we calculate the depletion distance. Figure 3 shows the resulting depletion zone thicknesses for different particle sizes and different actin concentrations c (0.5, 1, and

2 mg/ml). All particle sizes are bigger than the mesh size of the actin solutions, so the probe particles are prevented from simple diffusion through the porous mesh of polymers [16,9].

The model we used to calculate the depletion length assumes a step profile for the polymer concentration, going from zero in the shell to the macroscopic value outside the shell. In reality, however, there is a smooth concentration profile of filaments near the particle surface. Nevertheless, our results are consistent with a depletion zone that grows with particle size. In particular, these results are not consistent with a depletion length of the order of the mesh size between polymers, as would be expected for solutions of entangled flexible polymers.

The storage modulus measured with 1PMR exhibits a more complex particle size dependence than the loss modulus, as shown in Fig. 4, which compares macroscopic storage moduli (symbols) with moduli measured with 1PMR using particles with diameters of 0.52μm (black line), 1.16μm (black broken line), 2.56μm (line with symbol) and 5μm (line with cross).For all of the particle sizes used in these one-particle measurements underestimate the macroscopic modulus at frequencies above 10Hz, which is consistent with the depletion model (smaller particles measure a softer environment). However, at low frequencies an opposite trend with respect to the particle size occurs. The smallest particles of 0.5μm and 1.16μm even show a $G'(\omega)$ than was even larger than the macroscopic modulus and exhibit apparent elastic plateau that is not seen in the macroscopic data.

In addition at higher frequencies also the slope of $G'(\omega)$ was different for different particle sizes. This observation suggests a second non-continuum effect arising from the interaction of the particles with the surrounding network. As a small particle moves in the vicinity of a single stiff filament, it will displace the filament by an amount u perpendicular to the filament. The associated elastic energy due to bending is approximately $E_{bending} \sim ku^2/\lambda^3$, where λ is the characteristic length over which the filament bends and k is the bending modulus. In addition to this bending energy, the displaced filament will also displace the surrounding elastic continuum. Away from the particle, if we assume that $\lambda >> R$ (particle radius), this displacement of the surrounding medium gives an elastic energy that is approximately $E_{elastic} \sim Gu^2\lambda$, where *G* is the macroscopic complex shear modulus.

There is a balance or optimization of the total elastic energy, the sum of these terms, from which we find that [37] $\lambda \sim \lambda_0 = \sqrt[4]{k/G}$. Once we plug this back into the full elastic energy, we find an effective restoring force due to the filament given by $f \sim -Gu\lambda_0$. This picture of course assumes that λ is large compared with the particle radius R. However, since this length tends to decrease with increasing G, we can expect this to be violated in stiffer media. Of course, this resulting in the usual restoring force $f \sim -GuR$, for a particle in an elastic continuum. Thus, a transition is expected between a particle-dominated and a filament-dominated response. This transition is given by $\lambda_0 = \sqrt[4]{k/G} \sim R$, where we shall assume that *G* has the form of $G = Ac\omega^z$ above the plateau, and $G = G^{(0)}$ in the plateau region, which we also assume occurs below a frequency ω_e. Given all of this, the crossover frequency below which the filament mechanical effects should become apparent, is of order $\omega_0 \sim (k/cR^4)^{1/z}$.

In addition to this crossover, one can estimate the effect that this has on measurements of the shear modulus. In this picture, the restoring force below the crossover frequency begins to look as though the particle were of size λ_0. In other words, the particle looks larger than it is, due to its interactions with stiff filaments that tend to spread the force out. From the restoring force above, this means that, interpreted in terms of the particle radius R, the microrheology would yield an apparent *local* modulus given by $G_{local} \sim G\lambda/R \sim (c\omega)^{3z/4}/R$, where $G = Ac\omega^z$, with *z* = 3/4 is the high-frequency-dependence of the macroscopic shear modulus. Within this model we expect to see a probe-size-dependent "apparent" elastic modulus, when measured with 1PMR at low frequency with a $\omega^{9/16}$ frequency dependence, which connects to the expected macroscopic rheology (at high frequencies $\omega^{3/4}$).

In Fig. 4, from the high end of the frequency range to approximately two decades lower, the slope of $G'(\omega)$ for the two smallest probes with diameters *D* = 0.5μm (solid line) and 1.16 μm (black broken line) is 9/16, while for bigger particles, *D* = 2.56μm, (line with symbols) the slope equals 9/16 over the whole frequency range. The slope of $G'(\omega)$ for the largest particles (*D* = 5μm, line with cross) is similar to the macroscopic shear measurements and is close to 3/4 at high frequency. The particle size (*R*), crossover frequency (ω_0), scales with $R^{16/3}$ in actin solution with assumption that *z* = 3/4 is the high frequency dynamics.

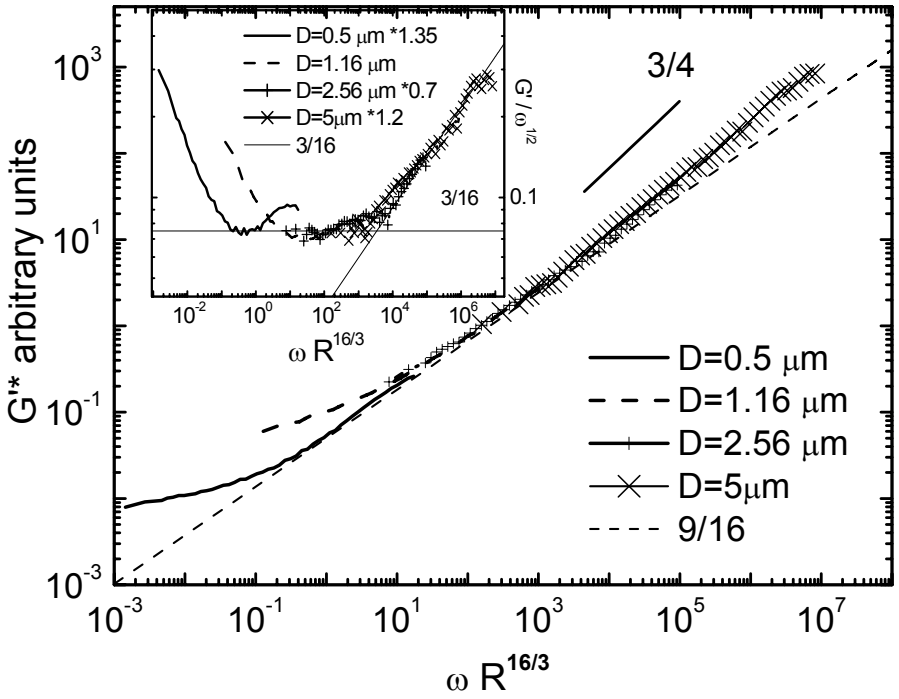

Figure 5: Normalized $G'(\omega)$ of 1mg/ml actin, measured with 1PMR for different particle diameters, are plotted versus frequency normalized by 2π $R^{16/3}$. $G'(\omega)$ are multiplied by arbitrary values to obtain a collapse of data on to $\omega^{9/16}$ (broken thin line). Insert: The same data where the $G'(\omega)$ multiplied by $\omega^{9/16}$, line with slope of 3/16 is expected 3/4 of high frequency actin rheology in this way of ploting.

In Fig. 5 the "local" storage modulus measured with 1PMR is plotted versus the scaled frequency with the particle size. $G'(\omega)$ is shifted to overlap the different particle sizes, which is necessary to compensate for the depletion effect. The values we used for the multiplication for different particle sizes were larger than the one calculated from the shell model using the loss modulus at high frequencies. The broken line in the plot represents $\omega^{9/16}$, and shows that the elastic modulus scales with $\omega^{9/16}$ for a large frequency range, changing to $\omega^{3/4}$ at high frequency. In the

inset we look closer at the scaling regime, by plotting $\omega^{9/16}G'(\omega)$ versus $\omega R^{16/3}$. The flat line is the region of scaling and at high frequency $\omega^{3/16}$ is the high frequency macroscopic shear scaling in this representation.

With this model the depletion affects G′ more than G″, we expostulate that this is because of polymers are depleted around particles, but there is still a viscous fluid around the particle which contributes to the loss modulus. However the smaller number of polymers does result in a smaller contribution to the elastic modulus. Using the Kramers-Kronig integral we introduce a cut-off on the frequency obtained in G′ and our data do not extend to higher than 5 kHz to test this hypothesis. This is consistent with our observation of the need for a greater depletion effect to be able to collapse the G' data on top of each other with the 9/16 scaling. This finding casts doubt on the interpretation of various video-based) low-frequency microrheology results in actin solutions, where a 1/2 power law exponent has been seen.

We have shown that the possibility of probing wide range of particle sizes (0.5 to 5μm) and frequencies (0.1 to 100 kHZ), with interferometric microrheology, provides an effective method to study size-dependence dynamical interactions between particles and their surrounding network.

8.4 Acknowledgments

We thank A. Levine, D. Head, D.C. Morse, M. Pasquali, K.M. Addas, J. Liu, D. Weitz and P.A. Janmey for helpful discussions, J. van Mameren, F. Gittes, J.I. Kwiecińska and M. Buchanan for help with data-evaluation software, K.C. Vermeulen for actin preparation. This work was supported by the Foundation for Fundamental Research on Matter (FOM).

8.5 References

[1] B. Alberts, A. Johnson, J. Lewis, et al., *Molecular Biology of the Cell* (Garland Publishing, Inc., New York&London, 2002).

[2] F. C. MacKintosh and C. F. Schmidt, Curr. Opin. Colloid Interf. Sci. **4**, 300 (1999).

[3] T. A. Waigh, Rep. Prog. Phys. **68**, 685 (2005).

[4] M.Buchanan, M.Atakhorrami, J. F. P. and, et al., Macromolecules **38**, 8840 (2005).**(Chapter 4)**

[5] M.Buchanan, M.Atakhorrami, J.F.Palierne, et al., Physical Review E **72**, 011504 (2005).**(Chapter 5)**

[6] K. M. Addas, C. F. Schmidt, and J. X. Tang, Phys. Rev. E **70**, 021503 (2004).

[7] J. C. Crocker, M. T. Valentine, E. R. Weeks, et al., Phys. Rev. Lett. **85**, 888 (2000).

[8] A. J. Levine and T. C. Lubensky, Physical Review E **65** (2002).

[9] M. L. Gardel, M. T. Valentine, J. C. Crocker, et al., Phys. Rev. Lett. **91**, 158302 (2003).

[10] D. C. Morse, Macromolecules **31**, 7044 (1998).

[11] J. Wilhelm and E. Frey, Physical Review Letters **91**, 108103 (2003).

[12] F. C. MacKintosh, J. Käs, and P. A. Janmey, Physical Review Letters **75**, 4425 (1995).

[13] K. Kroy and E. Frey, Phys. Rev. Lett. **77**, 306 (1996).

[14] D. A. Head, A. J. Levine, and F. C. MacKintosh, Phys. Rev. Lett. **91**, 108102 (2003).

[15] B. Schnurr, F. Gittes, F. C. MacKintosh, et al., Macromolecules **30**, 7781 (1997).

[16] A. C. Maggs, Phys. Rev. E **57**, 2091 (1998).

[17] J. D. Pardee and J. A. Spudich, in *Structural and Contractile Proteins (PartB: The Contractile Apparatus and the Cytoskeleton)*, edited by D. W. Frederiksen and L. W. Cunningham (Academic Press, Inc., San Diego, 1982), Vol. 85, p. 164.

[18] M. W. Allersma, F. Gittes, M. J. deCastro, et al., Biophys. J. 74, 1074 (1998).

[19] M.Atakhorrami et al, not published. **(Chapter2)**

[20] F. Gittes and C. F. Schmidt, Optics Lett. 23, 7 (1998).

[21] E. J. G. Peterman, M. A. van Dijk, L. C. Kapitein, et al., Review of Scientific Instruments 74, 3246 (2003).

[22] F. Gittes and C. F. Schmidt, Methods in Cell Biology, Vol 55 55, 129 (1998).

[23] M. Atakhorrami, G.H. Koenderink, C.F. Schmidt, et al. Phys.Rev.Lett. **95,** 208302 (**Chapter9**)

[24] T. B. Liverpool and a. F. C. MacKintosh, submitted to PRL.

[25] L. D. Landau and E. M. Lifshitz, (1980).

[26] P. M. Chaikin and T. C. Lubensky, Principles of Condensed Matter Physics (Cambridge University Press, Cambridge, New York, 1995).

[27] A. J. Levine and T. C. Lubensky, Phys. Rev. Lett. 85, 1774 (2000).

[28] C.W.Oseen, Neuere Methoden und ergebnisse in der hydrodynamik, Leipzig, 1927).

[29] P. Hebraud, F. Lequeux, and a. J. F. Palierne, Langmuir 16, 8296 (2000).

[30] M. Cagnon and G. Durand, Phys Rev Lett 45, 1418–1421 (1980).
[31] F. Gittes and F. C. MacKintosh, Phys. Rev. E 58, R1241 (1998).
[32] D. C. Morse, Phys. Rev. E 58, R1237 (1998).
[33] G.H. Koenderink, M. Atakhorrami, F.C. MacKintosh, et al. submitted to Phys.Rev.Letters. **(Chapter7)**
[34] M. Pasquali, V. Shankar, and D. C. Morse, Phys. Rev. E 64, 020802 (2001).
[35] F. Gittes and F. C. MacKintosh, (unpublished).
[36] D. T. Chen, E. R. Weeks, J. C. Crocker, et al., Physical Review Letters **90** (2003).
[37] L. D. Landau, E. M. Lifshitz, A. M. Kosevich, et al., *Theory of Elasticity* (Pergamon Press, Oxford, 1986).

High-Frequency Inertial Response of Fluids

IV

This part is based on the following papers:

1. **M. Atakhorrami**, G.H. Koenderink, C.F. Schmidt, and F.C. MacKintosh, "Short-time inertial response of viscoelastic fluids: observation of vortex propagation" Physical Review Letters (2005), 95:208302. (Chapter 9)
2. **M. Atakhorrami**, D. Mizuno, G.H. Koenderink, F.C. MacKintosh and C.F. Schmidt, "Inertial response of fluids probed with active and passive microrheology" (manuscript in preparation), (Chapter 10)

Chapter 9

Short-time inertial response of viscoelastic fluids: observation of vortex propagation

Abstract

We probe the response of viscous and viscoelastic fluids on micrometer and microsecond length and time scales using two optically trapped beads. In this way we resolve the flow field, which exhibits clear effects of fluid inertia. Specifically, we resolve the short time vortex flow and the corresponding evolution of this vortex, which propagates diffusively for simple liquids. For viscoelastic fluids, this propagation is shown to be faster than diffusive and the displacement correlations reflect the frequency- dependent shear modulus of the medium.

A fundamental problem in hydrodynamics is the response of a liquid to the motion of a small embedded particle. At sufficiently long times, the well known Stokes velocity field, which decreases as $1/r$ away from the particle, will describe this fluid response. For an initial disturbance due to a local force in the liquid, however, only a small region of the liquid can be set in motion because of the inertia of the liquid. If the liquid is incompressible, backflow occurs that is characterized by a vortex ring surrounding the point disturbance. Since vorticity diffuses within the (linearized) Navier-Stokes equation, propagation of stress in the fluid drives the expansion of this vortex ring as a function of time t as $\sqrt{t}$. The $1/r$ Stokes flow is established only in the wake of this vortex. While this basic picture has been known theoretically for simple liquids since Oseen [1], and has been observed in simulations since the 1960's [2], this vortex flow pattern has not been observed directly in experiment. Here, we use the correlations in thermal fluctuations of small probe particles to resolve this vortex flow field on the micrometer scale along with its diffusive propagation. We find good agreement between measured flow patterns and theoretical calculations for simple viscous fluids [1, 3]. Furthermore, we demonstrate similar vortex-like flow in viscoelastic media, consistent with theoretical predictions in the accompanying Letter [4]. In the viscoelastic case, interestingly, vorticity spreads super-diffusively.

We obtain the spatial structure of the vortices by measuring the cross-correlated displacements of pairs of thermally excited colloidal particles in a fluid at frequencies up to 100 kHz. This technique is related to recent high resolution one- and two-particle microrheology experiments [5-8] used to probe the shear moduli of complex fluids. A schematic illustration of the experiment is shown in the inset of Fig. 1. By measuring the displacement cross-correlations we obtain the mutual response functions of two spherical particles, labeled 1 and 2, where the coordinate axes are conveniently chosen to be parallel (x) to the line connecting the particle centers and perpendicular (y) to it. The mutual response function measures the displacement response of particle 2 to a force acting on particle 1 and vice versa in the linear response regime. For separation distances r much larger than the particle radius R, the response function depends on r but not on particle size or shape [8, 9].

The displacement $u_x^{(1)}$ of particle 1 in the *x* direction is related to the force $F_x^{(2)}$ acting on particle 2 according to $u_x^{(1)}(\omega) = \alpha_{\parallel}(\omega) F_x^{(2)}$, where $\alpha_{\parallel}(\omega) = \alpha'_{\parallel}(\omega) + i\alpha''_{\parallel}(\omega)$ is the parallel complex response function with real and imaginary parts, $\alpha'_{\parallel}(\omega)$ and $\alpha''_{\parallel}(\omega)$, and ω is the radial frequency. Similarly, we define $\alpha_{\perp}(\omega) = \alpha'_{\perp}(\omega) + i\alpha''_{\perp}(\omega)$, with $u_y^{(1)}(\omega) = \alpha_{\perp}(\omega) F_y^{(2)}$ for the perpendicular response function. The single-particle response functions for each *x,y* direction are defined as $u_{x,y}^{(1)}(\omega) = \alpha_{Auto}(\omega) F_{x,y}^{(1)}$. For homogeneous, isotropic media, these $\alpha_{\parallel,\perp}(\omega)$ completely characterize the linear response at any point in the medium to a force at another point. Both velocity and displacement response can be obtained from $\alpha_{\parallel,\perp}(\omega)$.

In the case of thermal excitations of two colloidal particles, $\alpha_{\parallel,\perp}(\omega)$ also determine the correlations of these thermal fluctuations, via the fluctuation-dissipation theorem of statistical mechanics [10]. Accordingly, the imaginary parts $\alpha''_{\parallel,\perp}(\omega)$ can be determined from the Fourier Transform of the cross-correlated displacement fluctuations $\left\langle u^{(1)}(t) u^{(2)}(0) \right\rangle$ of the two particles:

$$\alpha''_{\parallel}(\omega) = \frac{\omega \int \left\langle u_x^{(1)}(t) u_x^{(2)}(0) \right\rangle e^{i\omega t} dt}{2kT} \qquad \text{and} \qquad \alpha''_{\perp}(\omega) = \frac{\omega \int \left\langle u_y^{(1)}(t) u_y^{(2)}(0) \right\rangle e^{i\omega t} dt}{2kT} \tag{1}$$

where k is the Boltzmann constant and T is the temperature (in our experiments T = 21.5°C, stabilized). Implicit in $\alpha''_{\parallel,\perp}(\omega)$ is also a dependence on the (scalar) separation *r* between the two particles.

Our experiments were done with a custom-built inverted microscope [6, 11] that provides a pair of focused laser beams with wavelengths λ = 830 nm (diode laser), and λ = 1064 nm (NdVO4). A pair of silica particles of radius R = 0.580 μm±5% are weakly trapped (trap stiffness ≤ 3x10^{-6} N/m), in glass sample chamber with 140 μm inner height; the experiments were performed at least 25 μm from both surfaces. Displacements of the particles (*x*, *y*), detected by quadrant photo diodes [12], with spatial resolution of ~ 0.1 nm at 100 kHz bandwidth. For the 1064 nm laser light we used a specialized silicon PN photodiode (YAGG444-4A, Perkin Elmer), to avoid the low-pass filtering [13].

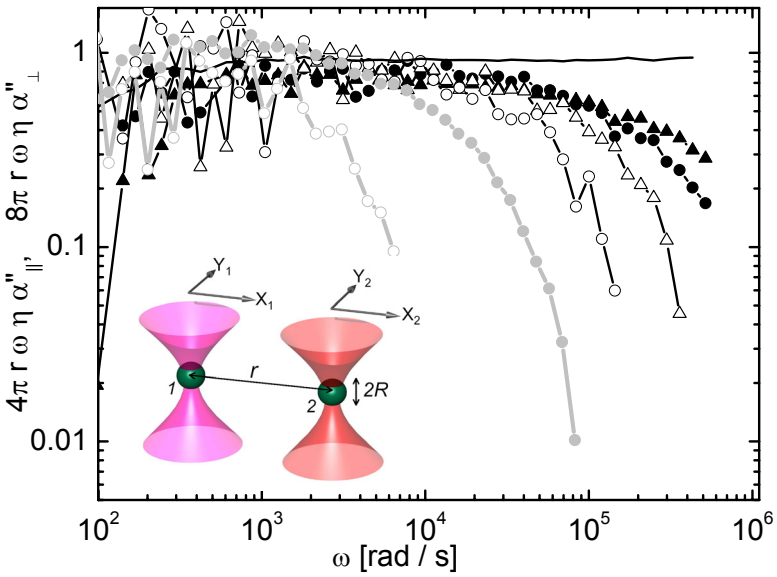

Figure 1: Normalized responses of two particles, ∥ (filled) and ⊥(open) in water/glycerol (r = 8.3μm; r = 5.7μm) compared to water (r = 8.3μm) in gray and to the normalized single-particleresponse function (horizontal line). For the same viscosity the decay shifts to lower frequency for larger r. Inset: Sketch of the experiment: Two particles separation r in two laser traps (λ = 830nm, 1064nm). Displacements in the plane normal to the laser, (parallel (x) and perpendicular (y)) to the line of centers, are detected using laser interferometry.

Output voltages were digitized with an A/D interface (200 kHz) and recorded in Labview (National Instruments). The output voltages were calibrated [1] as described in [14].

We consider first the spatial structure of vortices in simple viscous liquids. As samples we used two Newtonian fluids with different viscosities η and mass densities ρ, namely water (η = 0.969 m Pa s, ρ = 1000 kg m^{-3}) and a (1:1 v/v) water/glycerol mixture (η = 6.9 m Pa s, ρ = 1150 kg m^{-3}) for probe distances r between

[1] In viscous liquids the detection was calibrated using the same beads, as used for the correlation measurements; in the viscoelastic systems calibration was done separately in the water.

2.2 and 12 μm. Figure1 shows representative data for $\alpha''_{\parallel,\perp}(r,\omega)$ from pairs of silica particles, parallel to the center line (filled symbols) and perpendicular to it (open symbols) in water/glycerol, (r = 8.3 μm (blue, online); r = 5.7 μm, (red, online)) and in water (gray symbols), (r = 8.3 μm). Solid black is the measured displacement auto-correlations of one of the single particles from the same data. The experimental $\alpha''(\omega)$ are normalized by their low-frequency limit (i.e, the Oseen tensor and Stokes drag coefficient), not yet accounting for fluid inertia [1]: $\alpha''_{\parallel}(\omega) = 2\alpha''_{\perp}(\omega) = (4\pi r\omega\eta)^{-1}$ and $\alpha''_{Auto}(\omega) = (6\pi R\omega\eta)^{-1}$.With this normalization the data expected to superimpose as horizontal line for low frequencies. The response $\alpha''_{Auto}(\omega)$ does not deviate significantly from the Stokes limit over the full experimental frequency range. For $\alpha''_{\parallel,\perp}(\omega)$, however a systematic decrease is seen at high frequencies, which reflects the failure of instantaneous, long-range stress propagation. For a given probe distance r, $\alpha''_{\perp}(\omega)$ turns down at lower frequencies than $\alpha''_{\parallel}(\omega)$. In the perpendicular channel, displacements become eventually anti-correlated (negative values not plotted), as expected from the backflow of the vortex-displacement field. As r increases, such anti-correlations are visible at lower frequency (blue, online). For the same r, the anti-correlation occurs in water at a lower frequency than in the water/glycerol mixture. The one-particle $\alpha''_{Auto}(\omega)$ does not exhibit inertial effects in either of the two fluids studied, since the viscous penetration depths remain of order of or larger than the bead size [10, 13, 15].

The velocity response function for the fluid surrounding a moving sphere within the unsteady Stokes approximation was calculated by Oseen [1]. To compare with our $\alpha''_{\parallel,\perp}(\omega)$, we need the frequency dependence, which has the form [3 ,4]

$$\alpha''_{\parallel} = \frac{1}{4\pi r\omega\eta}\chi''_{\parallel}\left(r\sqrt{\frac{\rho\omega}{2\eta}}\right) \text{ and } \alpha''_{\perp} = \frac{1}{8\pi r\omega\eta}\chi''_{\perp}\left(r\sqrt{\frac{\rho\omega}{2\eta}}\right) \tag{2a}$$

where

$$\chi''_{\parallel}(x) = \frac{e^{-x}}{x^2}\left[(1+x)\sin(x) - x\cos(x)\right] \text{ and } \chi''_{\perp}(x) = \frac{e^{-x}}{x^2}\left[\left(x+2x^2\right)\cos(x) - (1+x)\sin(x)\right] \tag{2b}$$

Normalized $\alpha''_{\parallel,\perp}(\omega)$ (*e.g.*, $4\pi r\omega\eta\alpha''_{\parallel}$) for different viscous liquids should thus collapse onto these master curves $\chi''_{\parallel,\perp}$ when plotted versus distance normalized by the frequency dependent viscous penetration depth $\delta_v = \sqrt{\eta/\omega\rho}$.

Figure 2 demonstrates the expected collapse of our data for water and the water/glycerol mixture onto $\chi''_{\parallel,\perp}$, with no adjustable parameters.

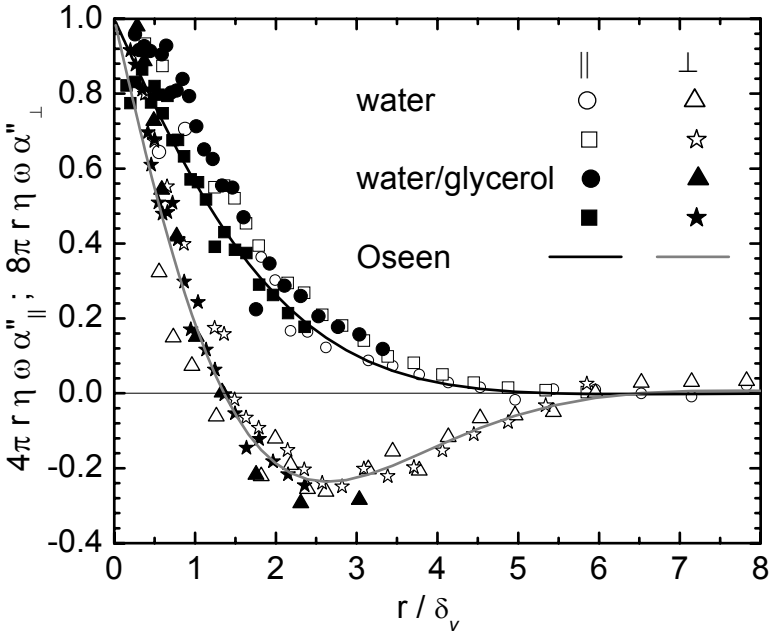

Figure 2: Normalized responses, collapsed by plotting versus scaled separation distance r/δ_v for r = 11.7 μm (circles, triangles), 8 μm (square, stars), in water (open symbols, η = 0.969 m Pa s) and water/glycerol (filled symbols, η =6.9 m Pa s). Normalized data fall onto the two master curves of Eqs. (2) (dark and gray lines). Data shown for ω > 200 rad/s, for ω < 2k rad /s one in every 5 data points.

Fig. 2 clearly shows the anti-correlation in the perpendicular channel at high frequencies, which is a direct consequence of the vortex flow. Scaling with $\omega^{1/2}$ implicit in the data collapse demonstrates the diffusive propagation of this vortex. Prior experiments have reported diffusive propagation in longitudinal correlations between two particles in a Newtonian liquid [16], although transverse correlations (where back-flow is apparent) were not observed. Here the $\chi''_{\parallel,\perp}$ are defined such that $\chi_{\parallel,\perp}(\omega) \to 1$ as $\omega \to 0$. Thus the data collapse at low ω is consistent with static Oseen tensor. The vortex propagation is faster in the glycerol/ water mixture than in water, since η/ρ is larger by a factor of 6.

In viscoelastic media, (see accompanying paper [4]), anti-correlations and oscillations are expected to be more pronounced. The vortex/stress propagation is also expected to be qualitatively different: it is no longer diffusive. In addition, polymer solutions are expected to have a larger penetration depth at a given frequency than a simple viscous fluid, given the higher modulus. We present experimental results from solutions of flexible, wormlike micelles, and solutions of entangled or sparsely cross-linked semiflexible actin filaments, both of which confirm the expectations.

We use worm-like micelles cetylpyridinium chloride (CPyCl) in brine (0.5M NaCl) with sodium salicylate (NaSal) as counterions, molar ratio Sal/CPy = 0.5 (diameter 3 nm, persistence length 10 nm, length several μm) [17]. We have measured $\alpha''_{\parallel}$ and $\alpha''_{\perp}$ for three different micelle concentrations (C_m), and varying distances between the particles. Figure 3a shows the results for a particular distance in each concentration (C_m = 0.5 wt%, r = 8 μm; 1 wt%, r = 10 μm; 2wt %, r = 10 μm).

We assume power-law behavior [4] for our viscoelastic solutions at high frequency, explicitly including the solvent: $G = A(-i\omega)^z - i\omega\eta$. Analogous to the viscous case presented in Fig. 2, the normalized compliances, $4\pi r|G|\alpha''_{\parallel}$ and $8\pi r|G|\alpha''_{\perp}$, are plotted against particles separation scaled by the viscoelastic penetration depth, $\delta_{ve} = \sqrt{|G|/\omega^2\rho}$. In order to collapse data for different distances r and micelle concentrations we need to determine two adjustable (highly correlated) parameters, the exponent z and the (concentration-dependent) prefactor A. The exponent z for a semidilute solution of flexible polymers is expected to lie between 1/2 and 2/3 depending on hydrodynamic effects [18]. We found the best collapse of all data sets with each other and with the model curves for all five probed distances r (3-10 μm) and three concentrations, using a single z = 0.68 ± 0.05 and A = 0.012 ± 0.0045, A = 0.028 ± 0.0085, and A = 0.0575 ± 0.012 $Pa\ s^z$ for 0.5, 1, and 2 wt% micelles, respectively (Fig. 3a) Our results are consistent with an expected linear concentration dependence of A (see inset). Furthermore, measured shear moduli in the low-frequency limit are in agreement with both macro- and micro-rheological measurements for worm-like micelles using different experimental methods [19]. The observed exponent z is consistent with the Zimm exponent of 2/3 [18].

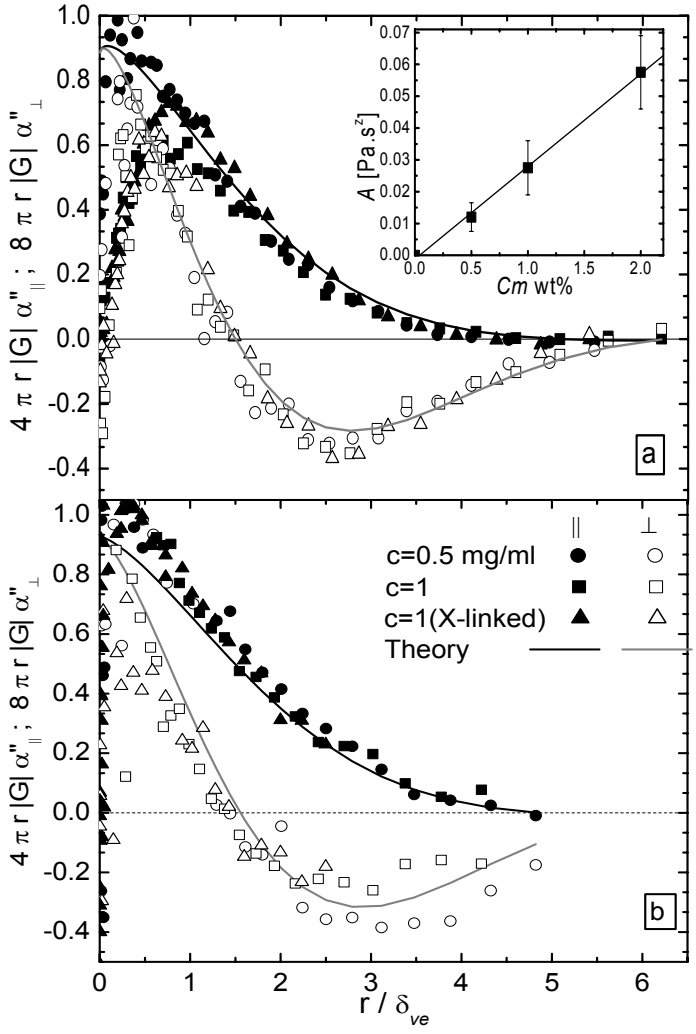

Figure 3: Normalized responses, $4\pi r|G|\alpha''_{\parallel}$ (filled) and $8\pi r|G|\alpha''_{\perp}$ (open) versus scaled distances r/δve, for solutions of wormlike micelles, (a) (Cm = 0.5 wt%, r = 8 μm (circles); 1 wt%, r = 10 μm (squares) and 2 wt%, r = 10 μm (triangles)). (b) entangled actin solutions with (C = 0.5 mg/ml, r = 13.6 μm (circles); 1 mg/ml, r = 16.2 μm (squares)) and for weakly cross-linked actin network (C = 1 mg/ml, r = 10.2 μm (triangles)). Solid lines: predictions for a viscoelastic fluid with z = 0.68, in micelles and z = 0.75 in actin. Inset a: the fit parameter A increases linearly with micelle concentration.

The appearance of an elastic-like plateau of the shear modulus at low frequencies accounts for the observed down-turn of both $\alpha''_{\parallel}$ and $\alpha''_{\perp}$ at low frequencies [11], which becomes more apparent for the concentrated micelle solutions.

F-actin is the polymeric form (filament diameter 7 nm, average length and persistence length ~17 μm) of the major cytoskeletal protein actin . Entangled networks of F-actin have high-frequency viscoelastic behavior qualitatively different from that of flexible polymer systems [20]. We looked at both entangled and weakly cross-linked networks of actin[2]. Figure 3b shows good data collapse after normalizing both $\alpha''_{\parallel}$ and $\alpha''_{\perp}$ for entangled actin at two concentrations (0.5 and 1 mg/ml) and for a weakly cross-linked actin gel (1 mg/ml). The best collapse of the data was found for parameters $z = 0.8 \pm 0.1$ and $A = 0.085 \pm 0.05$, 0.18 ± 0.13, 0.21 ± 0.13 *Pa* s^z respectively. The actin solutions have a larger shear modulus than the micelle solutions, so the vortex-caused anti-correlation occurs at higher frequencies or larger separations. This is most evident in the case of the cross-linked actin solutions, with the highest shear modulus of all samples. Here, we see anti-correlation (backflow) set in only at ~40 kHZ, which leads to a larger inaccuracy in the determination of A and z. The viscoelastic exponent z found for actin solutions is consistent with $z = 0.75$ [5, 6, 22] and because of the large error bars (particularly for A) we chose $z = 0.75$ to plot the data. The amplitude A is approximately a factor of two smaller than predicted [22].

We have shown how inertial flow in fluids can be directly resolved on micrometer and microsecond time scales using a new high-bandwidth laser interferometry technique. Inertia causes a vortex-like flow surrounding a localized disturbance at short times which leads to enhanced correlations in the thermal velocity fluctuations in liquids. A well studied consequence of these correlations is

---

[2] Monomeric actin (G-actin) isolated from rabbit skeletal muscle [21] mixed with silica beads, and polymerized for 1 hour at a concentration of 1 mg/ml by addition of concentrated buffer [final concentration 2 mM HEPES, 2 mM $MgCl_2$, 50 mM KCl, 1 mM Na_2ATPa, and 1 mM EGTA, pH 7]. Cross-linked networks with a low frequency plateau elastic modulus of 0.8 Pa obtained by copolymerizing a small fraction of biotinylated G-actin with unlabeled G-actin, and adding neutravidin (Pierce Biotechnology) at molar ratios actin/biotinylated actin = 50 and actin/neutravidin = 200.

the slow, algebraic decay of velocity correlations, known as the *long time tail* [2], as can be seen in the crossover from ballistic to Brownian motion of colloidal particles [23]. This vortex flow leads to a diffusive propagation of stress in liquids, which is evident in our results. In viscoelastic media, however, the propagation of stress becomes super-diffusive as shown here. The implications of this for colloidal motion (e.g., long time tail) in viscoelastic fluids have yet to be explored.

Acknowledgements

We thank T. Liverpool (theory), D. Mizuno (discussions), K.C. Vermeulen (Actin purification), C. van Kats (Si particles) and F. Gittes, J. Kwiecinska, J. van Mameren (software). This work was supported by the Foundation for Fundamental Research on Matter (FOM).

References

[1] C.W. Oseen, *Neuere Methoden und Ergebnisse in der Hydrodynamik*, Leipzig, 1927.

[2] B.J. Alder and T.E. Wainwright, Phys. Rev. Lett. 18, 988–990 (1967); Phys. Rev. A. 1,18 (1970).

[3] P. Mazur and D. Bedeaux, Physica 76, 235 (1974).

[4] T.B. Liverpool and F.C. MacKintosh, unpublished.

[5] F. Gittes, B. Schnurr, P. D. Olmsted, F.C. MacKintosh, C.F. Schmidt, Phys. Rev. Lett. 79, 3286 (1997);

[6] B. Schnurr, F. Gittes, F. C. MacKintosh, C.F. Schmidt, Macromolecules 30, 7781 (1997).

[7] J.C. Meiners and S.R. Quake, Phys. Rev. Lett. 82, 2211 (1999).

[8] J. C. Crocker, M. T. Valentine, E. R. Weeks, T. Gisler, P.D. Kaplan, A.G. Yodh, D.A. Weitz, Phys. Rev. Lett. 85, 888 (2000).

[9] A.J. Levine and T.C. Lubensky, Phys. Rev. Lett. 85, 1774 (2000).

[10] L.D. Landau and E.M. Lifshitz, *Fluid Mechanics*, Butterworth-Heinemann, (Oxford, 2000).

[11] M. Atakhorrami *et al*., not published.**(Chapter 2)**

[12] F. Gittes and C.F. Schmidt, Optics Lett. 23, 7 (1998).

[13] E. J. G. Peterman, M. A. van Dijk, L. C. Kapitein, C.F. Schmidt , Rev. Sci. Instrum 74, 3246 (2003).

[14] F. Gittes and C. F. Schmidt, *Meth. Cell. Biol.* (Academic Press, 1998), Vol. 55, p. 129.

[15] K. Berg-Sørensen and H. Flyvbjerg, Rev. Sci. Instrum. 75, 594 (2004).

[16] S. Henderson, S. Mitchell, and P. Bartlett, Phys. Rev. Lett. 88 (2002).

[17] J.A.J.F. Berret, and G. Porte, Langmuir 9, 2851 (1993).

[18] M. Doi and S.F. Edwards, Oxford University Press (New York, 1986).

[19] M. Buchanan, M. Atakhorrami, J.F. Palierne, F.C. MacKintosh, C.F. Schmidt, Phys. Rev. E Phys. Rev. E 72, 011504 (2005).**(Chapter 5)**

[20] F.C. MacKintosh and P.A. Janmey, Curr. Opin. Solid State. Mater. Sci. 2, 350 (1997).

[21] J.D. Pardee and J.A. Spudich, Meth. Enzymol. 85, 164 (1982).

[22] D.C. Morse, Phys. Rev. E 58, R1237 (1998); F. Gittes and F.C. MacKintosh, Phys. Rev. E 58, R1241 (1998).

[23] G.L. Paul and P. N. Pusey, Journal of Physics A 14, 3301 (1981); D.A. Weitz, D.J. Pine, P. N. Pusey, R.J.A. Tough, Phys. Rev. Lett. 63, 1747 (1989).

Chapter 10

Inertial response of fluids probed with active and passive microrheology

Abstract

We measure the inertial response and stress propagation in fluids using two optically trapped particles and interferometric particle-tracking techniques. We measure displacement correlations in the thermal motion of Brownian particles, as well as the response due to an actively oscillating particle. In this way we can directly resolve both the real and the imaginary parts of the inertial response function, which exhibits a vortex-like flow motion. This inertial vortex flow propagates diffusively for simple liquid, while for viscoelastic solutions the vortex propagation is super-diffusive, dependent on the viscoelastic properties of the medium.

10.1 Introduction

The response of a fluid to a point-force disturbance is characterized by Stokes-like flow at long times, which decays with distance r as $1/r$ away from the origin of the disturbance. In this limit, the fluid inertia can be neglected and the disturbance (force) propagates instantaneously from point to point within the medium. At short times or high frequencies, however, the fluid inertia limits the range of stress propagation, which in incompressible fluids results in a back-flow characterized by a vortex ring that resembles a smoke ring. In simple liquids, stress propagation is then characterized by the diffusive spreading of this vortex.

When a particle moves in a fluid, the initial momentum is carried out rapidly by a spherical sound wave to the neighboring particles. This establishes incompressibility in the medium. The inertia of the fluid together with incompressibility of the medium initiates a vortex ring, as noted above. This vortex ring then spreads in time and space, resulting in a long-range response of the medium. The less than instantaneous propagation of this vortex due to the inertia of the medium leads to persistence of fluid motion that manifests itself in a slow, algebraic decay of the velocity auto-correlation function of either a fluid element, or of a particle embedded in the fluid. This is known as the "long time tail" effect [1,2,3,4], which controls the transition from ballistic to Brownian motion of particles in simple liquids. The long time tail effect has been shown to be present even at the atomic level, for example, from neutron scattering experiments on liquid sodium [5].

Although this basic physical picture has been known theoretically for simple liquids since the work of Oseen in 1927 [6] and computer simulations in the 1960s [7,8], it has not been observed directly until now [9]. In the colloidal regime, such as we consider here, this has been difficult because of the high temporal and spatial resolution that is required. We recently showed that the inter-particle correlation and response functions of two particles in both viscous and viscoelastic media can resolve the dynamics of vortex propagation. We tracked the Brownian motion of two optically trapped spherical particles using an interferometric technique [10,11] with high temporal (up to 100 kHz) and spatial (sub-nanometer) resolution in both viscous and viscoelastic fluids. We were able to observe the anti-correlation in the inter-particle response function of thermally excited particles that is characteristic of

the vortex propagation [9,12]. This is also a method for passive two-particle microrheology [13, 14, 15,16].

The inter-particle response functions $\alpha(\omega)$, with real and imaginary parts defined by $\alpha(\omega) = \alpha'(\omega) + i\alpha''(\omega)$, are obtained for motion both parallel to ($\alpha_{\parallel}(\omega)$) and perpendicular to ($\alpha_{\perp}(\omega)$) the centerline between the two particles. In the passive approach, the imaginary part of the response function is directly measured from the position fluctuations of two particles via the Fluctuation-Dissipation Theorem (FDT) [17]. The real part of the response function is then obtained from the Kramers-Kronig relations, which leads to a cut-off at about 10 kHz. In order to directly measure both the real (in-phase) and imaginary (out-of-phase) parts of the response function up to high frequencies (100 kHz), we have also developed an active microrhelogy technique [18,19]. In this method, one of the optical traps oscillates a particle, and the response of another particle at separation *r* is measured.

In this paper, we present experimental results of both passive [9,12] and active approaches. The outline of the paper is as follows. In section II, we present the theoretical analysis. In section III, we present the materials and methods of sample preparation, as well as the experimental techniques we used for the measurement of the response functions for both passive and active microrheology. In section IV we describe our methods of data analysis used for the results presented in section V. In the results section (V), we first compare the data for simple liquids with the dynamic Oseen tensor, which demonstrates the diffusive propagation of the vortex flow. We also present (in section V) our results and a comparison with the theory for viscoelastic solutions, including evidence for superdiffusive stress propagation. Finally, we conclude with a discussion (section VI), including the implications of our results for microrheology in general.

I0.2 Theoretical background

Based on the linearized Navier-Stokes equation and its generalization to incompressible viscoelastic medium, the authors of Ref. [12] derived the frequency and spatial dependence of the inertial response tensor in viscoelastic fluids. For isotropic media, there are just two independent and non-zero components of the

linear response, corresponding to the motion parallel ($\|$) and perpendicular ($\perp$) to the line between disturbance and response:

$$\alpha_{\|} = \frac{1}{4\pi G(\omega) r}\chi_{\|}(r\sqrt{k}) \text{ and } \alpha_{\perp} = \frac{1}{8\pi G(\omega) r}\chi_{\perp}(r\sqrt{k}) \quad (1)$$

where r is the separation distance between two particles, $k = \frac{\rho\omega^2}{G(\omega)}$ is complex and

$$\chi_{\|}(x) = \frac{2}{x^2}((1-ix)e^{ix} - 1) \text{ and } \chi_{\perp}(x) = \frac{2}{x^2}(1 + (x^2 - 1 + ix)e^{ix}). \quad (2)$$

The magnitude of κ defines the viscoelastic penetration depth $\delta_{ve} = \sqrt{|G|/\rho\omega^2}$, where ρ is the fluid density, $\omega = 2\pi f$ is the angular frequency, and $|G|$ is the magnitude of the shear modulus. For a solution of polymer in a solvent, the modulus (at high frequencies) is expected to be of the form $G = A(-i\omega)^z - i\omega\eta = |G|e^{-i\Psi}$. The first term in this relation is the polymer contribution while the second term is the solvent contribution, where η is the solvent viscosity. The polymer contribution is characterized by a concentration-dependent pre-factor A and an exponent z that depends on the polymer dynamics. For instance, for the Rouse model, z = 1/2 [20] while for semiflexible polymers, z = 3/4 [21, 22,23,24, 25, 26]. The magnitude of the complex shear modulus is thus given by

$$|G| = \sqrt{(A\omega^z)^2 + (\omega\eta)^2 + 2\omega^{z+1}\eta A\sin(\pi z/2)} \quad (3)$$

For the phase, Ψ, we have the following useful expressions

$$\sin\Psi = \frac{(\omega\eta + A\omega^z \sin(\pi z/2))}{|G|}, \quad (4a)$$

$$\cos\Psi = \frac{A\omega^z \cos(\pi z/2)}{|G|}, \quad (4b)$$

$$\sin\frac{\Psi}{2} = \sqrt{\frac{1}{2}\left(1 - \frac{A\omega^z \cos(\pi z/2)}{|G|}\right)}, \quad (5a)$$

and

$$\cos\frac{\Psi}{2} = \sqrt{\frac{1}{2}\left(1 + \frac{A\omega^z \cos(\pi z/2)}{|G|}\right)}. \quad (5b)$$

We define the real parameter $\beta = r\sqrt{\rho\omega^2/|G|}$ and use the definitions in Eqs.(2) to obtain the compact expressions for the complex response functions ($\alpha_{\|}(\omega), \alpha_{\perp}(\omega)$), which can be expanded using the compound angle formulas and the definitions

above. The real ($\alpha'_{\parallel}(\omega), \alpha'_{\perp}(\omega)$) and imaginary ($\alpha''_{\parallel}(\omega), \alpha''_{\perp}(\omega)$) parts of the response functions can thus be found:

$$4\pi |G| r\,\alpha'_{\parallel} = \frac{2}{\beta^2}\left\{ e^{-\beta \sin\frac{\Psi}{2}}\left[\cos(\beta\cos\frac{\Psi}{2}) + \beta\sin(\frac{\Psi}{2} + \beta\cos\frac{\Psi}{2}) \right] - 1 \right\} \tag{6a}$$

$$4\pi |G| r\,\alpha''_{\parallel} = \frac{2\,e^{-\beta \sin\frac{\Psi}{2}}}{\beta^2}\left\{ \sin(\beta\cos\frac{\Psi}{2}) - \beta\cos(\frac{\Psi}{2} + \beta\cos\frac{\Psi}{2}) \right\} \tag{6b}$$

$$8\pi |G| r\,\alpha'_{\perp} = \frac{2}{\beta^2}\left\{ 1 - e^{-\beta \sin\frac{\Psi}{2}}\left[\cos(\beta\cos\frac{\Psi}{2}) + \beta\sin(\frac{\Psi}{2} + \beta\cos\frac{\Psi}{2}) - \beta^2\cos(\Psi + \beta\cos\frac{\Psi}{2}) \right] \right\} \tag{6c}$$

$$8\pi |G| r\,\alpha''_{\perp} = \frac{2\,e^{-\beta \sin\frac{\Psi}{2}}}{\beta^2}\left\{ -\sin(\beta\cos\frac{\Psi}{2}) + \beta\cos(\frac{\Psi}{2} + \beta\cos\frac{\Psi}{2}) + \beta^2\sin(\Psi + \beta\cos\frac{\Psi}{2}) \right\} \tag{6d}$$

We have written these response functions in a form in which the non-inertial limits ($r\sqrt{k} \to 0$) are simple. In this limit, $\chi_{\parallel,\perp}(r\sqrt{k}) \to 1$ in Eqs. (1 and2). Thus, for a simple liquid, for which $G(\omega) = -i\omega\eta$, the response functions reduce to a displacement response consistent with the (time-independent) Oseen tensor for the velocity field [27,28]. For finite *x*, these response functions also reduce to the dynamic Oseen tensor [29,6], for the case of simple liquids. Here, the velocity response function is given by

$$-i\omega\alpha_{\parallel} = \frac{1}{4\pi r\eta}\chi_{\parallel}\left(r\sqrt{\frac{\rho\omega}{2\eta}} \right) \quad \text{and} \quad -i\omega\alpha_{\perp} = \frac{1}{8\pi r\eta}\chi_{\perp}\left(r\sqrt{\frac{\rho\omega}{2\eta}} \right), \tag{7}$$

where

$$\chi'_{\parallel}(x) = \frac{\left[(1+x)\sin(x) - x\cos(x)\right]e^{-x}}{x^2}, \tag{8a}$$

$$\chi''_{\parallel}(x) = \frac{1 - \left[(1+x)\cos(x) + x\sin(x)\right]e^{-x}}{x^2}, \tag{8b}$$

$$\chi'_{\perp}(x) = \frac{\left[\left(x + 2x^2\right)\cos(x) - (1+x)\sin(x)\right]e^{-x}}{x^2}, \tag{8c}$$

and

$$\chi''_{\perp}(x) = \frac{\left[\left(x + 2x^2\right)\sin(x) + (1+x)\cos(x)\right]e^{-x} - 1}{x^2}. \tag{8d}$$

10.3 Materials and methods

10.3.1 Materials

For our experiments on simple liquids, we used two Newtonian fluids with different viscosities η and mass densities ρ, namely water (η = 0.969 mPa s and ρ = 1000 kg m^{-3}) and a (1:1 v/v) water/glycerol mixture (η = 6.9 m Pa s and ρ = 1150 kg m-3).

We also performed experiments on two different viscoelastic fluids, wormlike micelle solutions and solutions of the cytoskeletal biopolymer F-actin. Worm-like micelles are self-assemblies of cetylpyridinium chloride (CPyCl) in brine (0.5 M NaCl) with sodium salicylate (NaSal) as counterions, with a molar ratio of Sal/CPy = 0.5. Three different concentrations of wormlike micelles were used: c_m = 0.5, 1 and 2wt%. This system served as an example of flexible polymer solutions, having an average diameter of 3 nm, persistence length of 10 nm, and contour length of several μm [30]. Entangled F-actin solutions were polymerized from monomeric actin (G-actin) isolated from rabbit skeletal muscle [31]. G-actin (c = 0.5 or 1 mg/ml) was mixed with silica beads in the presence of concentrated buffer [final concentration 2 mM HEPES, 2 mM MgCl2, 50 mM KCl, 1 mM Na2ATPa, and 1 mM EGTA, pH 7] for 1 hour. These entangled actin solutions were studied as an example of semiflexible polymer solutions.

10.3.2 Experimental methods

We used a custom-built inverted microscope [32,11], that provides a pair of focused laser beams with two different wavelengths (λ=1064 nm, ND:YVO4, Compass, Coherent, Santa Clara, CA, USA) and λ = 830 nm (diode laser, CW, IQ1C140, Laser 2000). The role of the laser traps was two-fold. On the one hand, they served to detect the motion of a pair of thermally driven particles with high temporal and spatial resolution in the passive method. On the other hand, for in the active method, one optical trap could be used to apply a sinusoidal force to actively drive one particle, while the response of the other particle was detected.

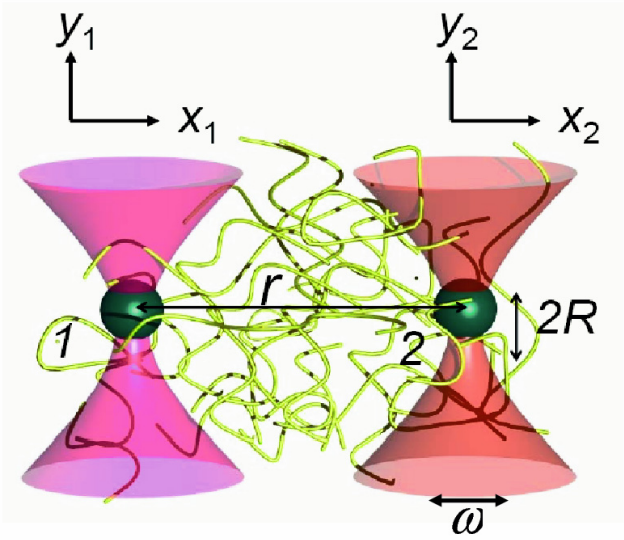

Figure 1: Schematic of the experiment. A pair of silica particles (radius R) is trapped by a pair of laser traps at a separation distance *r*. In the passive method, the position fluctuations of each particle in the *x* and *y* directions are detected simultaneously with quadrant photodiodes and the cross-correlated position fluctuations are measured parallel and perpendicular to the centerline. In the active method, one of the particles is oscillated using one laser trap and the resulting motion of the other particle is measured.

All the experiments were performed at least 25 μm away from both surfaces, in a glass sample chamber made from a glass slide and cover slip with a 70 μm inner height. The lab temperature is stabilized at T = 21.5°C. Below, a brief explanation of the experiments and methods of data analysis are given. More details can be found in [11, 19].

For the passive method, a pair of silica particles (Van't Hoff Laboratory, Utrecht University, Utrecht, Netherlands) of different radii (R = 0.5 μm±5%, 0.580 μm±5%, 1.28 μm±5% and 2.5 μm±5%) were weakly trapped (trap stiffness between 2μN/m and 5μN/m, with the larger particles requiring the higher laser intensities). The interference pattern of scattered light from each of the Brownian particles with

the unscattered laser light was imaged onto a quadrant photo diode. This detection method facilitated the independent detection of particle displacements u_x and u_y in the *x* and *y* directions [10]. A specialized silicon PN photodiode operated at a reverse bias voltage of 110 V (YAG444-4A, Perkin Elmer, Vaudreuil, Canada), was used for the 1064 nm light, while the 830nm laser light was detected by a standard silicon-type PN photodiode with a reverse bias voltage of 15V (10mm diameter, Spot9-DMI, UDT, Hawthorne, CA) [33]. The output voltages were digitized with an A/D interface (200 kHz) and recorded in Labview (National Instruments, Austin, TX, USA). Output voltages were converted to actual displacements using calibration methods described in [34].

For the active method, the 1064 nm laser was used as the drive laser for one particle, while the 830 nm laser trap was used for the detection of a second particle at a separation distance *r*. The driving laser oscillated the trapped particle through an Acousto-Optical Deflector (AOD) (TeO2 , Model DTD 276HB6, IntraAction). A piezo-electric transducer was driven by a voltage-controled oscillator (VCO) (DRF.40, AA OPTP-ELECTRONIC, Orsay Cedex, France) to generate the acoustic wavefronts in the AOD, which deflected the incoming laser light through a Bragg deflection angle. Thus, the VCO controlled the oscillatory motion of the laser beam, and hence of the particle. The force applied to this particle was calibrated by measuring the power spectral density (PSD) of the Brownian motion of a particle trapped in water with the same laser power [34]. The second (probe) laser detected the motion of the second particle. The output signal (from the QPD) was fed into a lock-in amplifier (SR830, Stanford Research Systems, Sunnyvale, CA, USA). In this way, the amplitude and phase of particle motion that was coherent with the driving signal of the VCO was separated from the background noise, including Brownian motion of the particle as well as shot noise.

10.4 Data Analysis

For both the active and passive methods, the particle displacements $u(\omega)$ were small. Thus, the complex response function $\alpha(\omega)$ can be found from the linear relation $u(\omega) = \alpha(\omega)F(\omega)$, where $F(\omega)$ is the applied force. Again, we consider separately the

real ($\alpha'(\omega)$) and imaginary parts ($\alpha''(\omega)$) of this response. In these experiments, the coordinate system was chosen in such a way that x was parallel to the centerline of particles ($\|$) and y is perpendicular to it ($\perp$). In order to map the flow field, these inter-particle response functions along these two directions were obtained as sketched in Fig. 1.

The displacement $u_x^{(1)}$ of particle 1 in the x direction is related to the force $F_x^{(2)}$ acting on particle 2 according to $u_x^{(1)}(\omega) = \alpha_{\|}(\omega)F_x^{(2)}$. Similarly, the perpendicular response function was derived from $u_y^{(1)}(\omega) = \alpha_{\perp}(\omega)F_y^{(2)}$. The single-particle response functions for each x and y directions are defined as $u_{x,y}^{(1)}(\omega) = \alpha_{Auto}(\omega)F_{x,y}^{(1)}$. For homogeneous, isotropic media, these $\alpha_{\|,\perp}(\omega)$ completely characterize the linear response at any point in the medium due to a force at another point. The displacement response functions $\alpha_{\|,\perp}$ determine both position and velocity ($-i\omega\alpha_{\|,\perp}$) response.

Experimentally, in the passive method, the medium is fluctuating about equilibrium, and the only forces on the particles are thermal/Brownian forces. Therefore the fluctuation-dissipation theorem (FDT) of statistical mechanics [35] relates the response of the medium to the displacement correlation functions. For two particles, these are the cross-correlated displacement fluctuations: $\left\langle u_x^{(1)}(t)u_x^{(2)}(0)\right\rangle$ and $\left\langle u_y^{(1)}(t)u_y^{(2)}(0)\right\rangle$. In frequency space, the Fourier transform was used and the frequency-dependent cross-correlated displacement fluctuations were used to obtain the imaginary parts of the complex response functions $\alpha''_{\|,\perp}(\omega)$ via the FDT:

$$\alpha''_{\|}(\omega) = \frac{\omega\int\left\langle u_x^{(1)}(t)u_x^{(2)}(0)\right\rangle e^{i\omega t}dt}{2kT} \text{ and } \alpha''_{\perp}(\omega) = \frac{\omega\int\left\langle u_y^{(1)}(t)u_y^{(2)}(0)\right\rangle e^{i\omega t}dt}{2kT} \qquad (9)$$

where k is the Boltzmann constant and T is the controlled laboratory temperature.

The real parts of the inter-particle response functions $\alpha'_{\|,\perp}(\omega)$ were obtained from the Kramers-Kronig relations:

$$\alpha'_{\|,\perp}(\omega) = \frac{2}{\pi}P\int_0^{\infty}\frac{\varsigma\alpha''_{\|,\perp}(\omega)}{\varsigma^2-\omega^2} = \frac{2}{\pi}\int_0^{\infty}\cos(t\omega)\int_0^{\infty}d\varsigma\,\alpha''_{\|,\perp}(\varsigma)\sin(t\varsigma), \qquad (10)$$

where P denotes a principal-value integral [21, 35,22]. The high frequency cut-off of the Kramers-Kronig integral limits the frequency range of the calculated $\alpha'_{\|,\perp}(\omega)$. Therefore, in order to obtain the real part of the response functions, up to 100kHz we used the active method. In the active method, the force applied to a driven particle

and the resulting motions in-phase and out-of-phase of the second particle can be determined from the real and imaginary parts of the inter-particle response functions ($\alpha'_{\parallel,\perp}(\omega)$ and $\alpha''_{\parallel,\perp}(\omega)$). This was done for several different driving frequencies.

10.5 Results

10.5.1 Simple liquids

In the low-frequency limit, where the fluid inertia can be neglected, the inter-particle response functions are inversely related to the shear modulus of the medium [36,37, 22]. For a simple viscous fluid the response functions in this limit are given by

$$\alpha_{\parallel} = 2\alpha_{\perp} = i/(4\pi r\omega\eta), \tag{11}$$

where r is the separation distance between the two particles and η is the viscosity. These relations contains the r dependence of the Fourier transform of the displacement cross-correlation functions:

$$S_{\parallel}(\omega) = \int \left\langle u_x^{(1)}(t)\, u_x^{(2)}(0) \right\rangle e^{i\omega t}\, dt \quad \text{and} \quad S_{\perp}(\omega) = \int \left\langle u_x^{(1)}(t)\, u_x^{(2)}(0) \right\rangle e^{i\omega t}\, dt\,. \tag{12}$$

In Fig. 2a and b, the normalized displacement cross-correlation functions ($4\pi r S_{\parallel}$ and $8\pi r S_{\perp}$) are plotted versus frequency for water (symbols). For comparison, the single-particle auto-correlation function normalized by the Stokes drag ($6\pi R S_{auto}$) is also plotted as the solid line, where R = 0.58 μm is the particle radius. The auto-correlation function follows a power-law of slope -2 in the whole probed frequency range up to 100 kHz. This is indeed expected from the Lorentzian shape of the PSD for a Brownian particle in a viscous fluid. The fluid inertia effect is clear in the displacement cross-correlation functions (symbols), where a clear systematic r-dependent decrease of the cross-correlations compared to the Lorentzian behavior is apparent at high frequencies for separations r ranging from 2.2 to 11.7 μm. The downturn of the cross-correlations is a manifestation of the lack of instantaneous long-range stress propagation in the medium. For larger r, the data clearly show that the decrease begins at a lower frequency, corresponding to larger viscous penetration depths.

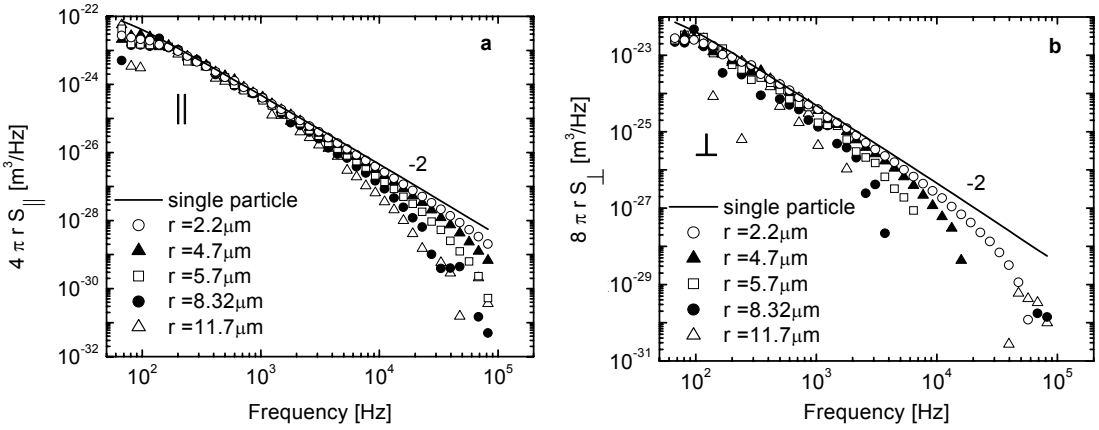

Figure 2: Normalized cross-correlated displacement correlation functions $4\pi r S_{\parallel}$ (**a**) and $8\pi r S_{\perp}$ (**b)** in water versus frequency, compared for different separation distances r (line and symbols). The (solid line) is the auto-correlation function of a single particle normalized by $6\pi R$ (R = 0.58 μm). The expected dependence for a single Brownian particle (slope of –2) is also shown (solid line).

Comparing Figs. 2a and b demonstrates that the decrease of the cross-correlation is more apparent (for the same separation distance) in the perpendicular channel than in the parallel channel. This is due to the counter-propagating flow of the vortex-like response in the direction perpendicular to the direction of an applied force. For r > 5μm (open squares), the cross-correlations become negative (not shown in the log-log plot). At higher frequencies, the displacement cross-correlation functions again become positive (Fig.2b), especially at larger separations such as r = 8.3 μm (filled circles) and r = 11.7 μm (open triangles). Again, this is consistent with the expected oscillation in the displacement cross-correlation functions in the frequency domain, and is a manifestation of the vortex-like flow apparent in the theoretical response functions [12]. This effect becomes more pronounced in viscoelastic media.

Spatial and temporal propagation of the vortex in a general viscoelastic medium is characterized by Eqs (6a-d) [9,6,12]. For a simple liquid, $A = \eta$ (viscosity) and z = 1. In order to quantitatively test these equations, we plot the scaled

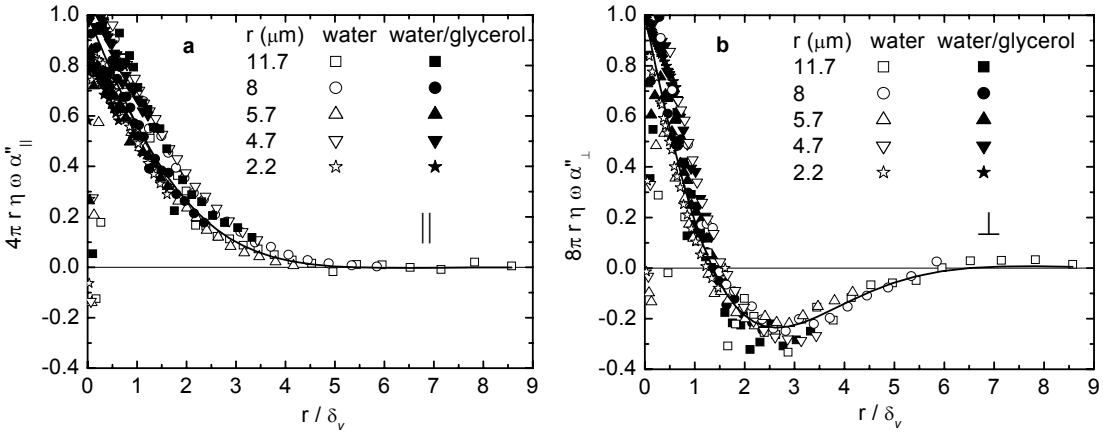

Figure 3: Normalized imaginary part of inter-particle response functions (**a**) $4\pi\eta\omega\alpha''_{\parallel}(\omega)$ and (**b**) $8\pi\eta\omega\alpha''_{\perp}(\omega)$ versus r scaled by the viscous penetration depth (δ_v) measured in water (η = 0.969 m Pa s) and water/glycerol (filled symbols, η = 6.9mPa s). Solid lines are the Oseen predictions for a simple liquid with no adjustable parameters. Data are shown for ω > 2k rad/s, and for ω < 200 rad /s one in every 5 data points are shown.

inter-particle response functions as a function of the separation distance *r scaled by* the viscous penetration depth, defined as $\delta_v = \sqrt{\eta/\rho\omega}$.

In Figs. 3a and b, we compare the imaginary part of the normalized inter-particle response functions $4\pi\eta r\omega\alpha''_{\parallel}(\omega)$ (Fig.3a) and $8\pi\eta r\omega\alpha''_{\perp}(\omega)$ (Fig.3b) for water and a (1:1 v/v) water/glycerol mixture. In accordance with Eqs. (1, 2, 7, 8), the rescaling procedure collapses all data onto a single master curve for all separations *r*, ranging from 2.2 to 11.7 μm, and for both the parallel (Fig.3a) and perpendicular (Fig.3b) inter-particle response functions. This is apparent for both water (open symbols) and water/glycerol (filled symbols) mixtures, where we have accounted for the different viscosities, which are known in both cases. Thus, no free fit parameters were used. Furthermore, the data are in quantitative agreement with the frequency-dependent dynamic Oseen tensor (Eqs. (7, 8)), shown by the solid lines. Here the region of negative response in the perpendicular case corresponds directly to the back-flow of the vortex described above.

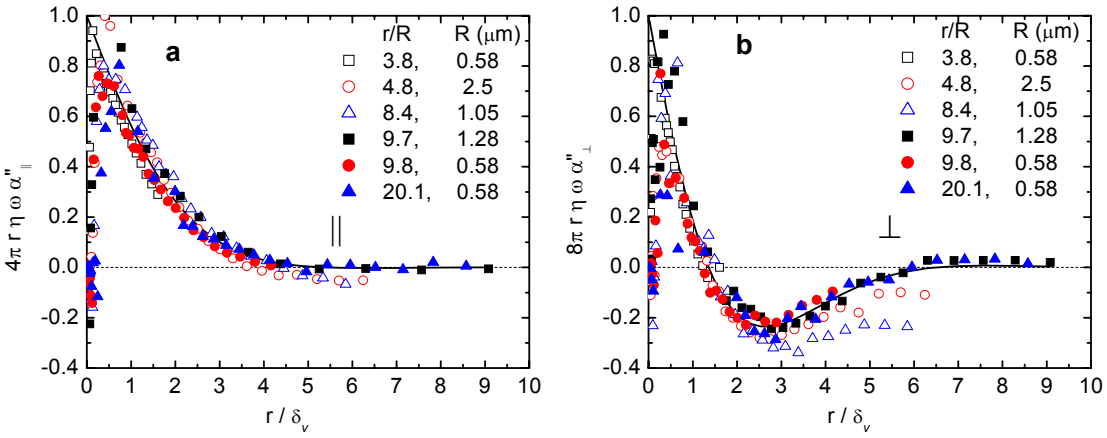

Figure 4: Normalized imaginary part of inter-particle displacement response functions (**a**) $4\pi\eta r\omega\alpha''_{\parallel}(\omega)$ and (**b**) $8\pi\eta r\omega\alpha''_{\perp}(\omega)$ versus r scaled by the frequency-dependent viscous penetration depth (δ_v) in water. These response functions also represent the in-phase velocity response normalized by the corresponding components of the Oseen tensor. Different particle sizes (R = 0.58, 1.05, 1.28 and 2.5 μm) were used at various separation distances r.

At large enough separations r, the inter-particle response functions are independent of the particle size and shape [37,38], resulting in a dependence on r and ω alone. In the analysis, we thus assume for simplicity that the particles are point-like. The inter-particle response functions were also measured with different size particles in order to check the validity of this approximation. In Figs. 4a and b, the imaginary part of the normalized response functions $4\pi\eta r\omega\alpha''_{\parallel}(\omega)$ (**a**) and $8\pi\eta r\omega\alpha''_{\perp}(\omega)$ (**b**) versus r/δ_v are plotted for water (symbols). Data for different particle radii (R = 0.58, 1.05, 1.28 and 2.5 μm) are shown for various separations r. We find no systematic bead size dependence, supporting our assumption. Again, all data fall onto one single plot for each channel, and agree well with the dynamic Oseen tensor (solid line). The deviation observed in the last data points for R = 1.05 μm (open triangle) and 2.5 μm (open circle) are most probably due to shot noise at high frequencies. Shot noise

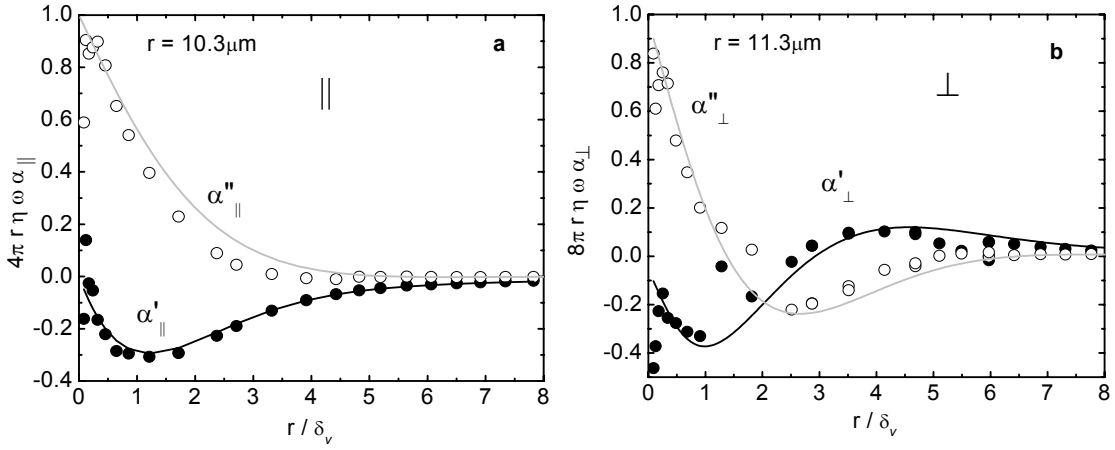

Figure 5: Normalized complex inter-particle response functions in water: (**a**) $4\pi\eta\omega r\alpha_{\parallel}(\omega)$ and (**b**) $8\pi\eta\omega r\alpha_{\perp}(\omega)$. These are plotted versus r (r = 11.3 μm for parallel, and r = 10.3 μm for perpendicular), scaled by the frequency-dependent viscous penetration depth (δ_v). Both real (filled symbols) and imaginary parts (empty symbols) are shown, for both parallel and perpendicular directions. These experiments were done using a bead radius R = 0.58μm. The corresponding predictions of the dynamic Oseen tensor from Eqs. (7, 8a-d) are also shown (black and gray lines), using the known parameters η = 0.969 m Pa s and ρ = 1000 kg m-3.

occurs because the large particles exhibit smaller fluctuations, which results in a smaller number of photons detected by the quadrant photodiodes. In any case, the deviations observed for these data are not consistent with the expected error due to the finite particle size, which should be larger for smaller r/R.

So far, we have just considered the passive fluctuations, which measure the imaginary (out-of phase) part of the inter-particle response functions ($\alpha''_{\parallel,\perp}(\omega)$). Using our active method, we can completely determine both the real (in-phase) and imaginary parts of the inertial response. In Figs. 5a and b, we show the normalized inter-particle response function measured by active microrheology (R = 0.58μm) in water. This is done for both the parallel (**a**) and perpendicular (**b**) directions. The data are shown by symbols: $\alpha''_{\parallel,\perp}(\omega)$ (open circles) and $\alpha'_{\parallel,\perp}(\omega)$ (filled circles). In

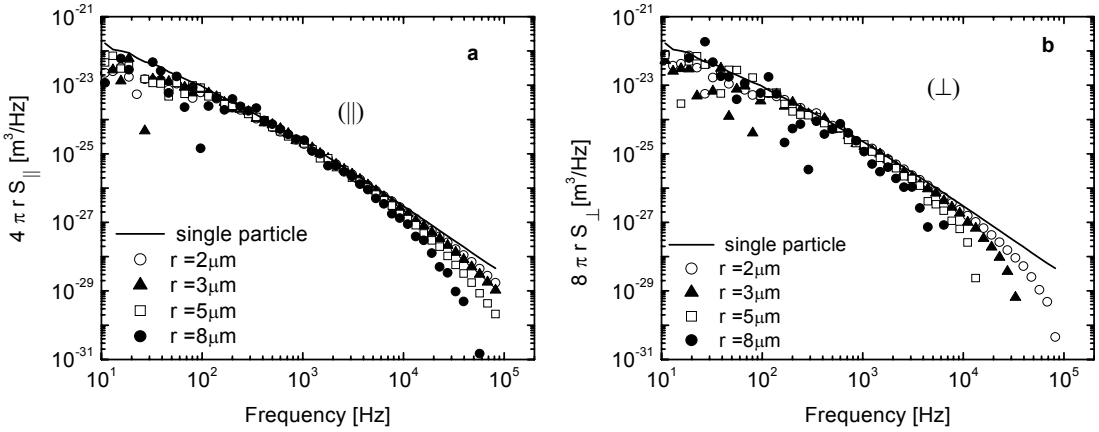

Figure 6: Scaled inter-particle displacement correlation functions $4\pi r S_{\parallel}$ (**a**) and $8\pi r S_{\perp}$ (**b)** in worm like micelle solutions (cm = 1 wt%) versus frequency, compared for different *r* (separation distance): (**a**) parallel and (**b)** perpendicular directions. In all cases, R = 0.58 μm.

each case, we find good agreement with Eqs. (7, 8a-d). The separation distances used for the parallel (r = 10.3 μm) and perpendicular (r = 11.3 μm) channel are different because these measurements were done in separate experiments (in contrast to the passive data, which are obtained simultaneously in a single experiment).

10.5.1 Viscoelastic solutions

In viscoelastic polymer solutions, the polymer contribution modifies the propagation of the inertial vortex. Here, we first discuss our results for wormlike micelle solutions [39,40]. The displacement cross-correlation functions ($4\pi r S_{\parallel}$ and $8\pi r S_{\perp}$) are plotted versus frequency in Fig. 6 for two particles at separation distances r of 2μm to 8 μm) in a 1wt% wormlike micelle solution. For comparison, the scaled auto-correlation function $6\pi R S_{auto}$ for a single particle (R = 0.58 μm) is also plotted (solid lines). In contrast with simple liquids, the particles are confined by the surrounding polymer network, and do not exhibit free diffusion. Thus, the frequency dependence is weaker than for Brownian motion (*i.e.*, the power-law slope is less than –2) 39, 41.

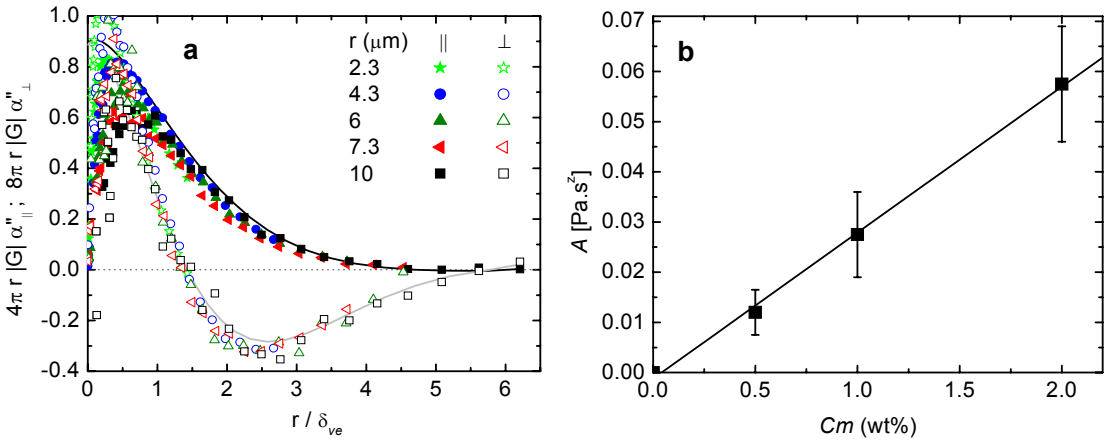

Figure 7: **(a)** Collapse of the inter-particle response functions (imaginary part) for different r in worm-like micelle solutions of 1wt%. Here, the viscoelastic penetration depths were determined via combined fits to Eqs. (3-6) with parameters $z = 0.68 \pm 0.05$ and $A = 0.028 \pm 0.008$Pa s^z , where the solvent (water) viscosity has been taken into account. In all cases, $R = 0.58$ μm. In **(b)**, we show the expected linear dependence of the parameter A on micelle concentration c_m.

As before, the displacement cross-correlation functions are used to determine the full vortex-like flow and its corresponding (superdiffusive) propagation. The r-dependent decrease of the cross-correlation functions occurs for both the parallel (Fig. 6a) and perpendicular (Fig. 6b) directions, but is more apparent in the latter case.

In order to collapse these data onto a single curve for each of the two channels (parallel and perpendicular), following Eqs. (3-6), we plot the normalized inter-particle response functions $4\pi |G| r\alpha''_{\parallel}(\omega)$ and $8\pi |G| r\alpha''_{\perp}(\omega)$ versus scaled r/δ_{ve}, where δ_{ve} is the viscoelastic penetration depth. Unlike the water and water/glycerol samples, we do not know the frequency-dependent shear modulus $G(\omega)$ *a priori*. Based on theoretical expectations for flexible polymer systems [20], as well as prior high-frequency rheology of worm-like micelle solutions [39, 41], however, we

assume that the shear modulus is as described in Eq. (3). Thus, we fit our data to determine the two correlated parameters A and z. We expect z to be independent of the micelle concentration, while A should depend linearly on the polymer/micelle concentration. In Fig. 7a, we show the resulting collapse of the normalized inter-particle response functions in the parallel (filled symbols) and perpendicular (empty symbols) directions, for the same data of Figs 6a and 6b. The predictions of Eqs. (1) and (2) are shown with black and gray lines [12]. The best overall collapse of the data for wormlike micelle solutions at all concentrations (0.5 , 1, and 2 wt%) and separations r (from 2 to 16 μm) was obtained using $z = 0.68 \pm 0.05$ and the values of A shown in Fig. 7b.

In order to test these ideas further, we also performed experiments on another viscoelastic fluid with a different frequency dependence, namely solutions of semiflexible F-actin filaments, which contribute to the viscoelasticity in a different way than the flexible polymers such as the wormlike micelle solutions studied above do [21, 22, 24-26, 16]. Accordingly, the spatial structure and propagation of the vortex are different. Figure 8 shows a collapse of the inter-particle response functions $4\pi |G| r\alpha''_{\parallel}(\omega)$ (fill symbols) and $8\pi |G| r\alpha''_{\perp}(\omega)$ (open symbols) versus scaled distance r/δ_{ve} onto two master curves for the parallel and perpendicular directions. The data are shown for an actin concentration of 1 mg/ml and for probe particles of radius 0.58 μm at various separation distances r (from 4.2 to 16.2 μm). In F-actin solutions, the magnitude of the shear modulus is large, so the vortex propagates faster, making it somewhat harder to observe in our experimental time window. In particular, it is harder to determine the parameters A and z in this case. Here, we find the best collapse with $z = 0.78 \pm 0.1$ and $A = 0.18 \pm 0.13$ Pa s^z. In order to reduce these error bars in the passive method, it would be necessary to perform our measurements at higher frequencies and/or larger separation distances. Nevertheless, our results are consistent with prior measurements and predictions of both parameters.

Independently, using active manipulation of one particle, both real and imaginary parts of the response functions can be measured directly. In Fig. 9a and b,

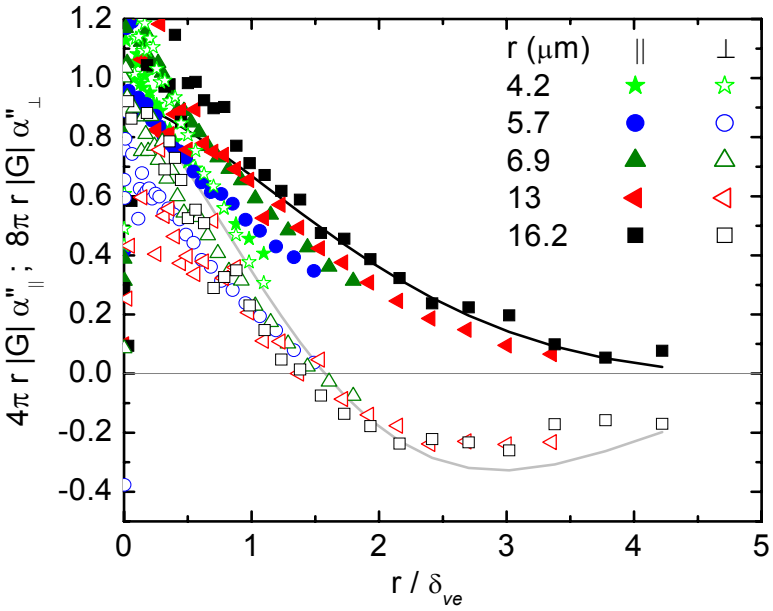

Figure 8: Collapse of the imaginary part of the inter-particle response functions at different r in F-actin solutions of concentration 1 mg/ml. A combined fit of all data sets to Eqs. (3-6) was made, accounting for the solvent (water) viscosity, using a single set of parameters $z = 0.78 \pm 0.1$ and $A = 0.18 \pm 0.13$. Data are presented for the parallel (closed symbols) and perpendicular (open symbols) directions, and for R = 0.58 μm. The solid black line represents Eq. (6b) and the gray line represents Eq. (6d), both with $z = 0.75$ and $A = 0.2$ Pa sz.

the parallel (Fig. 9a) and perpendicular (Fig. 9b) complex inter-particle response functions for c = 1 mg/ml F-actin solutions are shown, as probed with beads of radius 1.28 μm. These have also been fitted with Eq. (6a-d), indicated by black and gray lines, respectively. The measurements are shown by symbols for both $\alpha''_{\parallel,\perp}(\omega)$ (open circles) and $\alpha'_{\parallel,\perp}(\omega)$ (filled circles). Data for both the parallel (r = 12.1 μm) and perpendicular (r = 13.5μm) channel are in very good agreement with Eq (6a-d) using parameters $z = 0.78 \pm 0.01$ and $A = 0.22 \pm 0.05$ Pa s^z. In this method, the inter-particle response functions were first fitted for the parallel data. Then, the same z and A were used to compare the perpendicular data with formulae Eq (6c) and (6d). For this method, the error bars result from fitting the data. With the active method, the

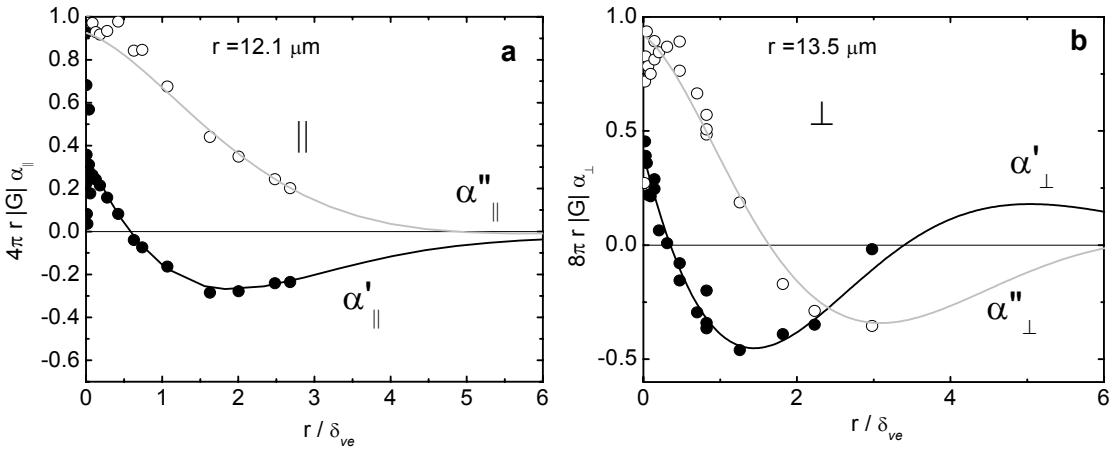

Figure 9: Normalized complex inter-particle response functions in c = 1 mg/ml entangled F-actin solutions probed with particles of radius R = 1.28μm. (**a**) $4\pi r\,|G|\,\alpha_{\parallel}(\omega)$ and (**b**) $8\pi r\,|G|\,\alpha_{\perp}(\omega)$ versus r (r = 11.3 μm for the parallel and r = 10.3 μm for the perpendicular direction), scaled by δ_{ve} as determined from Eqs. (3-6). Both the real (filled symbols) and imaginary (empty symbols) parts of both the parallel and perpendicular response functions are in a good agreement with Eq (6a-d) with fit parameters A = 0.22 ± 0.05 Pa sz and z = 0.78 ± 0.02. The corresponding theoretical lines are shown for z = 0.78 and A = 0.22.

inter-particle response functions for the parallel and perpendicular directions were measured separately (in two different experiments). In contrast in the passive experiments the parallel and perpendicular inter-particle response functions were obtained simultaneously.

For both methods, the high-frequency values of z and A found here are consistent with prior experimental microrhelogy and macrorheology experiments for both entangled actin solutions [21, 22, 24-26, 16] and wormlike micelle solutions [39,40, 41]. To obtain these values, it is essential to model the fluid inertia in viscoelastic solutions including both polymer and solvent contributions to the shear modulus. We observed that, although the high frequency rheology of the polymer solution is dominated by the polymer, the background solvent inertia has a larger contribution to the inertial vortex propagation. To demonstrate this, we excluded the solvent

shear modulus ($-i\omega\eta$) in Eq (6a-d), and analyzed our data with just the high frequency shear modulus with the form of $G = A\omega^z$. For both wormlike micelle solutions and entangled F-actin solutions, we found much larger values of z (~ 0.9) with a nonlinear concentration dependence of A, contrary to expectations.

10.6 Discussion

In these experiments we have directly resolved the inertial response/flow of fluids on micrometer and microsecond time scales using optical tweezers and interferometric particle-tracking techniques. Our results demonstrate that vorticity and stress propagate diffusively in simple liquids and superdiffusively in viscoelastic media. One consequence of the propagation of this vortex is the long time tail effect [1,42]. We computed the velocity auto-correlation of one single particle from the displacement fluctuations, to observe the long-time tail effect in liquid. However, the particle motion was affected by the laser trap potential at low frequencies and the results were not conclusive, as also reported in experiments by [2].

Inertia also sets a fundamental limit for the applicability of two-particle microrheology techniques, which are based on the cross-correlated position fluctuations of particles [13, 15, 16, 39, 41, 37]. Inertial effects limit the range of stress propagation at high frequencies, especially in soft media such as those studied here. Specifically, this can affect measurements at frequencies as low as 1 kHz for separations of order 10 micrometers. Since the stress propagation is diffusive, or nearly so, measurements may be affected even at video frame rates for separations of the order 50 micrometers. The effect would appear as a change in the frequency dependence of the measured shear moduli [41]. As shown here, these inertial effects are more pronounced in the perpendicular inter-particle response functions than the parallel ones, which suggests that the shear modulus obtained from the parallel inter-particle response functions are more reliable. Therefore, in the analysis of two-particle microrheology experiments, the fluid response function is not simply defined by the general Stokes-Einstein relationship, and the fluid response has to be corrected for the inertial effects, according to the probed frequency as well as the

particle separations. However, given the exponential attenuation of stress due to inertia, such corrections will necessarily be limited.

10.7 Acknowledgments

Actin was purified by K.C. Vermeulen and silica particles were kindly donated by C. van Kats (Utrecht University, the Netherlands). F. Gittes, J. Kwiecinska, J. van Mameren, and M. Buchanan helped with software development. We thank D. Frenkel, W. van Saarloos, A.J. Levine and K.M. Addas for helpful discussions. This work was supported by the Foundation for Fundamental Research on Matter (FOM).

10.8 References

[1] G.L. Paul and P. N.Pusey, Journal of Physics A 14, 3301 (1981).

[2] B. Lukic, S. Jeney, C. Tischer, et al., Phys.Rev.Lett 95, 160601 (2005).

[3] K. Ohbayashi, T. Kohno, and a. H. Utiyama, Phys Rev A 27, 2632 (1983).

[4] J. P. Boon and a. A. Bouiller, Phys. Lett. 55A, 391 (1967).

[5] C. Morkel, C. Gronemeyer, W. Glaser, et al., Physical Review Letters 58, 1873 (1987).

[6] C.W.Oseen, *Neuere Methoden und ergebnisse in der hydrodynamik* (Akademische Verlagsgesellschaft, Leipzig, 1927).

[7] B. J. Alder and T. E. Wainwright, Phys. Rev. Lett. 18, 988–990 (1967).

[8] B. J. Alder and T. E. Wainwright, Phys. Rev. A 1, 18 (1970).

[9] M. Atakhorrami, G.H. Koenderink, C.F. Schmidt, et al., Phys.Rev.Lett 95, 208302 (2005). **(Chapter 9)**

[10] F. Gittes and C. F. Schmidt, Optics Lett. 23, 7 (1998).

[11] M. Atakhorrami, (unpublished). **(Chapter 2)**

[12] T. B. Liverpool and a. F. C. MacKintosh, Phys.Rev.Lett 95, 208303 (2005).

[13] J. C. Crocker, M. T. Valentine, E. R. Weeks, et al., Phys. Rev. Lett. 85, 888 (2000).

[14] L. Starrs and P. Bartlett, Journal of Physics-Condensed Matter 15, S251 (2003).

[15] M. L. Gardel, M. T. Valentine, J. C. Crocker, et al., Phys. Rev. Lett. 91, 158302 (2003).

[16] G. H. Koenderink, M. Atakhorrami, F. C. MacKintosh, et al., Submitted to Phys.Rev.Letter. **(Chapter 7)**

[17] L. D. Landau and E. M. Lifshitz, (1980).

[18] L. A. Hough and H. D. Ou-Yang, Physical Review E 65, 021906 (2002).

[19] D. Mizuno, unpublished.

[20] M. Doi and S. Edwards, *The Theory of Polymer Dynamics* (Oxford Science Publications, Oxford, 1986).

[21] F. Gittes, B. Schnurr, P. D. Olmsted, et al., Phys. Rev. Lett. 79, 3286 (1997).

[22] B. Schnurr, F. Gittes, F. C. MacKintosh, et al., Macromolecules 30, 7781 (1997).

[23] D. C. Morse, Macromolecules 31, 7030 (1998).

[24] D. C. Morse, Macromolecules 31, 7044 (1998).

[25] D. C. Morse, Phys. Rev. E 58, R1237 (1998).

[26] F. Gittes and F. C. MacKintosh, Phys. Rev. E 58, R1241 (1998).

[27] D. Bedeaux and P. Mazur, Physica 76, 247 (1974).

[28] P. Mazur and D. Bedeaux, Physica 76, 235 (1974).

[29] J. H. a. H. Brenner, *Low Reynolds Number Hydrodynamics* (McGraw-Hill, New York, 1963).

[30] J. F. Berret, J. Appell, and a. G. Porte, Langmuir 9, 2851 (1993).

[31] J. D. Pardee and J. A. Spudich, in *Structural and Contractile Proteins (PartB: The Contractile Apparatus and the Cytoskeleton)*, edited by D. W. Frederiksen and L. W. Cunningham (Academic Press, Inc., San Diego, 1982), Vol. 85, p. 164.

[32] M. W. Allersma, F. Gittes, M. J. deCastro, et al., Biophys. J. 74, 1074 (1998).
[33] E. J. G. Peterman, M. A. van Dijk, L. C. Kapitein, et al., Review of Scientific Instruments 74, 3246 (2003).
[34] F. Gittes and C. F. Schmidt, in *Methods in Cell Biology* (Academic Press, 1998), Vol. 55, p. 129.
[35] L. D. Landau, E. M. Lifshitz, and L. P. Pitaevskii, *Statistical Physics* (Pergamon Press, Oxford, New York, 1980).
[36] T. G. Mason and D. A. Weitz, Phys. Rev. Lett. 75, 2770 (1995).
[37] A. J. Levine and T. C. Lubensky, Phys. Rev. Lett. 85, 1774 (2000).
[38] A. J. Levine and T. C. Lubensky, Physical Review E 65 (2002).
[39] M.Buchanan, M.Atakhorrami, J.F.Palierne, et al., Physical Review E 72, 011504 (2005). **(Chapter 5)**
[40] M.Buchanan, M.Atakhorrami, J. F. P. and, et al., Macromolecules 38, 8840 (2005).**(Chapter 4)**
[41] M. Atakhorrami and C. F. and Schmidt, Rheol. in print (2005). **(Chapter 6)**
[42] D. A. Weitz, D. J. Pine, P. N. Pusey, et al., Physical Review Letters 63, 1747 (1989).

Summary

Elastic and viscous properties are important characteristics of materials. “Soft materials”, such as many kinds of polymers and polymer solutions, colloidal solutions, but also many biological materials such as cells or tissues, are typically viscoelastic. Measuring the viscoelastic properties of soft materials accurately is an important part of understanding how the (underlying) microscopic dynamics of the material relate to the macroscopic response to applied shear/stress. Therefore various methods have been developed to quantify viscoelastity. Recent interest in the characterization of biomaterials and other complex fluids, which usually exhibit dynamics that vary over a wide range of time and length scales, necessitated the development of microrheology.

The aim of the research described in this thesis was to develop and examine high-bandwidth passive one- and two-particle microrheology. Our method is based on particle tracking with laser interferometric techniques. We used micron-sized optically trapped particles and detected both auto- and cross-correlated position fluctuations in thermal motion in equilibrium; from the correlation functions the single- and inter-particle response functions were obtained using linear response theory, to characterize viscoelastic properties. The results were compared with both existing and newly developed theoretical models.

A custom made dual set of optical tweezers operating with two different laser wavelengths of 830nm and 1064nm was used to trap and detect individual particles, as described in chapter 1. We chose to use two lasers with different wavelengths for position detection instead of two perpendicularly polarized beams in order to eliminate cross-talk caused by the depolarization of light occurring (such as in the objective lens at highly curved surfaces).

This setup was used throughout this thesis. Laser traps were used for two reasons: First, to move and hold particles against gravity in viscous and less elastic

solutions like wormlike micelles and simple liquids. Second, as a focussed light source to detect the particles position using an interferometric technique at high spatial (sub-nanometer) and temporal (100kHz) resolution.

It is important, however, to distinguish between the additional (anti) correlations due to effect of laser traps and the elasticity of the medium in the measured viscoelastic properties. This question is studied extensively in chapter 2, using a viscoelastic solution of fd viruses, and water as a simple viscous liquid without any elastic modulus. The single- and inter-particle response functions were obtained theoretically, accounting for the additional (anti) correlation caused by optical traps in the response functions. The quantitative agreement of the calculated and measured response functions in the simple liquid provides a solid basis for the application of the same method to viscoelastic solutions. This study showed that the effect of laser traps on the correlation of two particles especially at low frequencies, depends on the trap strength and the shear modulus of the viscoelastic medium and has to be corrected for using the presented correction methods to permit a quantitative measurement of viscoelastic properties in one- and two-particle microrheology using optical traps.

One of the essential assumptions in passive microrheology is the generalization of the Stokes-Einstein relationship with negligible fluid inertia. At high frequencies, such as studied in this thesis, however, contributions of fluid inertia cannot be ignored. In incompressible fluids due to the fluid inertia a local perturbation of fluid results in a vortex ring, which propagates through the liquid in a diffusive manner. This picture is known since 1927, when Oseen solved the Stokes equations with the time-dependent inertial term, but it had not been observed experimentally. In Part IV of this thesis, the structure of this inertially induced vortex has been observed by measuring the inter-particle displacement response function of the thermally and actively (using optical traps) driven particles for simple liquids (water and water/glycerol) and in viscoelastic solutions of actin and wormlike micelles. In a viscoelastic solution it is shown that the vortex propagates faster than diffusive and the displacement correlations reflect the frequency dependent shear modulus of the medium. The effects of fluid inertia can be seen in the measured shear modulus at high frequencies, as shown in chapter 6.

The dynamics of polymer solutions and networks greatly depends on the degree of flexibility of the individual polymers. We used two model systems of semiflexible polymers, wormlike micelles and cytoskeletal actin networks.. The rheological properties of these two systems are very different, originating from different dynamics associated to the network's characteristic length scales and relaxation times, probed by the micron-sized particles. We used wormlike micelles as an example of long flexible polymers with nanometer characteristic length scales (part II). F-actin filaments were studied as a model system for the cytoskeleton of the cell as well as prototypical semiflexible polymer networks with a large persistence length (17 μm) on the order of the polymer length itself (part III).

We applied one- and two-particle microrheology to these systems to verify that in certain conditions one- and two-particle microrheology can measure the same response as bulk rheology and also to study the micron-sized length-scale local dynamics. The motivation was that the prior works by different groups had suggested that one-particle microrheology, which is based on the single-particle response function, could be sensitive to the local medium properties in the direct vicinity of the probe particle, which could be different from bulk properties due to surface chemistry or steric (entropic) effects. In contrast, two-particle microrheology, based on the inter-particle response function, should be independent of particle size and interactions, and should report the unmodified bulk rheology.

In chapters 5 and 6, very good agreement between one- and two-particle microrheology in wormlike micelles is presented. This strongly confirms that one can measure bulk viscoelastic properties with one-particle microrheology in these polymer systems, provided that the network length scales are much smaller than probe size. The advantage is that it is a simpler and less noisy technique than two-particle microrheology (chapter 4). Such a confirmation had been lacking before. We further confirmed the validity of these methods by the comparison of one- and two-particle microrheology and bulk rheology (macrorheology) in a wide overlapping frequency range up to 10kHz. This was achieved for the first time using a special made piezo-rheometer. These results together unambiguously advocate that one-particle microrheology is a reliable high resolution and high bandwidth technique to study simple systems. At high frequencies we observed single-filament behavior

with a functional form of $\omega^{0.67}$, and an exponent somewhere between that of flexible polymers and that of semiflexible polymers.

In part III the same methods of one- and two- particle microrheology and high frequency macrorheology were applied to entangled and cross-linked actin networks. Particularly in actin systems, we explored a very large multitude of length and time scales network dynamics. The results of two-particle microrheology were in very good agreement for all the probed frequencies and different particle size with what measured in bulk rheology (chapter 8). We demonstrated the quantitative agreement with theory in both amplitude and functional form $\omega^{3/4}$ for the modulus at high frequencies, confirming the principal role of transverse thermal bending fluctuations in determining the network shear moduli. Furthermore, we showed compelling evidence for a recently predicted intermediate-frequency relaxation mode that is unique to semiflexible polymers with finite length; this mode is due to rapid stress propagation along the filament backbone that is abolished upon crosslinking and is more pronounced in entangled networks with shortened actin filament (chapter 7).

Finally we compared one- and two-particle microrheology obtained simultaneously to explore the complex dynamics of the interaction of particles with their environment. The results presented in chapter 8 show that one-particle microrheology consistently underestimates the bulk moduli by an amount that scales approximately linearly with particle size, which is likely due to steric depletion of polymers around the particles. Also non-affine deformations of the network around the particles resulted in an anomalous $\omega^{9/16}$ frequency dependence of the storage modulus at low frequencies for small probe sizes. This non affine deformation occurs when the particle size is smaller than the (introduced) length scales obtained from the force balance of the polymer bending and shear modulus of network. At higher frequency where the shear modulus of the network dominates storage modulus approaches the bulk behavior.

In conclusion, the combination of one- and two-particle microrheology provides a way to explore more complex length scale-dependent bulk and local dynamics of various polymers, biological and colloidal systems. More complexity can be added in the form of composite networks of biopolymers and cells. Active

micro-manipulation of particles in active microrheology in combination with passive microrheology can open a new window to study non equilibrium systems.

Samenvatting

Elasticiteit en viscositeit zijn belangrijke materiaaleigenschappen. “Zachte materialen”, zoals vele polymeren en polymeeroplossingen, colloïdale systemen, maar ook biologische materialen zoals cellen en weefsels, zijn in het algemeen *visco-elastisch*. Het meten van visco-elastische eigenschappen van zachte materialen is een krachtige methode om inzicht te verkrijgen in de microscopische dynamica die ten grondslag ligt aan de relaxatie van opgelegde spanningen in het medium. Voor het doen van dergelijke metingen zijn verschillende methoden ontwikkeld. Recentelijk is er veel belangstelling in de karakterisering van biologische materialen en andere complexe vloeistoffen, die moeilijk in grote hoeveelheden te verkrijgen zijn en die interessante dynamica vertonen over een groot aantal tijd- en lengteschalen. Dit heeft geleid tot de ontwikkeling van microreologie.

Het onderzoek dat in dit proefschrift wordt gepresenteerd had tot doel om hoogfrequente passieve een- en tweedeeltjesmicroreologie te ontwikkelen en toe te passen. De door ons gebruikte methode is gebaseerd op het volgen van deeltjes door middel van laserinterferometrie. We hebben metingen verricht aan de positiefluctuaties in thermisch evenwicht van deeltjes met een afmetingen op de micrometerschaal. Uit deze signalen hebben wij zowel de autocorrelatie van individuele deeltjes als de kruiscorrelatie van paren van deeltjes bepaald. Gebruik makend van de lineaire-responstheorie hebben wij hieruit de een- en tweedeeltjesresponsfunctie afgeleid, waaruit de viscoelastische eigenschappen bepaald konden worden. We hebben de resultaten vergeleken met zowel bestaande als nieuw ontwikkelde theoretische modellen.

In de experimentele opstelling hebben we gebruik gemaakt van een zelfgebouwde dubbele optische pincet met twee verschillende lasergolflengten van 830nm en 1064nm om individuele deeltjes te vangen en hun beweging te detecteren, zoals beschreven in hoofdstuk 1. We hebben ervoor gekozen om twee lasers met

verschillende golflengten te gebruiken in plaats van twee loodrecht gepolariseerde laserbundels, om geen last te hebben van de overspraak die ontstaat door de depolarisatie van licht aan sterk gekromde oppervlakken (zoals die van de lens).

Wij hebben de hierboven beschreven opstelling gebruikt voor alle experimenten die beschreven zijn in dit proefschrift. In deze opstelling werd op twee manieren gebruik gemaakt van de lasers. Ten eerste werden ze gebruikt als optische pincet om deeltjes te verplaatsen en vast te houden tegen de zwaartekracht in minder elastische oplossingen zoals wormachtige micellen en simpele vloeistoffen. Ten tweede fungeerden de lasers als een lichtbron voor de interferometrische techniek om de positie van de deeltjes te meten met een hoge resolutie in ruimte (sub-nanometer precisie) en tijd (100 kHz).

Bij het bepalen van de visco-elastische eigenschappen is het van belang om rekening te houden met de additionele (anti-)correlatie in de positiefluctuaties die het gevolg is van de optische pincet. Deze kwestie is uitgebreid behandeld in hoofdstuk 2, door te kijken naar een visco-elastische oplossing van fd-virussen en naar water als een simpele vloeistof zonder enige elastische modulus. De een- en tweedeeltjesresponsfuncties van simpele vloeistoffen kunnen theoretisch worden berekend, rekening houdend met de additionele (anti-)correlatie die wordt veroorzaakt door de optische pincet. De gevonden quantitatieve overeenstemming tussen de berekende en gemeten responsfuncties in de simpele vloeistof biedt een solide achtergrond voor het gebruik van dezelfde methode voor visco-elastische oplossingen. De resultaten tonen aan dat het effect van de laservallen op de bewegingscorrelatie van de twee deeltjes met name aanwezig is bij lage frequenties en afhankelijk is van de sterkte van de val en de glijdingsmodulus van het viscoelastische medium. Correcties hiervoor moeten dus worden toegepast voor een quantitatieve bepaling van visco-elastische eigenschappen met behulp van een- en tweedeeltjesmicroreologie gebaseerd op optische pincetten.

Een van de onderliggende aannamen in passieve microreologie is de generalisatie van de Stokes-Einsteinrelatie, die uitgaat van een verwaarloosbare traagheid van de vloeistof. Bij hoge frequenties echter, zoals die in dit proefschrift bestudeerd worden, kan de bijdrage hiervan niet worden genegeerd. In incomprimeerbare vloeistoffen zorgt de traagheid van de vloeistof ervoor dat een kleine verstoring leidt

tot het ontstaan van een vortexring, die zich op diffusieve wijze uitbreidt. Dit fenomeen is al bekend sinds 1927, toen Oseen de Stokes-vergelijkingen heeft opgelost met een tijdsafhankelijke inertiaalterm, maar was tot nog toe niet experimenteel waargenomen. In deel IV van dit proefschrift is beschreven hoe wij de structuur van deze inertie-geïnduceerde ring hebben waargenomen door het meten van de tweedeeltjesresponsfunctie van thermisch en actief (door middel van de optische pincet) bewogen deeltjes, zowel in simpele vloeistoffen (water en water/glycerol) als in visco-elastische oplossingen van actine en wormachtige micellen. Voor visco-elastische oplossingen laten we zien dat de vortex zich sneller dan diffusief uitbreidt en dat de positiefluctuatiecorrelaties tussen de deeltjes een afspiegeling zijn van de frequentie-afhankelijke glijdingsmodulus bij hoge frequenties, zoals beschreven in hoofdstuk 6.

De dynamica van polymeeroplossingen en -netwerken hangt in grote mate af van de mate van flexibiliteit van de individuele polymeren. We hebben gebruik gemaakt van twee modelsystemen om dit verband te onderzoeken: wormachtige micellen en actinenetwerken. De reologische eigenschappen van deze twee systemen zijn zeer verschillend vanwege de uiteenlopende lengteschalen en relexatietijden van de netwerken. Wormachtige micellen zijn een voorbeeld van lange flexibele eiwitten met een lengteschaal in de orde van nanometers (deel II). F-actine filamenten vormen een modelsysteem voor het cytoskelet en voor semi-flexibele polymeernetwerken met een grote persistentielengte (17 μm), vergelijkbaar met de polymeerlengte zelf.

We hebben een- en tweedeeltjesmicroreologie toegepast op deze systemen om te onderzoeken of – en in welke gevallen – deze methoden een goede weergave geven van de macroscopische reologie en om de lokale dynamica van een medium op de micrometerschaal te onderzoeken. De motivatie voor dit vergelijkende onderzoek was dat eerdere resultaten van verscheidene groepen suggereerden dat een-deeltjesmicroreologie, gebaseerd op de een-deeltjesresponsfunctie, gevoelig kan zijn voor de lokale mediumeigenschappen in de directe nabijheid van het sondeerdeeltje. Deze kunnen mogelijk verschillen van de macroscopische eigenschappen, vanwege de oppervlaktechemie van de deeltjes of sterische (entropische) effecten. In tegenstelling daarmee zou tweedeeltjesmicroreologie, gebaseerd op de

tweedeeltjesresponsfunctie, onafhankelijk moeten zijn van de grootte en interacties van de deeltjes, en de macroscopische visco-elastische eigenschappen moeten weergeven.

In hoofdstukken 5 en 6 wordt goede experimentele overeenkomst tussen een- en tweedeeltjesmicrorelogie in wormachtige micellen gepresenteerd. Dit onderbouwt de stelling dat in dergelijke netwerken, waarin de lengteschalen van het netwerk veel kleiner zijn dan het sondeerdeeltje, eendeeltjesmicroreologie een geschikte methode is om de macroscopische reologie te meten. Het voordeel hiervan is dat deze techniek simpeler en minder ruisgevoelig is dan tweedeeltjesmicroreologie (hoofdstuk 4). We hebben de validiteit van beide methoden verder onderzocht door de resultaten te vergelijken met macroreologieresultaten in een groot overlappend frequentiegebied tot 10kHz. Dit kon voor het eerst gedaan worden door gebruik te maken van een speciale piëzoreometer. De verzamelde resultaten tonen overduidelijk aan dat eendeeltjesmicroreologie een betrouwbare hoge-resolutie en hoge-bandbreedtetechniek is om simpele systemen te bestuderen. Een dergelijke experimentele bevestiging was niet eerder gegeven. In het systeem van wormachtige micellen hebben we bij hoge frequenties enkel-filament-gedrag waargenomen, gekenmerkt door een frequentie-afhankelijkheid van $\omega^{0.67}$, met een exponent tussen die van flexibele en semi-flexibele polymeren in.

In deel III hebben we dezelfde technieken (een- en tweedeeltjesmicroreologie en hoog-frequente macroreologie) ook toegepast op verstrengelde en verbonden actine-netwerken. Vooral in deze actinenetwerken hebben we de netwerkdynamica op een groot aantal lengte- en tijdschalen onderzocht. De resultaten uit tweedeeltjes-microreologie kwamen goed overeen met die uit macroreologie, voor alle gemeten frequenties en groottes van de sondeerdeeltjes (hoofdstuk 8). We hebben aangetoond dat de resultaten voor de glijdingsmodulus bij hoge frequenties quantitatief overeenkomen met de theorie, zowel in amplitude als in functionele vorm ($\omega^{3/4}$), wat de vooraanstaande rol van transverse buigingsfluctuaties in het bepalen van de glijdingsmodulus van het gehele netwerk bevestigt. Bovendien hebben we overtuigend bewijs laten zien voor een recent voorspelde tussenliggende-frequentie relaxatietoestand die uniek is voor semiflexibele polymeren van eindige lengte. Deze toestand ontstaat door de snelle propagatie van spanningen langs de ruggengraat

van het filament; deze toestand wordt onderdrukt door het maken van dwarsverbindingen tussen de polymeren en is meer uitgesproken aanwezig in verstrengelde netwerken van verkorte actinefilamenten (hoofdstuk 7).

We hebben de gegevens van een- en tweedeeltjesmicroreologie die gelijktijdig in hetzelfde experiment verkregen zijn bovendien gebruikt om de complexe dynamica van de interactie van deeltjes met hun omgeving te onderzoeken. De resultaten die in hoofdstuk 8 gepresenteerd worden laten zien dat eendeeltjesmicroreologie de macroscopische glijdingsmodulus structureel onderschat met een hoeveelheid die ongeveer lineair schaalt met de deeltjesgrootte, wat veroorzaakt zou kunnen worden door sterische depletie van de polymeren rondom de deeltjes. Bovendien zorgen niet-affiene deformaties van het netwerk rond de deeltjes voor een afwijkende frequentie-afhankelijkheid van de elastische modulus ($\omega^{9/16}$) bij het gebruik van kleine sondeerdeeltjes. Deze niet-affiene deformatie vindt plaats als het deeltje kleiner is dan de lengteschaal die volgt uit de krachtbalans tussen de polymeerbuiging en de glijdingsmodulus van het netwerk. Bij hogere frequenties, waar de glijdingsmodulus van het netwerk dominant is, nadert de gemeten elastische modulus het macroscopische gedrag.

We concluderen dat de combinatie van een- en tweedeeltjesmicroreologie de mogelijkheid biedt om onderzoek te doen naar complexe lengteschaalafhankelijke collectieve en lokale dynamica van diverse polymeren, biologische en colloïdale systemen. Toekomstige uitdagingen kunnen gevonden worden in de vorm van meer complexe systemen, zoals samengestelde netwerken van biopolymeren en zelfs cellen. Bovendien biedt actieve micromanipulatie van deeltjes in actieve microreologie in combinatie met passieve microreologie nieuwe mogelijkheden om systemen ook buiten het thermische evenwicht te bestuderen.

Curriculum Vitae

Maryam Atakhorrami was born on September 5, 1976 in Roodbar[1], Iran. She followed her basic education in different schools in Rasht, Roodbar and Tehran, Iran. In 1994, after passing the national entrance exam, she began her bachelor program in applied physics in the Physics Department of the Tehran University, Iran. She received her B.Sc. in solid state physics from Tehran University in 1999. In 2000, she moved to the Netherlands and started her M.Sc. program in the Leiden Institute of Physics, Universiteit Leiden, The Netherlands. The research for her master thesis was done in the group of Prof.dr. J.A. Mydosh, in the Kamerlingh Onnes Laboratory, under the supervision of Dr. Federica Galli and Dr. G.J. Nieuwenhuys. In 2001 her research culminated in the thesis "Tuning charge-density waves in $(Er_x\ Lu_{(x-1)})_5Ir_4Si_{10}$ compounds". In the same year she started her PhD program under the supervision of Prof.dr. C.F. Schmidt and Prof.dr. F.C. MacKintosh in the Department of Physics of Complex Systems in the Faculty of Sciences at the Vrije Universiteit Amsterdam in The Netherlands. This thesis describes the main results from her four years of PhD research, which were also presented in various national and international conferences. She received the award for the best article of 2005 from the LCVU (Laser Center Vrije Universiteit) for the paper "Short-time inertial response of viscoelastic fluids: observation of vortex propagation" (chapter 9 of this thesis).

[1] according to birth certificate

List of publications

This thesis is based on the following articles:

1. **M. Atakhorrami**, K.M. Addas and C.F. Schmidt," Twin optical traps for two-particle cross-correlation measurements: eliminating cross-talk" (manuscript in preparation), (Chapter 2)
2. **M. Atakhorrami**, J. Kwiecinska, K.M. Addas, G.H. Koenderink, J.X. Tang, A.J. Levine, F.C. MacKintosh and C.F. Schmidt, "Correlated fluctuations of microparticles in viscoelastic solutions: quantitative measurement of material properties by microrheology in the presence of optical traps" (submitted Physical Review E), (Chapter 3)
3. **M. Atakhorrami**, M. Buchanan, J.F. Palierne, and C.F. Schmidt, "Comparing macrorheology and one- and two-point microrheology in wormlike micelle solutions " Macromolecules 2005, 38(21)8840. (Chapter 4)
4. M. Buchanan, **M. Atakhorrami**, J.F. Palierne, F.C. MacKintosh, and C. F. Schmidt, "High-frequency microrheology of wormlike micelle" Phys. Rev. E (2005) 72: 011504. (Chapter 5)
5. **M. Atakhorrami** and C.F. Schmidt, "High-bandwidth one- and two-particle micrhorheology in solutions of wormlike micelles" (in print Rheologica Acta), (Chapter 6)
6. G.H. Koenderink, **M. Atakhorrami**, F.C. MacKintosh, and C.F. Schmidt," High-frequency stress relaxation in semi-flexible polymer solutions and networks" (submitted to Physical Review Letters), (Chapter 7)
7. **M. Atakhorrami**, G.H. Koenderink, J.F. Palierne, F.C. MacKintosh and C.F. Schmidt," Cytoskeleton networks at the micron scale: anomalous dynamics due to non-continuum elasticity" (manuscript in preparation), (Chapter 8)
8. **M. Atakhorrami**, G.H. Koenderink, C.F. Schmidt, and F.C. MacKintosh, "Short-time inertial response of viscoelastic fluids: observation of vortex propagation" Physical Review Letters (2005), 95:208302. (Chapter 9)

9. **M. Atakhorrami**, D. Mizuno, G.H. Koenderink, F.C. MacKintosh and C.F. Schmidt, "Inertial response of fluids probed with active and passive microrheology" (manuscript in preparation), (Chapter 10)
10. **M. Atakhorrami**, G.H. Koenderink, D. Mizuno, J.F. Palierne, C.F. Schmidt, and F.C. MacKintosh, "One- and Two-particle active and passive microrheology of semiflexible actin solutions" (manuscript in preparation)

Other Publications:

11. S. Jabbari-Farouji, D. Mizuno, **M. Athakhorrami**, F.C.Mackintosh, C.F. Schmidt, E. Eiser, G.H. Wegdam and D. Bonn, "Non-equilibrium fluctuation-dissipation theorem in an aging colloidal glass" (submitted to Physical Review Letters).
12. Karim M. Addas, **Maryam Atakhorrami**, Jay X. Tang, Alex.J. Levine, Frederick Mackintosh, Christoph F. Schmidt, "Two-bead microrheology of semiflexible fd virus solutions", (manuscript in preparation).
13. Fatima Bouchama, Maryam Atakhorrami, Christoph F. Schmidt, Erika Eiser, "Micro-rheology of Hyaluronic Acid gels" (manuscript in preparation)
14. S. Jabbari-Farouji, **M. Athakhorrami**, D. Mizuno, C.F. Schmidt, E. Eiser, D. Bonn and G.H. Wegdam," High frequency Microrheology of aging colloidal system" (manuscript in preparation)
15. **M. Atakhorrami**, K.M. Addas, M. Buchanan, G.H. Koenderink, F.C. MacKintosh, J.X. Tang, C.F. Schmidt,Molecular mechanics of cytoskeletal components
    Mechanics of the 21st Century, Warsaw, Poland, 15-21 August 2004. Gutkowski, Witold; Kowalewski, Tomasz A. (Eds.) 2005, LXXIV, 422 p., Hardcover ISBN: 1-4020-3456-3
16. Experimental study of effective temperature in an aging colloidal glass
    S. Jabbari-Farouji, D. Mizuno ,**M. Atakhorrami**, F.C. MacKintosh, C.F. Schmidt, E. Eiser, G.H. Wegdam and Daniel Bonn, Journal of Physics, Lecture Notes of Physics series of the Springer Verlag. (in process)

Acknowledgments

I cannot believe that I finished with writing *the* thesis! I'm very happy! And now I got to the most fun part of all, the acknowledgments. I think this is the great moment. Along the way I always looked forward to writing it and I kept thinking about the people I have spent time with in the last couple of years and especially during the last months of writing. Remembering the nice memories and the fun…That was an awesome drive. Their support and encouragement was always keeping me from loosing my sanity in the difficult days. Some people write this chapter in a more official way, with some philosophical start. I thought about it too, but I realized, while doing science and especially while doing my PhD, that I have changed "a little" some of my romantic views. So I write this more like a letter to all of the people whom I want to thank, and I hope I do not forget anybody. If I do, please accept my apology right now. The bottom line is that you have to read it all! It is just like a game! If you think it is too long just find your part and read! ;-)

I started my PhD research four years ago in the Complex Systems group. Fred and Christoph tried hard to get me into the totally unfamiliar field of microrheology. It has been a great pleasure working with them; I learned a lot. Christoph never runs out of ideas; he always has something to make you *very* busy! And Fred always finds some interesting theoretical questions out of your data. I really think that I have been very lucky to work with these enthusiastic researchers. I also learned that theoretical and experimental physics are not two separated islands. I really want to thank them for the opportunities they gave me, for their optimistic views and for being my friends as well as my supervisors. Christoph was all the time extremely generous with sending me to the meetings and conferences. Last year I stayed in Boston in the Dave Weitz lab and in Philadelphia, in the Paul Janmey lab. I appreciate this opportunity to be in such dynamic labs. I learned a lot of new science; I saw different ways of doing research and met very nice people. In addition I also got a feeling of what life could be like in the USA, a country that used to be the dreamland for many Iranian friends. Here I like to use the opportunity to thank Dave and Paul as well as their fantastic lab members for showing me around and making me familiar with

their research. In Boston, Peter Schall, Peter Lu, Margaret, Jiayu, Daniel, Cliff, Katie and Karen in Harvard and Zvonimir, Karim and Ed in the Rowland institute. I am very much thankful to Zvonimir for the generous hospitality and opportunity he gave me in his lab to do a lot of biochemistry together with Gijsje. In Philadelphia, Margaret, Kheya, Jérôme, Penelope and Sebastian. Getting familiar with some biochemistry, in the process of Neurofilament purification together with Paul, at last helped me to get over my fear of reading protocols. It was a great joy.

All of the research I have presented in this thesis has been conducted in collaborations with various people: Mark, Asia, Karim, Gijsje and Daisuke. Everybody taught me so much. Here I want to thank them for being with me to this point. Mark brought the collaboration with Jean-François Palierne. I want to thank Jean-François, for giving me the chance to use his valuable rheometer, for more experiments on actin, in Lyon. This was a real breakthrough for my thesis work. Asia helped with writing some of the programs for the data analysis. Karim was great in making me think more in-depth about different questions due to his perfectionism. I spent more than a year of the time with Gijsje; she is very efficient and has a great drive which is inspiring. She also helped me a lot with writing and proofreading. We had lots of fun and great talks besides doing research, in conferences that we attended together, while hiking in the White Mountains, and the very special place we shared in our Victorian-style room in the Gables, Philadelphia over our HUGE breakfasts ;-). I want to thank Daisuke, for his patience and creative ideas. I also enjoyed collaboration with people outside of the VU, from the UvA, Erika, Fatima, and Sara. Alex Levine, was a frequent visitor with whom I enjoyed many discussions about two-particle microrhology. I like to thank the people in the workshop, specially Mario Molenaar and Pierre Noordeloos .

Of course I could not enjoy my time as much if it was not such a great CoSy group. I want to thank you all, for your help, for your patience when having a noisy girl around, listening to me and supporting me in various stages in the last four years, for the “gezellige“ coffee and lunch breaks, for the group meetings and scientific discussions. The CoSy summer schools with the Amolf people were unforgettable memories, the campfires and driving to the local pubs with 19 people in a van! Could that be more fun? So, thanks to you all, Bram, Lukas, Maarten, Siet, Sander,

Tom, Remus, Joost, Iwan, Irena. Special thanks to Joost for being my always-reachable problem solver, particularly with computers! Iwan for his great personality and being so helpful in the chemical Lab. Irena for being one of my best friends, helping me sort out my mind. Also, for bringing us our new volunteer "lab member" Yana, with her sweet tiny smiles. To my great office mates, Mikhail and Karen, thanks to both of you, for keeping with me, I know it can be very difficult especially during the time I was constantly on the phone! Thanks to Karen for providing actin, for great talks and for our friendship. Your explanations about "Dutch" made life here much easier in a way. I like to thank Gijs and Erwin, for their helpful discussions and for reminding me that some times it is good to think twice (a little unusual for my nature!). Stefan and Catherine, who were always supportive and we had great talks about politics, science, and art. Thanks to the girls for the cheerful atmosphere they bring to the lab just by being around: Svenja, Beth and Marina. At the end I like to remember some other members of our group, Ola and Nikta. I had wonderful time with Ola when she was here, visiting museums and going out for drinks. I enjoyed a lot the time when Nikta was here; saying some words in Persian during the day at work was very comforting and so natural. During all this time Gerrie has been "geweldig": whenever I had to arrange some bureaucratic work and I would get stuck, she was there. She helped me to arrange my residence permit, a room in guesthouse when I needed it, and most importantly, my defense date. Thanks a lot!

Living in a totally different country and culture than you are used to is very exciting, but not ever totally smooth and easy. If it wasn't because of my friends I wouldn't ever feel as much at home in Amsterdam, as I feel now. This is besides of the charm of city itself of course ;-). My friends were always supporting me no matter where they are in this "small world", Australia: Mohammad and Leyla; Canada: Soheyla; USA: Tokameh, Rob, Azarmindokht, Katayoun, Petia, Solmaz, Parisa, Salomeh; England: Habib; Germany: Lili, Francesca, Salima, Jens, Esther, Tanja; Paris: Katerina; Athens: Thania; Hungary: Zoli; Iran: Arsham, Alireza, Elmira, Amirabbas, Saba, Talayeh, Bita and all the boys and girls of our hiking club; and in the Netherlands: Behnaz, Sara, Sharareh, Alireza, Babak, Nazanin, Mani, Adone, Federica, Calina, Didi, Mirjam. My youth friends, Azar and Lili, I sometimes forget

how fast time has passed, and still, wherever we meet in some part of the world, it feels like we are in Tehran and all the mutual connections pop up! Lili lives just across the border; her place fills the empty spot of home, whenever I miss Tehran. Although Azar lives in Washington DC, our hours long telephone talks always bring us all the news. And of course I remember my "Chinese queen style" bed, which was just big enough for my length! Tokameh, your friendship has always been very valuable to me, our discussions, going out and your spirit and all the good time we have shared, I miss you, and I am counting down the days until you and Rob come back to NL with your little new Avin ;-). Francesca, Salima, Katerina, Adone and Tokameh, the (in)sane parties in Berlin, the October feast in Munchen, wedding in Verona, and the fun we had in Iran by the Caspian sea, are all memorable. Katerina, your place in Paris, with the ice-cold Greek coffees in summer in our big cups! We definitely share the same passion. I'll visit you even if you go to Mars! Katy, it is a big prize for me to have you here from oversees, just on the exact day that I am going to submit this thesis; it keeps me going! Thousands of thanks to my friends and paranymphen, Halleh and Elke, for their never-ending friendships, and mutual understanding, for the encouragement you have offered me to keep going.

Many thanks to my dear friends in Amsterdam, Sharareh, Sara and Behnaz, for the Persian nights with delicious food that Sharareh would cook. Although she moved back to Iran, we always remember the great time, nice talks, jokes and gossip all night long ;-). Also to Ellen, the one and half year I lived in your place was just awesome! It was so relaxing, and easy. I felt very welcome; I still feel nostalgic for that small cozy room ;-). Here I would like to also thank the common friends I have with Simon for the crazy parties and going out. Toon, Sanne, Sanna, Laura, Rosa, Marjolijn, Dita, Tjerk, Willempje, Nienke, Sylvia. Tobias and Tessa for relaxed parties and barbecues in your pretty house, (I could even fall sleep during the party!). The Bad Taste parties have been fantastic Niels, and could any trip to NYC be funkier than the one last year? In that matter I would like to thank Bernardo too, for showing us underground life in NYC and having us in his place, and Jan Maarten for his excellent explanations in museums. Sietske, it is always great talking to you, also sharing a cigarette! I wish you luck with your research.

I like to express my gratitude to Simon's family. José, Peter and Arthur; they have been very supportive in all these times. José sent me to a very special Dutch course, (het was prima!) and I have been consulting Peter and José several times to find my way here in the Netherlands. I have spent great times at their place, with good wines and food. Also with Arthur and other cousins I have enjoyed the "Sinterklaas" and Christmas nights. For the latter I would like to thank Jan and Truus as well. I used to think that Christmas nights were the most boring, but now it is actually pretty relaxing, playing "Risk", eating "rijstevlaai" and drinking good wines!

Finally, I want to thank the most important people in my life, my family. Many thanks to them for believing in me, and accepting all of my decisions and for letting me experience what I want, even if it could be painful for them. In Iranian fashion, I like to first thank my grandmother, Maman bozorg, for her kindness, and "Shami Roodbary". I cannot wait to finish my defense and fly to her place with the huge garden, where I can climb up fruit trees. To my mother, Nabat, thanks for being so brave and going trough all you have gone through. You showed me that I must stay on my own feet. Thanks to Mahsa, my sister, for her love, for having such a happy personality and being my best friend ever. To Mazdak, my brother, as you grow up I am sometimes wonder how much we look like each other ;-) I'm not sure whether it is good! Watch out! I want to thank the other aunts, uncles and cousins, (Hadi, Sedigheh, Fazel, Masi, Zari, Tayeb, Shahnaz, Ebrahim, Fayez, Taher, Mansoureh, Ata, Mehrnoosh, Kooshyar, Sara, Elnaz, Omid, Arezo, Babak,…) special thanks to Marzieh va Naser for always being my intellectual supports. They are indeed my second parents.

Simon! I do not know how to thank you for all of the support and comfort during the previous (almost) two and a half years; you have been a great partner! Also, you are very fun person to hang out with. More professionally(!), thanks for proofreading my thesis, translating my "samenvatting" and spending so much time on the design of the book cover, etc. We are going to relax the applied (shear) stress in another of *the* vacations ;-).

Maryam,
December 15, 2005, Amsterdam

چکیده

خواص کشسانی و گرانرَوی را می توان از ویژگی‌های مهم مواد نرم بشمار آورد. مواد نرم از جمله انواع پلیمرها و محلول‌های کولئیدی و همچنین بسیاری از مواد بیولوژیکی مانند سلول‌ها و بافت‌ها دارای خواص ویسکوالاستیک نیز هستند.
نحوه شارش مواد نرم به ساختارهای میکروسکوپی و واکنش این مواد نسبت به برش و تنش اعمال‌شده بستگی دارد. یکی از موارد لازم برای درک بهتر این نحوه شارش، اندازه‌گیری خواص ویسکوالاستیسیته ماده می‌باشد. این خواص در هریک از مواد نرم متفاوت است.
گرایش روبه‌رشد دانشمندان به شناخت مواد زیستی و شاره‌های خاص، امروزه باعث ایجاد شاخه‌ای جدید از علم به نام ریزشاره‌شناسی (میکروریولوژی) شده است.

هدف از پژوهش ارائه‌شده در این پایان‌نامه، بررسی و تکمیل تکنیک‌های جدید میکروریولوژی با فرکانس بالا (تا ۱۰۰ کیلوهرتز) با توجه به رفتارهای موضعی و کلی شاره‌ها می‌باشد. روشی که ما در اینجا به این منظور بکار برده‌ایم روش تداخل‌سنجی لیزری می‌باشد.

برای این منظور میکروسکوپ ویژه ای ساخته شد که قادر به کانونی کردن نور لیزر در محیط نمونه است. از این راه تله ای برای به دام انداختن ذرات میکرونی کروی در محیط مزبور فراهم شد. با استفاده از این تله لیزری می توان جابجایی میکرونی ذراتی که دارای حرکت براونی هستند را اندازه‌گیری نمود و از این طریق درک بهتری از ویژگی‌های ویسکوالاستیک ماده بدست آورد.

در این تحقیق، دو نوع سیستم به عنوان مدل مورد بررسی قرار گرفته اند.
نوع اول میسل است که به عنوان یک نوع محلول پلیمری انعطاف‌پذیر شناخته شده است. نوع دوم آکتین می‌باشد که یکی از مهمترین پلیمرهای ساختار سلول است. آکتین همچنین به عنوان یک سیستم الگو برای محلول‌های پلیمری نیمه‌انعطافی کاربرد دارد.

نظریه‌ای برای بررسی خواص لَختی مایعات از سال ۱۹۲۷ موجود بوده است ولی تاکنون تکنیک های لازم برای مشاهده و اثبات این نظریه در دست نبوده است.
تکنیک‌های میکروریولوژیک بکاررفته در این پژوهش، با قابلیت دسترسی به فرکانس‌های بالا، امکان اثبات این نظریه را فراهم نموده است.